The Electropolymerisation of Indolo{3,2,1-jk}carbazole and Pyrrolo{3,2,1-jk}carbazole: An Electrochemical, Computational and Spectroscopic Study.

Madelaine A.Chapman

Degree of Doctor of Philosophy

The University of Edinburgh

2004

Abstract

The electropolymerisation of a range of 5-substituted indoles has been shown previously to result in the formation of redox-active films. The oxidation potentials of both the indole monomers and their polymers can be altered by substitution of the monomer with different electron-withdrawing groups. Both the indole monomers and polymers also have high fluorescence quantum yields. However, the fluorescence wavelengths of the indole polymers are not tuneable by substitution. In this thesis, the work on the electropolymerisation of indoles is extended to two monomers which have larger conjugated systems than the indoles; indolo{3,2,1-*jk*}carbazole (IC) and pyrrolo{3,2,1-*jk*} carbazole (PC). A combination of computational, electrochemical and spectroscopic techniques has been employed to investigate both these monomers and their polymers.

Computational confidence tests have been performed on a range of small organic molecules to assess methods of calculating oxidation potentials, radical cation spin density distributions and excited states using the software Gaussian 98. Calculations have predicted the oxidation potentials of such molecules to within 0.19 V of their experimental values. These calculated oxidation potentials are systematically underestimated. Gaussian 98 has been used to calculate the radical cation spin density distribution of indole and has been found to reproduce the results of previous calculations performed using the software DMol^3. Configuration interaction singles (CIS) incorrectly predicted the energetic ordering of the two lowest singlet excited states of indole and carbazole. However CIS correctly predicted the dipole moment of the ^1L_a state to be larger than the dipole moment of the ^1L_b state of indole.

The oxidation potentials of IC and PC have been measured experimentally and calculated. IC and PC have both been electropolymerised to form redox-active polymers. IC forms a conducting film which has been shown to contain two different dimers by mass spectroscopy and NMR. Although successful in predicting the ring positions at which indoles link during electropolymerisation, radical cation spin density calculations have been shown to be unsuccessful in predicting the linkage sites for IC. The mechanism of electropolymerisation of IC has been shown to be similar to the mechanism of electropolymerisation of indoles, with initial film formation occurring in solution, followed by linkage of IC radical cations adsorbed on the electrode surface. The diffusion coefficient has been measured from Koutecky-Levich plots as 5.9×10^{-5} cm^2 s^{-1} ($\pm$ 2.0×10^{-5}). The rate of film formation for IC

has been shown to be approximately 0.9 times that of indole-5-carboxylic acid and 0.4 times that of 5-cyanoindole.

Steady-state fluorescence spectroscopy in solution at room temperature has shown both the IC and PC monomers and their polymers to be highly fluorescent. There is no significant difference between the equilibrium geometries and potential energy surfaces of the IC monomer in the ground and first singlet excited states. However, such a difference does exist between the ground and first singlet excited states of the PC monomer. The electropolymerisation of each monomer produces a number of emitting species which have more extensive π-electron delocalisation than the monomers. The emission from the IC dimer peaks at 408 nm. IC electropolymerisation has been shown to proceed in a similar manner to indole electropolymerisation; the first step is the formation of dimer, followed by the linkage of dimer units to form longer polymer species. The IC polymer has been found to be fluorescent in the solid state.

Time correlated single photon counting (TCSPC) experiments have been performed on solutions of the IC and PC monomers and their polymers. Altogether seven emitting species were observed in the emission from the IC polymer. The lifetimes ranged from 2.6 to 10.0 ns, indicating that the size of polymer produced by the electropolymerisation of IC is limited. The lifetime of the IC dimer is 10.0 ns. Altogether seven emitting species were observed in the emission from the PC polymer, with lifetimes ranging from 1.3 to 14.3 ns. This is a greater range of lifetimes than observed for the IC polymer, which suggests the existence of a wider range of polymer chain lengths in the PC polymer than in the IC polymer.

Declaration

I hereby declare that the work presented in this thesis is my own unless otherwise stated by reference.

Madelaine Chapman
March 2004

Acknowledgements

A great deal of thanks go to my supervisors; both official, Dr Anita Jones and Dr Andy Mount, and unofficial, Dr Simon Bates. Without their patience and encouragement this work would never have been completed.

I am also grateful to the EPSRC, for providing the funding.

I would like to thank Lynne Crawford and Stuart Wharton, both members of Hamish MacNab's group, for providing the samples of IC and PC.

I have received lots of help from other members of the Mount/Jones groups. Particular thanks go to Tricia, who was very helpful with my calculations, Lorna Kettle, who showed me how to do the electrochemistry experiments, Neil Speirs, who showed me how to use the Fluoromax and Steve Magennis who helped with the COSMIC experiments. Alice Williams played perhaps the most crucial role in helping me to go for tea breaks and taking me to visit Scout.

I would like to thank everyone in the room 252 and all my fellow tea break enthusiasts, including Alex, Ian, Rob, Orange Mike and Dave.

Finally, I thank Mum, Marie-Clare and Catherine for all their support and encouragement.

To Mum and Dad

CONTENTS

Chapter One

INTRODUCTION

1.1 Introduction

In this thesis, the electropolymerisation of two organic heterocycles, indolo{3,2,1-*jk*}carbazole (IC) and pyrrolo{3,2,1-*jk*}carbazole (PC), is described for the first time. The molecular structures of these monomers are shown in Figure 1.1. The polymers formed from IC and PC were then studied using both electrochemical and spectroscopic techniques. In this chapter a brief introduction to the field of conducting polymers and their applications is provided. In particular previous work on the electropolymerisation of indoles, which are related to the monomers IC and PC, is discussed. Finally, the motivation for the work described in this thesis is explained.

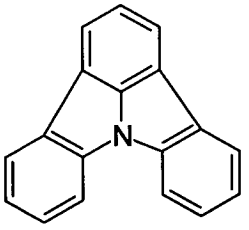

IC
(indolo{3,2,1-*jk*}carbazole)

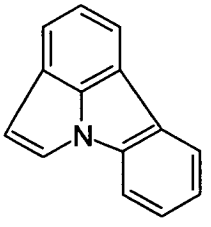

PC
(pyrrolo{3,2,1-*jk*}carbazole)

Figure 1.1: Molecular structures of IC and PC.

1.2 Conducting Polymers

Organic polymers which have extended π-systems are known as conjugated polymers. These materials contain a chain of sp^2 hybridised carbon atoms, whose p_z orbitals overlap to form π valence and π* conducting bands. The structures of some common conjugated polymer systems are shown in Figure 1.2.

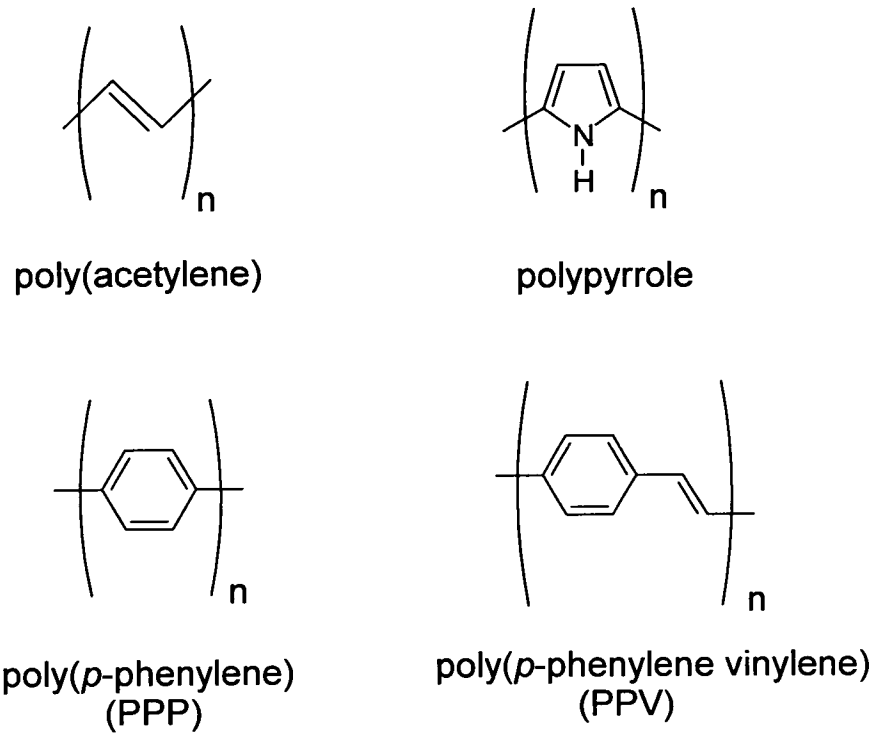

Figure 1.2: The structures of some common conjugated polymer systems.

Traditionally, polymers have been seen as insulating materials. However in 1977 it was reported that the conjugated polymer poly(acetylene) exhibits electrical conductivities of up to 1,000 S cm^{-1} at room temperature when doped with iodine [1, 2]. Such a high level of conductivity had not previously been observed for organic polymers and this discovery prompted interest in the development of organic materials which combine semiconducting properties with attractive polymer characteristics, such as excellent mechanical properties. Although at first it was believed that having a conjugated backbone is necessary for a polymer to be electrically conducting, it was later shown that this is not the case, as with appropriate substituents a nonconjugated polymer such as 1,4-*cis*-polyisoprene, may also become conducting [3, 4, 5]. Conducting polymers have many potential applications [6], for example in biosensors [7], light-emitting diodes (LEDs) [8, 9], photovoltaics [10], polymer-based lasers [11, 12, 13] and field-effect transistors [14].

Much of the research into conducting polymers over the past 25 years has focussed on improving the synthesis and properties of conducting polymers which are already known, such as polyacetylene and poly(phenylenevinylene) (PPV). In particular, PPV-based conducting polymers have been the subject of a great deal of research, since these polymers display electroluminescence and may therefore be used as the light-emitting layer in LEDs[15]. The range of conductivities of conducting polymers have been increased dramatically and conductivities greater than 10^4 S cm^{-1} have been obtained for iodine-doped poly(acetylene)[16]. Such conductivies are approaching the conductivity of copper at room temperature (500,000 S cm^{-1}). One of the original drawbacks to the use of conducting polymers in devices was the poor solubility and high melting points of many of these materials, due to the rigidity of the polymer backbone. These characteristics, whilst desirable in the device structure, make such materials difficult to process. A variety of approaches have been developed to overcome this problem, such as the attachment of side groups to increase solubility [9], or processing *via* a solution-processible precursor with *in situ* conversion to the intractable conjugated form after processing [15, 17]. Examples of these approaches applied to PPV are illustrated in Figure 1.3. Another limitation on the applicability of such polymers in commercial devices has been their chemical stability. For example poly(acetylene) is unstable in the presence of oxygen and this has prevented the use of this particular polymer in such devices.

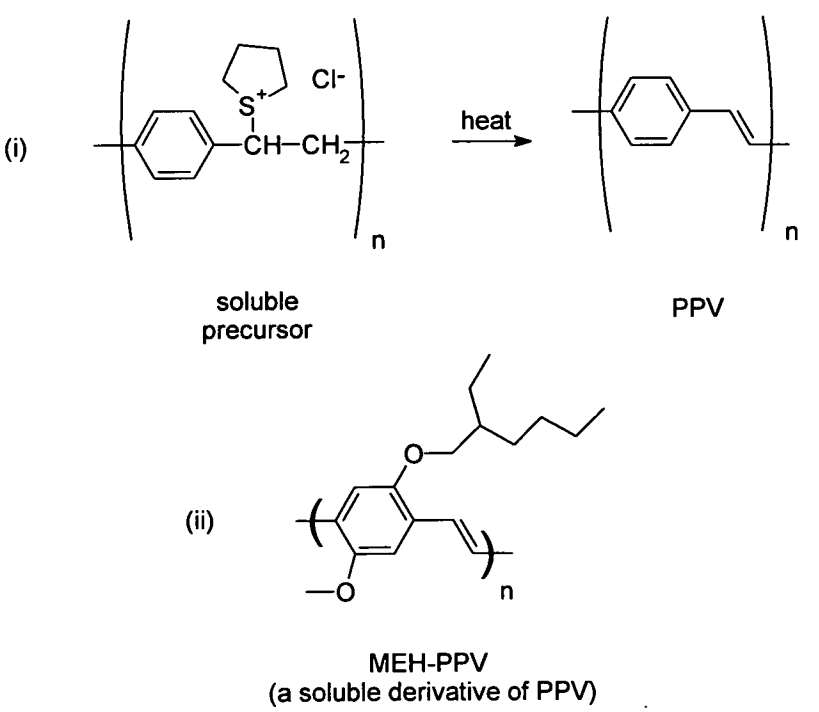

Figure 1.3: (i) A route to PPV via soluble precursor and (ii) MEH-PPV, a soluble derivative of PPV formed by the attachment of alkoxy side-groups.

In addition to poly(acetylene) and PPV, a number of other conducting polymers have also been studied, many of which are based on heterocyclic monomers. These include polypyrrole [18, 19], polyaniline [20, 21], polythiophene [22], polycarbazole [23] and polyindole [24, 25]. In particular, polypyrrole has been the subject of many studies and both it and polyaniline have been found to exhibit a relatively high level of environmental stability. Polypyrrole and polythiophene have been shown to polymerise *via* similar mechanisms to give linear polymers. In contrast, indole has been shown to polymerise to give discrete indole trimer units, which may then undergo further linkage to form polymer. This work on indole is particularly relevant to the work presented in this thesis and is described in more detail in section 1.3 of this chapter.

1.2.1 Synthesis of conducting polymers

Conducting polymers may be synthesised by both electrochemical and chemical methods. In this thesis the polymers of IC and PC were prepared using electrochemical oxidation. Whilst both methods have their own advantages, electrochemical methods are particularly useful for investigating novel conducting polymers. This is because such methods allow control of the polymerisation reaction through control of such variables as electrode potential, and also offer a means of *in situ* analysis of the polymerisation process. Chemical methods are suited to the large scale synthesis of conducting polymers for commercial devices.

An electrochemical synthesis of a conducting polymer typically starts with a solution of the monomer dissolved in electrolyte. This solution is placed in contact with an electrode held at a suitable potential to allow oxidation of the monomer. The monomer is oxidised to form radical cations, which then link to form polymer and where this polymer is insoluble in the electrolyte, it precipitates out onto the electrode surface. The oxidised film formed on the electrode surface incorporates anions from the solution which act as dopant ions and therefore the film is conducting in its oxidised form. In its reduced form the anions are expelled from the film into the solution and the film becomes insulating. Such films may be cycled between their conducting and insulating forms. These processes are illustrated in Figure 1.4.

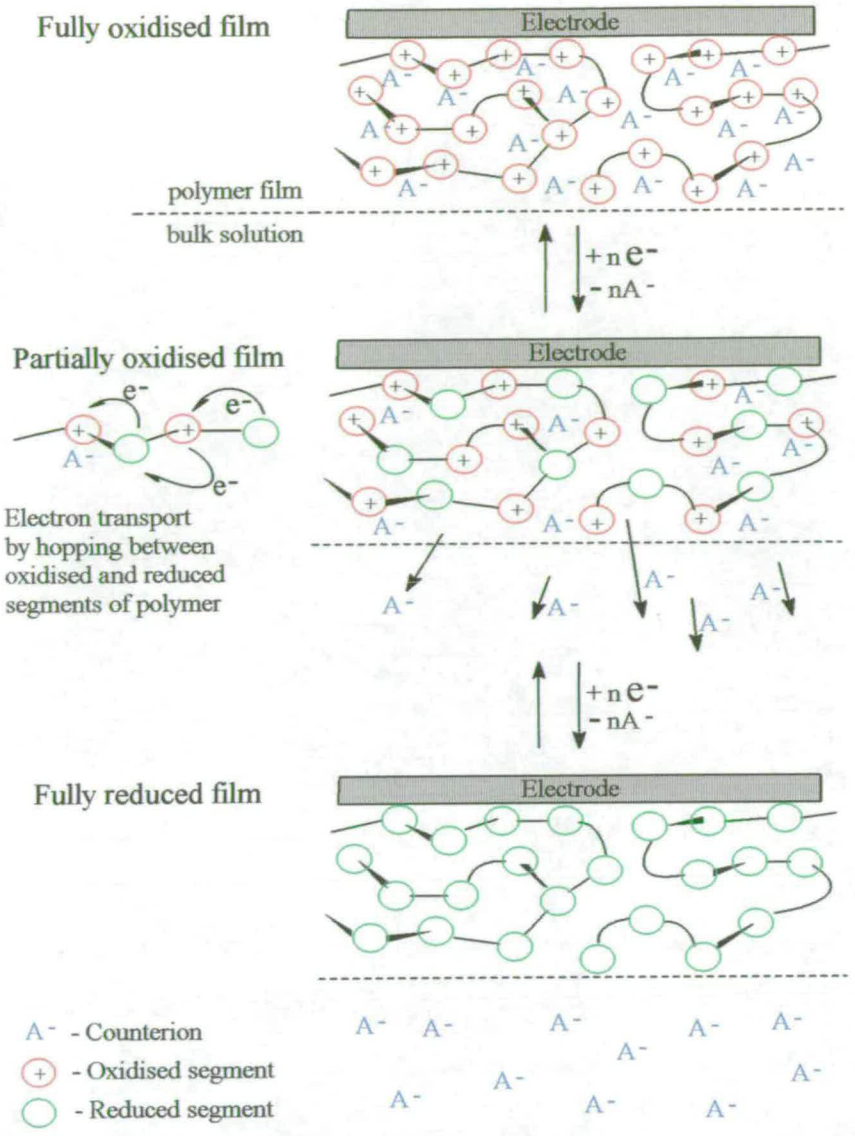

Figure 1.4: The reversible uptake of counterions by a conducting polymer film, reproduced from reference 26

1.2.2 Photophysics of conducting polymers

Since the discovery in 1990 of electroluminescence in a thin PPV layer, there has been a great deal of interest in the field of organic polymer LEDs [15]. The advantages offered by organic LEDs over the more conventional inorganic LEDs include flexibility, low cost, low operating voltage and ease of processing, which allows the possibility of making large area devices [6]. Most of the work to date in this area has focussed on the optimisation of PPV, polyfluorene and their derivatives.

In a LED the mechanism of light emission is by electroluminescence. However most studies of the phenomenon of light emission from conducting polymers have used

photoluminescence, in which luminescence is stimulated by another photon. The photon is absorbed by the polymer, promoting an electron from the highest occupied molecular orbital (HOMO) to the lowest unoccupied molecular orbital (LUMO). This results in the formation of a singlet excited state, which is sometimes referred to as a singlet exciton. The singlet excited state may then decay to the ground state by emitting a photon, which always has a longer wavelength than the absorbed photon. This difference in wavelength is known as the Stokes shift. In electroluminescence the singlet exciton is generated through a different mechanism [27], which is illustrated in Figure 1.5. An electron is injected into the material at the cathode, producing a negatively charged polaron, and a hole is injected at the anode, producing a positively charged polaron. These two species migrate through the material under the influence of an electric field and may combine to form a singlet exciton. This exciton is indistinguishable from that obtained by photo-excitation and, as in photoluminescence, may decay to the ground state by emitting a photon.

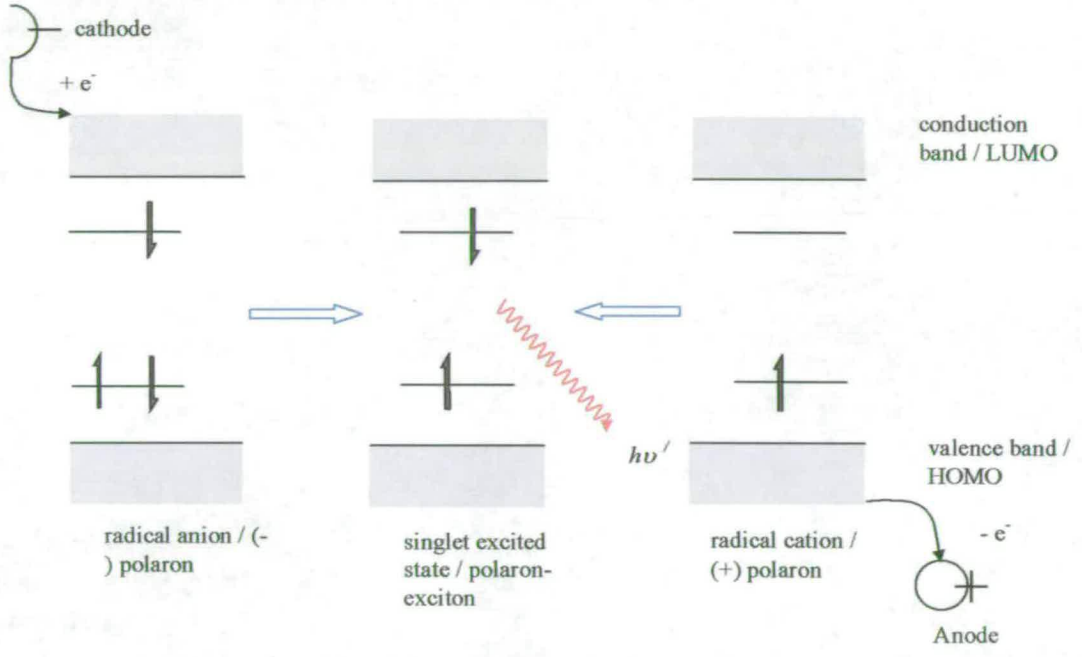

Figure 1.5: Electroluminescence from a conjugated polymer, reproduced from reference 27.

One of the limits to the efficiency of devices based on electroluminescence from conjugated polymers is that triplet excitons may be formed as well as singlet excitons, and decay from triplet excitons to the ground state is largely non-radiative. From spin statistics the probability of singlet formation is 0.25 and therefore there is a restriction on the maximum efficiency of such devices, measured as the ratio of the number of photons emitted per electron injected, of 25 %. Some research has been directed into increasing the efficiency of

devices by utilising the triplet excitons as well as the singlet excitons, for example by doping PPV with the phosphorescent molecule fac-tris(2-phenylpyridine) [28]. In such a device energy transfer occurs from both the singlet and triplet excitons to the phosphorescent molecule. Some studies combining theoretical and experimental work have suggested that the value of 25 % may be wrong and that the true value for the probability of forming a singlet exciton is higher than this [29, 30]. However, recently the fraction of excitons formed as singlets has been measured as 20 % (± 4) for MEH-PPV, thus confirming the value of 25 % for this polymer, although the possibility that the fraction is material dependent has not been ruled out [31].

A simple LED, such as the one shown in Figure 1.6 is made up of four layers [32]. The substrate layer is some optically transparent material such as glass. On the substrate there is a layer of some high work-function, optically transparent, electrical conductor such as indium-tin-oxide (ITO), which serves as the anode or positive contact. This is followed by the light-emitting layer, which is typically no more than 100 nm thick, and finally a layer of low work-function metal such as Ca or Al, which serves as the cathode or negative contact. An electrical potential is created between the two electrodes which forces electrons in through the cathode and holes in through the anode. As described above, the electrons and holes meet and combine in the emissive layer, forming a singlet exciton which then decays to the ground state by emitting a photon of light.

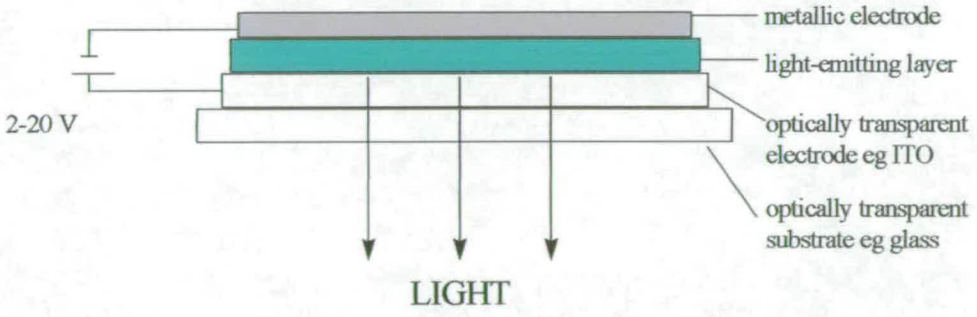

Figure 1.6: Schematic diagram of a basic light-emitting diode (LED).

LEDs for commercial applications must be both efficient and reliable. The efficiency of a device depends on a number of factors, such as the efficiency with which singlet excitons are generated, the proportion of such excitons which decay radiatively rather than non-radiatively and the efficiency with which the photons can escape from the device [30]. In order to improve efficiency and reliability, both the device structure and the nature of the emitting layer have been optimised. For example, quenching at the cathode may decrease the

efficiency of single-layer devices such as the one shown in Figure 1.6. This is a particular problem since exciton formation tends to occur close to the cathode because, for the majority of conducting polymers investigated, electron mobility is lower than hole mobility. A method of correcting for this has been to introduce an extra layer of an organic charge transporting material between the conducting polymer and the cathode [33]. This layer, known as an electron-conducting/hole-blocking (ECHB) layer, ensures that recombination occurs away from the metal electrode by preventing the passage of holes and allowing the passage of electrons. It also has the effect of balancing the rates of electron and hole injection.

Another area of investigation has been into extending the range of colours of light emitted by polymer LEDs. In particular, the colours red, green and blue are required for multicolour display applications. PPV itself has emission maxima at 551 and 520 nm in the yellow-green region of the visible spectrum [15] and a variety of strategies have been utilised in the search for emission of different colours. Among these have been the use of substituents to alter the structures and band gaps of polymers, for example substitution of PPV at the 2- and 5-positions on the phenyl ring with alkoxy groups gives orange-red emission [32]. An alternative strategy has been to use copolymers in which the conjugation length of the polymer is limited by the incorporation of a non-conjugated copolymer into the chain [34]. This enables tuning of the colour of emission by changing the relative amounts of the two polymers. The use of polymers other than PPV has also been investigated, for example poly(3-alkylthienylenes), which give red emission [32]. The main challenge in this area has been to obtain a bright blue light-emitting polymer with the characteristics required for device applications. The first blue emitting polymer LED was made by Yoshino *et al* using poly(9,9-dihexylfluorene) [35] and since then there has been research obtaining blue light emitting diodes with polyfluorenes [36] and polyindenofluorenes [37]. A problem associated with these materials is that green or yellow emission, which has been attributed to keto defects, appears upon heating during device formation or operation [38]. Recently, however, stable blue emission in the solid state from an aryl-substituted polyindenofluorene [37] and an alkoxyphenyl-substituted polyfluorene [39] have been reported.

1.3 Electropolymerisation of indole

Indole was first electropolymerised in 1982 by Tourillon and Garnier [40] and since then polyindole films have been the subject of investigation by several groups. A variety of applications have been proposed for such films, for example the use of poly(indole-5-carboxylic acid) as a fast-response pH sensor [41, 42]. Initially it was believed that indole would

form linear polymers in a similar manner to pyrrole and thiophene. For example, Tourillon and Garnier [40] proposed a linear, N-N bonded structure, based on the observation that N-methyl indole does not give a conducting film. However Waltman *et al* [43] proposed a different, 1-3 linked polymer based on the observation that indoles substituted at the 1, 2 or 3 positions do not polymerise. However subsequent work by the Mount group has shown that indoles do not polymerise to give linear polymers, but rather form indole trimers which may then link further to form polymer.

1.3.1 Structural characterisation of polyindoles

The electropolymerisation of a range of 5-substituted indoles has been the subject of investigation by Mount *et al* over the last ten years. Initially, this work focussed on the electropolymerisation of indole-5-carboxylic acid [24, 44, 45] and 5-cyanoindole [46], both of which may be electropolymerised to form an electroactive, conducting polymer film. Both of these films were found to be separable into two components by their differential solubility in DMF. The DMF-soluble component was characterised in each case using ^{1}H NMR spectroscopy and two-step laser desorption laser photo-ionization time-of-flight mass spectrometry (L^{2}TOFMS) and found to consist of an asymmetric trimer. The structure of this trimer is shown in Figure 1.7. It may be noted that this structure accounts for the observation by Waltman *et al* that indoles substituted at the 1, 2 and 3-positions do not polymerise. ^{1}H NMR spectroscopy on the DMF-insoluble component was consistent with it being polymer in each case and UV-visible and fluorescence spectroscopy showed that the DMF-soluble and insoluble components absorb and emit *via* similar chromophores. On the basis of this evidence, along with L^{2}TOFMS and IR spectroscopy results, the DMF-insoluble components were characterised as polymer made up of trimer units linked *via* the indole ring nitrogens in the trimer. The linkage of the trimer units *via* the ring nitrogens to form polymer was also supported by the results of a study of the electropolymerisation of N-methylindole [47], which found no evidence of such polymer formation where the ring nitrogens are blocked by methyl groups.

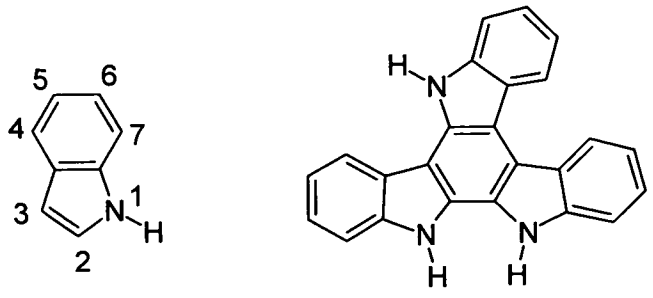

Figure 1.7: The indole monomer and the asymmetric indole trimer.

1.3.2 The mechanism of electropolymerisation of indoles

The polymerisation mechanisms of indole-5-carboxylic acid [24] and 5-cyanoindole [44] were investigated using electrochemical techniques. Both were found to polymerise *via* the same mechanism, which is illustrated in Figure 1.8. Initially, monomer is oxidised to form radical cations, which link to form asymmetric trimer in the diffusion layer close to the electrode surface. This trimer is insoluble in acetonitrile and precipitates out onto the electrode surface where it forms a surface onto which monomer may be adsorbed. Reaction then proceeds *via* adsorption and oxidation of monomer followed by linkage to form trimer (1). Trimer formation is thought to proceed *via* initial formation of the symmetric 3,3'-dimer. There is indirect evidence for this from both density functional theory (DFT) calculations [48] and the chemical synthesis of the symmetric trimer [49], which occurs *via* the unsymmetric 2,3'-dimer. Recently, the asymmetric trimer has also been chemically synthesised [50]. The asymmetric trimer thus formed may be further linked to form polymer (2), which has been found to have an average of two bonds per trimer unit.

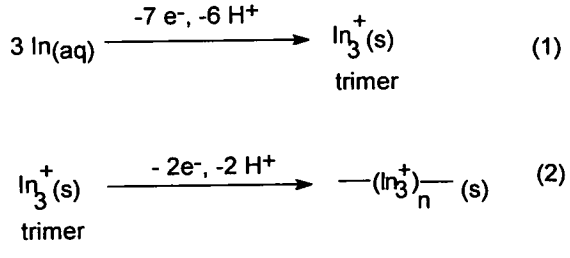

Figure 1.8: Mechanism of formation of indole trimer (1) followed by linkage of trimer units to form polymer (2).

The extent to which linkage of trimer units to form polymer occurs depends on the polymerisation conditions. A fast rotation speed of the rotating disc electrode (RDE) and high bulk concentration of monomer leads to formation of a trimer-rich film, whereas a slow rotation speed and low bulk concentration of monomer leads to more linkage and therefore

the proportion of polymer in the film is increased with respect to trimer. An additional study of the copolymerisation of 5-cyanoindole and indole-5-carboxylic acid [51] found that trimers of mixed functionality could be formed and that this occurred *via* a similar mechanism to that described above.

The electrochemical responses of the films formed from the electropolymerisation of 5-cyanoindole and indole-5-carboxylic acid were further investigated by the analysis of ac impedance data [52]. Both the films were both found to show high electronic conduction consistent with the films behaving as porous metals. However, with prolonged cycling between the oxidised (conducting) form and the reduced (insulating) form, the indole-5-carboxylic acid film showed a change in structure and redox mechanism, moving from metallic behaviour to redox hopping between trimer centres. This change was not observed for the 5-cyanoindole film and was attributed to the effects of an irreversible deprotonation of the carboxylic acid side group.

1.3.3 The effects of substitution

The electropolymerisation reactions of a range of other 5-substituted indoles were also studied by Mount *et al* [25]. This work showed that indole itself and indoles substituted with electron-withdrawing groups at the 5-position may be electropolymerised to form films made up of asymmetric trimer units. In contrast, indoles substituted with electron-donating groups, such as hydroxy, only form films if electrooxidised onto a preformed indole film layer. At first this difference was attributed to surface effects, but density functional calculations [48] showed that there is a fundamental difference in the electron distribution around the ring between the indole radical cations of monomers substituted with electron-withdrawing groups and those substituted with electron-donating groups. Such calculations were also used to successfully predict the monomer oxidation potentials. It was found for the 5-substituted indoles substituted with electron-withdrawing groups, that the oxidation potentials of both the monomers and the trimers are dependent on the strength of the substituent electron-withdrawing effect, and therefore are tuneable.

1.3.4 Studies of the fluorescence of polyindoles

The steady-state fluorescence of the indole monomers, and the trimers and polymers formed from various 5-substituted indoles, has also been investigated [53]. All three species are fluorescent and the 5-cyanoindole trimer has been found to have a have a fluorescence quantum yield in ethanol which is 1.3 times that of indole. The quantum yield of indole in

ethanol has been reported to be 0.4 [54]. The emission maxima of the indole-5-carboxylic acid trimer occurs at 408 and 428 nm in ethanol at room temperature. The trimer and polymer emission is very different to the monomer emission, showing a shift to longer wavelengths which is characteristic of more delocalised aromatic systems. The emission spectra of the trimers show little dependence on the polarity of the solvent or the nature of the 5-substituent. This means that the wavelength of emission of the trimers cannot be tuned by using different substitutents. The polymer emission occurs at longer wavelengths than the trimer emission and has a lower intensity. It is also broad, suggesting that a range of emitting species, which probably correspond to a distribution of different conformations, each having a different degree of delocalisation, are present. The fluorescence of 5-cyanoindole and indole-5-carboxylic acid films were also studied during electrochemical redox cycling using a novel *in situ* spectroelectrochemical cell [55]. It was found that intact oxidised films do not give any fluorescence emission, indicating the presence of an efficient quenching process. However, the reduced intact film and both oxidised and reduced drop-coated films do show fluorescence emission.

The time-resolved fluorescence of 5-bromoindole trimer and polymer species has been studied [56, 57]. The linked (quenched) trimer species has a lifetime of ~150 ps, whereas the lifetime of the free trimer is 5.5 ns. It has been suggested that the large difference between the lifetimes of these two species is due to efficient non-radiative energy transfer from the linked trimer species to lower energy, longer conjugation length segments of polymer. Also observed were a number of longer conjugation emitting species with a range of lifetimes.

1.4 Aims of this work

As discussed above, indoles have been shown to polymerise to form fluorescent conducting polymers. However substitution of indole monomers at the 5-position has been shown to have little effect on the emission wavelengths of the indole trimers and polymers. In this thesis the electropolymerisation of the monomers IC and PC is reported for the first time. The photophysical behaviour of the resulting polymers is also examined using both steady-state and time-resolved techniques. IC and PC are both similar to indole, being nitrogen containing heterocycles, indeed they may be thought of as a fused indole and carbazole and a fused indole and pyrrole respectively. Therefore, it was thought that these monomers may electropolymerise in a similar manner to indole to give fluorescent conducting polymers. However, their extended aromatic systems, when compared to indole, may result in the formation of polymer which emits at different wavelengths to the indole trimer and

polymers. This would therefore provide a means of tuning the fluoroscence wavelengths of such polymers.

In the following chapter, aspects of the theory behind the various computational and experimental techniques used in this work are described. In chapter three, the experimental details are discussed and in chapter four, the results of confidence tests of various calculation methods which may be used to calculate different properties of the monomers, such as oxidation potentials, are given. In chapter five, the electropolymerisation of IC and PC is described and the characterisation of the IC films is given. Chapters six and seven are both concerned with the photophysical properties of the monomers and their polymers. In chapter six, the results of steady-state fluorescence measurements are given and in chapter seven, the results of the time-resolved measurements are discussed.

1.5 References

1. C.K.Chiang, C.R.Fincher Jr., Y.W.Park, A.J.Heeger, H.Shirakawa, E.J.Louis, S.C.Gau and A.G.MacDiarmid, *Phys.Rev.Lett.*, 1977, **39(17)**, 1098-1100

2. H.Shirakawa, E.J.Louis, A.G.MacDiarmid, C.K.Chiang and A.J.Heeger, *J.Chem.Soc.Chem.Comm.*, 1977, 578-580

3. M.Thakur, *Macromolecules*, 1988, **21**, 661-664

4. M.Thakur and B.S.Elman, *J.Chem.Phys.*, 1989, **90(3)**, 2042-2044

5. A.L.Cholli and M.Thakur, *J.Chem.Phys.*, 1989, **91(12)**, 7912-7915

6. V.Saxena and B.D.Malhotra, *Current Appl.Phys.*, 2003, **3**, 293-305

7. G.Bidan, M.Billon, T.Livache, G.Mathis, A.Roget and L.M.Torres-Rodriguez, *Synth.Met.*, 1999, **102**, 1363-1365

8. Richard Friend, Donal Bradley and Andrew Holmes, *Physics World*, Nov. 1992, 42-46

9. R.H.Friend, R.W.Gymer, A.B.Holmes, J.H.Burroughes, R.N.Marks, C.Taliani, D.D.C.Bradley, D.A.Dos Santos, J.L.Brédas, M.Lögdlund and W.R.Salaneck, *Nature*, 1999, **397**, 121-128

10. N.S.Sariciftci, L.Smilowitz, A.J.Heeger and F.Wudl, *Science*, 1992, **258**, 1474

11. N.Tessler, G.J.Denton and R.H.Friend, *Nature*, 1996, **382**, 695-697

12. A.J.Heeger, *Solid State Com.*, 1998, **107(11)**, 673-679

13. G.Heliotis, R.Xia, D.D.C.Bradley, G.A.Turnbull, I.D.W.Samuel, P.Andrew and W.L.Barnes, *Appl. Phys.Lett.*, 2003, **83(11)**, 2118-2120

14. Tsumara A., Koezuka H. and Ando T., *Appl.Phys.Lett.*, 1986, **49(18)**, 1210-1212

15. J.H.Burroughes, D.D.C.Bradley, A.R.Brown, R.N.Marks, K.Mackay, R.H.Friend, P.L.Burns and A.B.Holmes, *Nature*, 1990, **347**, 539-541

16. N.Basecu, Z.-X.Liu, D.Moses, A.J.Heeger, H.Naarman and N.Theophilou, *Nature*, 1987, **327**, 403-405

17. G.Padmanaban and S.Ramakrishnon, *J.Am.Chem.Soc.*, 2000, **122**, 2244-2251

18. A.F.Diaz, K.Kanazawa and G.P.Gardini, *J.Chem.Soc.Chem.Comm.*, 1979, 635

19. K.Kanazawa, A.F.Diaz, R.H.Geiss, W.D.Gill, J.F.Kwak, J.A.Logan, J.F.Rabolt and G.B.Street, *J.Chem.Soc.Chem.Comm.*, 1979, 854

20. J.Yue and A.J.Epstein, *J.Am.Chem.Soc.*, 1990, **112**, 2800-2801

21. P.M.McManus, R.J.Cushman and S.C.Yang, *J.Phys.Chem.*, 1987, **91**, 744-747

22. R.J.Waltman, J.Bargon and A.F.Diaz, *J.Phys.Chem.*, 1983, **87**, 1459-1463

23. S.Y.Abe, J.C.Bernede, M.A.Delvalle, Y.Tregouet, F.Ragot, F.R.Diaz and S.Lefrant, *Synth.Met.*, 2002, **126(1)**, 1-6

24. J.Gordon Mackintosh and Andrew R.Mount, *J.Chem.Soc.Faraday Trans.*, 1994, **90(8)**, 1121-1125

25. P.Jennings, A.C.Jones, A.R.Mount and A.D.Thomson, *J.Chem.Soc. Faraday Trans.*, 1997, **93(21)**, 3791-3797

26. A.D.Thomson, PhD Thesis, The University of Edinburgh, 1996

27. A.B.Holmes, D.D.C.Bradley, A.R.Brown, P.L.Burns, J.H.Burroughes, R.H.Friend, N.C.Greenham, R.W.Gymer, D.A.Halliday, R.W.Jackson, A.Kraft, J.H.F.Martens, K.Pichler and I.D.W.Samuel, *Synth.Met.*, 1993, **57(1)**, 4031

28. K.M.Vaeth and J.Dicillo, *J.Polymer Science Part B – Polymer Physics*, 2003, 41(21), 2715-2725

29. J.S.Kim, P.K.H.Ho, N.C.Greenham and R.H.Friend, *J.Applied Phys.*, 2000, **88(2)**, 1073-1081

30. J.A.E.Wasey, A.Safonov, I.D.W.Samuel and W.L.Barnes, *Phys.Rev.B.*, 2001, **64**, art.no.205201

31. M.Segal, M.A.Baldo, R.J.Holmes, S.R.Forrest and Z.G.Soos, *Physical Rev.B*, 2003, **68**, art.no. 075211

32. A.Kraft, A.C.Grimsdale and A.B.Holmes, *Angew.Chem.Int.Ed.*, 1998, **37**, 402-428

33. A.R.Brown, D.D.C.Bradley, J.H.Burroughes, R.H.Friend, N.C.Greenham, P.L.Burn, A.B.Holmes and A.Kraft, *Appl.Phys.Lett.*, 1992, **61(23)**, 2793-2795

34. M.Hay and F.L.Klavetter, *J.Am.Chem.Soc.*, 1995, **117**, 7112-7118

35. Y.Ohmori, K.Uchida, K.Muro, K.Yoshino, *Jpn.J.Appl.Phys.*, 1991, **30**, L1941-L1943

36. A.W.Grice, D.D.C.Bradley, M.T.Bernius, M.Inbasekaren, W.W.Wu and E.P.Woo, *Applied Phys.Lett.*, 1998, **73(5)**, 629-631

37. J.Jacob, J.Zhang, A.C.Grimsdale, K.Müllen, M.Gaal and E.J.W.List, *Macromolecules*, 2003, **36**, 8240-8245

38. E.J.W.List, M.Gaal, R.Guentner, P.Scandiucci de Freitas and U.Scherf, *Synth.Met.*, 2003, **139**, 759-763

39. J-H. Lee and D-H.Hwang, *Chem.Comm.*, 2003, 2836-2837

40. G.Tourillon and F.Garnier, *J.Electroanal.Chem.*, 1982, **135(1)**, 173-178

41. P.N.Bartlett and J.Farrington, *Bull. Electrochem.*, 1992, **8(5)**, 208-211

42. P.N.Bartlett, D.H.Dawson and J.Farrington, *J.Chem.Soc. Faraday Trans.*, 1992, **88(18)**, 2685-2695

43. R.J.Waltman, A.F.Diaz and J.Bargon, *J.Phys.Chem.*, 1984, **88**, 4343-4346

44. J.G.Mackintosh, C.R.Redpath, A.C.Jones, P.R.R.Langridge-Smith, D.Reed and A.R.Mount, *J.Electroanal.Chem.*, 1994, **375**, 163-168

45. J.G.Mackintosh, A.R.Mount and D.Reed, *Mag.Res.Chem.*, 1994, **32(9)**, 559-561

46. J.G.Mackintosh, C.R.Redpath, A.C.Jones, P.R.R.Langridge-Smith and A.R.Mount, *J.Electroanal.Chem.*, 1995, **388(1-2)**, 179-185

47. A.R.Mount and A.D.Thomson, *J.Chem.Soc. Faraday Trans.*, 1998, **94(4)**, 553-558

48. L.J.Kettle, S.P.Bates and A.R.Mount, *Phys.Chem.Chem.Phys.*, 2000, **2**, 195-201

49. N.Robertson, S.Parsons, E.J.Maclean, R.A.Coxall and A.R.Mount, *J.Mater.Chem.*, 2000, **10**, 2043-2047

50. L.Greci, G.Tommasi, R.Petrucci, G.Marrosu, A.Trazza, P.Sgarabotto, L.Righi and A.Alberti, *J.Chem.Soc. Perkin Trans.*, 2000, **2**, 2337-2342

51. J.G.Mackintosh, S.J.Wright, P.R.R.Langridge-Smith and A.R.Mount, *J.Chem.Soc. Faraday Trans.*, 1996, **92(20)**, 4109-4114

52. A.R.Mount and M.T.Robertson, *Phys.Chem.Chem.Phys*, 1999, **1**, 5169-5177

53. P.Jennings, A.C.Jones and A.R.Mount, *J.Chem.Soc. Faraday Trans.*, 1998, **94**, 3619-3624

54. *Handbook of Fluorescence Spectra of Aromatic Molecules* by I.B.Berlman, Academic Press, New York, 1971

55. P.Jennings, A.C.Jones and A.R.Mount, *Phys.Chem.Chem.Phys.*, 2000, **2**, 1241-1248

56. P.Jennings, PhD Thesis, University of Edinburgh, 1999

57. Private communications, Alice Williams, University of Edinburgh

Chapter Two

THEORY

2.1 Introduction

The research presented in this thesis utilised a wide range of experimental and computational techniques including techniques from electrochemistry, spectroscopy and computational modelling. This chapter presents a summary of the relevant theory behind each of these areas.

2.2 Electrochemistry

2.2.1 Introduction

Electrochemical techniques were used in this thesis to generate and study the polymeric films of IC and PC. All the electrochemical experiments were carried out using a three electrode system comprising a working, reference and counter electrode and voltammetric techniques, where the current is monitored as a function of the potential of the working electrode, were used. Potential step voltammetry was used to polymerise IC and PC and investigate the kinetics of the polymerisation process. Potential sweep voltammetry was used to measure the oxidation potentials of the monomers and study their polymer films. Although the method of electrooxidation to form polymer films is small-scale and not appropriate for an industrial synthesis, it has advantages in that it allows greater control and measurement of the conditions in which films are formed than chemical oxidation.

2.2.2 The electrochemical cell

The simplest electrochemical cell consists of two electrodes in contact with an electrolyte. Chemical reactants are dissolved in the electrolyte and the electrodes are connected by an external electrical circuit. Such a cell may be used to drive a non-spontaneous reaction by application of a potential difference between the electrodes (electrolytic cell) or to produce an electric current as a result of spontaneous reactions at each electrode (galvanic cell).

An electrochemical cell may be thought of as a collection of interfaces across which charges may pass. The cell voltage is the total potential difference between the two electrodes and it is typically non-zero, even when there is no current flowing through the cell. In an electrolytic cell, typically there is an electrode at which the reaction of interest occurs; this is

called the working electrode. In order to study the reaction of interest it is necessary to measure the changes in potential at this electrode. As it is impossible experimentally to look at one interface in isolation, in order to measure how the potential at the working electrode is changing a reference electrode such as the standard hydrogen electrode (SHE) is used. The potential difference across a reference electrode is a constant and by convention the potential of the SHE is defined as zero.

In the electrochemical experiments performed for this thesis a three-electrode system was used, comprising a working, reference and counter electrode. This third, counter, electrode is used in systems where there is a large iR drop. The term iR drop refers to the potential drop across the solution between the electrodes where i is the current passed during electrolysis and R is the electrical resistance of the solution. The iR drop will be large where the currents passed are high due to the use of electrodes of conventional size (greater than mm) or where the electrical resistance is high, for example in non-aqueous solutions. In such circumstances a three-electrode system may be used, with a potentiostat to control the three electrodes and ensure that current only flows between the working and counter electrode. This removes the iR drop term from the potential across the reference and working electrodes and stabilises the reference electrode.

For a reaction R→O+ne the equilibrium potential of the working electrode, E_{eq}, is given by the Nernst equation, which is:

$$E_{eq} = E^{\theta} + \frac{RT}{nF} \ln \frac{(c_R)_0}{(c_O)_0} \qquad \textbf{(2.1)}$$

assuming the activity coefficients of O and R are equal. In Equation 2.1 E^{θ} is the standard electrode potential, R is the gas constant, T is the temperature, F Faradays constant, $(c_R)_0$ the concentration of the reduced species at the electrode surface and $(c_O)_0$ the concentration of the oxidised species at the electrode surface. Application of a potential, E, to the working electrode that is different from E_{eq} results in electrolysis becoming thermodynamically viable. Application of a negative potential leads to an oxidation reaction and application of a positive potential to a reduction reaction.

The current passed by the working electrode during electrolysis is related directly to the rate of the electrochemical reaction. This rate may be controlled either by the kinetics of the electrode reaction, which are in turn controlled by the potential at the working electrode, or by the transport of reactants/products to/from the electrode surface. Therefore experiments

must be performed either under conditions where the mass transport of reactants/products is controlled, for example by using a rotating disc electrode (RDE), or, for reactions performed in a stagnant solution, the effects of mass transport by diffusion must be taken into account.

2.2.3 The rotating disc electrode

Control of the rate of mass transport of reactant to the electrode surface during an electrochemical experiment allows quantitative information on the kinetics of an electrode reaction to be obtained. There are three mass transfer processes that are important in electrochemistry; migration, diffusion and convection (natural and forced). The effects of migration can be removed by using a background electrolyte concentration of ≥0.05 M. In order to control diffusion and convection a hydrodynamic electrode, such as the rotating disc electrode (RDE), is used. A hydrodynamic electrode uses controlled forced convection to determine the mass transfer of reactant to the electrode surface. The need to consider the effects of natural convection is thereby removed but both diffusion and forced convection must still be considered.

A typical RDE, such as that shown in Figure 2.1, has the form of a Pt disc embedded in an insulating mantle made of an insulator, such as epoxy resin. The Pt disc should be polished smooth and lie flush with the plastic housing.

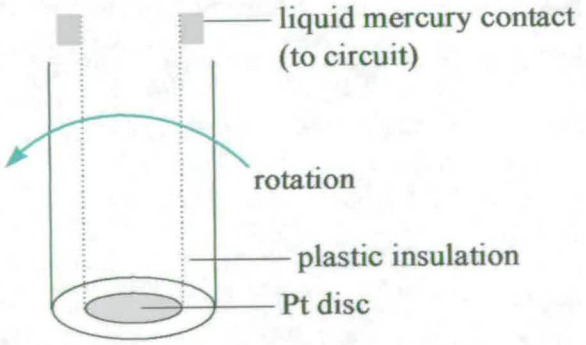

Figure 2.1: Schematic of a rotating disc electrode (RDE).

The RDE is placed in the electrolyte solution so that the Pt disc is horizontal, and is then rotated at a constant speed, W. Control of W allows control of the rate of mass transfer. The hydrodynamic behaviour of the solution under these conditions can be solved analytically and so the rate and pattern of mass transport is well understood. As the RDE rotates the solution at the surface is dragged along with it and then thrown out radially by the centrifugal force. Fresh solution is then drawn up vertically (in the z direction) from the bulk. The flow of the solution during rotation of the RDE is illustrated in Figure 2.2.

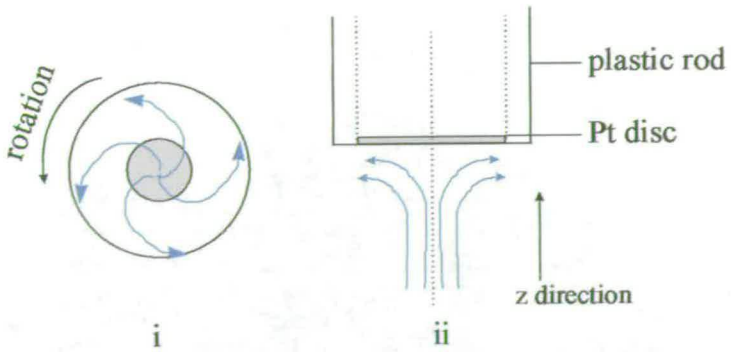

Figure 2.2: Flow of solution with RDE: i. from below and ii. side view

The concentration profile of a solution species in the z direction of the RDE is shown in Figure 2.3.

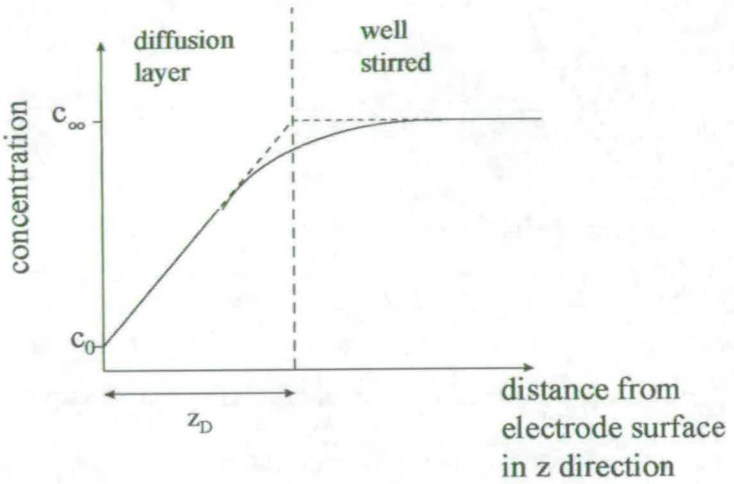

Figure 2.3: The concentration profile of a species in solution in the z direction at a RDE.

Rotation of the RDE causes a diffusion layer of thickness z_D to be formed, within which the velocity of a species in solution in the z direction is zero and mass transport is by diffusion only. Outside this diffusion layer the solution is well stirred and the concentration of the species is that of the bulk solution, c_∞. The variation in concentration across the diffusion layer from c_∞ to the surface concentration of the species, c_0, is approximately linear, which means that there is a uniform concentration gradient. Since the rate of diffusion to a planar surface is directly proportional to the concentration gradient (Ficks law), control of the concentration gradient allows control of mass transport to the electrode surface. The diffusion layer thickness, z_D, for a particular species at a RDE is given by Equation 2.2:

$$Z_D = 0.6435 v^{1/6} W^{-1/2} D^{1/3} \qquad \textbf{(2.2)}$$

where ν is the kinematic viscosity of the solution ($cm^2\ s^{-1}$), W is the rotation speed of the RDE (Hz) and D is the diffusion coefficient of the species ($cm^2\ s^{-1}$). Therefore the thickness of the diffusion layer can be controlled by the rotation speed of the RDE and this allows control of the concentration gradient within the diffusion layer.

Under conditions where the rate of the reaction occurring at the RDE is limited only by the rate of mass transfer and the concentration of reactant at the electrode surface is so small it may be assumed to be zero, the RDE mass transport limited current, i_L, for a reaction is predicted by the Levich equation:

$$i_L = nFA\frac{Dc_\infty}{z_D} = 1.554nFAD^{2/3}W^{1/2}\nu^{-1/6}c_\infty \qquad \textbf{(2.3)}$$

where n is the number of electrons needed to reduce or oxidise one molecule of reactant, F is Faradays constant, A is the area of the Pt disc, D is the diffusion coefficient of the reactant ($cm^2\ s^{-1}$), c_∞ is the bulk concentration of reactant, z_D is the thickness of the diffusion layer, W is the rotation speed of the RDE (Hz) and ν is the kinematic viscosity of the solution ($cm^2\ s^{-1}$). The Levich equation applies when the rate of reaction is limited solely by the rate of mass transfer of reactant to the RDE surface and under these conditions a plot of i vs $W^{1/2}$ will give a straight line passing through the origin. The slope of such a plot may be used to calculate the number of redox electrons, n.

A reaction which is first order in monomer and which has a mass transport independent step at the electrode surface with a rate constant, k', which is much greater than the rate constant for mass transport, k_{MT}, may be described by Scheme 2.1:

$$c_\infty \xrightarrow{k_{MT}} c_0 \xrightarrow[-ne^- / +ne^-]{k'_{ox}/k'_{red}} \text{product} \qquad \textbf{(Scheme 2.1)}$$

In such a case the Koutecky-Levich equation may be applied, where

$$\left|\frac{1}{i_{obs}}\right| = \left(\frac{0.6435\nu^{1/6}}{nFAc_\infty D^{2/3}W^{1/2}}\right) + \frac{1}{k'} \qquad \textbf{(2.4)}$$

where i_{obs} is the observed current. A plot of $|1/i_{obs}|$ vs $1/W^{1/2}$ will give a straight line, the gradient of which may be used to calculate n, if the diffusion coefficient is known. The intercept gives a measure of the rate of the electrode reaction when the concentration of reactant at the electrode surface is equal to the bulk concentration and therefore there are no mass transport effects.

2.2.4 Potential step voltammetry

At the start of a potential step voltammetry experiment the potential of the working electrode is held at an initial value E_1, where no reaction occurs. During the experiment the potential is instantaneously stepped (rather than scanned) to E_2 and held constant while the change in current with time is recorded. In this thesis the technique of potential step voltammetry was used to polymerise the monomers IC and PC and all such experiments were carried out on non-stagnant solutions. Mass transport to the working electrode was controlled by use of a RDE rotated at a constant speed so that the rate of mass transport of material to the electrode surface remained constant. A schematic of a typical current-time transient for such an experiment is shown in Figure 2.4.

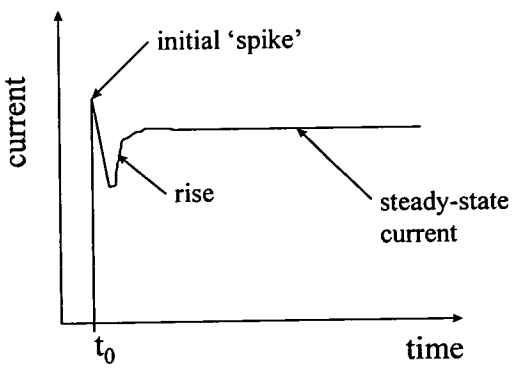

Figure 2.4: A typical potential step voltammogram.

There are three important regions shown in Figure 2.4. These are the initial 'spike', the decrease in current immediately following this and then the 'rise'. On stepping the potential from E_1 to E_2, provided that E_2 is in the mass transport region of the CV of the monomer (see section 2.2.5), all the monomer at the surface of the RDE will immediately undergo oxidation. At this point the current increases sharply to form the initial 'spike'. The oxidised monomer can then react to form the initial layer of polymeric film on the surface of the RDE. The 'spike' also includes the current passed during double layer charging, which is a nonfaradaic process occurring on a timescale of ~1 ms. As the diffusion layer is depleted of monomer the current drops with time according to the Cottrell equation:

$$i = \frac{nFAD_R^{1/2}c_\infty^R}{\pi^{1/2}t^{1/2}} \qquad (2.5)$$

In a stagnant solution this drop in current with time would continue, ultimately to zero. However in a non-stagnant solution, for example with a RDE, the diffusion layer is constantly replenished with monomer from the bulk solution. At a constant rotation speed the concentration of monomer at the surface of the working electrode becomes constant and the current reaches a steady-state value. However if polymer produced in such an

experiment is insoluble in the solvent and is adsorbed onto the surface of the Pt disc, the surface of the electrode will get coated in polymeric film. Therefore in order for the steady-state current to be maintained the polymeric film must be conducting. Where the film is non-conducting i will decrease with time. The 'rise' in Figure 2.4 is due to the fact that it is easier to polymerise onto a surface already coated with polymer than onto the bare Pt surface.

2.2.5 Potential sweep voltammetry

There are two types of potential sweep voltammetry, linear-sweep voltammetry (LSV) and cyclic voltammetry (CV). Both LSV and CV experiments are performed on a stagnant (or stationary) solution so that material is only transported to the working electrode surface by diffusion and natural convection. In LSV the potential is swept from a start value E_1 to an end value E_2 at a constant sweep rate, ν, and the current passed across the working electrode during the sweep is plotted as a function of E. In CV the LSV experiment described above is performed but upon reaching E_2 the potential sweep is reversed back to E_1. One CV cycle is where the potential changes from E_1 to E_2 and then back to E_1 and further cycles are recorded as required. Typical linear-sweep and cyclic voltammograms are shown in Figure 2.5.

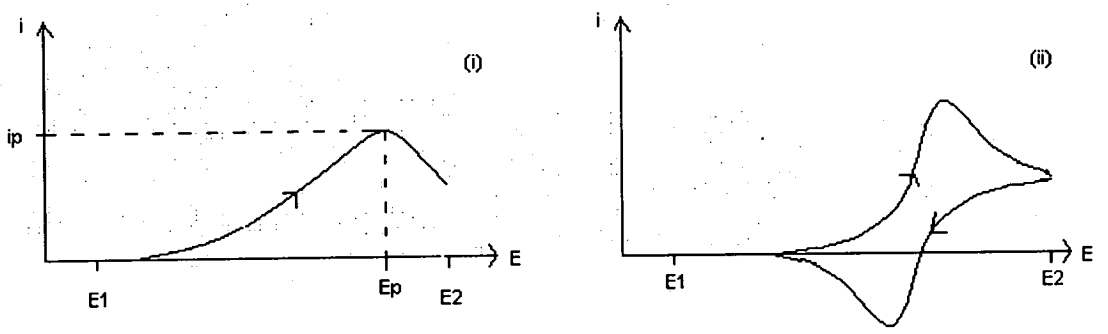

Figure 2.5: Typical current responses for an oxidation during (i) linear-sweep and (ii) cyclic voltammetry.

The shape of a typical linear-sweep or cyclic voltammogram can be explained by considering the oxidation reaction R→O+ne. The current, i, is zero at E_1 where no reaction takes place. As E becomes more positive i will increase approximately exponentially with E as the electrochemical rate constant, k_{ox}, increases. At this point the linear-sweep voltammogram is under electrochemical control. As E increases further the concentration of R at the electrode surface drops. Eventually i reaches a peak value, i_p, representing the balance between the increasing electrochemical rate constant and the decreasing surface

concentration of R. As E is increased beyond E_p, the current falls as the diffusion layer at the electrode surface becomes thicker and mass transport to the electrode becomes less efficient. The linear-sweep voltammogram is now under mass-transport control. In the case of CV the reverse portion of the voltammogram is subject to the same effects but for the reduction of the products formed during the initial sweep. This produces a reducing current superimposed on the oxidation reaction.

The shape of a linear-sweep or cyclic voltammogram can give information on whether a redox reaction is electrochemically reversible (Nernstian) or irreversible. A reversible reaction is characterised by fast electrode kinetics and therefore c_R and c_O at the electrode surface will be equal to the concentrations predicted from the Nernst equation (Equation 2.1) for a particular working electrode potential, even when the system is not at equilibrium. A diagnostic for a one electron reversible reaction is that $|E_p - E_{p/2}|$ is $\frac{56.5}{n}$ mV at 25 ^{0}C, and E_p is independent of sweep rate, ν. In the CV of a reversible reaction $E_p(red) = E_{p/2}(ox)$ and vice versa. $E_{1/2}$ is the potential halfway between E_p and $E_{p/2}$ and, assuming the diffusion coefficients for the reduced and oxidised species are the same, which is nearly always the case, $E_{1/2}$ is equal to the standard reduction potential for the electrode reaction. The standard potential of a reaction can be used to calculate the standard Gibbs free energy of the reaction and so thermodynamic information may be obtained for a reversible reaction from potential sweep voltammetry experiments.

An irreversible reaction has slow electrode kinetics. An appreciable overpotential is necessary for current to flow and so the increase in current with potential is slower than for a reversible reaction. E_p will be shifted to more positive potential for an oxidation than for a reversible reaction at the same ν and as ν is increased E_p will be pushed to increasingly positive potential. For both reversible and irreversible systems where the redox active species is in solution i_p is proportional to $\nu^{1/2}$, which demonstrates diffusion control. However where the redox active species forms a film which is adsorbed onto the electrode surface this relation will only hold true as long as the whole film is not reduced/oxidised on each sweep. Where the whole film is reduced/oxidised on each sweep i_p will be proportional to ν.

2.3 Spectroscopy

2.3.1 Introduction

Modern spectroscopy encompasses a wide range of techniques, with applications in many areas of the physical sciences ranging from organic chemistry to astrophysics. It is primarily an experimental discipline, but is closely related to the theory of quantum mechanics so that a basic understanding of quantum mechanics is necessary for an understanding of spectroscopy. This section provides a brief introduction to the aspects of both the theory of quantum mechanics and the practice of spectroscopy which are relevant to this thesis.

2.3.2 Theoretical background

2.3.2.1 Molecular spectroscopy

The total energy of a molecule can be separated into electronic, vibrational, rotational and translational components. The electronic, vibrational and rotational components of the energy are quantised, which means that they can only take discrete values. Since the energy differences between the vibrational and rotational levels of a molecule are over a magnitude smaller than those between electronic states, each electronic state can be thought of as having a series of vibrational and rotational energy levels associated with it. Molecular spectroscopy is based on the observation, known as the Bohr frequency condition, that a photon of frequency, ν, may be absorbed or emitted by a molecule when $\Delta E=h\nu$, where ΔE is the energy difference between the initial and final states of the molecule and h is Planck's constant. The energy differences between electronic states in molecules correspond to the frequencies of the UV and visible regions of the electromagnetic spectrum and the energy differences between vibrational levels correspond to the frequencies of the infrared region. Since the energy states of a molecule are characteristic of its structure, analysis of the frequencies of light absorbed and emitted by a molecule can give valuable information on many molecular properties such as dipole moments and bond strengths.

The lowest electronic state of a molecule is known as the ground state. In aromatic molecules this is usually a singlet state and is given the label S_0. There exist a series of electronic states higher in energy than the S_0 state, with a different arrangement of electrons but with the same spin multiplicity, which are labelled S_1, S_2 etc. There are also triplet states and the lowest energy triplet state is labelled T_1. Although the S_1 and T_1 states have the same electron configuration, T_1 is always lower in energy than S_1. This is because the two electrons with parallel spins in T_1 are always subject to Fermi correlation, which acts to lower the energy (see section 2.4.9), but the spin paired electrons in S_1 are not. Each of the

electronic states of a molecule, S_0, T_1, S_1 etc have a series of vibrational energy levels, for each normal mode of the molecule, associated with them. The vibrational levels within a vibrational mode are given quantum numbers, v = 0, 1, 2, 3, ..., n. For a particular electronic state, the lowest energy vibrational level, v = 0, has the lowest, or zero-point energy that the molecule may have in that state, even at 0 K.

2.3.2.2 Selection rules

Absorption of a photon by a molecule promotes an electron to a higher energy state and results in a separation of charge within the molecule. This gives rise to a radiation induced dipole moment in the molecule known as the transition dipole moment. The transition dipole moment, $\underline{\mu}_{fi}$, for a transition which occurs by interaction with the electric component of the radiation, between initial and final states with wavefunctions Ψ_i and Ψ_f respectively, is defined as:

$$\underline{\mu}_{fi} = \int \Psi_f^* \hat{\mu} \Psi_i d\tau \qquad \textbf{(2.6)}$$

where $\hat{\mu}$ is the dipole moment operator. The transition moment is a vector quantity and so has both a direction and a magnitude. The transition probability is the square of the magnitude of the transition moment, $|\mu_{fi}|^2$, and is related to selection rules, which govern whether or not a transition may occur. Selection rules do not give any information on the intensity of a transition, only whether it is allowed or forbidden. For a transition to be allowed, the transition probability must be non-zero. For an allowed transition, the transition probability is proportional to the intensity of the transition.

Equation 2.6 may be broken down into electronic, spin and nuclear components to give Equation 2.7, where the subscript e denotes the electronic, s the spin and v the nuclear wavefunctions.

$$\underline{\mu}_{fi} = \int \Psi_{e,f}^* \hat{\mu} \Psi_{e,i} d\tau \int \Psi_{s,f}^* \Psi_{s,i} d\tau \int \Psi_{v,f}^* \Psi_{v,i} d\tau \qquad \textbf{(2.7)}$$

If any of the integrals in Equation 2.7 are zero, then the overall transition moment will be zero and the transition will be forbidden. For example, the spin integral is zero if the change in spin multiplicity accompanying the transition is non-zero. This means that a $S_1 \leftarrow S_0$ transition is allowed, but a $T_1 \leftarrow S_0$ transition is forbidden.

The third term in Equation 2.7 is called the vibrational overlap integral and this term determines which, if any, vibrational bands are observed in the electronic spectrum. The intensity of a vibrational band in the electronic transition is given by the square of the

vibrational overlap integral, which is also known as the Franck-Condon factor. The most intense transition will occur where the vibrational wavefunctions of the initial and final states are most similar. This is the mathematical formulation of the Franck-Condon principle, which states that the most probable electronic transitions within a molecule occur with no change in nuclear geometry or velocity.

The operation of the Franck-Condon principle can be illustrated in a diagram such as the one in Figure 2.6, which shows the potential energy curves for two electronic states of a diatomic molecule. The electronic transitions are said to be vertical because the nuclear configurations before and after the electronic transition has taken place must be the same. The higher electronic state in Figure 2.6 has been shown with a larger equilibrium interatomic distance than the lower electronic state. This is because an electronic transition usually involves movement of an electron from a bonding to an anti-bonding orbital, which results in a decrease in bond strength and an increase in bond length.

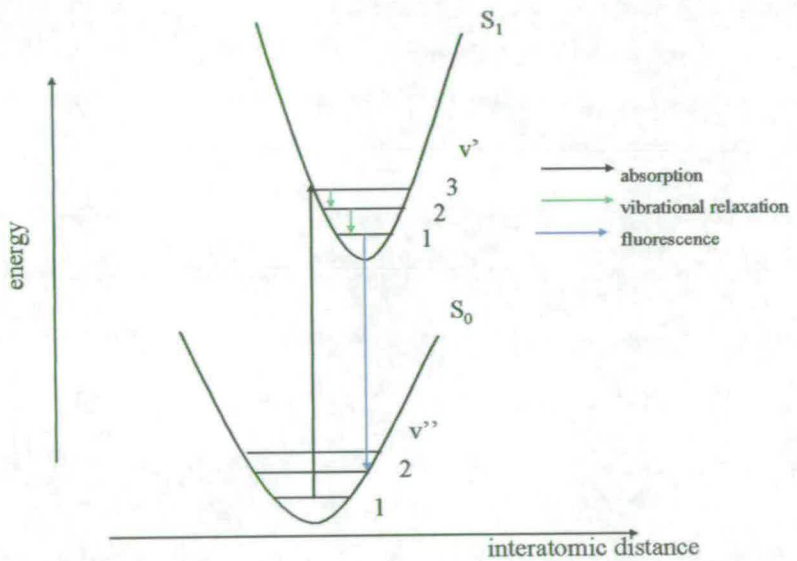

Fig.2.6: Diagram showing two electronic states for a diatomic molecule and the vertical transitions between them.

2.3.2.3 Oscillator strengths

The oscillator strength, f, is measure of the intensity of an electronic transition.

$$f = \left(\frac{4m_e c\varepsilon_0}{N_A e^2} \ln 10 \right) \times A \qquad (2.8)$$

where c is the speed of light, ε_0 is the vacuum permittivity, N_A is Avogadros constant and A is the integrated absorption coefficient. The integrated absorption coefficient is the sum of the absorption coefficients over the entire band and is obtained from the spectrum of the molecule. It is related to the transition probability of a transition by:

$$f = \frac{8\pi^2 m_e \nu}{3he^2} \times \left|\underline{\mu}_{fi}\right|^2 \qquad \textbf{(2.9)}$$

where m_e is the mass of the electron. The constants in Equation 2.9 ensure that the oscillator strength is a dimensionless quantity and the maximum value of f is usually 1. It can be seen from Equation 2.9 that the square of the transition probability is proportional to the intensity of the transition. The oscillator strength is a useful measure as it relates the transition moment to the experimentally available spectrum of a molecule.

2.3.3 Decay of electronically excited states

A Jablonski diagram is commonly used to show the different states of a molecule and the possible transitions between them. An example of a Jablonski diagram is shown in Figure 2.7

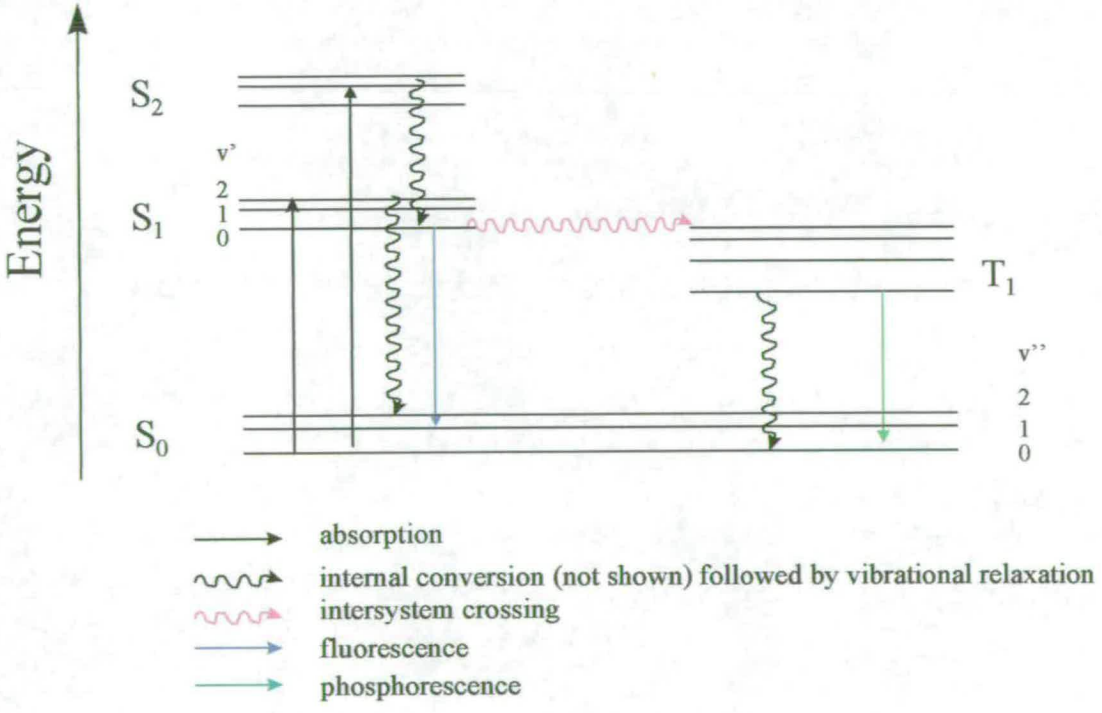

Figure 2.7: Jablonski diagram

A molecule may be excited from the ground state to an electronic state higher in energy by absorption of a photon of the appropriate frequency. An example of such an excitation is the $S_1 \leftarrow S_0$ transition shown in Figure 2.7. The molecule is now in an excited state, which is

inherently unstable and will therefore decay to the ground state. The processes involved in the de-excitation or inter-conversion of electronic states may be described as either non-radiative (wavy arrows) or radiative (straight arrows).

2.3.3.1 Non-radiative transitions

Internal conversion and intersystem crossing are both non-radiative intramolecular processes whereby a molecule crosses from one electronic state to another. In internal conversion both states have the same spin multiplicity, for example the molecule may cross from the S_2 state to the S_1 state. Internal conversion from the higher singlet excited states to S_1 is very efficient and it is therefore rare to measure emission spectra from these higher excited states. However internal conversion from the S_1 to the S_0 state is hindered by the large energy difference between the two states. In intersystem crossing, which is illustrated in Figure 2.7, the two states have different spin multiplicities, for example the molecule may cross from the S_1 to the T_1 state. Intersystem crossing is spin forbidden, but spin-orbit coupling relaxes this selection rule and therefore intersystem crossing is particularly important for molecules containing the heavier atoms, such as sulphur, in which spin-orbit coupling is large. An excited state molecule which is subject to collisions with surrounding molecules will undergo vibrational relaxation, where its vibrational energy is given up to the surrounding molecules until v'=0 is reached. Vibrational relaxation is also illustrated in Figure 2.7.

2.3.3.2 Radiative transitions

Emission of light is called luminescence and can be divided into two types, fluorescence and phosphorescence, both of which are illustrated in Figure 2.7. Fluorescence is a spin-allowed radiative transition in which both the initial and final electronic states have the same spin multiplicity. Typically both states are singlets. In solution vibrational relaxation occurs on a timescale of about 10^{-3} ns and it is usually complete before fluorescence occurs. Therefore fluorescence almost always occurs from the lowest vibrational level of the excited state, v'=0. Phosphorescence is light emission where the initial and final electronic states have different spin multiplicities. Although phosphorescence is spin-forbidden it can occur where spin-orbit coupling is present, but it is slow. Phosphorescence lifetimes are typically $1\text{-}10^{-3}$ s. It is not usually observed in solution at room temperature because other processes such as collisional quenching compete with it. However if a fluorophore is dissolved in a solvent such as ethanol which may be frozen to form a clear glass, phosphorescence may be observed. This is because the fluorophore molecule trapped in the glass cannot undergo

collisions with other molecules and so the lifetime of the triplet state is extended long enough for phosphorescence to occur.

2.3.3.3 Decay kinetics

As described above, molecules in their excited states decay to the ground state by either radiative or nonradiative transitions. The decay of an excited state, M*, is a first order process, with a first order rate constant, k_F. k_F is the sum of the rate constants of the radiative, k_r, and nonradiative, k_{nr}, decay processes:

$$k_F = k_r + \sum k_{nr} \tag{2.10}$$

The rate of change of the concentration of M*, [M*], with time is given by:

$$-\frac{d[M^*]}{dt} = k_F[M^*] \tag{2.11}$$

which can be rearranged and integrated to give:

$$[M^*]_t = [M^*]_0 \exp(-k_F t) \tag{2.12}$$

where $[M^*]_0$ is the initial concentration of excited state molecules. The intensity of emission at time t, I(t), is directly proportional to $[M^*]_t$. Therefore

$$I(t) = I_0 \exp(-k_F t) \tag{2.13}$$

where I_0 is the intensity at t = 0.

The lifetime of an excited state, τ_F, is the time taken for the concentration of molecules in the excited state to reach 1/e of the initially excited concentration and is given by:

$$\tau_F = \frac{1}{k_F} \tag{2.14}$$

τ_F is usually referred to as the fluorescence lifetime. For aromatic molecules τ_F is typically of the order of 10 - 100 ns.

The quantum yield, ϕ, is defined as the ratio of the number of photons emitted to the number of photons absorbed and is given by:

$$\Phi = \frac{k_r}{k_r + \sum k_{nr}} \tag{2.15}$$

2.3.4 Experimental electronic spectroscopy

2.3.4.1 UV-vis spectroscopy

In UV-vis spectroscopy a sample is exposed to UV or visible radiation of a particular wavelength and the ratio of the intensity of the transmitted light, I, to the intensity of the incident light, I_0, is measured. The relationship between I and I_0 is given by the Beer-Lambert law:

$$I = I_0 \times 10^{-\varepsilon.c.l} \tag{2.16}$$

where ε is the molar absorption coefficient, c is the concentration of the absorbing species in solution and l is the pathlength of the sample. ε is dependent on the wavelength of the incident light. By defining the absorbance, A, as

$$A = \log \frac{I_0}{I} \tag{2.17}$$

the Beer-Lambert law may be simplified to

$$A = \varepsilon.c.l \tag{2.18}$$

The absorbance is plotted against the wavelength of the incident light to give a UV-vis spectrum and according to Equation 2.18 a plot of A vs (c.l) for a variety of concentrations will give a straight line with gradient ε.

Deviation from the Beer-Lambert law takes place where (ground state) aggregation occurs and the aggregate and monomer both contribute to the UV-vis spectrum. Examples of aggregation are the formation of dimers, trimers etc by, for example, π-stacking. At a wavelength where both monomer and aggregate absorb, the total molar absorption coefficient, ε_{total}, will be a function of both the individual ε's. Since the proportion of aggregate to monomer increases as the concentration of monomer in solution increases, and provided the monomer and aggregate have different values of ε, ε_{total} will change with concentration. Therefore a plot of A vs (c.l) will no longer give a straight line and the Beer-Lambert law will no longer hold true.

2.3.4.2 Steady-state fluorescence spectroscopy

There are two types of steady-state fluorescence spectroscopy, fluorescence emission and fluorescence excitation. In emission spectroscopy, a sample is excited with a particular wavelength of UV-vis radiation, λ_{ex}, and the intensity of emission as a function of emission wavelength is measured. In excitation spectroscopy, the sample is excited at a range of wavelengths and the emission intensity at a chosen wavelength, λ_{em}, is measured as a

function of excitation wavelength. Typical shapes of emission and excitation spectra and the transitions involved are shown in Figure 2.8.

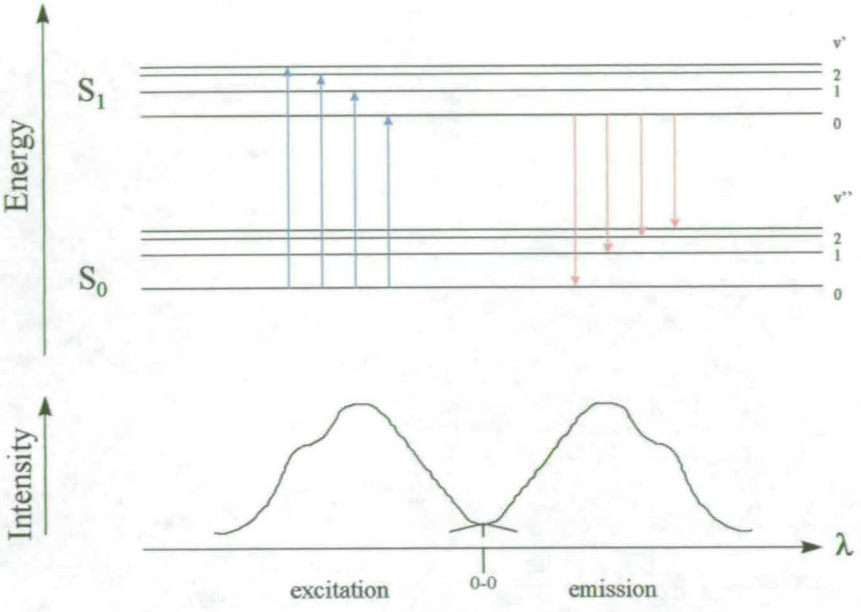

Figure 2.8: Typical emission and excitation spectra and the transitions whose intensities are measured.

The shape of an excitation spectrum is characteristic of the vibrational structure of the excited state because at room temperature most molecules in a sample are in v''=0 and so excitation occurs from this level. Conversely, the shape of an emission spectrum is characteristic of the vibrational structure of the ground state, since vibrational relaxation ensures that most molecules in a sample are in the v'=0 level of the S_1 state before fluorescence occurs. Since all emission usually occurs from the v'=0 level, emission spectra are generally independent of λ_{ex}. This is known as Kasha's rule. In general, a dependence of the emission spectrum on the excitation wavelength implies the presence of more than one fluorescent species. For example, an exception to Kashas rule may occur where there is some (ground state) aggregation present. If ground state dimers are formed and the energy difference between the excited and ground state monomers is larger than the energy difference between the excited and ground state dimers, exciting on the long wavelength edge of the excitation spectrum will increase the intensity of long wavelength emission. In the case of aggregation the shape of the emission will also be concentration dependent as the proportion of aggregate to monomer in the solution will increase with concentration.

Another general characteristic of excitation and emission spectra is that, where there is little difference between the equilibrium geometries of the S_0 and S_1 states and their potential

energy surfaces are similar, the $S_1 \leftarrow S_0$ portion of the excitation spectrum and the emission spectrum should appear as mirror images. This is because the Franck-Condon factors and hence intensities and relative positions of the vibronic transitions will be the same. Exceptions to this mirror-image rule may be caused by large differences between equilibrium excited and ground state geometries but could also be due to excited state reactions such as excimer (excited state dimer) formation. The formation of excimers will result in increased emission to long wavelengths, which may distort the symmetry of the spectra. In such a case, the shape of the emission spectrum will be concentration dependent but Kasha's rule will still be obeyed.

In solution, fluorescence occurs at lower energies than excitation. In other words, the light emitted by a fluorophore is of a longer wavelength than the light absorbed. This is known as the Stokes shift. The most common reasons for this are the loss of vibrational energy in the excited state due to vibrational relaxation before emission and the emission from v'=0 to higher ground state vibrational levels. This suggests that the origin, or (0-0), transition will have the same energy in both the emission and excitation spectra. However, other factors may contribute to the Stokes shift such as solvent effects and complex formation and these may cause the emission origin to be shifted to longer wavelengths than the excitation origin. For example, the solvent molecules surrounding the excited state are initially in the most stable arrangement for the equilibrium geometry of the ground state. As the solvent molecules rearrange around the excited state during its lifetime, the excited state is lowered in energy, increasing the Stokes shift. Also, where there is an increase in dipole moment between the ground state and the excited state of the fluorophore, the Stokes shift will increase with the polarity of the solvent as the interaction between the polar solvent molecules and the excited state molecule increases. Measuring the fluorescence emission spectrum in a frozen glass removes the effects of solvent reorganisation.

2.3.4.3 Re-absorption and the inner filter effect

When measuring steady-state fluorescence emission and excitation spectra, it is important to avoid the re-absorption and inner filter effects.

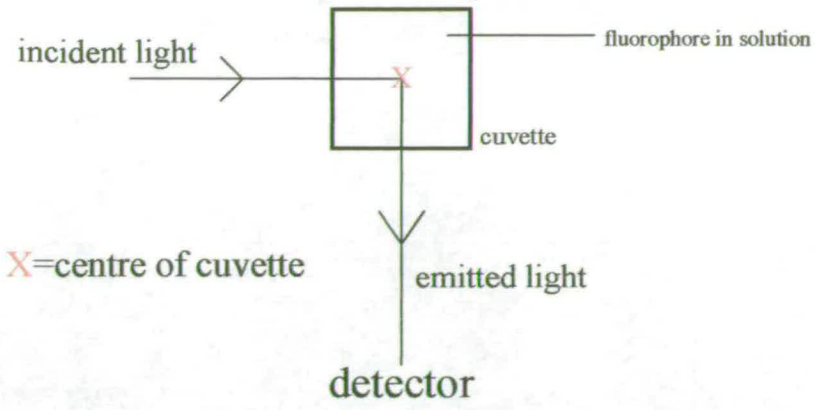

Figure 2.9: View from above of paths of incident and detected light through a cuvette during a steady-state fluorescence excitation or emission experiment.

The inner filter effect is concerned with how much incident light reaches the detection volume at the centre of the cuvette, shown as point X in Figure 2.9. When the concentration of fluorophore in solution is high, all the incident light is absorbed by fluorophores in solution before reaching X and, due to the detection geometry, no excitation or emission spectra can be measured. At low concentrations, little or no incident light is absorbed before X and the excitation and emission spectra are unaffected. At intermediate concentrations the shape of the excitation spectrum will be altered by absorption of the incident light before it reaches X. This distortion occurs because the amount of incident light absorbed before X will vary for the different wavelengths across the absorption spectrum. As the absorbance increases in the absorption spectrum, the intensity of incident light reaching X for those wavelengths will be reduced. Therefore there will be a false decrease in intensity of the excitation spectrum in regions corresponding to peaks in the absorption spectrum. The shape of the emission spectrum is unaffected by the inner filter effect.

The re-absorption effect is concerned with what happens to the emitted light between point X and the detector. At wavelengths where the excitation and emission spectra overlap, light emitted at point X may be re-absorbed before reaching the detector. This results in a decrease in the intensity of the emission over this wavelength region, changing the shape of the emission spectrum. The excitation spectrum will only be affected if λ_{em} is within the overlap region, and if affected its shape will be unaltered but there will be a loss of intensity over the whole spectrum.

The inner filter and re-absorption effects may be avoided by reducing the concentration of fluorophore in solution until both the emission and excitation spectra are independent of concentration.

2.3.4.4 Solvation effects on steady-state spectra

The shapes and positions of solution phase steady-state fluorescence spectra may be affected by both the dielectric properties of the solvent and specific interactions between the fluorophore and surrounding solvent molecules. Usually, excitation spectra are only slightly affected by the nature of the solvent, whereas emission spectra are more sensitive. Initially, the solvent molecules closest to the fluorophore are arranged around the ground state molecule in a configuration which minimises the energy of the complex. Immediately upon excitation of the fluorophore to the excited state, the solvent molecules remain in the ground state configuration. However, before fluorescence occurs the solvent molecules may rearrange (or relax) around the excited state molecule in response to the change in electron distribution on excitation. If there is an increase in the permanent dipole moment of the fluorophore from the ground to the excited state, solvent relaxation will result in increased stabilisation of the excited state in a polar solvent compared to a non-polar solvent. Therefore the Stokes shift observed will increase as the solvent polarity increases, and the emission spectrum is shifted to longer wavelengths as the polarity of the solvent is increased.

2.3.4.5 Introduction to lifetime measurements

Although the measurement of fluorescence lifetimes is far more complex than the measurement of steady-state fluorescence spectra, it is often worthwhile because of the extra information it can provide. For example, fluorescence lifetime measurements can show the presence of more than one molecular conformer in a sample where different conformers have different lifetimes. In this project such lifetime measurements were used to analyse how the type and weighting of different components in polymer films changes with polymerisation conditions.

In this project fluorescence lifetimes were measured using the technique of time-correlated single photon counting (TCSPC). In a TCSPC experiment a laser pulse is directed at the sample. This pulse excites the sample and simultaneously starts a 'clock'. When the first photon to be emitted from the sample is detected, the 'clock' is stopped. Typically this process is repeated 10,000 to 20,000 times and a histogram of the number of counts vs time is built up. This histogram is known as the decay curve. A schematic of a single exponential decay curve from a TCSPC experiment is shown in Figure 2.10(a).

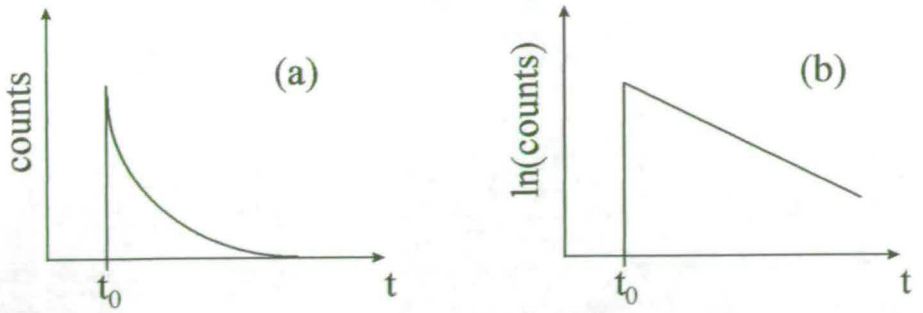

Figure 2.10: Schematic of (a) single exponential decay curve (b) decay curve in (a) plotted with ln(counts).

When a single exponential decay curve is plotted as ln(counts) vs t, the lifetime of the fluorophore, τ, is the inverse of the gradient of the line. Such a plot is shown in Figure 2.10(b). Where there is more than one fluorescence lifetime contributing to the data, ie the decay curve is multiexponential, the extraction of lifetimes is more complicated (see section 2.3.4.6).

A schematic diagram of the apparatus used for the TCSPC experiments is shown in Figure 2.11.

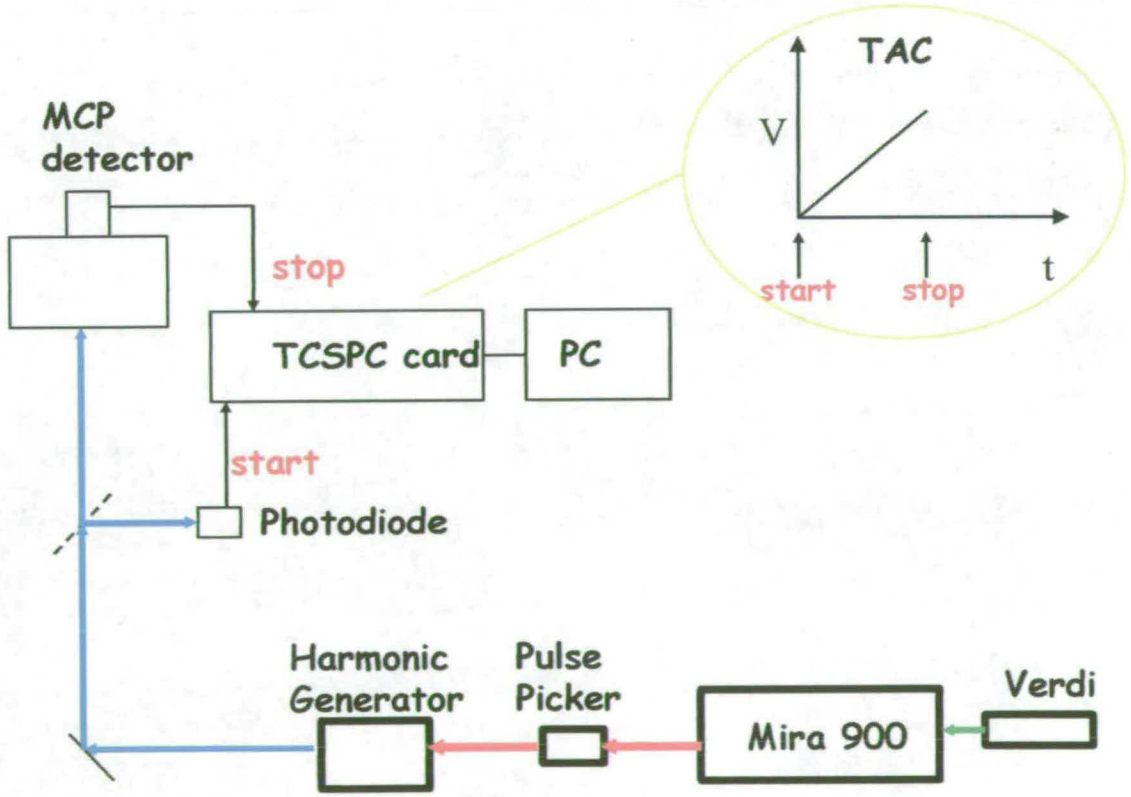

Figure 2.11: Schematic diagram of the TCSPC set-up used for this project.

A TCSPC experiment is complex but can be broken down into stages as follows:

1. Generation of laser pulse

In the experimental set-up used for this project, which is illustrated in Figure 2.11, a non-tunable diode laser is used to pump the tunable, pulsed titanium:sapphire (Ti:sapphire) laser. The Ti:sapphire laser has a repetition rate of 76 MHz and each pulse generated has a width of 100-200 fs. This repetition rate is too high as it does not allow a full decay curve to be measured for one exciting laser pulse before the next laser pulse arrives. Therefore a pulse picker is used. The pulse picker selects one out of sixteen pulses and so reduces the repetition rate to ~4 MHz. The use of a pulse picker has the disadvantage of resulting in the loss of some of the laser power generated by the Ti:sapphire laser. The Ti:sapphire laser is tunable and can produce light of any wavelength within the wavelength range 720 to 1,000 nm. However to excite most fluorophores photons with wavelengths lower than 720 nm are required. In such cases a harmonic generator may be used to increase the range of wavelengths available for sample excitation by frequency doubling or frequency tripling the light from the Ti:sapphire laser.

2. Start signal

The excitation pulse generated in 1. is passed through a beam splitter that reflects part of the laser pulse onto a photodiode, triggering the start of the 'clock'. The rest of the pulse passes through the beam splitter and goes on to excite the sample. The 'clock' is a time-to-amplitude converter (TAC), which is capable of measuring the subnanosecond time differences required in a TCSPC experiment.

3. Excitation of sample

The laser pulse used to excite the sample is vertically polarised and the emission from the sample is passed through an emission polariser oriented at 54.7^0 from the vertical. This is called the 'magic angle' and is the angle at which anisotropy effects resulting from excitation by vertically polarised light are cancelled out. The emission then passes through a monochromator, which allows control of the emission wavelength that is detected.

4. Detection of emitted photons

The first photon emitted by the sample for each light pulse is detected by a microchannel plate photomultiplier tube (MCP PMT). The MCP PMT has a higher time resolution than an ordinary PMT and so gives a more accurate stop signal. Plotting the time between excitation and emission for only the first photon emitted from the sample for each laser pulse skews the data towards shorter times. However plotting the results from at most only one in 100 laser pulses, or 1% of the repetition rate, removes this bias towards short lifetimes. In fact, for this project a count rate of ~20,000 counts/s, or 0.5 % of the repetition rate, was used. Therefore

the results from no more than 1 in 200 excitation laser pulses were used to plot the decay curves.

5. Stop signal

Once the emitted photon is detected, it is passed to a constant fraction discriminator (CFD) and then onto the TAC where it forms the stop signal for the voltage ramp. The final voltage produced by the TAC is proportional to the time between excitation and emission events.

6. Instrument response

In TCSPC experiments it is important to measure the instrument response function (IRF). The IRF is the response of the whole detection system to an infinately short pulse and gives the time resolution of the system. It is measured using a scattering solution, such as colloidal silica (Ludox), which scatters the exciting pulse rather than absorbing and re-emitting it. Under the experimental conditions used for this thesis the full width half maximum of the IRF was 50 ps.

2.3.4.6 TCSPC data analysis

In a sample of polymer film, such as those analysed by TCSPC for this thesis, there are frequently more than one fluorescent species (and hence more than one lifetime) contributing to the decay curve. Such a decay curve can be fitted to a multiexponential function where the intensity at time t, I(t), is given by:

$$I(t) = \sum_i \alpha_i \exp(-t / \tau_i) \qquad \textbf{(2.19)}$$

In Equation 2.19 α_i is the pre-exponential factor of excited state i, $\sum_i \alpha_i$ is normalised to 1 and τ_i is the fluorescence lifetime of species i. The value of α_i corresponds to the fraction of the total number of fluorescing species in the sample which have a lifetime of τ_i. The aim of the data-fitting procedure is to arrive at the most probable values of α_i and τ_i for a particular data set. Since there is no method for measuring the exact number of exponents contributing to a particular decay curve, this is assumed. It is usual practice to start the fitting procedure with one exponent and progressively add in exponents to improve the fit. However, since adding more exponents will always result in a better fit, once a 'good fit' (based on the goodness of fit criteria outlined below) is obtained it is assumed that it is based on the correct number of exponents, unless there is a good justification for adding more. However, if the data will not fit, within the stated criteria, to three exponentials or less then the results must be interpreted with some caution.

The method used to analyse the decay curves measured for this thesis is called iterative non-linear least-squares analysis. For a particular assumption of the number of exponents, the parameters α_i and τ_i in Equation 2.19 are varied until the best match between the experimental and calculated data is found. This is achieved when the weighted sum of the squares of the deviation of the experimental points I(i) from the theoretical function Y(i) is at a minimum. This is expressed as:

$$\sum_{i=1}^{n} R(i)^2 = \sum_{i=1}^{n} w_i^2 [I(i) - Y(i)]^2 \qquad \textbf{(2.20)}$$

R(i) is the weighted residual for point i and w_i is the weighting factor for point i. Since the decay curve is a histogram, each channel represents an estimate of the mean of a Poisson distribution of counts in that channel. In a Poisson distribution the mean is equal to the variance and therefore the weighting factor, w_i, can be shown to be

$$w_i = [I(i)]^{-1/2} \qquad \textbf{(2.21)}$$

Therefore Equation 2.20 becomes:

$$\sum_{i=1}^{n} R(i)^2 = \sum_{i=1}^{n} \frac{[I(i) - Y(i)]^2}{I(i)} \qquad \textbf{(2.22)}$$

The quality of the fit of the calculated function to the experimental data may be assessed using the reduced chi-squared value, χ^2, where

$$\chi^2 = \chi_v^2 = \frac{1}{v} \sum_{i=1}^{n} \frac{[I(i) - Y(i)]^2}{I(i)} \qquad \textbf{(2.23)}$$

where v is the number of degrees of freedom left after fitting n data points with r parameters (v = n-r-1). For a large data set such as the ones used for this thesis v can be approximated as n. For a perfect fit of the calculated decay to the experimental decay $\chi^2 = 1$ because the deviation between the fitted function and the experimental point is equal to the standard deviation in the experimental point. For the experimental set-up used in this thesis values of χ^2 less than or equal to 1.2 were deemed acceptable. A plot of the weighted residuals against time may also be used to assess the quality of the fit. This is a visual test and for a good fit they should be randomly distributed around zero with no correlation between residuals.

2.4 Computational modelling

2.4.1 Introduction

Over the last few decades the range and availability of computer modelling techniques available to the chemist has increased dramatically through both improvements in theory and computer power. There are now commercially available packages which are relatively simple to use, can be run on a desk-top PC and which may be used to model a wide range of systems. However, it is important to understand the theory upon which these calculations are based in order to use them correctly and effectively. If this is done, computer modelling can be a powerful technique with applications in many areas of chemistry. It can be used, for example, to assist in the interpretation of experimental results or to predict the behaviour of molecules or systems under extreme conditions where conventional experimental techniques cannot be applied. The advantages of computer modelling "experiments" over more conventional experiments include the greater control over experimental conditions that they allow and their cost-effectiveness - only one piece of apparatus is required for *ab initio* calculations from which a wide range of physical and chemical properties can be obtained, whereas a number of different pieces of apparatus may be required to obtain the same information experimentally. However, computer modelling should not be seen as a replacement for conventional experimentation but as an additional tool for the experimenter. New techniques in computer modelling must be validated and this can be done by comparing the results generated with data from tried and tested experimental methods.

In this section, the theory behind the computational modelling techniques used in this thesis are explained. All the calculations done were quantum chemical calculations. The gas phase is ideally suited to computational modelling as the atoms or molecules in this phase at low to moderate pressures do not interact with each other and may be considered individually. Both ground state and excited state gas phase calculations were performed for this thesis. Calculations using the implicit solvation model COSMO were also performed.

2.4.2 Quantum chemical calculations

A complete mathematical description of a system of nuclei and electrons, including quantum mechanical and relativistic effects, would be extremely complex even for a small system. However, using quantum mechanics it is possible to predict the total energy of a system of nuclei and electrons by solving the Schrödinger equation and from the total energy of such a system, or the differences in total energies between such systems it is then possible to calculate many physical and chemical properties. The predictions of quantum mechanics are

very accurate, in fact the equations of quantum mechanics have yet to be shown to fail. However even the most theoretically rigorous approaches to solving the Schrödinger equation involve approximations.

The first of these approximations takes into account the huge difference between the masses of the nuclei and the masses of the electrons and the fact that the forces acting on them are the same. The electrons respond almost instantaneously to the motion of the nuclei, remaining in the ground state and this means that the motion of the nuclei and the electrons can be decoupled, i.e. treated separately. This is known as the Born-Oppenheimer (or adiabatic) approximation and it is very reliable for systems where the electrons are in the ground state but less reliable for excited states. It results in two equations, one for the motion of the electrons in a fixed field of nuclei, the electronic Schrödinger equation and one for the nuclei, the nuclear Schrödinger equation. Quantum chemical calculations aim to solve the electronic Schrödinger equation whereas molecular mechanics calculations aim to solve the nuclear Schrödinger equation. However, even with the Born-Oppenheimer approximation the only molecular species for which the electronic Schrödinger equation can be solved exactly is H_2^+ which contains only one electron.

The electronic, nonrelativistic, time-independent Schrödinger equation for a fixed set of nuclear positions, which computational quantum chemical calculations aim to solve, is given by Equation 2.24.

$$\hat{H}\,\Psi(\mathbf{r};\mathbf{R}) = E(\mathbf{R})\Psi(\mathbf{r};\mathbf{R}) \qquad \textbf{(2.24)}$$

where E is the electronic energy and $\Psi(\mathbf{r};\mathbf{R})$ is the electronic wavefunction with electronic positions $\mathbf{r}$ and nuclear positions $\mathbf{R}$. The Hamiltonian operator $\hat{H}$ is:

$$\hat{H} = \frac{-\eta^2}{2m_e}\sum_{i}^{n}\nabla_i^2 - \sum_{i}^{n}\sum_{I}^{N}\frac{Z_I e^2}{4\pi\varepsilon_0 r_{Ii}} + \frac{1}{2}\sum_{i,j}^{n}\frac{e^2}{4\pi\varepsilon_0 r_{ij}} \qquad \textbf{(2.25)}$$

for a system of n electrons with coordinates i and N nuclei with coordinates I. Z_I is the charge of nucleus I. The first term in Equation 2.25 describes the kinetic energy of a system of non-interacting electrons and the second term the attractive nuclei-electron Coulomb potential energy. The third term is the electron-electron repulsive Coulomb potential energy and it is this term that causes problems in computing the energies of systems containing more than one electron. Conventionally the nucleus-nucleus repulsion energy is added in as a classical term at the end of calculations.

The aim of quantum mechanical calculations is to obtain the total electronic wavefunction for the system (in reality an approximation to it) using the Hamiltonian operator, and from this solve the Schrödinger equation for the energy of the system. Since it is impossible to solve the Schrödinger equation exactly, within the Born-Oppenheimer approximation, for any system with more than one electron using the Hamiltonian operator given in Equation 2.25, an approximation to the Hamiltonian is used. For a particular quantum chemical calculation the method of approximating the Hamiltonian is described as the level of theory. The electronic wavefunction of the system to be modelled needs a mathematical form and this is known as the basis set. The accuracy of a calculation is completely specified by the basis set and level of theory used. The options available can be presented on a two-dimensional diagram such as that shown in Figure 2.12.

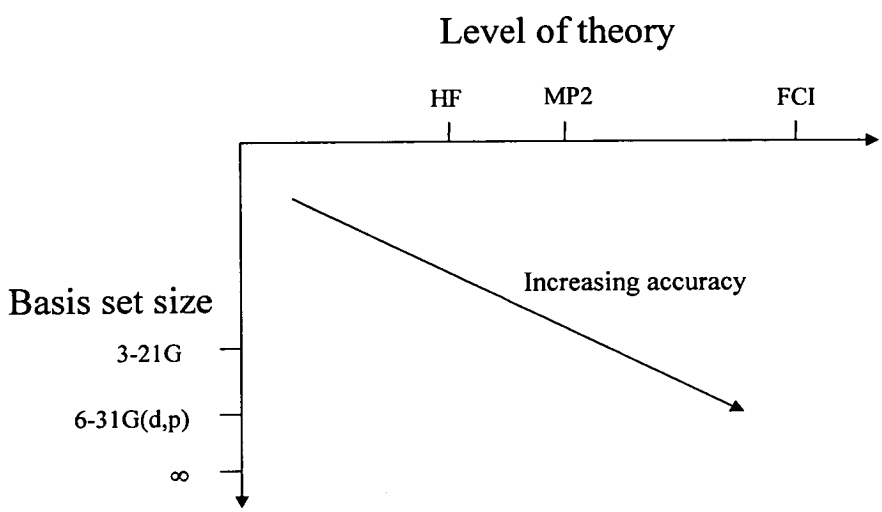

Figure 2.12: A two-dimensional diagram illustrating the relation of the level of theory and the basis set size to the accuracy of a calculation.

At the bottom right hand corner is the true energy of the system which, in practice, it is not possible to calculate. However, as the basis set size is increased and the level of theory improved the energies obtained will converge on the true energy. The methods and basis sets can be tested to find out the minimum computational expense required to obtain good agreement between experiment and theory.

2.4.3 Level of theory

There are two major approaches to the problem of approximating the Hamiltonian operator given in Equation 2.25. In *ab initio* (from first principles) methods a model is chosen for the electronic wavefunction and the electronic Schrödinger equation is solved using only the fundamental constants and the positions and atomic numbers of the nuclei as input. In

semiempirical methods a simplified form of the Hamiltonian operator is used as well as adjustable parameters with values obtained from experimental data. *Ab initio* methods are more computationally demanding than semiempirical methods and the time taken for an *ab initio* calculation often scales up very quickly with the size of the system being studied. However *ab initio* methods are not dependent on the particular system that has been used for parameterisation and so are more generally applicable than semiempirical methods. Although semiempirical calculations are less computationally demanding than *ab initio* calculations, care must be taken to ensure that the method used is parameterised for the particular system being studied. The sections of this chapter from 2.4.8 onwards describe the various *ab initio* and semiempirical approaches to the approximation of the Hamiltonian, which were used in the calculations, performed for this thesis.

2.4.4 Basis sets

In quantum chemical calculations the many-electron wavefunction in Equation 2.24 is approximated as a normalised Slater determinant composed of one-electron spinorbitals. A spinorbital is a product of a molecular orbital wavefunction, the normalised square modulus of which gives the probability of finding that electron at any point in space, and a spin function. Each molecular orbital wavefunction is a linear combination of mathematical functions known as basis functions and the total set of basis functions used for the system is known as the basis set. This may be expressed as:

$$\psi_i = \sum_{\mu=1}^{N} c_{\mu i}\phi_\mu \qquad \textbf{(2.26)}$$

where ψ_i is the molecular orbital wavefunction for the i^{th} electron in the system, ϕ_μ is a basis function, $c_{\mu i}$ is the molecular orbital expansion coefficient and N is the number of basis functions used for each molecular orbital. In principle an exact description of the molecular orbital wavefunction may be obtained by using an infinite number of basis functions, and this is called a complete basis set. However the use of a complete basis set is impossible in practice and so a finite number of basis functions must be used. In general a larger basis set will give more accurate results for a given calculation. However the computational expense of a calculation is dependent on the number of basis functions used, for example for the Hartree-Fock (HF) method the total number of two-electron integrals increases as M^4, where M is the total number of basis functions. Therefore the size of basis set used must be limited to make calculations feasible. The type of basis functions used is also important as they can be chosen to improve the efficiency of a calculation, therefore enabling a larger basis set to

be used. However there is always a trade-off between accuracy and computational expense when choosing a basis set.

There are a variety of types of basis function which may be used in quantum chemical calculations. Two commonly used types are the Slater type orbitals (STOs) and the Gaussian type orbitals (GTOs), both of which consist of individual basis functions centred on nuclei. STOs have a cusp at the nucleus and drop off exponentially with distance from the nucleus and so are good models for a 1s atomic orbital. STOs do not have any radial nodes, but these may be introduced by making linear combinations of STOs to model orbitals with angular momentum quantum numbers of one or more ie p, d orbitals etc. However the great drawback to STOs is that solving the two-electron integrals over more than two atomic centres is mathematically very difficult and so calculations using STOs become impractical for polyatomic molecules. This problem is overcome by the use of GTOs, with which all the two-electron integrals over more than 2 atomic centres may be reduced to two-electron integrals over two atomic centres. They are therefore much better adapted for computational work than STOs. However GTOs, unlike STOs, do not have a cusp at the nucleus. This problem is overcome by using a linear combination of GTOs to model each orbital. To reduce the number of unknown expansion coefficients to be evaluated during a calculation the coefficients of this linear combination are fixed and the new GTO is called a contracted Gaussian type function, CGTF. All the calculations performed in this thesis were done with Gaussian basis sets.

The simplest type of basis set is called the minimal basis set. In the minimal basis set the minimum number of basis set functions is used to accommodate all the electrons of the system while maintaining overall spherical symmetry. For example the minimal basis set for H would contain one basis function for the 1s orbital and the minimal basis set for B would contain five basis functions, one each for the 1s and 2s orbitals and three for the 2p orbitals. However minimal basis sets have been found to be inadequate to produce accurate calculation results and generally basis sets with more basis functions are required. A basis set where two CGTFs are used for each valence orbital and one for each core orbital is called a split-valence basis set. The use of two CGTFs for each valence orbital allows these orbitals to expand and contract radially. An example of such a basis set is the 6-31G, where 6 primitives are used to form a single CGTF for each of the core orbitals and two CGTFs are constructed for each of the valence orbitals, one made up of three primitives and one made up of one diffuse function. In a split-valence basis set such as 6-31G, spherical symmetry is still imposed around each nucleus. This may not be appropriate for the orbitals in a

molecular environment, especially in molecules containing polar bonds. Therefore polarisation functions, which represent orbitals with higher angular momentum quantum numbers than the valence orbitals, may be included, for example p-type basis functions may be introduced on all the hydrogen atoms in the molecule. In a split-valence basis set the addition of polarisation functions is denoted by the symbol p for the addition of p-type functions to the hydrogens and d for the addition of d-type functions to all other carbon, nitrogen etc. The p and d are sometimes replaced by asterisks so that 6-31G(d,p) and 6-31G** mean the same thing. Additional sets of diffuse functions may be included in a basis set and this is denoted by +, for example 6-31+G** denotes addition of one set of diffuse s and p functions on non-hydrogens. Such diffuse functions are particularly important when calculating the energies of anions.

2.4.5 The variation principle

The variation principle states that where an arbitrary wavefunction, called the trial wavefunction, Ψ_{trial}, is used to calculate the energy of a system, the energy calculated, ε, is never less than the true energy. Variation theory, which is based on the variation principle, is a method of systematically improving a trial wavefunction. In variation theory the expansion coefficients of the basis set used to model the wavefunction of a system are varied to obtain the lowest possible energy. This is done by minimising the Rayleigh ratio, which is:

$$\frac{\int \Psi_{trial}^{*} \hat{H} \Psi_{trial} d\tau}{\int \Psi_{trial}^{*} \Psi_{trial} d\tau} \qquad (2.27)$$

The Rayleigh ratio is equal to ε, and $\varepsilon \geq E_0$ where E_0 is the true energy of the system. The basis set with these expansion coefficients will be the closest model possible to the true wavefunction of the system for that set of basis functions and the value of ε will be an upper bound for the energy of the system. Examples of calculation methods where a trial wavefunction is formed (initial guess) and then improved using the variation method are Hartree-Fock (HF) and configuration interaction (CI). Calculation methods that are based on perturbation theory, for example MP2, are not variational.

2.4.6 Geometry optimisation

Variation theory may be used to optimise the electronic wavefunction of a molecule and find the energy at a fixed input geometry. This is known as a single-point calculation. If an

optimisation of the geometry as well as the wavefunction is required the calculation becomes more complicated. In Figure 2.13 the various stages of such a calculation are shown.

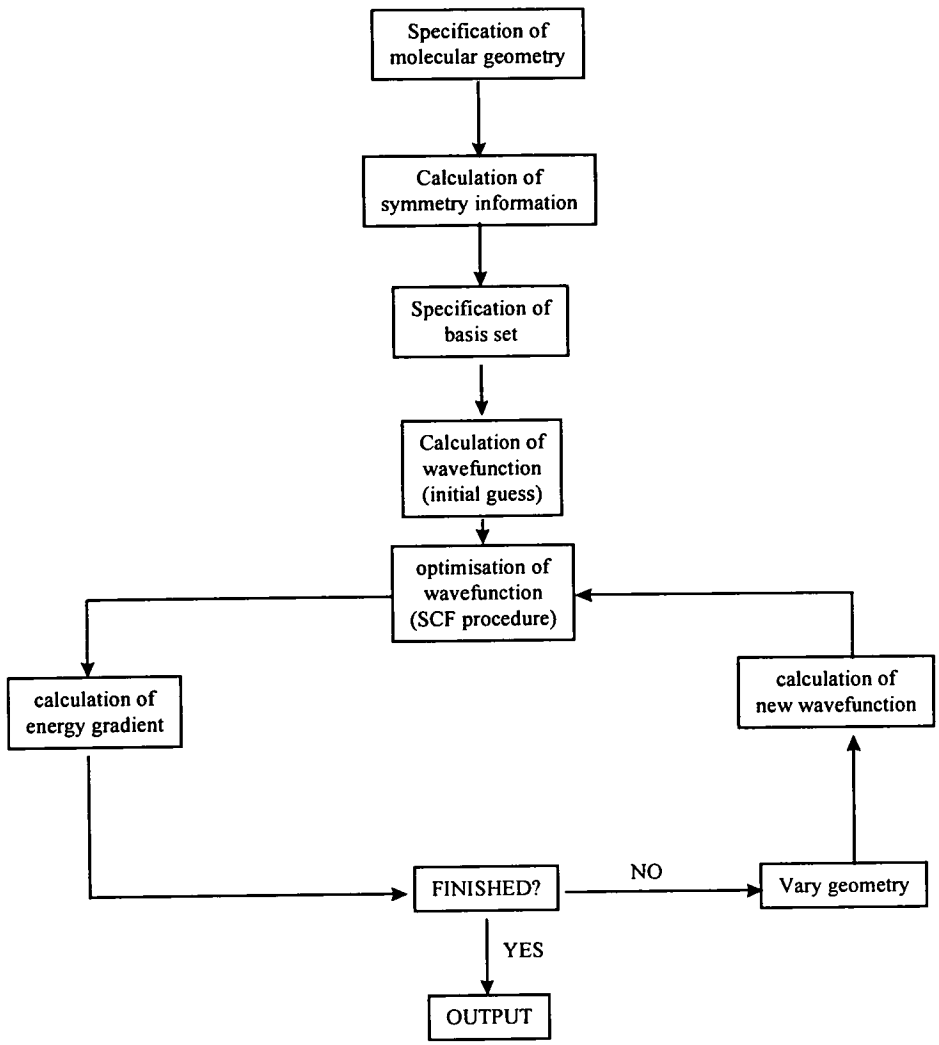

Figure 2.13: Various stages of a typical geometry optimisation.

The calculation of the energy gradient is the calculation of the change in potential energy with geometry, ie the calculation of the first derivative of the potential energy surface (PES). The aim of a geometry optimisation is to find a point on the PES, called a stationary point, where the energy gradient is zero. The calculation is deemed finished when the energy gradient is below some preset limit. There are three types of stationary point. These are minima, where any change in geometry increases the potential energy of the molecule, maxima, where any change in geometry decreases the potential energy of the molecule and saddle points, which are a maxima with respect to a change in geometry in one or more directions and minima with respect to geometry changes in all other directions. Saddle points correspond to transition structures connecting two or more equilibrium structures. Therefore once a geometry optimisation is complete it is important to check which type of

stationary point has been reached. Maxima, saddle points and minima may be distinguished by inspecting the matrix of the second derivative of the energy with respect to geometry (the Hessian matrix). For minima all matrix elements are positive, for maxima all are negative and for saddle points there are one or more negative elements. The elements of the Hessian are the force constants of vibrations within the harmonic approximation and so negative elements in the Hessian matrix correspond to imaginary frequencies.

2.4.7 Excited state methods

The electronic ground state of a molecule is the lowest energy state for a given spin multiplicity. Higher energy states of the same spin multiplicity are called excited states. In the development of quantum chemical calculation methods most of the effort has focussed on optimising the ground state electronic wavefunctions and geometries of molecules. This is because variational methods such as HF and DFT work by trying to minimise the energy of the system using a self-consistent field (SCF) procedure. With such methods it is difficult to prevent an excited state from dropping to the ground state during a calculation. This is known as variational collapse and is the reason these methods are only suitable for ground state calculations. However, recently, with developments in theory and computer power, the calculation of excited states has become feasible. Two of the methods described below may be used to optimise both the wavefunctions and geometries of ground and excited states, for example configuration interaction (CI) and complete active space (CAS). There has also been work carried out to extend density function theory (DFT) to the calculation of excited states resulting in a method called time-dependent DFT (TD-DFT).

2.4.8 Hartree-Fock (SCF) theory

Hartree-Fock (HF) or self-consistent field (SCF) theory was developed to enable a solution to the Schrödinger equation to be found which includes some of the effects of the electrostatic repulsion of the electrons (the 3rd term in Equation 2.25). It is purely a ground state method and cannot be applied to excited states. In the HF approach each electron is modelled as moving in an average potential generated by all the other electrons and the nuclei. Initially, for a system containing n electrons, a trial set of n spinorbitals is formulated. This set of spinorbitals is then used to generate and then solve the HF equations to generate a new set of spinorbitals. The process is repeated until the spinorbitals generated in a cycle are the same as the spinorbitals generated in the previous cycle to within the convergence criteria.

The HF equations are obtained by application of variation theory to the set of n spinorbitals, with the constraint that they are orthonormal i.e. normalized and mutually orthogonal. They are of the form:

$$\hat{f}_1\phi_a(1) = \varepsilon_a\phi_a(1) \tag{2.28}$$

where $\hat{f}_1$ is the Fock operator, $\phi_a(1)$ is the spinorbital ϕ_a containing electron 1 and ε_a is the energy of spinorbital ϕ_a. The Fock operator is:

$$\hat{f} = h_1 + \sum_u \{\hat{J}_u(1) - \hat{K}_u(1)\} \tag{2.29}$$

where h_1 is the core Hamiltonian for electron 1, the Hamiltonian operator in Equation 2.25 excluding the term for the electron-electron repulsion. $\hat{J}_u$ is the Coulomb operator and $\hat{K}_u$ is the exchange operator. Both of these operators are defined in terms of all the other spinorbitals apart from $\phi_a(1)$, the one being calculated in the HF equation. More than n optimised spinorbitals can be obtained from this procedure since the Fock operator has an infinite number of eigenfunctions but of course it is only practical to obtain a finite number of these optimised spinorbitals. These can then be arranged in order of increasing energy and the n spinorbitals of lowest energy, the occupied orbitals, combined to give the HF ground state wavefunction of the system. HF calculations have the advantage of being both variational and size-consistent. A size-consistent method is one for which the energy calculated is proportional to the number of electrons. This means that the accuracy of the results will not be dependent on the size of the molecule under study.

HF calculations where each of the n spinorbitals has a separate spatial component as well as a spin component are known as unrestricted HF (UHF) calculations. In restricted HF (RHF) calculations electrons which are paired in the same orbital, for example the two 1s electrons in ground state He, are assumed to have the same spatial wavefunction but different spin functions. RHF calculations are applicable to closed-shell systems only whereas UHF calculations are applicable to both closed and open-shell systems. A disadvantage of UHF calculations is that spin contamination, where the calculated wavefunction of the system does not have the correct spin symmetry, can occur. A UHF calculation on the ground state of Li illustrates this problem. There are two α spinorbitals, 1s and 2s, and one β spinorbital, 1s. The calculated energy of the 1sα spinorbital is lower than the energy of the 1sβ spinorbital because the effects of spin correlation between the electron in the 1sα spinorbital and the electron in the 2sα spinorbital are taken into account in the calculation. The two 1s orbitals therefore have different energies. This results in spin impurities in the computed

wavefunction. The extent of spin contamination can be measured by calculating the expectation value of $\hat{S}^2$, the spin operator, in the computed wavefunction and comparing it with the true value of S(S+1), where S is the total spin angular momentum, for the system.

2.4.9 Correlation energy

A HF(SCF) calculation will find almost all the true energy of a system but the remaining energy, the correlation energy, is very important for chemical systems and cannot be ignored if accurate results are to be obtained. The correlation energy is more accurately called the Coulombic correlation energy as there are, in fact, two types of correlation, Fermi and Coulombic. Fermi (interorbital or spin) correlation occurs between electrons in different orbitals with parallel spins. It exists as a consequence of the Pauli exclusion principle which states that no more than two electrons may occupy a single orbital and if two electrons do occupy a single orbital their spins must be paired. This means that electrons with parallel spins must occupy different orbitals and must be spatially separated. Therefore there is a large decrease in the probability of finding two electrons with parallel spins close in space, which is known as a 'Fermi hole'. As a result, the electrostatic repulsion between electrons of parallel spin is reduced and the energy of the system lowered by what is referred to as the exchange energy.

Coulombic correlation occurs between all electrons in a system. The electrons interact with each other, exerting forces upon one another so that the motion of one electron instantaneously affects the motion of all the other electrons. The motion of all the electrons is correlated. This again has the effect of keeping the electrons apart and so lowers the electrostatic energy of the system still further. However, for electrons with parallel spins the Fermi correlation masks the Coulombic correlation. Therefore it can be assumed that Coulombic correlation only acts on electrons with paired spins. Calculations based on HF theory include the energy from Fermi correlation but not Coulombic. There are various ways of adding the effects of Coulombic correlation into the HF wavefunction. The calculation methods used to do this in this thesis were Møller-Plesset perturbation theory (MPPT), configuration interaction (CI) and complete active space (CAS).

2.4.10 Multiconfiguration methods

In theory, a HF (SCF) calculation on a system containing n electrons results in an infinite number of spinorbitals which can be arranged in order of increasing energy. In the HF (SCF) method the n lowest energy spinorbitals are combined as a Slater determinant to form

the electronic wavefunction of the system. This arrangement of electrons can be thought of as corresponding to a single, ground state electronic configuration of the molecule. However, there are many other Slater determinants that can be formed by utilising the remaining higher energy spinorbitals. For example, many determinants corresponding to singly excited configurations can be formed by removing an electron from an occupied spinorbital in the HF ground state wavefunction and placing it in a previously unoccupied or virtual spinorbital. Similarly, determinants corresponding to doubly excited configurations can be formed by removing two electrons from occupied spinorbitals in the HF ground state wavefunction and placing them in virtual spinorbitals.

Mathematically, the exact electronic wavefunction, Ψ, for a system can be expressed as a linear combination of all possible n-electron determinants arising from a complete set of spinorbitals as shown in Equation 2.30.

$$\Psi = C_0\Phi_0 + \sum C_S\Phi_S + \sum C_D\Phi_D + \ldots\ldots \qquad \textbf{(2.30)}$$

where C is an expansion coefficient, Φ is an n-electron determinant, the subscript 0 denotes the HF ground-state determinant, the subscript S denotes singly excited determinants and the subscript D denotes doubly excited determinants. Each particular determinant is included in the summation only once. This result can be used to improve the HF ground state wavefunction by forming a linear combination of such determinants and applying variation theory to optimise the expansion coefficients. This is effectively a way of incorporating some of the effects of Coulombic electron correlation into the HF wavefunction. Multiconfiguration methods can also be used to calculate the wavefunctions of excited states (see section 2.4.11). However, to obtain the exact wavefunction of a system a complete set of spinorbitals, which consists of an infinite number of spinorbitals, would have to be used, and all possible determinants corresponding to all possible electronic configurations constructed from these spinorbitals must be included in Equation 2.30. This is clearly impossible in practice and so some method of choosing the determinants to be included in the linear combination is required. Since the number of determinants that can be obtained from a finite set of spinorbitals increases rapidly with the number of spinorbitals and it is very computationally demanding to deal with large numbers of determinants, in most cases only a fraction of the total number of available determinants are used. Two widely used

methods of choosing the determinants for a multiconfiguration calculation are configuration interaction (CI) and complete active space (CAS).

In a full CI (FCI) calculation all the determinants of the correct symmetry for the finite number of spinorbitals from the HF calculation are included. Nearly always, FCI still involves too many determinants to be practical and more have to be excluded. A systematic way of choosing the determinants to be included in a CI calculation is to include only the determinants which correspond to a certain number of electrons being excited. For example, CI calculations that include only singly excited determinants are known as CI-singles (CIS). However the HF ground state wavefunction will not be improved by using CIS, so for ground state calculations with CI only doubles (CID) or singles and doubles (CISD) are used. In a CAS calculation a small number of spinorbitals of the correct symmetry, including some occupied and some virtual orbitals, are chosen to form the active space and all single, double, triple, etc excitations within the active space are included in the calculation. The selection of the correct active space is the crucial step in performing a CAS calculation.

Both CI and CAS calculation are variational and so provide an upper limit on the energy of a molecular state. However they have the disadvantage of not being size-consistent, so the accuracy of the results will vary with the size of the molecule for the same level of theory and basis set. They are also computationally expensive. However, the results of ground state CI calculations, and in particular FCI calculations, are used as a standard to evaluate newly developed calculation methods. They can also both be used for excited state calculation optimisations of wavefunctions and geometries.

2.4.11 Møller-Plesset perturbation theory

The ground state wavefunction of a system obtained from a HF calculation can be improved by using Møller-Plesset perturbation theory (MPPT), which is a special case of many-body perturbation theory. In perturbation theory an exact solution to the Schrödinger equation is found for a system which resembles the true system. This wavefunction is then used as a guide to the true wavefunction by noting how the Hamiltonians of the two systems differ. The Hamiltonian operator for the true system, $\hat{H}$, is given by Equation 2.31.

$$\hat{H} = \hat{H}_0 + \lambda \hat{H}_1 \qquad \textbf{(2.31)}$$

where $\hat{H}_0$ is the Hamiltonian of the approximate system for which an exact solution is known and $\hat{H}_1$ is the perturbation. In MPPT $\hat{H}_0$ is taken to be the sum of the n Fock operators obtained from the HF calculation and the procedure involves expanding the eigenvalues and eigenfunctions of $\hat{H}$ as series. The first term of the series is the zero-order correction; the second term is the first-order correction and so on. Each successive correction term is calculated until the calculation is terminated at some level. A calculation up to and including the second-order correction is denoted MP2, up to and including third-order correction MP3 and so on. The MP1 energy is identical to the Hartree-Fock value so MP2 is the simplest level that includes correlation energy using MPPT. MPPT has the advantage of being size consistent if computations are carried out completely at any given order. This means that the energy is proportional to the number of electrons. However it is not variational so it doesn't provide an upper limit to the energy. Also it becomes difficult and costly to apply at higher orders. The technique of using perturbation theory to include more of the correlation energy can be applied to the HF ground state wavefunction and the CI and CAS excited state wavefunctions. However, it is not a technique that can be used with geometry optimisations and it is not variational. However MP calculations are size-consistent.

2.4.12 Density functional theory

An alternative approach to quantum chemical calulations, which is not based on HF theory, is that based on density-functional theory (DFT). DFT may be used to perform a geometry optimisation on the ground state of a system of nuclei and electrons and an extension to the theory called time-dependent-DFT (TD-DFT) may be used to obtain the electronic wavefunctions of excited states. DFT was developed by Hohenberg and Kohn (1964) and Kohn and Sham (1965) and is based on the proof by Hohenberg and Kohn that the total electronic energy of a system of electrons is a functional of the electron density. This means that for a given electron density distribution in a molecule there is a unique value of the electronic energy. The minimum value of this energy is the exact ground-state electronic energy of the molecule. The next step in the development of DFT came when Kohn and Sham showed that for an n-electron system the electronic energy can be written in terms of one electron spatial orbitals. As in HF theory, variation theory is then used to generate a set of equations that can be solved for the one-electron orbitals using the SCF method.

The problem in DFT is that the exact form of the functional dependence of the exchange-correlation energy on the electron density is unknown and so an approximation must be used.

In its simplest form DFT uses the local density approximation (LDA) in which it is assumed that the exchange-correlation energy per electron at each point in space is the same as it would be for a uniform gas of interacting electrons, accurate values of which are known from theoretical work. However, better results are obtained for chemical systems when general gradient approximations (GGA), which take into account gradients in the electron density, are used. DFT has the advantage over HF in that it includes some of the effects of Coulombic correlation. It is also much less computationally expensive than the more traditional MPPT, CI or CAS methods. Geometry optimisations carried out on ground state molecules using DFT give bond lengths very similar to those obtained using MP2, but taking a fraction of the time. The DFT method is also variational and size-consistent.

Unfortunately, DFT cannot be applied directly to excited states. Time-dependent TD-DFT is an extension of DFT that involves modelling the time-evolution of many-electron systems under a perturbation. Excited states arise under such conditions and it is possible to calculate excitation energies using TD-DFT. Such methods have been successfully applied to the low-lying electronic excitations of N_2, ethylene, formaldehyde and pyridine [1] and the results were found to be more accurate than HF based methods such as HF-CIS for a similar level of computational expense. However, a disadvantage of TD-DFT methods is that structural parameters such as geometries or dipole moments cannot be obtained.

2.4.13 ZINDO

ZINDO is a series of molecular electronic structure programmes, which have been developed over the last 20 years. The programmes were developed by Professor M.C. Zerner amongst others and the name ZINDO stands for Zerners INDO (intermediate neglect of differential overlap). The programmes can use a wide variety of electronic structure methods but INDO is the most widely used. INDO is one of a group of semiempirical methods in which certain two-electron integrals are set to zero in order to simplify the calculations. These methods only deal explicitly with the valence electrons of a system. ZINDO is parameterised for a variety of elements including the first and second row transition metals. It can be used to calculate various molecular properties such as total energies of molecules, ionisation potentials and UV-vis spectra, but not optimised geometries. Vertical excitation energies in ZINDO are calculated by performing a CIS calculation using a simplified Hamiltonian that has been parameterised using *ab initio* CI results. It is most accurate in predicting low-lying π-π^* and n-π^* bands of molecules containing hydrogen and first and second-row elements. Calculated higher-energy states usually agree less well with experiment. The use of ZINDO

to calculate vertical excitation energies has the advantage of being extremely fast compared to *ab initio* and DFT methods. However, ZINDO is a valence only method and so cannot accurately model properties which involve the core electrons and care must be taken that it is parameterised for a particular system before being used as it is a semiempirical method.

2.4.14 Solvation models

So far methods of optimising ground or excited states wavefunctions and/or geometries for isolated molecules have been discussed. Such calculations correspond to molecules in a low to moderate pressure gas phase, where they may be assumed to be non-interacting. However most chemistry occurs in condensed phases, with solution phases being of particular importance. Therefore it is often useful to be able to perform calculations which model solvated molecules.

In the solution phase solute molecules can no longer be thought of as isolated. The interaction with the surrounding solvent molecules becomes important. There are two principle means of modelling this interaction. In explicit solvation calculations individual solvent molecules are modelled in addition to the solute molecule. This is very computationally demanding and the number of solvent molecules that can be included is limited. In implicit (or continuum) solvation models the solvent is modelled as an isotropic dielectric continuum. The perturbation of the solute caused by the electric properties of the solvent is included but individual interactions such as H-bonding are not. The calculations on solvated molecules performed for this thesis used a continuum solvation model called the conductor-like screening model (COSMO) [2].

In the COSMO model the solute molecule is placed at the centre of a cavity. The shape of the cavity is formed by centring overlapping spheres on the nuclei of the solute. Surrounding this cavity, the solvent is modelled as an isotropic, dielectric continuum with a relative permitivitty ε_r. The charge distribution of the solute causes so called screening charges to be distributed on the surface of the cavity representing the response of the solvent to the solute. To simplify the calculation of these screening charges the solvent is assumed to be conducting, ie with $\varepsilon_r=\infty$. To take into account the finite permittivity of real solvents the calculated screening charges are then scaled by a factor incorporating the ε_r of the solvent being modelled. COSMO is available for use with semi-empirical, *ab initio* (HF,CI etc) and DFT calculations. For polar solvents such as water, deviations from the exact solution for the calculation of the screening charges arising from the approximations of COSMO are

about 1%, whereas for nonpolar solvents with $\varepsilon_r<2$ they may reach up to 10%. However for nonpolar solvents the screening effects will be small and therefore the absolute error will also be small.

2.5 References

1. Rüdiger Bauernschmitt and Reinhart Ahlrichs, *Chem.Phys.Lett.*, 1996, **256**, 454-464

2. A.Klamt and G. Schüürmann, *J.Chem.Soc. Perkin Trans.*, 1993, **2**, 799

2.6 Bibliography

The following texts were used in the writing of this chapter:

Physical Chemistry, 6th Ed. by P.W.Atkins, Oxford University Press, 1999

Electrode Dynamics by A.C.Fisher, Oxford University Press, 1998

Electrochemical Methods by A.J.Bard and L.R.Faulkner, John Wiley & Sons, 1980

The Theory of the Electronic Spectra of Organic Molecules by J.N.Murrell, Methuen & Co. Ltd., 1963

Modern Spectroscopy, 3rd Ed. by J.M.Hollas, John Wiley & Sons, 1996

Principles of Fluorescence Spectroscopy, 2nd Ed. by J.R.Lakowicz, Kluwer Academic / Plenum Publishers, 1999

Introduction to Computational Chemistry by F.Jensen, John Wiley & Sons, 1999

Molecular Quantum Mechanics, 3rd Ed. by P.W.Atkins and R.S.Friedman, Oxford University Press, 1997

Ab Initio Molecular Orbital Theory by W.J.Hehre, L.Radom, P.v.R.Schleyer and J.A.Pople, John Wiley & Sons, 1986

Essentials of Computational Chemistry, Theories and Models by C.J.Cramer, John Wiley & Sons, 2002

Chapter Three

EXPERIMENTAL

In this chapter the experimental and computational methods used in this thesis are described.

3.1 Chemicals

3.1.1 Chemicals synthesised in house

Indolo{3,2,1-*jk*}carbazole (IC) and pyrrolo{3,2,1-*jk*}carbazole (PC) were both synthesised in the department by Lynne Crawford [1] and Stuart Wharton, both members of Dr H. McNab's group, using the technique of Flash Vacuum Pyrrolysis (FVP).

IC

The method of synthesis of IC is outlined in Figure 3.1. The samples were purified by flash chromatography.

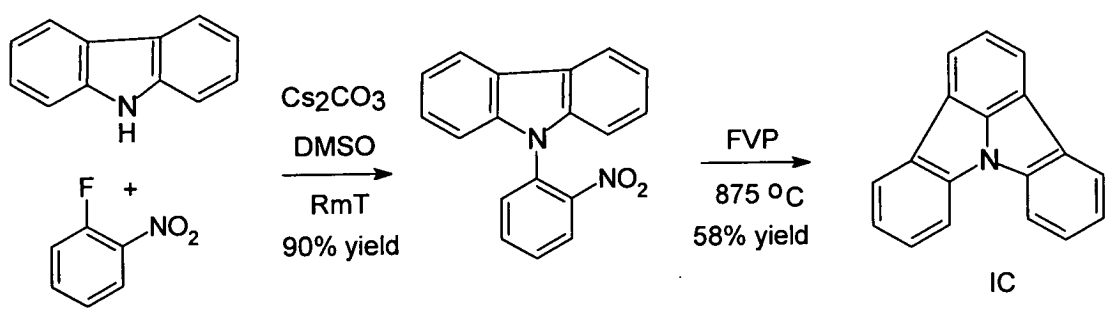

Figure 3.1: Synthetic route to IC

PC

The method of synthesis of PC is outlined in Figure 3.2. The samples were purified by flash chromatography.

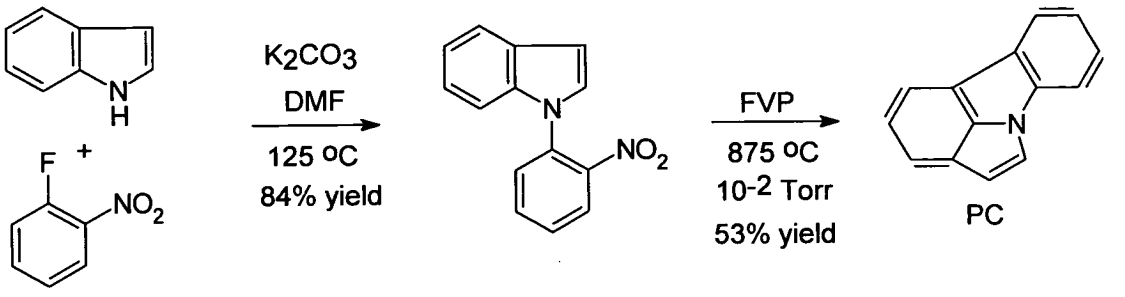

Figure 3.2: Synthetic route to PC

3.1.2 Commercial chemicals

Lithium perchlorate (Aldrich, 99.99%), silver perchlorate hydrate (Aldrich, 99%), ferrocene (Fluka AG >98% Fe), carbazole (Acros Organics 96%), pyrrole (Aldrich 98%) were all used as received.

3.1.3 Solvents

Acetonitrile (MeCN, Fisher Scientific, HPLC grade), N,N-dimethylformamide (DMF, Acros Organics, spectrophotometric grade 99+%), cyclohexane (Aldrich, HPLC grade, 99.9+% or Prolabo, Rectapur™, 99%), ethyl alcohol (EtOH, Aldrich, spectrophotometric grade) were all used as received. All water was doubly deionised by means of a Millipore water system.

3.2 Electrochemistry

All electrochemical experiments were carried out using a modular potentiostant/galvanostat with combined waveform generator and voltage sources (Oxford Electrodes Ltd). The rotating disc electrode (RDE) was controlled using a rotator and a motor controller (Oxford Electrodes Ltd). Data are collected on a PC with tailored programmes compiled using Visual Designer software (Intelligent Instruments).

The working electrode was a Pt rotating disc electrode (Oxford Electrodes Ltd) with a disc area of 0.387 cm^2. It was polished on a polishing cloth with a slurry of micropolish 0.3 μm alpha alumina (Buehler Ltd) in doubly deionised water. The counter electrode was a 2 cm^2 Pt gauze which was cleaned by rinsing in acetone and flaming in a bunsen burner. The reference electrode (Bioanalytical Systems Inc.) consisted of a silver wire dipped in a 0.01 M solution of $AgClO_4$ in electrolyte in a glass body separated from the bulk electrolyte by a VYCOR plug.

The electrolyte was a 0.1 M solution of $LiClO_4$ in acetonitrile. The Ag/Ag^+ reference electrode has a potential of +0.437 V [2] with respect to the saturated calomel electrode and +0.681 V with respect to the standard hydrogen electrode. During electrochemistry experiments the electrolyte solution was degassed with N_2 gas. Polymer films were dissolved off the electrode surface into DMF for analysis by spectroscopy.

3.3 Spectroscopy

3.3.1 Steady-state fluorescence spectroscopy

All steady-state fluorescence spectra were measured using a Jobin Yvon Spex Fluoromax™ spectrofluorometer (Instruments S.A. group). A diagram of the components of this spectrofluorometer is shown in Figure 3.3. The excitation source is a 150 W continuous ozone-free xenon lamp, with modified Czerny-Turner spectrometers in both the emission and excitation positions. The data acquisition and data manipulation software used was Instruments S.A. Datamax. All experiments were carried out with disposable poly(methyl methacrylate) (PMMA) cuvettes (Fisons 4.5 ml), which have 100 % transmission above 280 nm with a 1 cm path length.

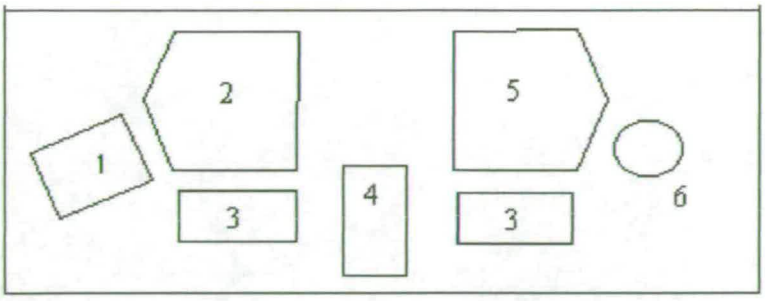

1 Illuminator
2 Excitation spectrometer
3 Sample compartment coupling optics
4 Sample compartment
5 Emission spectrometer
6 Emission detector

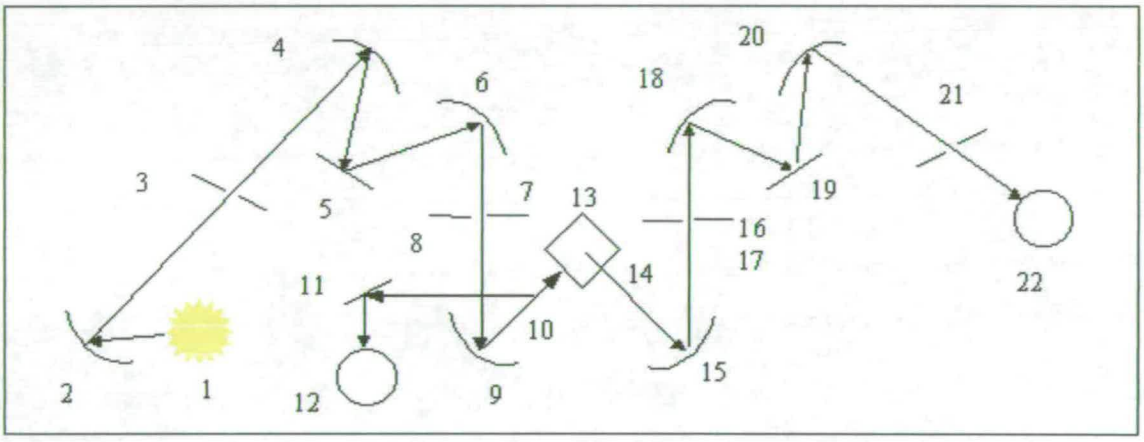

1 150 W ozone free lamp
2 Collection mirror (excitation spectrometer)
3 Entrance slit (excitation spectrometer)
4 Collection mirror (excitation spectrometer)
5 Grating
6 Focussing mirror (excitation spectrometer)
7 Excitation slit (excitation spectrometer)
8 Excitation shutter
9 Collection mirror (excitation spectrometer)
10 Beam splitter
11 Deflection mirror
12 Photodiode reference collector
13 Sample position
14 Window
15 Sample collection mirror
16 Emission shutter
17 Entrance slit
18 Collection mirror
19 Grating (1200 gr./mm)
20 Focussing mirror
21 Exit slit (emission spectrometer)
22 Emission detector

Figure 3.3: Schematic diagram of the components of the fluorescence spectrometer

3.3.2 UV-visible absorption spectroscopy

UV-visible spectra were measured with a Unicam spectrometer using a matched pair of 1 cm pathlength quartz cuvettes.

3.3.3 Time correlated single photon counting (TCSPC)

All experiments were performed at the Collaborative Optical Spectroscopy Micromanipulation and Imaging Centre (COSMIC) at the University of Edinburgh. An outline of a typical TCSPC experimental set up was described in chapter two. All decays were measured using an Edinburgh Instruments TCSPC spectrometer coupled with a Hammamatsu R3809U-50 series microchannel plate detector. Samples were excited using a mode-locked Ti-sapphire laser.

3.4 Computational

The computational work carried out for this thesis was done in conjunction with Dr. Simon Bates of the School of Physics, University of Edinburgh. All calculations were carried out using the software package Gaussian 98 [3] (G98) running under the Linux operating system on a PC. Default convergence criteria were used for all G98 calculations (maximum force = 0.00045, RMS force = 0.0003, maximum displacement = 0.0018 and RMS displacement = 0.0012).

For all molecules studied computationally (indole, carbazole, pyrrole, 5-cyanoindole, 5-hydroxyindole, pyrrolo{3,2,1-*jk*}carbazole and indolo{3,2,1-*jk*}carbazole), a frequency calculation was performed for each optimised geometry to ensure that a minimum in the potential energy hypersurface had been reached. This is shown by the absence of imaginary frequencies.

The spin density distribution for the radical cations was evaluated using a cube calculation with the default grid of 80^3 points. The spin density distribution plots were made using the software gOpenMol [4].

Due to a bug in the G98 software, in order to complete the CAS(SCF) geometry optimisation of the excited state of indole, it was necessary to add 'IOp(5/38=6) ExtraLinks=405' to the route section of the input file of this calculation.

3.5 References

1. Lynne A.Crawford, PhD thesis, University of Edinburgh, 2002

2. J.G.Mackintosh and A.R.Mount, *J.Chem.Soc. Faraday Trans.*, 1994, **90(8)**, 1121-1125

3. Gaussian 98, Revision A.7, M.J.Frisch, G.W.Trucks, H.B.Schlegel, G.E.Scuseria, M.A.Robb, J.R.Cheeseman, V.G.Zakrzewski, J.A.Montgomery, Jr., R.E.Stratmann, J.C.Burant, S.Dapprich, J.M.Millam, A.D.Daniels, K.N.Kudin, M. C.Strain, O.Farkas, J.Tomasi, V.Barone, M.Cossi, R.Cammi, B.Mennucci, C.Pomelli, C.Adamo, S.Clifford, J.Ochterski, G.A.Petersson, P.Y.Ayala, Q.Cui, K.Morokuma, D.K.Malick, A.D.Rabuck, K.Raghavachari, J.B.Foresman, J.Cioslowski, J.V.Ortiz, A.G.Baboul, B.B.Stefanov, G.Liu, A.Liashenko, P.Piskorz, I.Komaromi, R.Gomperts, R.L.Martin, D.J.Fox, T.Keith, M.A.Al-Laham, C.Y.Peng, A.Nanayakkara, C Gonzalez, M.Challacombe, P.M.W.Gill, B.Johnson, W.Chen, M.W.Wong, J.L.Andres, C.Gonzalez, M.Head-Gordon, E.S.Replogle, and J.A.Pople, Gaussian, Inc., Pittsburgh PA, 1998.

4. Copyright Leif Laaksonen (1997-2002), Engineering: Kevin Boyd, Eero Häkkinen and Leif Laaksonen

CHAPTER FOUR

COMPUTATIONAL CONFIDENCE TESTS

4.1 Introduction

Computational methods may be used to predict many of the properties of molecules, such as equilibrium geometries or excitation energies. They may therefore be useful for the screening of prospective heterocyclic monomers for electroluminescent applications. Computational confidence tests are used to assess the accuracy and cost of different calculation methods. The results of such tests may then be used to guide the choice of method used for the system of interest. For this thesis methods of calculating oxidation potentials, radical cation spin density distributions and the excited state energies and geometries of heterocyclic molecules were tested with a view to applying them to the indolo{3,2,1-*jk*}carbazole (IC) and pyrrolo{3,2,1-*jk*}carbazole (PC) monomers. The results of these tests are given in this chapter.

4.2 Oxidation potentials

The oxidation of a molecule, M, is shown in Scheme 4.1.

$$M \rightarrow M^{+} + e^{-} \qquad \textbf{(Scheme 4.1)}$$

In principle the standard redox potential of M, E^{θ}, may be calculated relative to another molecule, N, whose oxidation is shown in Scheme 4.2,

$$N \rightarrow N^{+} + e^{-} \qquad \textbf{(Scheme 4.2)}$$

by calculating the energy difference, ΔG^{θ}, for the reaction shown in Scheme 4.3

$$M^{+} + N \rightarrow M + N^{+} \qquad \textbf{(Scheme 4.3)}$$

and using the relation $\Delta G^{\theta}=nFE^{\theta}$. In this way, calculation of the energy of the solvated electrons may be avoided. In this thesis the standard redox potentials for the oxidation of a range of organic molecules (oxidation potentials) were each calculated relative to the standard redox potential of ferrocene (Fc). These were compared to the half wave potentials of these molecules measured experimentally. These measurements were made at room temperature (298K) and with the molecules in the solution phase. Therefore to compare calculated and experimental potentials the effects of temperature and solvation should be incorporated into the calculations.

In a previous study [1] density functional theory (DFT) calculations were successfully used to calculate the oxidation potentials relative to Fc/Fc^+ of a range of eleven 5-substituted indoles using the software package DMol^3. In these calculations the energy and geometry of the neutral and radical cation of each species were optimised and the effects of solvation were included using the COSMO solvation model (see section 2.4.14). The solvent was modelled as pure acetonitrile (MeCN) with a relative permittivity of 37.5. The basis set used in these calculations was a double-numeric basis set augmented by polarisation functions on all atoms. Generalised gradient corrections (GGA) were applied to the local density approximation *via* the PW91 functionals (see section 2.4.12) and temperature corrections to 300K were included from semiempirical frequency analyses carried out on the DFT optimised geometries. The difference in temperature corrections at 275 and 300K was found to be negligible so the error introduced by calculating the oxidation potentials at 300K rather than the 298K at which the experimental half wave potentials were measured was assumed to be negligible. The oxidation potentials predicted using this method were all within 0.2 V of the experimentally measured half-wave potentials.

The software package DMol^3 was no longer available for the work in this thesis, and so the aim of the oxidation potential test calculations described here was to reproduce the level of accuracy obtained with DMol^3 using the software package Gaussian 98 (G98). The five test molecules chosen for these confidence tests were indole, 5-hydroxyindole, 5-cyanoindole, carbazole and pyrrole. Indole, 5-hydroxyindole and 5-cyanoindole were chosen because the results for these molecules could be compared directly with the calculations done previously using DMol^3. Carbazole and pyrrole, together with indole, were chosen to provide a range of aromatic system sizes in nitrogen-containing heterocycles, bearing in mind the intended application to IC and PC. The structures of these molecules are shown in Figure 4.1. There are two possible conformers for 5-hydroxyindole. Both have the O-H bond in the plane of the aromatic system, one with the O-H bond lying approximately parallel to the C5-C6 bond (syn) and one with the O-H bond lying approximately parallel to the C4-C5 bond (anti). All calculations for this thesis were carried out on the anti conformer as previous calculations at the HF/6-31G* level [2] have predicted it to be slightly more stable (0.03 eV) than the syn conformer.

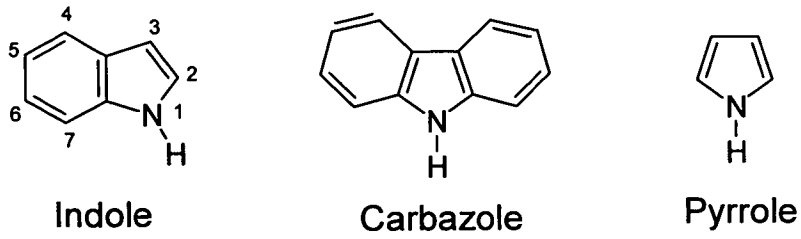

Figure 4.1: Molecular structures of indole, carbazole and pyrrole.

The method chosen for these test calculations was B3PW91/6-31G(d,p). B3PW91 is a hybrid DFT functional which incorporates some HF exchange energy into the DFT exchange-correlation energy. The correlation functional in this method, PW91, is the same as that used in the DMol[3] calculations. Numeric basis sets are not available in G98 so a basis set based on Gaussian functions was used. The 6-31G(d,p) basis set is a Gaussian split-valence basis set (see section 2.4.4) and has a comparable size to the double numeric basis set used in the DMol[3] calculations [3]. B3PW91/6-31G(d,p) geometry optimisations were performed for the neutral and radical cations of each of the test molecules and Fc and Fc^+. Frequency calculations were performed on these optimised geometries both to check that a local minima had been reached, shown by the absence of imaginary frequencies, and provide a temperature correction (from 0K to 298.15 K) to be used on the solvated energies. The solvated energies were then obtained from B3PW91/6-31G(d,p)/COSMO calculations started from the gas phase optimised geometries and using the default G98 relative permittivity of acetonitrile of 36.64.

The calculated oxidation potentials for the five test molecules were compared with experimental potentials measured using linear sweep voltammetry (LSV). These measurements were taken at low concentrations (≤1 mM) of monomer in electrolyte to minimise any potential coupling of monomer to form polymer, which could interfere with the shape of the LSV curve [4]. Values of the potential at maximum current (the peak potential), E_p, were obtained from the LSVs for each molecule. A diagnostic for a reversible (Nernstian) system is that $|E_p-E_{p/2}|$ is 56.5mV at 298 K where $E_{p/2}$ is the potential when the current has dropped to half its maximum value (the half peak potential). For a reversible system, the polarographic half wave potential, $E_{1/2}$, is located approximately midway between E_p and $E_{p/2}$ and so E_p-28.3 mV (at 298 K) gives a fairly accurate estimate of $E_{1/2}$. $E_{1/2}$ is related to the standard redox potential, E^θ, by

$$E_{1/2} = E^\theta + \frac{RT}{nF}\ln\frac{D_R^{1/2}}{D_O^{1/2}} \qquad \textbf{(4.1)}$$

where D_R is the diffusion coefficient of the reduced species and D_O is the diffusion coefficient of the oxidised species. If D_R and D_O are equal, which is generally a reasonable approximation, $E_{1/2}$ and E^θ are equal. Therefore the experimentally measured value of $E_{1/2}$ can be compared directly to the calculated value of E^θ.

Linear sweep voltammograms have previously been measured for indole, 5-cyanoindole and 5-hydroxyindole and found to show electrochemical reversibility [5]. Values of $E_{1/2}$ for these molecules, shown in Table 4.1, are taken from the literature. Linear sweep voltammograms for ferrocene, pyrrole and carbazole were measured for this thesis. The redox reaction between Fc and Fc^+ is known to be electrochemically reversible and is frequently employed as a standard in non-aqueous systems. However in the system employed for this thesis both E_p and $|E_p-E_{p/2}|$ for Fc/Fc^+ were found to show some dependence on sweep rate, with $|E_p-E_{p/2}|$ ranging from 85 mV at 20 mV/s to 111 mV at 100 mV/s. This is likely to be caused by a significant iR drop still present in the system despite the use of three electrodes. This is where there is some resistance across the electrolyte between the working and reference electrodes and is a particular problem in systems using non-aqueous electrolytes, such as the acetonitrile used here. However as $|E_p-E_{p/2}|$ for Fc/Fc^+ was closest to 56.5 mV at a sweep rate of 20 mV/s, and at this sweep rate carbazole and pyrrole both showed values of $|E_p-E_{p/2}|$ close to that of Fc/Fc^+ it was assumed for the purposes of this thesis that the oxidation of carbazole and pyrrole is essentially electrochemically reversible. Therefore $E_{1/2}$ was estimated from E_p as described above. The experimental and calculated values of $E_{1/2}$ and E^θ are given in Table 4.1.

Molecule	Experimental $E_{1/2}$ / V, 298K vs Fc/Fc^+	Calculated E^θ / V vs Fc/Fc^+		
		DMol[3], 300K*	B3PW91, 298K	
			6-31G(d,p)	6-311G(2d,2p)
indole	0.80*	0.71	0.58	0.54
5-OHindole	0.67*	0.56	0.38	0.34
5-CNindole	1.14*	1.07	0.94	0.90
carbazole	0.80	-	0.55	0.51
pyrrole	1.01	-	0.77	0.65

*A computational and electrochemical study of electropolymerised indoles by L.J.Kettle, PhD thesis, University of Edinburgh, 2000

Table 4.1: Calculated standard reduction potentials, E^θ, and experimental half wave potentials, $E_{1/2}$, for various heterocycles.

The results in Table 4.1 show that the oxidation potentials predicted using B3PW91/6-31G(d,p) are less accurate than those predicted with DMol[3]. For indole, 5-hydroxyindole

and 5-cyanoindole the DMol^3 oxidation potentials were all within 0.11 V of the experimental values whereas with B3PW91/6-31G(d,p) the calculated oxidation potentials were all systematically more than 0.20 V lower than the experimental values. The most important difference between the two methods was the type of basis functions used. Numerical basis sets are known to be more accurate than Gaussian basis sets of equivalent size [3] and therefore the G98 calculations were repeated using the larger Gaussian basis set 6-311G(2d,2p). These results are also shown in Table 4.1. Use of the larger basis set, however, did not improve the results, but actually made them worse. The B3PW91/6-311G(2d,2p) calculated oxidation potentials were all more than 0.24 V lower than the experimental values.

There is clearly some effect other than the type of basis functions used causing the G98 results to be worse than the DMol^3 results. When the B3PW91/6-311G(2d,2p) E^θ values are recalculated using the energies of Fc and Fc^+ obtained with the 6-31G(d,p) basis set, the results are much closer to those obtained using DMol^3, as shown in Table 4.2. This indicates that the error may be caused by the 6-311G(2d,2p) calculation of the Fc/Fc^+ couple

Molecule	Experimental $E_{1/2}$ / eV, 298K vs Fc/Fc^+	Calculated E^θ / V vs Fc/Fc^+		
		DMol^3, 300K*	B3PW91	
			6-31G(d,p)	6-311G(2d,2p)
indole	0.80*	0.71	0.57	0.70
5-OHindole	0.67*	0.56	0.36	0.51
5-CNindole	1.14*	1.07	0.93	1.07
carbazole	0.80	-	0.54	0.68
pyrrole	1.01	-	0.76	0.82

Table 4.2: Calculated standard reduction potentials, E^θ, and experimental half wave potentials, $E_{1/2}$, for various heterocycles. All G98 calculated E^θs in this table are calculated using Fc and Fc^+ energies from calculations using the 6-31G(d,p) basis set.

The best method for reproducing the results from DMol^3 in G98 appears to be B3PW91/6-311G(2d,2p) for the organic molecules and the 6-31G(d,p) basis set for Fc and Fc^+. Referencing the results to a basis set of different size is not ideal. The fact that the oxidation potentials are closer to the DMol^3 values when the energies from the 6-311G(2d,2p) calculations for the organic molecules are used rather than the 6-31G(d,p) energies is most likely because Gaussian basis sets are less good than numerical basis sets of equivalent size. The fact that the 6-31G(d,p) basis set must be used to calculate the energies of Fc and Fc^+ indicates that the G98 software is not very good for calculating transition metals with large basis sets. This reflects the fact that, with Gaussian basis sets, an increase in size does not

necessarily result in an increase in accuracy. However it is encouraging that the oxidation potentials calculated using G98 follow the same trends as the experimental half wave potentials and the calculated oxidation potentials for carbazole and pyrrole are of similar accuracy to those for the indoles.

4.3 Spin density calculations

It has been proposed that the first step in the electrooxidation of indole to form polymer occurs by the linkage of two indole radical cations, with the unpaired electrons on each cation forming a new bond. Reaction of this dimer with another indole radical and further oxidation results in the formation an asymmetric indole trimer [6, 7]. In order for an asymmetric trimer to be formed the first step is likely to involve linkage of two indole radical cations at the 3-position forming a 3,3'-dimer. This is illustrated in Figure 4.2.

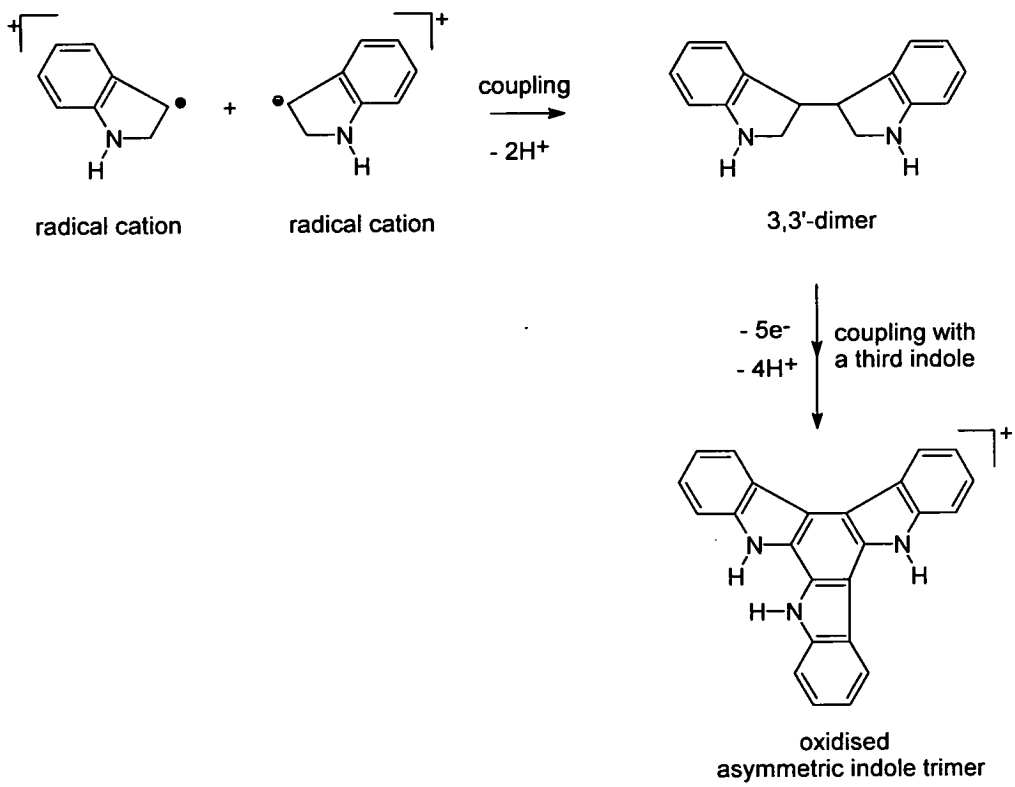

Figure 4.2: Linkage of two indole radical cations to form a 3,3'- indole dimer and structure of the asymmetric indole trimer formed from this dimer.

A spin density calculation is a calculation of the difference in the electron density distribution between the α and β electrons in a molecule. Such a calculation may be performed using the optimised wavefunction and geometry of a radical cation to show the most probable location of the unpaired electron in the molecule. Calculation of the spin

density distribution in indole$^{\bullet+}$, using DMol^3 with the method and basis set described in the previous section, predicts a high spin density at the proposed linkage site of the radical cation, the 3-position. This suggests that such calculations may be used to predict the linkage sites of other monomers that polymerise in a similar way. In previous work this calculation was extended to several 5-substituted indoles and it was found that the spin density distributions of the radical cations of indoles substituted with electron withdrawing groups such as cyano were very similar to that of indole$^{\bullet+}$ itself. In contrast the radical cations of indoles substituted with electron donating groups such as hydroxy showed very different spin distributions, with most spin density on the substituent and the carbon atom adjacent to it in the aromatic ring rather than on the 3-position of the aromatic ring.

As DMol^3 was no longer available for calculations for this thesis the aim of these confidence tests were to check that spin density distribution calculations performed using the software package G98 would give the same qualitative results as obtained using DMol^3. The spin density distribution in indole$^{\bullet+}$ calculated using B3PW91/6-31G(d,p) was compared to that calculated with B3PW91/6-311G(2d,2p) and, as both were found to be qualitatively the same, all other calculations were performed using the smaller basis set. Spin density distribution calculations were performed on indole$^{\bullet+}$, 5-hydroxyindole$^{\bullet+}$ and 5-cyanoindole$^{\bullet+}$ using B3PW91/6-31G(d,p) and the results are shown in Figure 4.3. The pictures show the spin density in a plane parallel to the plane of each molecule. As the unpaired electron is a π electron there is little or no spin density in the plane cutting through the nuclei, and therefore the planes are situated at the distance from the nuclei showing the most density.

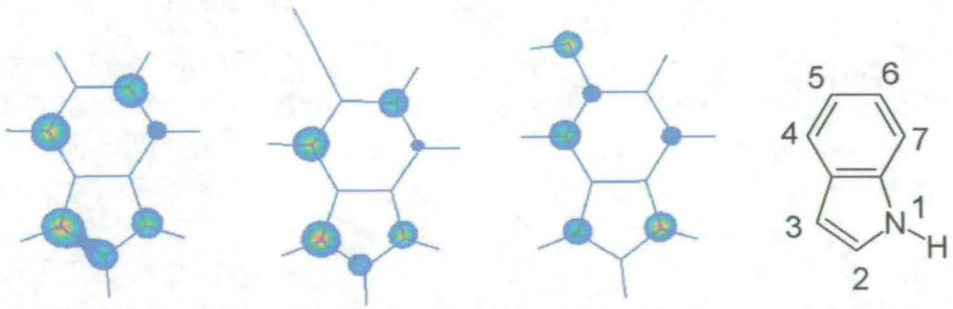

Figure 4.3: Schematic of the spin density distributions in indole$^{\bullet+}$, 5-cyanoindole$^{\bullet+}$ and 5-hydroxyindole$^{\bullet+}$ calculated using B3PW91/6-31G(d,p). Red indicates a higher spin density and blue a lower. The molecular structures are shown in blue.

The results obtained with G98 for the spin density distributions are qualitatively the same as those obtained with DMol^3, even though G98 was shown to be less accurate than DMol^3 for

the prediction of oxidation potentials. Therefore the method B3PW91/6-31G(d,p) was used for calculations of the spin density distributions of $IC^{\bullet+}$ and $PC^{\bullet+}$ for this thesis.

4.4 Calculations of excited states

There are several different methods available for the calculation of excited state energies and geometries. The theory behind the methods used in this project is explained in chapter two. In order to select the best method, calculations were carried out on the two test molecules indole and carbazole and the structures and numbering systems for these molecules are shown in Figure 4.4. The results of these calculations were then compared with experimental results and the most accurate method chosen for further calculations on PC and IC. All the excited state calculations carried out for this thesis were performed on isolated molecules and therefore, where possible, the results were compared to experimental results on jet-cooled or gas phase molecules.

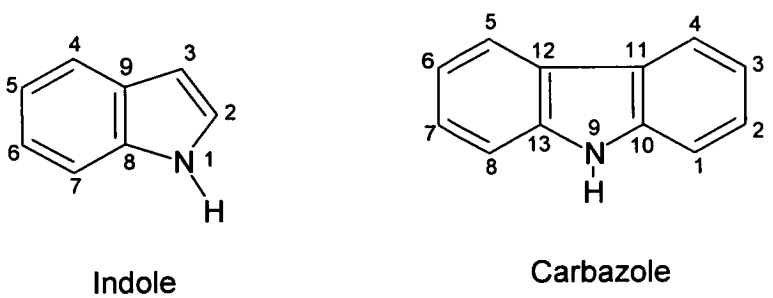

Figure 4.4: The structures and numbering systems of indole and carbazole.

There are a number of reasons why indole and carbazole were chosen for the confidence tests. Spectroscopic studies yield valuable information, such as energy differences between states, which can be compared with calculation results. As both molecules have high fluorescence quantum yields they can be studied using a variety of spectroscopic techniques such as fluorescence excitation spectroscopy. Both carbazole and indole have been the subject of a large number of such spectroscopic studies and there is a great deal of experimental data available. Indole in particular has been studied as it is the chromophore of the amino acid tryptophan, which is the most important emissive source in proteins. These studies have shown that the two lowest singlet excited states, ^1L_a and ^1L_b, of indole are nearly degenerate and the absorption and emission of the two low-lying bands is very sensitive to the environmental conditions. This is very unusual and means that accurate modelling of the excited states of indole will provide a significant test for the various calculation methods.

In the following sections a review of the relevant experimental and calculation results from the literature for indole and carbazole is given. In section 4.4.3 of this chapter the results of the excited state calculations carried out for this project are discussed.

4.4.1 Literature review for carbazole

The spectroscopic properties of carbazole have been studied experimentally in the solid state [8, 9, 10], in solution [11, 12], in the vapour phase [13] and under supersonic jet conditions [14, 15, 16, 17]. Some theoretical and computational studies have also been published [11, 18, 19, 20].

An early theoretical study of carbazole [11] predicted that the lowest energy transition $S_1 \leftarrow S_0$ should be weak and polarised along the short molecular axis, while the second transition should be stronger and long axis polarised. Analysis of the absorption spectrum of a carbazole crystal [10] confirmed the directions of the two transition dipole moments. The fact that the transition dipole moment directions for the two transitions are known allows the two lowest singlet excited states to be distinguished in calculation results. The oscillator strengths are approximately 0.05 for the transition from the ground state, S_0, to the lowest energy singlet excited state, S_1, [21, 9] and 0.15 for the transition from the S_0 state to the second singlet excited state, S_2, [22, 9]. The vertical excitation energies of carbazole have been reported at 30,300 and 34,280 cm^{-1}, for the $S_1 \leftarrow S_0$ and $S_2 \leftarrow S_0$ transitions respectively, from the absorption spectrum of carbazole in hexane [18].

The development of supersonic jets in the early 1980s meant that spectroscopic techniques could be performed on cold, isolated molecules to give very detailed spectra, and there have been a number of spectroscopic studies carried out on carbazole under supersonic jet conditions. Such spectra allow the exact positions of origin bands to be measured. The origin band of the $S_1 \leftarrow S_0$ transition has been reported at 30,809 cm^{-1} in the LIF excitation spectrum of jet-cooled carbazole by Honegger *et al* [14] and at 30,824 cm^{-1} by both Bombach *et al* [15] and Lubman *et al* [17], using one-colour resonant two-photon ionisation methods. Therefore an intermediate value of 30,820 cm^{-1} was taken for this thesis. The $S_2 \leftarrow S_0$ transition origin lies approximately 4,500 cm^{-1} above the $S_1 \leftarrow S_0$ origin at 35,320 cm^{-1} [14].

X-ray studies have shown that the ground state structure of carbazole is planar with C_{2v} symmetry [23]. The absence of out-of plane vibronic transitions and the excellent correlation between S_0 and S_1 vibrational modes observed in the LIF excitation spectrum of jet-cooled carbazole are strong indications that carbazole retains its planarity in the S_1 state [14]. Also,

the absence of any long progressions in the absorption spectrum of a carbazole crystal shows that any change in geometry between the S_0 and S_1 states must be small [9]. The geometry of the ground state of carbazole has also been studied using *ab initio* computational methods [19]. The closest agreement with the experimental X-ray values for the bond lengths and angles was obtained with the MP2 method.

4.4.2 Literature review for indole

4.4.2.1 States of indole

The electronic states of indole are usually labelled using the Platt system of nomenclature for aromatic systems [24, 25]. The states of interest here are the two lowest lying singlet excited states, which are labelled ^1L_a and ^1L_b. When performing excited state calculations on indole it is important to be able to distinguish the a and b states in calculation results. This is because the ^1L_b and ^1L_a states of indole are nearly degenerate and their relative energies are dependent on the environment of the molecule and can be altered by substitution. For example, in the gas phase the lowest energy singlet excited state, S_1, of indole is the ^1L_b state whereas in 2,3-dimethylindole it is the ^1L_a state [26]. For a molecule with a two-fold axis of symmetry the a and b states can be distinguished by the direction of their transition dipole moment from the ground state relative to that axis. Conventionally, the subscript a is used for states which have the transition dipole moment parallel to this axis and the subscript b used for states which have the transition dipole moment perpendicular to this axis. Since indole does not have any axes of symmetry the subscripts a and b are assigned by analogy with other molecules. The lowest energy triplet state ^3L_a and the singlet state ^1L_a have transition dipole moments from the ground state approximately parallel to the a 'axis' in Figure 4.5. The ^1L_b state has a transition dipole moment from the ground state approximately parallel to the b 'axis' in Figure 4.5.

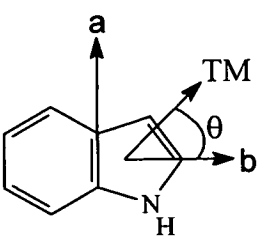

Figure 4.5: Diagram showing a and b 'axes' of indole and the angle, θ, between the b 'axis' and the transition dipole moment, TM.

4.4.2.2 Experimental work on indole

The absorption spectrum of indole has been studied in both the vapour [27] and solution phases [11, 28]. It is made up of two overlapping electronic bands between 240 and 300nm involving the ^1L_a and ^1L_b transitions. The oscillator strengths for these two electronic transitions have been estimated as 0.12 and 0.05 respectively [29] and the transition dipole moments have been shown, by a polarisation study of 3-indolylacetic acid crystals [30], to be approximately perpendicular. The band to lower energy shows vibronic structure and has been assigned to the ^1L_b transition whereas the band to higher energy is less structured and has been assigned to the ^1L_a transition. The vibronic bands belonging to the ^1L_a transition are more sensitive to perturbation by a solvent than those belonging to the ^1L_b transition and this observation has been used to distinguish the vibronic bands belonging to each [28]. Polarisation techniques have also been used to resolve the absorption and excitation spectra of indole into contributions from the two bands [31, 32, 33]. The vertical excitation energies of the ^1L_b and ^1L_a transitions have been measured as 35,250 and 38,460 cm^{-1} respectively from the vapour phase absorption spectrum of indole [28].

The jet-cooled excitation spectrum of indole has been reported by several groups [34, 35, 36] and shows the origin of the ^1L_b transition at 35,233±10 cm^{-1}. Distinguishing the ^1L_a origin band from vibronic lines in the spectrum of indole has proved more of a challenge. It was suggested by Nibu *et al* that the ^1L_a origin lies more than 2000 cm^{-1} above the ^1L_b origin, as no great change in the quantum yield of the excitation spectrum of jet-cooled indole was observed at lower energies [35]. Bersohn *et al* similarly suggested that the ^1L_a origin lies more than 1500 cm^{-1} above the ^1L_b origin based on the pattern of decay lifetimes of photoselected states of jet-cooled indole [36]. To explain the failure to observe the ^1L_a origin in the excitation spectrum of indole a dissociative pathway *via* N-H bond cleavage was proposed for the ^1L_a state [37]. However the polarised two-photon fluorescence excitation spectrum of indole showed that excitation of ^1L_a states definitely leads to fluorescence and a pair of lines at 455 and 480 cm^{-1} above the ^1L_b origin were assigned as the ^1L_a split origin [38]. It was later shown that these are in fact ^1L_b vibronic lines which obtain their ^1L_a character from Herzberg-Teller vibronic coupling with the nearby ^1L_a state [39]. A study of the differential shifts in the polarised fluorescence excitation and dispersed fluorescence spectra of indole in a solid Ar matrix showed that the true ^1L_a origin lies about 1,400 cm^{-1} above the ^1L_b origin [39]. However the exact location of the ^1L_a origin is unknown, although it has been proposed that it is split into a number of components in the 1400 cm^{-1} region *via* coupling with the underlying ^1L_b

manifold. The lowest triplet state of indole is the ^3L_a state and the phosphorescence origin lies at 24,930 cm^{-1} in a solid argon matrix [40].

The angle, θ (see Figure 4.5), of the transition dipole moment of the $^1L_b \leftarrow ^1A_1$ transition of indole with the b 'axis' has been obtained experimentally by analysis of the rotationally resolved excitation spectrum of indole. Rotational analysis of the room temperature gas phase spectrum gave a value of $\pm 33^0$ [41] whereas analysis of the high resolution spectrum of jet-cooled indole gave a value of $\pm 45^0$ [42]. However both of these investigations used only part of the spectrum and ignored the axis reorientation effect, where, as a result of the low symmetry of indole, different equilibrium molecule-fixed axis systems can exist for ground and electronically excited states. Analysis of the jet-cooled, laser induced fluorescence (LIF) excitation spectrum of indole taking into account both these points gave a value of $\pm 38.3^0$ (± 0.2) [43]. Such analysis gives only the absolute value and not its sign. A plus sign refers to a counter-clockwise rotation from the b 'axis', away from the ring nitrogen (see Figure 4.5), and a negative sign to a clockwise rotation from the b 'axis', towards the ring nitrogen. However rotational analysis of the jet-cooled spectrum of tryptamine, which contains the indole chromophore, showed that the plus sign should be taken for indole and thereby confirmed that the lowest energy excited state of indole in the gas phase is the ^1L_b state [44]. The direction of both the $^1L_b \leftarrow ^1A_1$ and $^1L_a \leftarrow ^1A_1$ transition dipole moments have also been measured using the technique of linear dichroism on indole in stretched polyethylene films [45, 46]. These studies gave a value for the direction of the $^1L_b \leftarrow ^1A_1$ transition dipole moment of $+42^0$ (± 2), which is close to that obtained by Berden *et al*, and for the direction of the $^1L_a \leftarrow ^1A_1$ transition dipole moment of -54^0 (± 7).

The relevant spectroscopic data on the transitions from the ground state to the two lowest singlet excited states and the lowest triplet state of indole is summarised in Table 4.3.

Transition	Origin band energy / cm^{-1}	Vertical excitation energy / cm^{-1}	Oscillator strength, f	Direction of transition dipole moment, θ
$^1L_b \leftarrow ^1A_1$	35,230	35,230	0.05	$+38.3^0$
$^1L_a \leftarrow ^1A_1$	36,630	38,460	0.12	-54^0

Table 4.3: Experimental values for the transition energies, oscillator strengths and directions of transition dipole moments from the b 'axis' for transitions from the ground state, $^1A_1$, to the ^1L_b and ^1L_a states of indole in the gas phase.

Indole is difficult to crystallise and no X-ray crystal structure is available in the literature. However crystal structures of molecules containing the indole chromophore, such as tryptophan [47], have been published. These, together with microwave measurements [48], show that indole is planar. Since the origin of the ^1L_b transition coincides with the maximum of the ^1L_b absorption band and no long progression is found, the geometry change in indole between the S_0 and ^1L_b states must be very small [27]. In fact, rotational analysis of the origin band of the $^1L_b \leftarrow ^1A$ transition [41, 43] shows a change in the rotational constants upon excitation, but this change is small and an average increase in bond lengths of only 1% is sufficient to account it. The maximum intensity of excitation to the ^1L_a state is to the blue of the ^1L_a origin band in the gas phase, which indicates that there is a greater geometry change between the ground and ^1L_a states than between the ground and ^1L_b states.

The classical method for measuring changes in permanent dipole moments between the ground and excited states of a molecule is to measure the fluorescence spectrum in a series of solvents of known polarity. There have been a number of such studies performed on indole and molecules which contain the indole chromophore, such as tryptophan [11, 49 50, 51]. However, early attempts to measure the dipole moment changes of indole using solvatochromic shifts were complicated by the fact that the emitting state of indole is dependent on the solvent polarity [49]. A study which took such dependence into account, as well as considering the effects of field-induced mixing of the two excited states, gave dipole moment values of 2.13 ± 0.02 D for the ground state, 2.39 ± 0.05 D for the ^1L_b state and 5.16 ± 0.09 D for the ^1L_a state [51].

4.4.2.3 Previous calculations of indole

The electronic structure of indole has been the subject of a number of computational studies using both semiempirical [52, 53] and *ab initio* [54, 55, 56, 57] methods.

In general semiempirical methods have been successful in predicting certain observables such as transition dipole moments, oscillator strengths and vertical excitation energies. However, accurate geometries cannot be calculated for excited states using semiempirical methods, as this would require the introduction of too many parameters. Therefore these methods do not give reliable information on the nature of the excited states themselves, for example excited state dipole moments, and cannot be used to calculate origin band or vertical emission energies. The results also depend on the particular parameter set used. Table 4.4 shows the results from a representative selection of semiempirical calculations on

the excited states of indole. INDO/SCI and INDO/SDCI refer to the semiempirical intermediate neglect of differential overlap (INDO) with configuration interaction singles (SCI) and singles and double (SDCI) methods respectively. PPP refers to the semiempririal Pariser-Parr-Pople configuration interaction method.

Observable	Transition	Exp	INDO/SCI [53]	INDO/SDCI [53]	PPP-CI [52]
Vertical excitation energies / cm^{-1}	$^1L_b \leftarrow {}^1A$	35,230	34,100	36,300	36,084
	$^1L_a \leftarrow {}^1A$	38,460	38,000	42,900	39,998
Oscillator strengths	$^1L_b \leftarrow {}^1A$	0.05	0.013	0.010	0.05
	$^1L_a \leftarrow {}^1A$	0.12	0.206	0.077	0.19
Transition dipole moment direction / degrees[a]	$^1L_b \leftarrow {}^1A$	+38.3	49	59	-
	$^1L_a \leftarrow {}^1A$	-54	-37	-50	-

[a] the transition dipole moment direction is measured from the long or b 'axis' (shown in Figure 4.5) with the direction away from the N as positive.

Table 4.4: Representative results of semiempirical calculations on the ^1L_b and ^1L_a states of indole with experimental data for comparison.

Studies of the singlet excited states of indole based on two different *ab initio* methods have been published. The first was based on the method of configuration interaction singles (CIS) [54] and also included the results of CIS_MP2 calculations, which incorporate more electron correlation into the CIS wavefunction through an MP2 correction [58]. This study used the 3-21G Gaussian-style basis set for the excited state calculations. The second study was based on the method of complete active space (CAS) [56]. In this study CASPT2 calculations, which are second order perturbation corrections to the CAS wavefunction, were also performed. This study used atomic natural orbital (ANO) style basis sets. In both studies the two excited states were distinguished by the relative directions of their transition dipole moments. The results of the two studies are summarised in Table 4.5.

Observable	Transition or state	Exp	CIS[54]	CIS-MP2[54]	CASSCF[56]	CASPT2[56]
Origin band energies / cm^{-1}	$^1L_b \leftarrow {}^1A$	35,230	-	-	-	35,037
	$^1L_a \leftarrow {}^1A$	36,630	-	-	-	37,534
Vertical excitation energies / cm^{-1}	$^1L_b \leftarrow {}^1A$	35,230	47,200[a]	57,400[a]	-	35,681
	$^1L_a \leftarrow {}^1A$	38,460	46,500[a]	63,200[a]	-	38,098
Dipole moments / Debye	^1A	2.13	2.12[b]	-	1.86	-
	^1L_b	2.39	2.15	-	0.85	-
	^1L_a	5.16	3.22	-	5.69	-

[a] referenced to MP2/6-31G* ground state energy
[b] for MP2/6-31G* with a SCF density matrix

Table 4.5: Results of *ab initio* calculations on the ^1L_b and ^1L_a states of indole with experimental data for comparison.

In the CIS/CIS-MP2 study, geometry optimisations of the two lowest singlet excited states of indole were performed using CIS/3-21G. These calculations correctly predicted the ^1L_a state to have a greater dipole moment than the ^1L_b state. However it was found that the CIS/3-21G calculations predicted the ^1L_a state to lie 940 cm^{-1} below the ^1L_b state, whereas experimentally it lies 1,400 cm^{-1} above the ^1L_b state in the gas phase. CIS-MP2/3-21G calculations of the excited state wavefunctions, however, correctly predicted the order of the two states in the gas phase, but with an energy separation between the two states of 5,510 cm^{-1}, which is much higher than the experimentally observed energy separation. The change in the ordering of the two excited states in going from CIS to CIS-MP2 is because the ^1L_b state is more sensitive to the inclusion of multiply excited determinants than the ^1L_a state.

The ground state of indole was optimised using HF with a series of basis sets of increasing size, and with MP2 with a 6-31G* basis set. The MP2/6-31G* ground state geometry optimisation gave the dipole moment closest to the experimental value and this geometry and wavefunction was then used as the reference ground state for the calculation of vertical excitation energies. Again, the CIS/3-21G method predicted the wrong ordering for the $^1L_a \leftarrow {}^1A$ and $^1L_b \leftarrow {}^1A$ transitions, whereas the CIS-MP2/3-21G method got this right. However, the vertical excitation energies calculated with CIS-MP2 were much greater than those observed experimentally.

In the CASSCF/CASPT2 study the ground and first two singlet excited states of indole were optimised using CASSCF. The ground state geometry obtained using this method was compared to a theoretical MP2/6-31G* structure of indole and an X-ray crystal structure of tryptophan. All three ground state geometries were found to be in good agreement. In

contrast to the CIS/3-21G calculations, the CASSCF calculations did not correctly predict the ordering of the dipole moments of the three electronic states. This appears to be due to a severe underestimation of the ^1L_b state dipole moment, although the predicted dipole moment of the ^1L_a state was closer to the experimental value than that obtained with CIS/3-21G, and suggests that the CIS optimised geometry is more accurate than the CASSCF for the ^1L_b state and vice versa for the ^1L_a state.

The energies of the three electronics states were then predicted using the CASPT2 calculation method, which correctly predicted the ^1L_b state to be the lowest singlet excited state in the gas phase. The energy difference between the ^1L_a and ^1L_b states from the CASPT2 calculations was 2,497 cm^{-1}, which is closer to the experimental difference than the results of the CIS-MP2 calculations. Also, the vertical excitation energies obtained with the CASPT2 method were closer to the experimental values than those obtained with either the CIS or CIS-MP2 methods.

4.4.3 Results of calculations of indole and carbazole

4.4.3.1 Ground states

Experimentally, the energies of the electronic states of molecules cannot be measured directly, but are measured in reference to other electronic states. The energies of excited states are principally measured in reference to the ground state, S_0. Therefore in order to compare the computational results with experimental results it is necessary to calculate the energies of both the ground and excited states and compute the difference. The method used to calculate the ground state energy should be the one appropriate for the excited state method, for example if using a time-dependent DFT excited state method, it should be referenced to the ground state DFT energy. Therefore geometry optimisations of the ground state, S_0, of carbazole and indole were carried out at the HF/3-21G, HF/6-31G(d,p), HF/6-311G(2d,p), MP2/6-31G(d,p) and DFT/6-31G(d,p) levels of theory/basis set size. Obviously the accuracy of the final excitation energies will depend, in part, on the accuracy of the ground state calculations used as reference. Therefore in this section the effects of both basis set size and method on the accuracies of these calculations are discussed.

In Tables 4.6 and 4.7 bond lengths and dipole moments from the ground state optimisations are given for carbazole and indole respectively, together with experimental bond lengths taken from X-ray crystal structures for both molecules and the experimental value for the dipole moment of indole. There is no experimental value for the dipole moment of carbazole

available. The equilibrium geometry of a molecule may differ between the gas and solid (crystal) phases. Therefore, when comparing the calculated and experimental bond lengths, the fact that the experimental values are applicable to molecules in a crystal, whereas the calculated values are applicable to gas phase molecules, must be taken into account.

Bond	Bond length / Å					
	HF/ 3-21G	HF/ 6-31G(d,p)	HF/ 6-311G(2d,p)	MP2/ 6-31G(d,p)	DFT/ 6-31G(d,p)	Exp[23]
C_1-C_2	1.380	1.381	1.382	1.391	1.390	1.390
C_2-C_3	1.395	1.397	1.399	1.408	1.404	1.398
C_3-C_4	1.380	1.380	1.382	1.389	1.390	1.395
C_4-C_{11}	1.386	1.390	1.392	1.402	1.398	1.400
C_{11}-C_{12}	1.456	1.456	1.455	1.444	1.448	1.467
C_1-C_{10}	1.385	1.388	1.391	1.398	1.395	1.395
C_{10}-C_{11}	1.403	1.401	1.401	1.418	1.417	1.404
C_{10}-N	1.387	1.378	1.378	1.384	1.382	1.414
μ / D	1.39	1.44	1.51	1.47	1.67	-

Table: 4.6: Calculated and experimental bond lengths and dipole moments of the ground state of carbazole. The numbering system of carbazole is shown in Figure 4.4.

Bond	Bond length / Å					
	HF/ 3-21G	HF/ 6-31G(d,p)	HF/ 6-311G(2d,p)	MP2/ 6-31G(d,p)	DFT/ 6-31G(d,p)	Exp[47]
N-C_2	1.388	1.373	1.373	1.379	1.378	1.377
C_2-C_3	1.349	1.348	1.348	1.375	1.368	1.344
C_3-C_9	1.446	1.442	1.442	1.430	1.434	1.451
C_9-C_4	1.394	1.399	1.399	1.408	1.404	1.412
C_4-C_5	1.374	1.374	1.374	1.387	1.386	1.397
C_5-C_6	1.402	1.404	1.404	1.412	1.408	1.386
C_6-C_7	1.374	1.375	1.375	1.388	1.387	1.391
C_7-C_8	1.391	1.394	1.394	1.401	1.398	1.400
C_8-C_9	1.404	1.401	1.401	1.423	1.421	1.380
C_8-N	1.377	1.371	1.371	1.376	1.375	1.391
μ / D	2.02	2.04	2.09	2.11	2.19	2.13

Table: 4.7: Calculated and experimental bond lengths and dipole moments, μ, of the ground state of indole. The numbering system of indole is shown in Figure 4.4.

The effect of the basis set size on the calculation of ground state geometries may be judged by comparing the bond lengths calculated with HF using the basis sets 3-21G, 6-31G(d,p) and 6-311G(2d,p). In moving from the 3-21G to the 6-31G(d,p) basis set the bond lengths change by between 0 and 0.015 Å, and for thirteen out of the eighteen bonds ring bonds for the two molecules, the bond lengths are closer to those obtained experimentally in the 6-31G(d,p) calculation than in the 3-21G calculation. Therefore increasing the basis set size

from 3-21G to 6-31G(d,p) improves the calculated geometry. However, increasing the basis set size from 6-31G(d,p) to 6-311G(2d,p), changes the bond lengths by only a small amount, between 0 and 0.003 Å. In fact the bond lengths obtained for indole using the 6-31G(d,p) basis set are the same as those obtained with the 6-311G(2d,p) basis set. Therefore it can be concluded that there is no advantage in using the larger 6-311G(2d,p) basis set for ground state geometries over the 6-31G(d,p) basis set.

The HF method is known to underestimate bond lengths, as it does not include the effects of electron correlation [3]. This is reflected in the computed values for indole and carbazole shown in Tables 4.6 and 4.7, which are, in general, shorter than the experimental values by between 0 and 0.036 Å. The few bonds in indole where the HF computed bond lengths are longer than the experimental values (eg C_8-C_9, C_5-C_6, C_2-C_3) are also predicted to be longer than the experimental values by the DFT and MP2 methods, and may be attributed to differences between the indole bond lengths in the gas and solid (crystal) phases. The effects of including electron correlation in the calculations may be judged by comparing the HF calculated bond lengths with the DFT and MP2 calculated bond lengths. The bond lengths change by between 0.004 Å and 0.027 Å in moving from the HF to DFT or MP2 methods and, in the majority of cases, the inclusion of electron correlation brings the bond lengths closer to the experimental values. The DFT and MP2 bond lengths are very similar, varying only by between 0.001 Å and 0.007 Å. However, since MP2 is a much more computationally expensive method than DFT, with calculations taking about four times as long, where resources are limited DFT would be recommended.

A very accurate prediction of the ground state dipole moment for indole was obtained with MP2/6-31G(d,p). The value of 2.11 D obtained with this method is within 0.02 D of the experimental value of 2.13 D. However the dipole moments of 2.19 D and 2.09 D, calculated with DFT/6-31G(d,p) and HF/6-311G(2d,p) respectively, are also close to the experimental value. The smaller basis sets 6-31G(d,p) and 3-21G used with HF give relatively poor values of the dipole moment. The calculated dipole moments for carbazole follow a similar trend to those for indole, with DFT predicting the largest dipole moment and HF/3-21G the lowest.

4.4.3.2 Vertical excitation energies

The calculation methods ZINDO and TD-DFT predict the energy of the excited state at the ground state equilibrium geometry. Energy differences computed between the ground and

excited states using these methods should therefore be compared to vertical excitation energies rather than origin band energies. The calculated and experimental vertical excitation energies and oscillator strengths for the $S_1 \leftarrow S_0$ and $S_2 \leftarrow S_0$ transitions of carbazole are given in Table 4.8, and for the $^1L_b \leftarrow {}^1A$ and $^1L_a \leftarrow {}^1A$ transitions of indole in Table 4.9. The S_1 and S_2 transitions of carbazole were assigned based on the calculated directions of the two transition dipole moments, as experiments have shown that the $S_1 \leftarrow S_0$ transition is short axis polarised and the $S_2 \leftarrow S_0$ long axis polarised [10]. The ^1L_b and ^1L_a transitions of indole were also assigned based on the relative calculated directions of their transition dipole moments, which are $+38^0$ and -54^0 from the b 'axis' shown in Figure 4.5 [43, 45].

Calculation method (ground state level of theory/basis set – excited state method)	S_1		S_2	
	$S_1 \leftarrow S_0$ vertical excitation energy / cm^{-1}	f	$S_2 \leftarrow S_0$ vertical excitation energy / cm^{-1}	f
HF/6-31G(d,p) - ZINDO	32,598	0.02	35,422	0.21
DFT/6-31G(d,p) - ZINDO	31,978	0.02	34,777	0.23
MP2/6-31G(d,p) - ZINDO	31,870	0.02	34,604	0.24
DFT/6-31G(d,p) – TDDFT	33,610	0.03	37,174	0.12
Experimental*, [18]	30,300	0.05	34,280	0.15

* in hexane

Table 4.8: Calculated and experimental vertical excitation energies and oscillator strengths, f, for carbazole.

Calculation method (ground state level of theory/basis set – excited state method)	^1L_b		^1L_a	
	$^1L_b \leftarrow {}^1A$ vertical excitation energy / cm^{-1}	f	$^1L_a \leftarrow {}^1A$ vertical excitation energy / cm^{-1}	f
HF/6-31G(d,p) - ZINDO	34,375	0.01	39,149	0.23
DFT/6-31G(d,p) - ZINDO	33,668	0.01	38,217	0.26
MP2/6-31G(d,p) - ZINDO	33,765	0.01	38,284	0.29
DFT/6-31G(d,p) – TDDFT	40,633	0.04	39,633	0.07
Experimental*, [28]	35,250	0.05	38,460	0.12

* vapour phase

Table 4.9: Calculated and experimental vertical excitation energies and oscillator strengths, f, for indole.

All the calculations performed on carbazole and indole predict the correct state, based on the directions of their transition dipole moments, to be the lowest energy excited state, except for the TD-DFT calculation on indole. Also, for both molecules the vertical excitation energies calculated using ZINDO are closer to the experimental energies than those calculated using

TD-DFT. The superiority of the semiempirical ZINDO method over the TD-DFT method is probably because ZINDO is parametrised using many common organic molecules and so gives very good results for such molecules.

Of the ZINDO calculations, that based on the MP2 ground state calculation gives excitation energies which are closest to the experimental values for all except the $^1L_b \leftarrow ^1A$ transition of indole, for which HF gives the closest excitation energy to the experimental value. It is unclear why HF should give a particularly good result for this transition. The excitation energies obtained with MP2 are very similar to those obtained with DFT, which is unsurprising as they both gave similar results for the ground state geometry calculations. Since DFT calculations are less computationally demanding than MP2 calculations, but give results of a similar level of accuracy, it is recommended that ZINDO based on a DFT ground state calculation is used for calculations of vertical excitation energies, where computational resources are limited.

4.4.3.3 Origin band energies and excited state geometries

Configuration interaction calculations may be used to calculate the energies of excited states at the optimised excited state geometry. Energy differences between the ground and excited states calculated using this method should therefore be compared to the experimental origin band energies. Configuration interaction singles (CIS) calculations were performed for the S_1 and S_2 states of carbazole and ^1L_b and ^1L_a states of indole. As in the previous section, the two states for each molecule were identified in the calculation results by the directions of their transition dipole moments. The results of these calculations were referenced to the Hartree-Fock (HF) ground state optimisations of the same basis set and the resulting calculated origin band energies and oscillator strengths are given in Table 4.10 for carbazole and Table 4.11 for indole, together with the relevant experimental data.

Calculation method (ground state level of theory/basis set – excited state method)	S_1		S_2	
	$S_1 \leftarrow S_0$ origin band energy / cm^{-1}	f	$S_2 \leftarrow S_0$ origin band energy / cm^{-1}	f
HF/3-21G - CIS	43,656	0.06	41,528	0.49
HF/6-31G(d,p) - CIS	42,142	0.05	39,574	0.48
HF/6-311G(2d,2p) - CIS	41,249	0.05	38,667	0.50
Experimental	30,820	0.05	35,320	0.15

Table 4.10: Calculated and experimental origin band energies and oscillator strengths, f, for carbazole.

Calculation method (ground state level of theory/basis set – excited state method)	^1L_b		^1L_a	
	$^1L_b \leftarrow {}^1A$ origin band energy / cm^{-1}	f	$^1L_a \leftarrow {}^1A$ origin band energy / cm^{-1}	f
HF/3-21G - CIS	48,133	0.03	44,727	0.35
HF/6-31G(d,p) - CIS	46,360	0.02	43,076	0.32
HF/6-311G(2d,2p) - CIS	45,530	0.02	41,977	0.32
Experimental	35,230	0.05	36,630	0.12

Table 4.11: Calculated and experimental origin band energies and oscillator strengths, f, for indole.

It has previously been reported that CIS/3-21G calculations predict the wrong ordering for the energies of the two lowest excited states of indole [54]. It can be seen in Tables 4.10 and 4.11 that this is also the case for carbazole, and that CIS calculations with the larger basis sets of 6-31G(d,p) and 6-311G(2d,p), although bringing the calculated origin band energies of indole closer to the experimental values, do not alter their relative magnitudes. For both indole and carbazole the predicted origin band energies of the S_1 (or ^1L_b) transitions are further away from the experimental values than the origin band energies of the S_2 (or ^1L_a) transitions. This is due to the greater sensitivity of the $S_1(^1L_b)$ state to the inclusion of multiply excited determinants in the CI wavefunction than the $S_2(^1L_a)$ state [54], and suggests that a calculation method which includes such determinants, such as complete active space (CAS), would be more accurate. CAS calculations also have the advantage that they may be used to improve the HF ground state wavefunction of molecules, thereby providing a more accurate ground state reference for the excited states than that used for CIS calculations.

CAS(SCF)/6-31G(d,p) geometry optimisations on the ground and first singlet excited states of indole were performed. These gave dipole moments of 1.50 and 1.88 D respectively and an origin band energy of 37,453 cm^{-1}. It was not possible to check the direction of the transition dipole moment of the transition between these states and therefore the excited state could not be assigned as ^1L_a or ^1L_b. However, since the experimental values of the dipole moments of the ^1A and ^1L_b states are very similar at 2.13 and 2.39 D respectively, and the experimental dipole moment of the ^1L_a state is much higher at 5.16 D [51], the calculated excited state may be assigned as ^1L_b. The origin band energy of 37,456 cm^{-1} obtained from the CAS/6-31G(d,p) calculations is closer to the experimental value of 35,230 cm^{-1} than the origin band energies for this transition obtained from the CIS calculations. However it proved impossible to complete a CAS calculation of the second excited state of indole, or any CAS calculations on carbazole, due to a problem with the G98 software. In private communications with the G98 software company it emerged that there is a bug in the

software which sometimes causes problems with a CAS calculation when a molecule contains a nitrogen lone pair. Therefore it is uncertain whether CAS calculations predict the correct order for the excited states of indole.

The dipole moments predicted with the CIS/6-31G(d,p) and CAS/6-31G(d,p) calculation methods for the excited states of indole, together with experimental values, are shown in Table 4.12.

Calculation method	Dipole moment / D		
	^1A	^1L_b	^1L_a
CIS/6-31G(d,p)	2.04*	2.47	3.19
CAS/6-31G(d,p)	1.50	1.88	-
exp[51]	2.13	2.39	5.16

*HF/6-31G(d,p) value

Table 4.12: Dipole moments for the three lowest singlet electronic states of indole predicted with CIS/6-31G(2d,p) and CAS/6-31G(d,p), and experimental values.

It can be seen in Table 4.12 that the dipole moments predicted for the ground and ^1L_b states of indole, with HF/6-31G(d,p) and CIS/6-31G(s,p) respectively, are in good agreement with experiment, with both predicted values within 0.09 D of the experimental values. In contrast, the dipole moment predicted for the ^1L_a state with CIS/6-31G(d,p) is almost 2 D lower than the experimental value. The calculated dipole moments do not appear to be significantly improved by use of the larger 6-31G(d,p) basis set compared to the 3-21G basis set (see data in Table 4.5) [54]. However, despite the error in the ^1L_a calculated dipole moment, the CIS/6-31G(d,p) calculations still predict the correct order for the dipole moments of the ^1L_b and ^1L_a states of indole, although these calculations predicted the incorrect order for the energies of these states. This appears to be because the prediction of the dipole moment is better for the ^1L_b state than the ^1L_a state, whereas the prediction of excited state energies was better for the ^1L_a state than the ^1L_b state. The dipole moments obtained from the CAS/6-31G(d,p) calculations for the ground and ^1L_b states of indole are actually further from the experimental values than those obtained with CIS/6-31G(d,p), although, again, they are in the correct order. These results suggest that, although CIS calculations are inferior to CAS calculations for the prediction of excited state energies, they may be used successfully to predict the relative magnitudes of excited state dipole moments.

4.5 Conclusions

Computational confidence tests have been performed for the calculation of the oxidation potentials, radical cation spin density distributions and excited state energies and dipole moments of heterocyclic organic molecules.

The oxidation potentials of indole, 5-hydroxyindole, 5-cyanoindole, carbazole and pyrrole have been calculated relative to the Fc/Fc^+ couple using the software G98, with the DFT functional B3PW91 and Gaussian-type basis sets. The effects of solvation were included with the continuum solvation model COSMO. The results of these calculations have been compared to calculations previously published using the $DMol^3$ software with a similar DFT functional, numerical basis sets and COSMO [1]. The G98 calculation method which gave the best agreement with the experimentally observed oxidation potentials was a combination of the 6-311G(2d,2p) basis set for the organic molecules and the 6-31G(d,p) basis set for the transition metal complexes. This method has been shown to systematically underestimate the oxidation potentials and reproduces the experimental oxidation potentials to within 0.19 V. These results are slightly worse than those obtained with $DMol^3$, which predicted the oxidation potentials to within 0.11 V.

The radical cation spin density distributions of indole, 5-hydroxyindole and 5-cyanoindole have also been calculated using the software G98, with the calculation method B3PW91/6-31G(d,p). This method has been shown to successfully reproduce the qualitative spin density distributions previously obtained with $DMol^3$, which are known to predict the highest spin density at the site at which the indole monomers link to form indole trimer [1].

The ground state geometries of indole and carbazole have been calculated with HF/3-21G, HF/6-31G(d,p), HF/6-311G(2d,p), DFT/6-31G(d,p) and MP2/6-31G(d,p). The effect of basis set size on the calculated geometries has been assesed by comparing the aromatic ring bond lengths obtained with HF/3-21G, HF/6-31G(d,p) and HF/6-311G(2d,p) with experimental bond lengths obtained from X-ray crystallography. Moving from the 3-21G to the 6-31G(d,p) basis sets improves the bond lengths with respect to experiment, but increasing the basis set size from 6-31G(d,p) to 6-311G(2d,p) does not significantly change the calculated bond lengths. The effect of the inclusion of electron correlation in the calculation of the ground state geometries of indole and carbazole has been assessed by comparing the bond lengths obtained with HF/6-31G(d,p), DFT/6-31G(d,p) and MP2/6-31G(d,p) with the experimental bond lengths. There is a significant improvement in the

bond lengths obtained by using the methods, DFT and MP2, which include electron correlation. However the bond lengths obtained with DFT and MP2 are very similar to each other. The value of the dipole moment of the ground state of indole obtained from the MP2/6-31G(d,p) calculation was found to be closest to the experimental value.

Vertical excitation energies to the two lowest excited states of indole and carbazole have been calculated using TD-DFT and ZINDO. Those obtained with ZINDO were found to be closer to the experimental values than those obtained with TD-DFT. ZINDO also correctly predicted the order of the energies of the two lowest excited states of both indole and carbazole. The ZINDO excitation energies based on the MP2 ground state calculation were found to be the closer to the experimental values than those based on HF or DFT ground state calculations in most cases.

The origin band energies for the two lowest excited states of indole and carbazole have been calculated using HF/3-21G-CIS, HF/6-31G(d,p)-CIS and HF/6-311G(2d,p)-CIS. All three calculation methods incorrectly predicted the energetic ordering of the two lowest excited states of both molecules. A CAS(SCF)/6-31G(d,p) calculation gave a value for the origin band for the ^1L_b transition of indole which was closer to the experimental value than that obtained from the CIS/6-31G(d,p) calculation. However the value of the dipole moment of the ^1L_b state obtained from the CAS calculation was further from the experimental value than that obtained from the CIS/6-31G(d,p) calculation, which was within 0.08 D of the experimental value. However the dipole moment of the ^1L_a state predicted with CIS was underestimated by almost 2 D. The CIS method correctly predicted the dipole moment of the ^1L_a state to be larger than the dipole moment of the ^1L_b state of indole.

4.6 References

1. L.J.Kettle, S.P.Bates and A.R.Mount, *Phys.Chem.Chem.Phys.*, 2000, **2**, 195-201

2. G.Alagona, C.Ghio and S.Monti, *Theo.Chem.*, 1998, **433**, 203-216

3. *A brief guide to molecular mechanics and quantum chemical calculations* by W.J.Hehre, J.Yu, P.E.Klunzinger and L.Lou, Wavefunction, Inc., 1998

4. *Electrochemical Methods: Fundamentals and Applications* by A.J.Bard and L.R.Faulkner, John Wiley and Sons, 1980

5. L.J.Kettle, PhD Thesis, University of Edinburgh, 2000

6. J.G.Mackintosh and A.R.Mount, *J.Chem.Soc. Faraday Trans.*, 1994, **90(8)**, 1121-1125

7. P.Jennings, A.C.Jones, A.R.Mount and A.D.Thomson, *J.Chem.Soc. Faraday Trans.*, 1997, **93(21)**, 3791-3797

8. A.Bree and R.Zwarich, *J.Chem.Phys.*, 1968, **49(8)**, 3344-3355

9. A.Bree and R.Zwarich, *J.Chem.Phys.*, 1968, **49(8)**, 3355-3358

10. S.C.Chakravorty and S.C.Ganguly, *J.Chem.Phys.*, 1970, **52(5)**, 2760-2762

11. N.Mataga, Y.Torihashi and K.Ezumi, *Theoret.Chim.Acta*, 1964, **2**, 158-167

12. J.E.Adams, W.W.Mantulin and J.R.Huber, *J.Am.Chem.Soc.*, 1973, **95(17)**, 5477-5481

13. C.H.Pinkham and S.C.Wait, Jr., *J.Mol.Spec.*, 1968, **27**, 326-342

14. E.Honegger, R.Bombach and S.Leutwyler, *J.Chem.Phys.*, 1986, **85(3)**, 1234-1246

15. R.Bombach, E.Honegger and S.Leutwyler, *Chem.Phys.Lett.*, 1985, **118(5)**, 449-454

16. A.R.Auty, A.C.Jones and D.Phillips, *Chem.Phys.*, 1986, **103**, 163-182

17. D.M.Lubman, L.Li and T.M.Dunn, *J.Phys.Chem.*, 1989, **93**, 3444-3448

18. R.W.Bigelow and G.E.Johnson, *J.Chem.Phys.*, 1977, **66(11)**, 4861-4871

19. S.Y.Lee, B.H.Boo, *J.Phys.Chem.*, 1996, **100**, 15073-15078

20. S.M.Zain, R.Hashim, A.G.Taylor and D.Phillips, *J.Mol.Structure (Theochem)*, 1997, **401**, 287-300

21. G.E.Johnson, *J.Phys.Chem.*, 1974, **78(15)**, 1512-1521

22. R.W.Bigelow and G.P.Ceasar, *J.Phys.Chem.*, 1979, **83(13)**, 1790-1795

23. R.N.Lahiri, *Acta Crystallogr.A*, 1969, S3, 5

24. J.R.Platt, *J.Chem.Phys.*, 1949, **17(5)**, 484-495

25. *The Theory of the Electronic Spectra of Organic Molecules* by J.N.Murrell, Methuen & Co. Ltd., 1963

26. B.Fender and P.R.Callis, *Chem.Phys.Lett.*, 1996, **262**, 343-348

27. J.M.Hollas, *Spec.Acta*, 1963, **19**, 753-767

28. E.H.Strickland, J.Horowitz and C.Billups, *Biochemistry*, 1970, **9(25)**, 4914-4921

29. A.Z.Britten and G.Lockwood, *Spectrochim.Acta*, 1976, **32(6)**, 1335-1338

30. Y.Yamamoto and J.Tanaka, *Bull.Chem.Soc.Jpn.*, 1972, **45**, 1362-1366

31. B.Valeur and G.Weber, *Photochem.Photobiol.*, 1977, **25**, 441-444

32. A.A.Rehms and P.R.Callis, *Chem.Phys.Lett.*, 1987, **140(1)**, 83-89

33. J.R.Cable, *J.Chem.Phys.*, 1990, **92(3)**, 1627-1633

34. J.Hager and S.C.Wallace, *J.Phys.Chem.*, 1983, **87**, 2121-2127

35. Y.Nibu, H.Abe, N.Mikami and M.Ito, *J.Phys.Chem.*, 1983, **87**, 3898-3901

36. R.Bersohn, U.Even and J.Jortner, *J.Chem.Phys.*, 1984, **80(3)**, 1050-1058

37. J.W.Hager, D.R.Demmer and S.C.Wallace, *J.Phys.Chem.*, 1987, **91**, 1375-1382

38. D.M.Sammeth, S.Yan, L.H.Spangler and P.R.Callis, *J.Phys.Chem.*, 1990, **94**, 7340-7342

39. B.J.Fender, D.M.Sammeth, P.R.Callis, *Chem.Phys.Lett.*, 1995, **239**, 31-37

40. B.J.Fender, K.W.Short, D.K.Hahn and P.R.Callis, *Int.J.Quantum Chem.*, 1999, **72**, 347-356

41. A.Mani and J.R.Lombardi, *J.Mol.Spec.*, 1969, **31**, 308-317

42. L.A.Phillips and D.H.Levy, *J.Chem.Phys.*, 1986, **85(3)**, 1327-1332

43. B.Berden, W.L.Meerts and E.Jalviste, *J.Chem.Phys.*, 1995, **103(22)**, 9596-9606

44. L.A.Phillips and D.H.Levy, *J.Phys.Chem.*, 1986, **90**, 4921-4923

45. B.Albinsson, M.Kubista, B.Nordén and E.Thulstrup, *J.Phys.Chem.*, 1989, **93**, 6646-6654

46. B.Albinsson and B.Nordén, *J.Phys.Chem.*, 1992, **96**, 6204-6212

47. T.Takigawa, T.Ashida, Y.Sasada and M.Kakudo, *Bull.Chem.Soc.Jpn.*, 1966, **39**, 2369

48. W.Caminati and S.di Bernardo, *J.Mol.Structure*, 1990, **240**, 253-262

49. H.Lami and N.Glasser, *J.Chem.Phys.*, 1986, **84(2)**, 597-604

50. D.W.Pierce and S.G.Boxer, *Biophysical J.*, 1995, **68**, 1583-1591

51. J.R.Lombardi, *J.Phys.Chem.A*, 1999, **103**, 6335-6338

52. P-S.Song and W.E.Kurtin, *J.Am.Chem.Soc.*, 1969, **91(17)**, 4892-4906

53. P.R.Callis, *J.Chem.Phys.*, 1991, **95(6)**, 4230-4240

54. L.S.Slater and P.R.Callis, *J.Phys.Chem.*, 1995, **99**, 8572-8581

55. D.K.Hahn and P.R.Callis, *J.Phys.Chem A*, 1997, **101**, 2686-2691

56. L.Serrano-Andres and B.O.Roos, *J.Am.Chem.Soc.*,1996, **118**, 185-195

57. A.L.Sobolewski and W.Domcke, *Chem.Phys.Lett.*, 1999, **315**, 293-298

58. J.B.Foresman, M.Head-Gordon, J.A.Pople and M.J.Frisch, *J.Phys.Chem.*, 1992, **96**, 135-149

Chapter Five

ELECTROPOLYMERISATION OF INDOLO{3,2,1-*jk*}CARBAZOLE AND PYRROLO{3,2,1-*jk*}CARBAZOLE

5.1 Introduction

The electrochemical behaviour of indole and various substituted indoles has been the subject of extensive investigation by Mount and co-workers. In particular the electropolymerisation of indoles to form redox-active polymers and the nature of these polymers have been studied. It has been shown that indoles may be electropolymerised to form electroactive conducting polymers [1, 2, 3, 4]. The oxidation potentials of both the indole monomers and their polymers can be altered by substitution of the monomers at the 5-position with different electron-withdrawing groups such as cyano and carboxylic acid [3, 5]. Both the indole monomers and polymers also have high fluorescence quantum yields and therefore have a possible application as the light-emitting layer in organic light emitting diodes (LEDs) [6]. However, unlike the oxidation potentials, the fluorescence wavelengths of the indole polymers are not tuneable by substitution. In this thesis the electropolymerisation of the indole-based monomers indolo{3,2,1-*jk*}carbazole (IC) and pyrrolo{3,2,1-*jk*}carbazole (PC), the structures of which are shown in Figure 5.1, is investigated. These monomers have larger conjugated systems than the indoles and this increase in the extent of conjugation of the monomers may result in the formation of polymers with different fluorescence emission wavelengths to those of the indole polymers, whilst retaining the desirable electrochemical properties exhibited by the indole polymers.

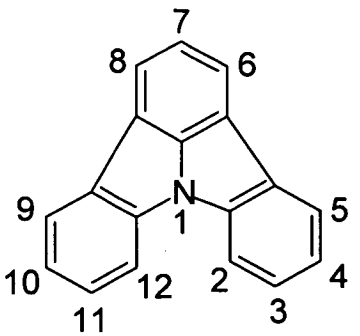

IC

(indolo{3,2,1-*jk*}carbazole)

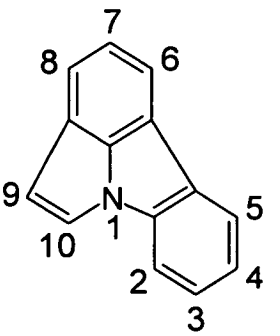

PC

(pyrrolo{3,2,1-*jk*}carbazole)

Figure 5.1: Molecular structures of IC and PC and the numbering system adopted for this thesis.

In this chapter the electrochemical behaviour of IC and PC and the formation of the polymers is described. The experimental set-up for all the electrochemical work described here is given in chapter three.

5.2 Prediction and measurement of oxidation potentials

The potentials at maximum current or peak oxidation potentials, E_p, of the monomers IC and PC were measured using linear sweep voltammetry (LSV). In similar studies on indoles it was found that indole monomers are oxidised to form radical cations which then couple to form polymer [3]. The rate of such a coupling is given by:

$$\text{rate} = k[m^{+\bullet}]^2 \qquad (5.1)$$

where k is the rate constant and $[m^{+\bullet}]$ is the concentration of the radical cation, $m^{+\bullet}$. The presence of such coupling of monomer to form polymer could affect the shape of the LSV curve of the monomer. Therefore to minimise any such effects low concentration (0.6 mM) solutions of monomer in electrolyte were used to measure E_p.

The results, together with results for indole for comparison, are given in Table 5.1. The experimental oxidation potentials are all quoted relative to the standard electrode potential of Fc/Fc^+. They were measured against a Ag/Ag^+ (0.01 M) reference electrode and the standard electrode potential of the Fc/Fc^+ couple was measured against this reference electrode for each experiment to allow conversion.

	Indole	IC	PC
E_p/ V	0.91*	1.03	0.79
$\|E_p-E_{p/2}\|$ / mV	-	62	79
$E_{1/2}$ / V	0.80*	1.00	0.76
E^{θ}_{calc} / V	0.70	0.79	0.82
E_{pol} / V	1.31*	1.10	0.82

* A computational and electrochemical study of electropolymerised indoles by L.J.Kettle, PhD Thesis, University of Edinburgh, 2000.

Table 5.1: Monomer peak oxidation potentials E_p, difference between E_p and the potential at the half peak height $E_{p/2}$, polarographic half-wave potential $E_{1/2}$, predicted oxidation potentials E^{θ}_{calc} and polymerisation potentials (see text) E_{pol} for indole, IC and PC. All are quoted relative to the standard electrode potential for Fc/Fc^+.

The expected value of $|E_p-E_{p/2}|$ for an electrochemically reversible one electron (Nernstian) system is 56.5 mV at 298 K. The values of $|E_p-E_{p/2}|$ for IC and PC shown in Table 5.1 are both larger than 56.5 mV which suggests that the one electron oxidation of these molecules is not electrochemically reversible. However, as discussed in chapter four, values of $|E_p-E_{p/2}|$ for the Fc/Fc^+ couple, which is known to be electrochemically reversible, were greater than 56.5 mV when measured using the same system. They also showed an increase with increasing sweep rate and this suggests the presence of a significant iR drop in the system. This is where there is some resistance across the electrolyte between the working and reference electrodes and is a particular problem in systems using non-aqueous solvents, such as the acetonitrile used here. Since the value of $|E_p-E_{p/2}|$ of 85 mV at a sweep rate of 100 mV s^{-1} for Fc/Fc^+ is similar to those recorded for IC and PC of 62 and 79 mV at the same sweep rate and similar concentrations, this is consistent with one electron electrochemically reversible behaviour for both monomers.

This assumption of electrochemical reversibility allows the values of $E_{1/2}$ to be calculated as $E_{1/2}$=Ep-28.3 mV in this case, and these values may be compared directly to the calculated values of E^{θ}, assuming that the diffusion coefficients of the oxidised and reduced species are equal, as discussed in chapter four. The method and basis set used to calculate E^{θ} was B3PW91/6-311G(2d,2p) for the organic neutral and radical cations and B3PW91/6-31G(d,p) for Fc and Fc^+, with the effects of solvation included using the COSMO solvation model, as described in chapter four. The experiments show that IC has the highest oxidation potential of the three molecules and PC has the lowest. However this trend is not followed by the calculations which predict PC to have the highest oxidation potential and indole to have the lowest. The results shown in Table 5.1 appear to show that the predicted oxidation potential for

PC is closest to the experimental oxidation potential. However in chapter four the results of similar calculations on indole, 5-hydroxyindole, 5-cyanoindole, carbazole and pyrrole were discussed. It was found that the method of calculating oxidation potentials used here correctly predicted the ordering of the oxidation potentials of these five molecules. In each case the calculated oxidation potential was lower than the measured oxidation potential by between 0.07 and 0.19 V, suggesting the presence of a systematic error. The oxidation potential calculated for IC is 0.21 V lower than the experimental value, which is close to maximum error of 0.19 V obtained for the five test molecules in chapter four. Also this method correctly predicts the oxidation potential of IC to be greater than the oxidation potential of indole. However out of all the seven molecules calculated, PC is the only one for which the calculated oxidation potential is greater than the experimental oxidation potential. This suggests that either there is something different about the oxidation of PC at the electrode surface compared to the oxidation of the other molecules at the electrode surface or there is some unsystematic error involved with this calculation. Such an error in the calculation seems unlikely. One possible source of deviation of the experimental measurement of the oxidation potential is from adsorption of PC onto the electrode surface. This may change the energetics of electron transfer sufficiently to affect the measured E^{θ} value. This was found to occur for both 5-hydroxy and 5-aminoindole [3]. However it is unlikely that such binding occurs for PC as, unlike for 5-hydroxy and 5-aminoindole, the nitrogen or oxygen lone pairs are not available to facilitate binding, but are delocalised around the ring. Also, it is hard to see why IC and PC would behave so differently. Therefore it is unclear what is causing the difference in the calculated and experimental oxidation potentials for PC compared to the other molecules.

The polymerisation potentials, E_{pol}, shown in Table 5.1 were chosen by examination of the CVs recorded for IC and PC at 0.6 mM. Ideally the polymerisation potential to be used in the potential step voltammetry experiments should be well past the peak, in the mass-transport region of the CV, to ensure that all the monomer reaching the electrode surface reacts rapidly. This minimises the effect of the change in surface electrochemical reactivity when forming a surface film. However, it is also advisable not to choose a polymerisation potential so high as to cause further oxidation reactions. The CVs for IC and PC at 0.6 mM are shown in Figure 5.2 and 5.3 respectively. In Figure 5.2 it is possible to see the oxidation peak of the IC monomer at 1.03 V vs Fc/Fc^{+}. There is also a small reduction peak at ~0.91 V vs Fc/Fc^{+}, which is probably due to small amounts of unreacted monomer radical cation being reduced. In the CV of an

electrochemically reversible reaction the reduction peak lies at the same potential as the half peak potential, $E_{p/2}$, of the oxidation peak and therefore the oxidation and reduction peaks will be 56.5 mV apart. In the case of IC the oxidation and reduction peaks are ~120 mV apart. This is again likely to be due to iR drop in the system as the oxidation and reduction peaks for the reversible Fc/Fc^+ couple at comparable concentrations were 140 mV apart when measured using the same system and sweep rate. Although the concentration is low, which will reduce the ability of radical cations to couple to form a polymer film, redox peaks for the a polymer film are seen growing with each cycle. Indeed, a green film, insoluble in acetonitrile, was formed on the surface of the working electrode during this experiment.

The CV for PC at the same concentration shown in Figure 5.3 is similar to that for IC, but there is no discernable evidence of redox peaks for a polymer although a small precipitate of brown solid was observed on the surface of the working electrode. Also there is no PC reduction peak visible.

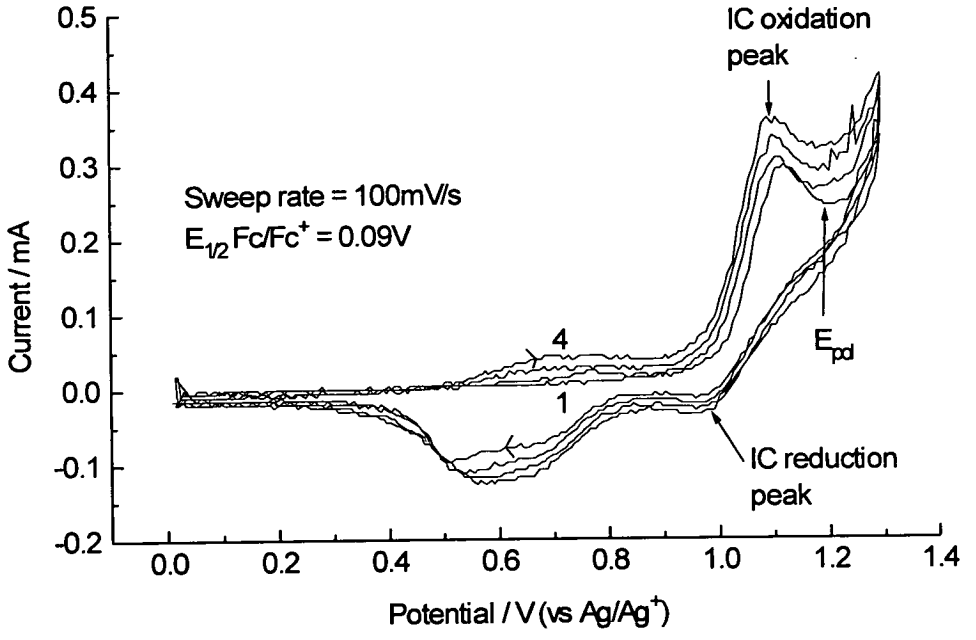

Figure 5.2: CV, cycles 1 to 4, recorded for 0.6 mM IC in electrolyte showing monomer oxidation peak, E_p, at 1.03 V vs Fc/Fc$^+$, polymerisation potential, E_{pol}, at 1.10 V vs Fc/Fc$^+$ and polymer film redox peaks at ~0.7 (oxidation) and 0.45-0.80 V (reduction).

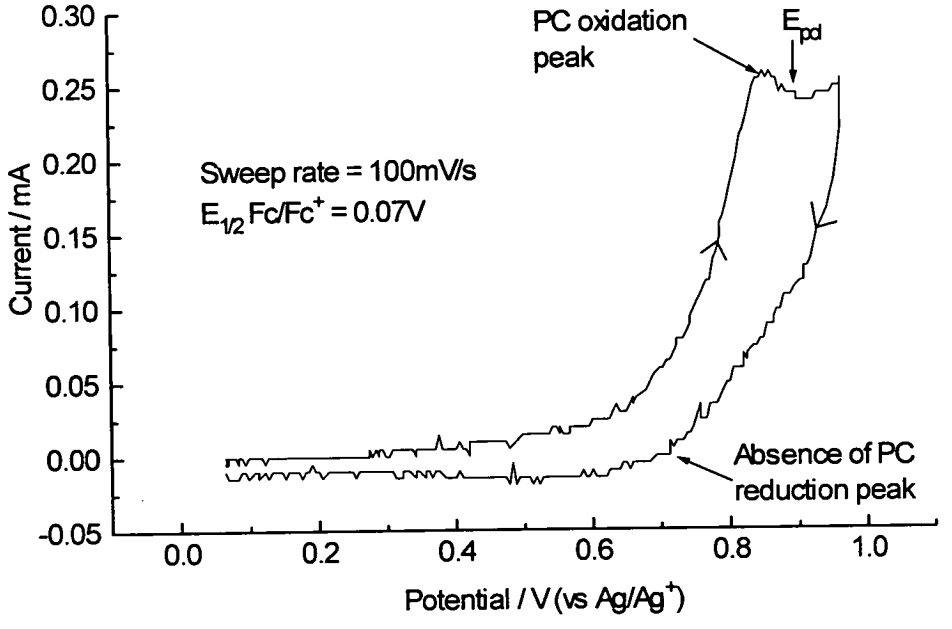

Figure 5.3: CV recorded for 0.6 mM PC in electrolyte showing monomer oxidation peak, E_p, at 0.79 V vs Fc/Fc$^+$ and polymerisation potential E_{pol} at 0.82 V vs Fc/Fc$^+$.

5.3 Spin density distributions of the IC and PC radical cations

It has been suggested that indole electropolymerises to form a trimer *via* linkage of two indole radical cations (indole$^{\bullet+}$) at the 3-position followed by reaction with another indole$^{\bullet+}$. In support of this, spin density calculations using the software DMol^3 have predicted the highest spin density to lie at this 3-position in indole$^{\bullet+}$ [5], and it could be expected that coupling would occur between sites of the highest radical electron density. Therefore it may be possible to predict the linkage sites of other monomers using such spin density calculations. Calculations discussed in chapter four showed that the method and basis set B3PW91/6-31G(d,p) using the software G98 also predicted the highest spin density at the 3-position of the indole$^{\bullet+}$ and so the spin density distributions of IC$^{\bullet+}$ and PC$^{\bullet+}$ were calculated using this method. The results are shown in Figure 5.4. The numbering systems for these molecules are shown in Figure 5.1.

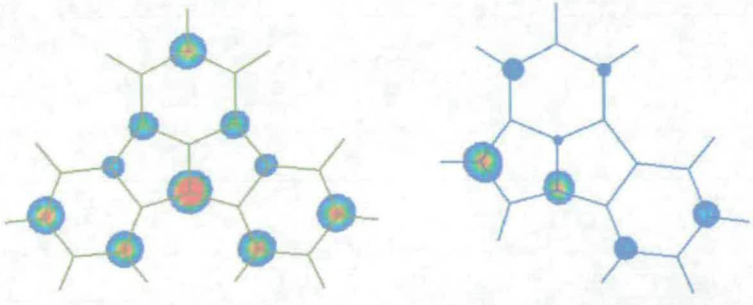

Figure 5.4: Spin density distributions in IC$^{\bullet+}$ and PC$^{\bullet+}$ calculated with B3PW91/6-31G(d,p). Red is the maximum and blue is the minimum spin density.

The IC$^{\bullet+}$ spin electron appears to be more widely delocalised than the PC$^{\bullet+}$ spin electron. Its distribution also reflects the C_{2V} symmetry of the molecule. Apart from the N, on which the most spin density is located, there are four positions, 2, 4, 10 and 12 (see Figure 5.1), which have approximately the same spin density and one position, 7, showing slightly less. This means there could be five likely linkage positions per molecule. The first step in any polymerisation is likely to be the formation of a dimer and it is interesting to consider the possible products of dimerisation given the above spin density distribution of IC$^{\bullet+}$. From five linkage positions there are twenty-five possible dimers. However this number may be reduced to six ((12,2'), (4,2'), (7,2'), (10,4'), (7,4') and (7,7')) using symmetry. Flat geometries are likely to be more stable than twisted geometries as they will have greater delocalisation of the π-system. Assuming the dimers are flat (or nearly flat), there will be two possible orientations of each dimer,

corresponding to 180^0 rotation about the linking bond (cis and trans), for all except the ones involving the 7 position. This increases the possible combinations to nine, which is rather a lot to consider. However some of these dimers are less likely to be formed than others due to steric hindrance. If the dimers are flat, one of the (12,2') and one of the (4,2') dimers may be definitely discounted on steric grounds. The remaining (12,2'), (4,2') and (7,2') dimers are unlikely to be stable due to steric hindrance, which leaves the four dimers involving the 4 and 7 positions (7,4'), (7,7'), (cis-10,4') and (trans-10,4') as the most likely products of dimerisation. Of course such reasoning involves a number of assumptions, such as that the loss of protons occurs after coupling and that the thermodynamics of the product determine which is formed, and is not based on experimental evidence. Therefore the conclusions drawn should only be used as a guide to subsequent investigations into the polymerisation of IC.

The spin density distribution of $PC^{\bullet+}$ is much simpler than that of $IC^{\bullet+}$, with the spin electron distributed approximately equally between the N and position 9 of the ring. If PC is thought of as two fused indoles, position 9 is in fact the linkage position for one of the indoles, ie the 3 position, where the spin electron of $indole^{\bullet+}$ is most likely to be. The 3 position of the other indole shows no spin density and is not available for linkage anyway. This suggests that a 9,9' dimer of PC is the most likely route for polymerisation. However formation of a trimer from the 9,9' dimer in the manner observed for indole is not possible for steric reasons, as illustrated in Figure 5.5. It must be remembered, though, that the spin density of $PC^{\bullet+}$ may be less reliable than that for $IC^{\bullet+}$ as the calculation of the oxidation potential may be suffering from an unsystematic error, as described above.

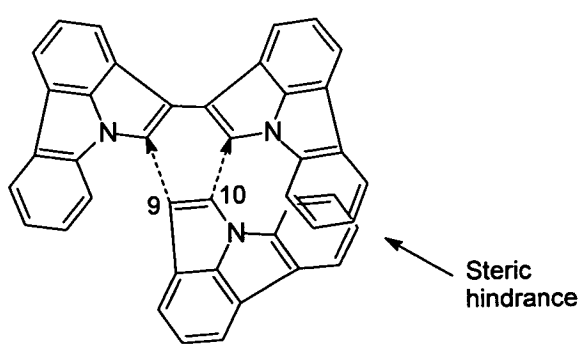

Figure 5.5: Illustration of how steric hindrance would prevent the formation of a PC trimer in the manner observed for indole. The numbering system for PC is shown in Figure 5.1.

5.4 Electropolymerisation of IC

IC was polymerised at 1.10 V vs Fc/Fc^+, at concentrations of 10 mM, 20 mM and 30 mM in electrolyte, at rotation speeds of 1 to 9 Hz, using the technique of potential step voltammetry as described in chapter two. The maximum obtainable concentration of IC in electrolyte before the solution became saturated was found to be ~30 mM. Figure 5.6 shows a typical current-time transient for such an experiment, in this case at a rotation speed of 2 Hz and concentration of 30 mM. During each of these experiments a green-black, electroactive film was formed on the surface of the rotating disc electrode (RDE). This film was found to be completely soluble in both DMF and DMSO in contrast to indole films which were partially soluble in DMF and completely soluble in DMSO [1]. Polymerisation at a constant potential and rotation speed was found to produce a current which was constant with time at rotation speeds from 1 to 9 Hz, indicating that the film formed is conducting. For a non-conducting (insulating) film the current would be expected to decrease with time as the coat became progressively thicker.

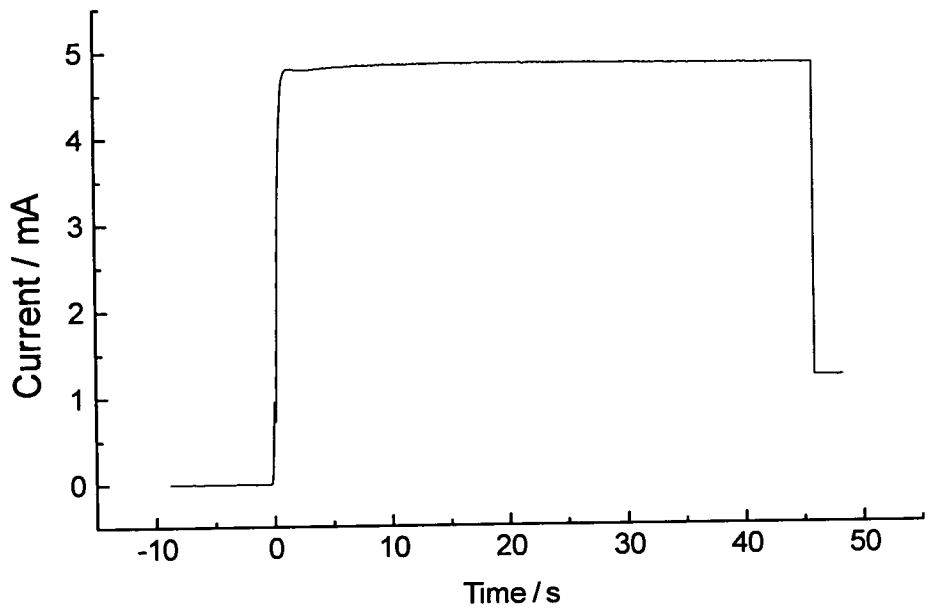

Figure 5.6: Current-time transient for polymerisation of IC from a 30 mM solution of IC in electrolyte at 2 Hz rotation speed.

Where the rate-determining step is linkage of radical cations and this occurs in solution at a RDE, as the rotation speed increases the efficiency of the removal of solution species from the diffusion layer increases and therefore the concentration of radical cation in the diffusion layer decreases. As the rate of polymer film formation will depend on the radical cation

concentration, the time taken to form a polymer film under such conditions will increase as the rotation speed increases. Where the rate-determining step is transport of monomer to the electrode to react and form radical cations, however, the time taken to reach a steady-state will decrease as the rotation speed increases. It was found that the electropolymerisation of indoles initially proceeds *via* linkage of radical cations in solution until a polymer film is deposited on the electrode surface. The mechanism then involves adsorption and oxidation of monomer on the electrode surface followed by linkage [1]. The different times taken to reach a steady-state current at various rotation speeds for the electropolymerisation of IC are given in Table 5.2.

Rotation speed / Hz	Time taken to reach steady-state / s
1	1.8
2	1.7
4	7.6
9	7.2

Table 5.2: Times taken to reach a steady-state current in the electropolymerisation of IC at various rotation speeds of the RDE.

The time taken to reach a steady-state increases from ~1.8 s at slow rotation speeds (1 and 2 Hz) to ~7.5 s at fast (rotation speeds). This is consistent with initial film formation occuring in solution.

One monolayer of thionine (bis-amino phenothiazonium cation) π-stacked flat on a gold surface has been found [7] to have a mole density of 3×10^{-10} moles cm^{-2}. $IC^{\bullet+}$ is similar to thionine in that it is a flat heterocyclic aromatic cation and it is likely that it also π-stacks flat on the Pt electrode surface. However thionine is a slightly smaller molecule than $IC^{\bullet+}$ and so this value of the mole density can be taken as an upper limit on the mole density of a monolayer of $IC^{\bullet+}$. In fact the area covered by one $IC^{\bullet+}$ molecule was calculated as approximately 1×10^{-14} cm^2 from a B3PW91/6-311G(2d,2p) geometry optimisation incorporating solvation by acetonitrile using the continuum solvation model COSMO (see chapter two). Allowing a factor of two for the presence of anions and the spacings between the molecules this gives an approximate mole density of 7.9×10^{-11} mol cm^2. Using this mole density value and assuming that 1.5 electrons are removed per molecule (see section 5.5 of this chapter), the approximate charge required to coat the surface of the electrode of area 0.387 cm^2 with a monolayer of $IC^{\bullet+}$ molecules is 4.5×10^{-6} C.

For all experiments the charge passed during the time required for the current to reach a steady-state was greater than 1×10^{-3} C, and was therefore three orders of magnitude greater than the charge required to coat the surface of the electrode with a monolayer of $IC^{\bullet+}$ molecules. This suggests that by the time a steady-state current is reached the electrode surface is completely covered with IC polymer film. Therefore, as with indole, the steady-state current observed in these experiments can be attributed to the current associated with electrooxidation of IC onto an oxidised polymer film surface.

The polymer films were rinsed in acetonitrile to remove any residual monomer IC and studied by cyclic voltammetry (CV) in background electrolyte. Such CVs of IC films show two overlapping oxidation peaks and two overlapping reduction peaks. Similar behaviour has previously been observed in the CVs of films of indole-5-carboxylic acid and 5-cyanoindole formed under similar conditions [1, 2]. In the indole films the redox peaks to higher potential were found to decrease in intensity with repeated cycling in background electrolyte and were attributed to the chemically irreversible polymerisation of the trimer units. The redox peaks to lower potential were found to be relatively stable with repeated cycling and were attributed to the one electron oxidation and reduction of the trimer units. To investigate the behaviour of the IC films a film formed at 4 Hz from a 20 mM solution of IC in electrolyte was cycled in background electrolyte at a constant sweep rate of 20 mV s^{-1}. The resulting CV is shown in Figure 5.7. During the recording of the CV shown in Figure 5.7, the film was held at a reducing potential between each cycle so that the whole film was in its reduced state at the start of each cycle.

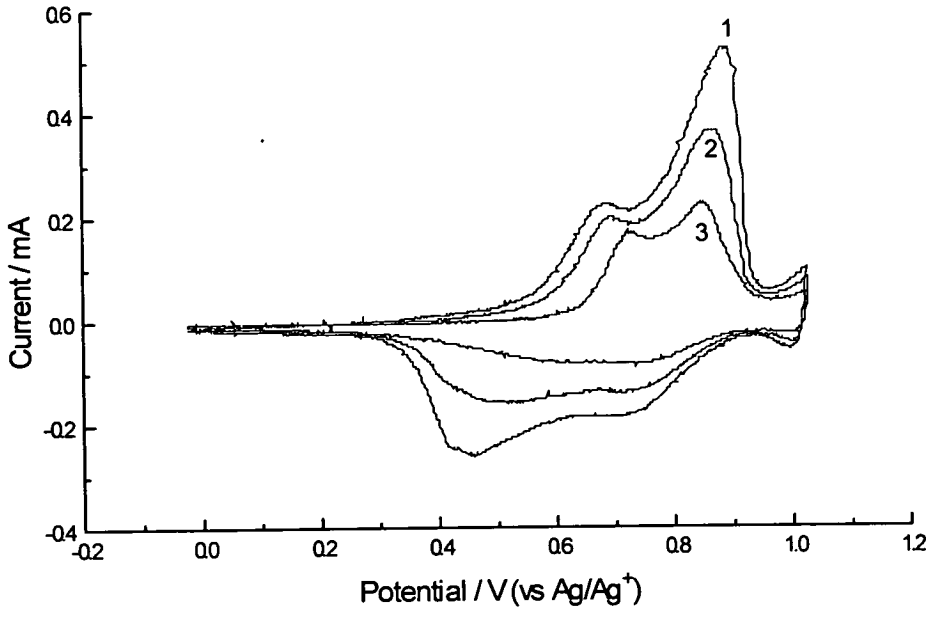

Figure 5.7: Cycles 1, 2 and 3 of an IC film formed from a 20 mM solution of IC in electrolyte at 4 Hz rotation speed, in background electrolyte at a sweep rate of 20 mV s^{-1}.

In the first cycle shown in Figure 5.7 the two oxidation peaks can be seen at 0.73 (first oxidation peak) and 0.85 V (second oxidation peak) and the two reduction peaks at 0.40-0.45 and 0.70-0.75 V. The small rise in current and the back peak at ~1.0 V may be due to the oxidation and reduction of some IC monomer which did not dissolve when the film was washed in acetonitrile, remaining trapped in the film.

In contrast to the behaviour observed for the indole films, neither set of redox peaks for the IC film is stable with repeated cycling. Rather, as shown in Figure 5.7, the intensities of all the redox peaks decrease with each cycle. In fact it was found that with repeated cycling eventually the redox peaks disappear. At the start of the experiment the electrode surface was coated with a thick film which, by the end of the experiment, had largely disappeared leaving only a thin coating. This suggests that the loss of intensity of all the redox peaks with cycling is due to solubility of the IC film in the electrolyte. It can be seen in Figure 5.7 that, in the first two cycles of the CV shown in Figure 5.7, the intensity of the second (0.85 V) oxidation peak drops more from cycle 1 to 2 than the intensity of the first (0.73 V) oxidation peak, although the shapes and positions of these peaks are very similar in the two cycles. This is consistent with the second oxidation peak being due to chemically irreversible linkage of small polymer units in the

film, as observed for indoles, or with this peak causing the solubility of the film in electrolyte. In the third cycle, however, the first oxidation peak has shifted to higher potential and become sharper than the first oxidation peaks in cycles one and two. There is also a noticeable difference in the reduction portion of the CV in the third cycle compared with the first two cycles. This indicates that there is a change in the coat structure as the film becomes thinner. The shift in the first oxidation peak to higher potential indicates that the kinetic barrier to the oxidation of the film, which arises from the necessity of the coat structure opening up to allow anions to enter the film and balance the positive charges, has increased for the thinner film, even though the film has become thinner, which would normally increase reaction kinetics.

CVs were measured at different sweep rates, v, from 10 to 200 mV s^{-1} for an IC film in background electrolyte. This film was polymerised at 4 Hz from a 20 mM solution of IC in electrolyte, as was the film used for the CVs in Figure 5.7. Examples of these CVs are shown in Figure 5.8. Again, during the recording of these CVs the film was held at a reducing potential between each cycle so that the whole film was in its reduced state at the start of each cycle. The CV for the slowest sweep rate was recorded first and the fastest last.

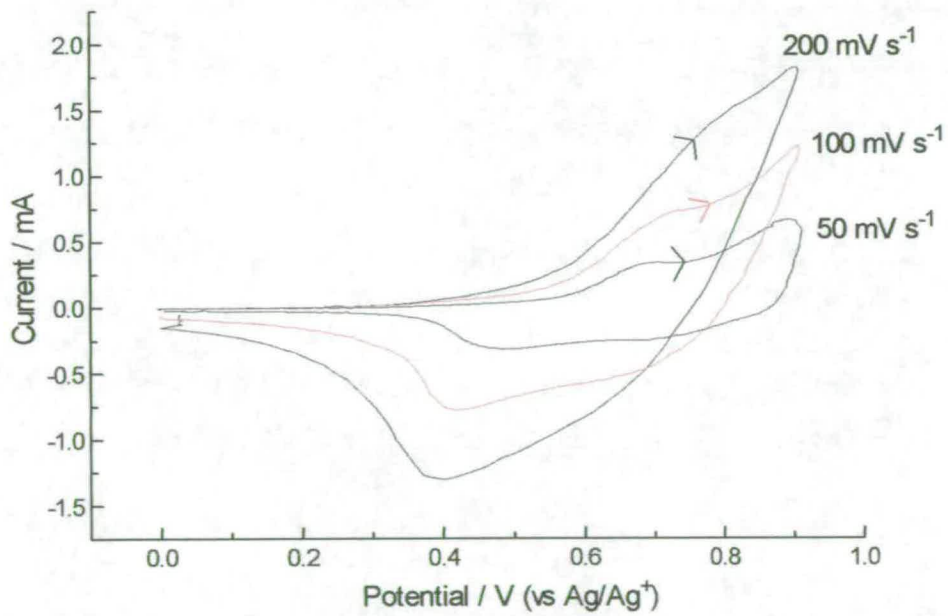

Figure 5.8: CVs, at sweep rates of 50, 100 and 200 mV s^{-1}, of a film formed from a 20 mM solution of IC in electrolyte.

As discussed in chapter two, where the redox active species forms a film which is adsorbed onto the electrode surface i_p is proportional to $v^{1/2}$ when film kinetics are slow with respect to v and the whole film is not reduced/oxidised on each sweep. Where film kinetics are fast and the whole film is reduced/oxidised on each sweep i_p is proportional to v. For this latter relationship to hold true the amount of film adsorbed onto the electrode surface must be the same for each sweep and therefore such a plot may be used to test if a film is dissolving off the electrode surface. A plot of the peak oxidation currents and peak reduction currents of the first (lowest potential) set of redox peaks against sweep rate is shown in Figure 5.9.

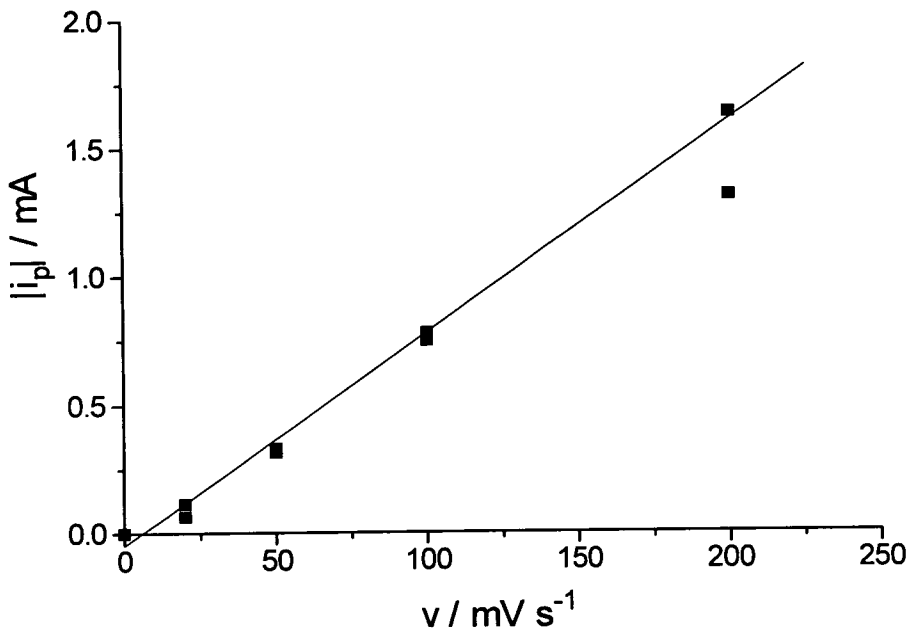

Figure 5.9: A plot of the peak oxidation and reduction currents, $|i_p|$, of the first oxidation peak against sweep rate, v, from the CVs of a film formed from 20 mM IC in electrolyte at a rotation speed of 4 Hz shown in Figure 5.8.

Figure 5.9 shows that at sweep rates up to and including 200 mV s^{-1}, both the peak oxidation and reduction currents are proportional to v. Therefore at these sweep rates the whole film is being oxidised and reduced on each sweep. This is not true for all IC films as it depends on the thickness of the film, which may be controlled by the polymerisation time and rotation speed of the RDE. For thicker IC films it has been observed that the proportional relationship of peak current to sweep rate fails. This failure occurs for the fastest sweep rates first. The fact that the peak currents are proportional to sweep rate in Figure 5.9 also means that this film is not

dissolving off the electrode surface. This is contrast to the CVs shown in Figure 5.7, which suggested that IC films are soluble in electrolyte. However the upper potential of the CVs shown in Figure 5.8 is 0.9 V, which is lower than the upper potential of 1.0 V of the CVs shown in Figure 5.7. Also, the sweep rate used for the CVs shown in Figure 5.7 was only 20 mV s^{-1}. At faster sweep rates the oxidation peaks are shifted to higher potential, as shown in Figure 5.8. Therefore the film in Figure 5.8 is not undergoing the second oxidation which peaks at ~0.85 V in Figure 5.7 and therefore these results are consistent with the solubility of the IC film being caused by the second oxidation peak at ~0.9 V.

The change in steady-state current with rotation speed was measured for bulk concentrations of 30, 20 and 10 mM of IC in electrolyte. The data for a particular concentration was recorded in a single experiment so that any surface changes to the RDE between experiments would not affect the results. An example of the current-time transient obtained during such an experiment is shown in Figure 5.10, in this case for the 10 mM solution. There is a slight increase in the current during the experiment, which can be seen in Figure 5.10 by comparing the current associated with a 1 Hz rotation speed at the start and end of the experiment. This increase is due to the increase in the surface area of the electrode as it is coated with polymer film.

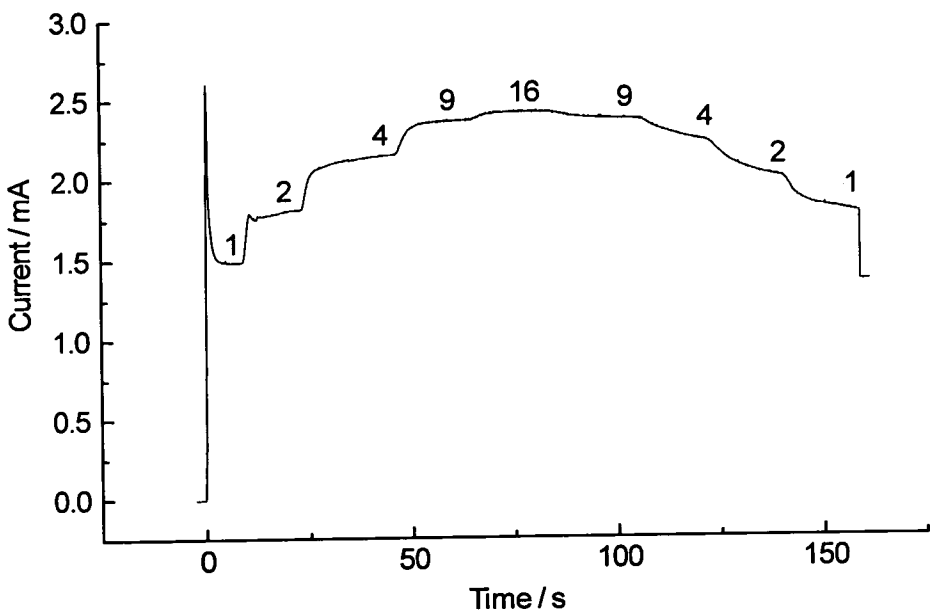

Figure 5.10: Current-time transient for the electropolymerisation of 10 mM IC in electrolyte at E_{pol} at rotation speeds 1, 2, 4, 9 and 16 Hz.

The data was plotted according to the Koutecky-Levich equation:

$$\frac{1}{i_{obs}} = \left(\frac{0.6435 \nu_{MeCN}^{1/6}}{nFAc_{\infty,IC} D_{IC}^{2/3} W^{1/2}} \right) + \frac{1}{i_{\infty}} \qquad (5.2)$$

where i_{obs} is the observed (steady-state) current, n is the number of electrons needed to reduce or oxidise one molecule of reactant, F is Faradays constant, A is the area of the Pt disc (0.387 cm^2), D_{IC} is the diffusion coefficient of the reactant IC (cm^2 s^{-1}), W is the rotation speed of the RDE (Hz), ν_{MeCN} is the kinematic viscosity of acetonitrile (cm^2 s^{-1}), $c_{\infty,IC}$ is the bulk concentration of reactant (IC) and i_{∞} is the current observed as W tends to infinity, when the current is independent of mass transport. Examples of Koutecky-Levich plots for each bulk concentration are shown in Figure 5.11. In each case the steady-state currents observed at the start of the experiment were used.

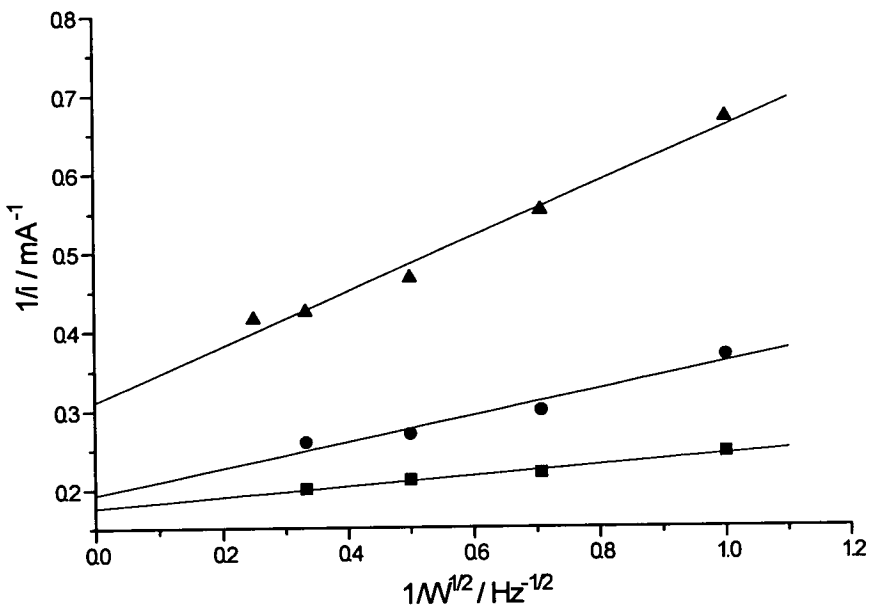

Figure 5.11: Koutecky-Levich plots for 10 mM (▲), 20 mM (●) and 30 mM (■) solutions of IC in electrolyte.

The data in Figure 5.11 lie on a straight line for each bulk concentration. Therefore the oxidation reaction is first order in monomer as this is an assumption of the Koutecky-Levich equation. This was also found to be the case for the electropolymerisation of indoles [1, 2, 3]. The gradients of the Koutecky-Levich lines such as those shown in Figure 5.11 can be used to estimate a value of the diffusion coefficient of IC, D_{IC}, if the value of n is known. Mass spectroscopy and NMR studies of the product of IC electropolymerisation (see section 5.5 of this

chapter) have shown oxidised IC dimer is formed, and therefore n is 1.5. Using this value of n the overall average value of D_{IC} was calculated as 5.9×10^{-5} cm^2 s^{-1} ($\pm$ 2.0×10^{-5}). This was calculated from all the experiments carried out on the 10 and 20 mM concentrations (five in all) and two out of the six experiments carried out on the 30 mM solution. For all these experiments the values of D_{IC} calculated were the same within their error limits. The values of D_{IC} calculated for the remaining four experiments carried out on the 30 mM solution were discounted as they were an order of magnitude greater than this with an average of 2.4×10^{-4} cm^2 s^{-1}. An anomalously high diffusion coefficient has previously been observed for 5-hydroxyindole [3], and this was attributed to the effects of 5-hydroxyindole aggregating in solution. The overall average calculated value of D_{IC} of 5.9×10^{-5} cm^2 s^{-1} ($\pm$ 2.0×10^{-5}) is the correct order of magnitude for the diffusion coefficient of an organic molecule of this size and similar analysis of Koutecky-Levich plots gave a value of 3×10^{-5} cm^2 s^{-1} for the diffusion coefficient of indole-5-carboxylic acid [1]. It might be expected that IC would be less well solvated than indole-5-carboxylic acid, and therefore would have a lower solvodynamic radius and hence a higher value of D.

The intercepts of the lines in Figure 5.11 give the value of the mass transport independent current, i_∞, for that bulk concentration. This gives the current where the concentration of IC at the electrode surface is equal to the bulk concentration of IC. The values of i_∞ calculated from the intercepts of the Koutecky-Levich plots at the three different concentrations are given in Table 5.3 together with their error limits.

Bulk concentration of IC in electrolyte / mM	i_∞ / mA
10	3.01 ± 0.30
20	5.06 ± 0.50
30	5.53 ± 0.24

Table 5.3: Values of the mass transport limited current, i_∞, at various bulk concentrations of monomer in electrolyte, taken from the intercepts of Koutecky-Levich plots.

It was found for the indole systems [1, 2, 3] that at bulk concentrations of indole of 10 mM or less the value of i_∞ decreases as the concentration decreases. This is because the electropolymerisation of indoles proceeds *via* a surface adsorbed intermediate and at these

concentrations there is no longer complete surface coverage of the electrode. Therefore the rate of film formation is limited by the surface coverage, controlled by the bulk concentration. At bulk concentrations greater than 10 mM it was found that the value of i_∞ remains constant as the concentration is varied, as there is complete surface coverage of the electrode and the rate of film formation is now limited by the area of the electrode. The results for the electropolymerisation of IC are similar to those for the indoles. The lowest value of i_∞ for the electropolymerisation of IC is 3.01 mA at 10 mM. As the bulk concentration of IC is increased to 20 mM the value of i_∞ increases to 5.06 mA and then to 5.53 mA for 30 mM. However the values of i_∞ for the 20 and 30 mM solutions are the same within their error limits. Therefore at concentrations above 10 mM the rate of film formation is limited by the area of the electrode surface and is independent of the bulk concentration of IC. The limiting value of i_∞ at large concentration can be taken as that for the 30 mM solution and is 5.5 mA (± 0.6). These results suggest that IC film formation proceeds *via* a surface adsorbed intermediate in a similar mechanism to indole film formation.

The limiting values of i_∞ at large concentration have been measured for indole-5-carboxylic acid and 5-cyanoindole in the same manner as that for IC and are 10 mA and 20 mA respectively [2]. This allows the rates of film formation for these three monomers to be compared. However it must be remembered that the rate of film formation will be dependent on the value of n as well as the value of the limiting i_∞ and the values of n are different for indole and IC electropolymerisation. For indole trimer formation n is $2^1/_3$ and for IC dimer formation n is 1.5. The ratio of the limiting i_∞ to the value of n is 3.67 for IC, 4.29 for indole-5-carboxylic acid and 8.57 for 5-cyanoindole. Therefore the rate of film formation for IC is approximately 0.9 times that of indole-5-carboxylic acid and 0.4 times that of 5-cyanoindole.

5.5 Structural characterisation of IC films

5.5.1 Mass spectrometry

Fast-atom bombardment (FAB) mass spectrometry was carried out by Stuart Wharton on an IC film in a 3-nitrobenzyl alcohol (3-NOBA) matrix. The parent ion peak was observed at 480 atomic mass units (amu). Given that the molar mass of the monomer is 241.278 g, this is the consistent with the species being a dimer in which the IC monomers have coupled to form one bond, and each has lost one H.

5.5.2 NMR

The ^{1}H NMR spectrum of an IC film in acetone d_6/DMSO d_6 was recorded by Stuart Wharton. The film was formed from a 20 mM solution of IC in electrolyte, by polymerisation at 1.10 V vs Fc/Fc^+ at a rotating disc electrode rotating at 4Hz. The spectrum is shown in Figure 5.12.

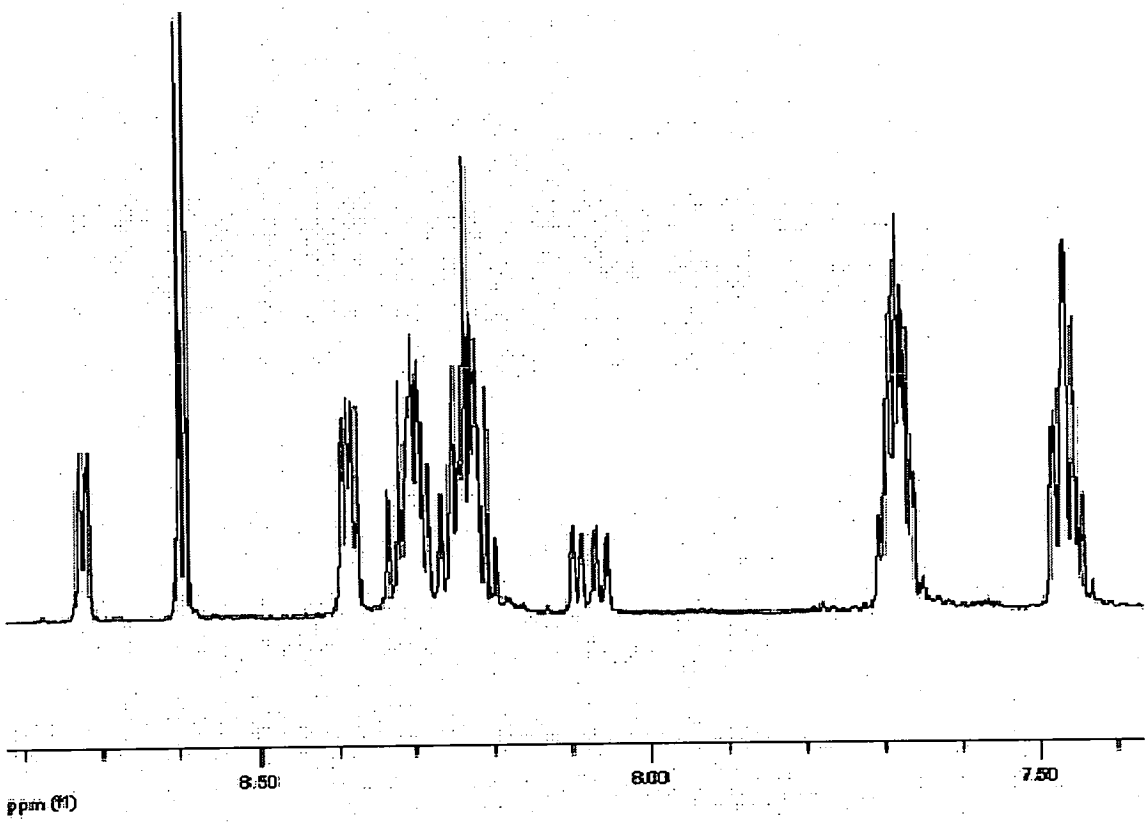

Figure 5.12: ^{1}H NMR spectrum of an IC film in acetone d_6/DMSO d_6.

The spectrum in Figure 5.12 shows well resolved peaks. This shows that the sample does not contain significant amounts of large polymer, as the slow tumbling rate of polymer in solution gives rise to broad unresolved peaks. The 1D and 2D ^{1}H NMR spectra of IC films were recorded and analysed and confirmed that the IC film is composed of dimer. The NMR shows the presence of 40 protons which corresponds to two different IC dimers and the peak integrals are comparable for all forty protons, which means that these two dimers are present in equal amounts. The two different dimer species present were shown to be likely to be the 7,3'-IC_2 dimer and the 7,4'-IC_2 dimer, the structures of which are shown in Figure 5.13.

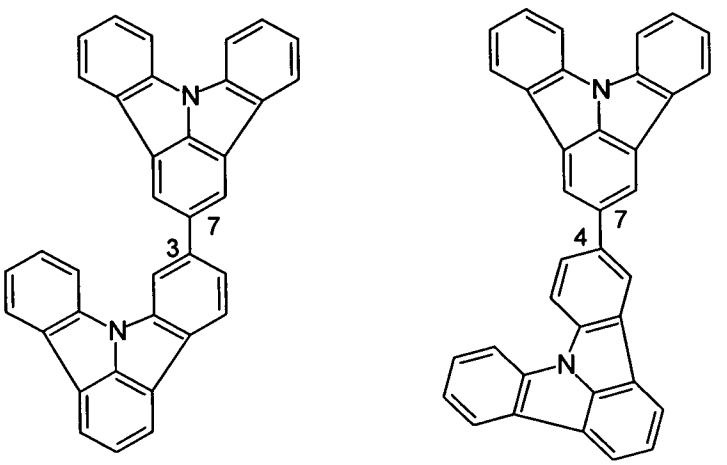

7,3'-IC2 7,4'-IC2

Figure 5.13: The structures of the two dimer species present in the IC film inferred from the NMR data.

The spin density distribution of $IC^{\bullet+}$ shown in Figure 5.4 shows spin density on the 2, 4 and 7 positions of the $IC^{\bullet+}$ ring. From this distribution four possible IC dimers were predicted involving the 4, 7 and 10 positions; 7,4', 7,7', cis-10,4' and trans-10,4'. Only one of these products, the 7,4'-dimer, is observed in the ^1H NMR of the IC film. This raises the question of why neither the 7,7' or the 10,4' dimers are formed, even though there does not appear to be any obvious steric hindrance preventing the molecules from coupling in any of these positions. The other dimer observed in the ^1H NMR is linked *via* the 3 position, which did not show any significant spin density in the calculation. Therefore, although successful in predicting the linkage site in indole electropolymerisation, the spin density calculation was unsuccessful in predicting the linkage sites of IC.

One possible explanation for the lack of success of these calculations is that they do not take into account a pertubation of the electron density of the radical cation caused by the approach of a second radical cation prior to linkage, which alters the positions at which the spin electron density is high from those predicted by the calculation. However if this were the dominant effect linkage would be expected to occur at all the available sites around the molecule. In fact there are only two products formed from the electropolymerisation of IC. This indicates that there is some other factor involved in determining the products of the electropolymerisation, for example the radical cations may be surface adsorbed only in specific orientations with respect to

one another, thus allowing linkage at only a limited number of sites. Overall these results show that the success of such spin density calculations in predicting the linkage site in indole electropolymerisation cannot necessarily be extrapolated to other aromatic monomers, especially where the spin density distribution contains more than one site of high density.

5.6 Electropolymerisation of PC

PC was polymerised at 0.82 V vs Fc/Fc^+ at a concentration of 30 mM PC in electrolyte, at rotation speeds of 1 to 9 Hz, using the technique of potential step voltammetry as described in chapter two. As for IC, polymerisation of PC resulted in the formation of a brown-black, electroactive film on the surface of the RDE. However, in contrast to the potential step voltammetry experiments performed with the IC monomer, a steady-state current was not obtained for any voltammetry experiment with the PC monomer. Rather, for each experiment performed, the current was found to decrease with time. This decrease in current as the coat becomes progressively thicker suggests that the PC film may be non-conducting.

For a non-conducting film it would be expected that as the rotation speed is increased, the rate of decrease of the polymerisation current with time should also increase. This is because as the rotation speed increases, the rate at which monomer is brought to the electrode surface increases, and hence the rate of growth of the film on the electrode surface increases. However this was not observed for PC polymerisation. Instead, as the rotation speed was increased, the rate of decrease of the polymerisation current with time decreased. This is illustrated by the typical current-time transients for such experiments shown in Figure 5.14.

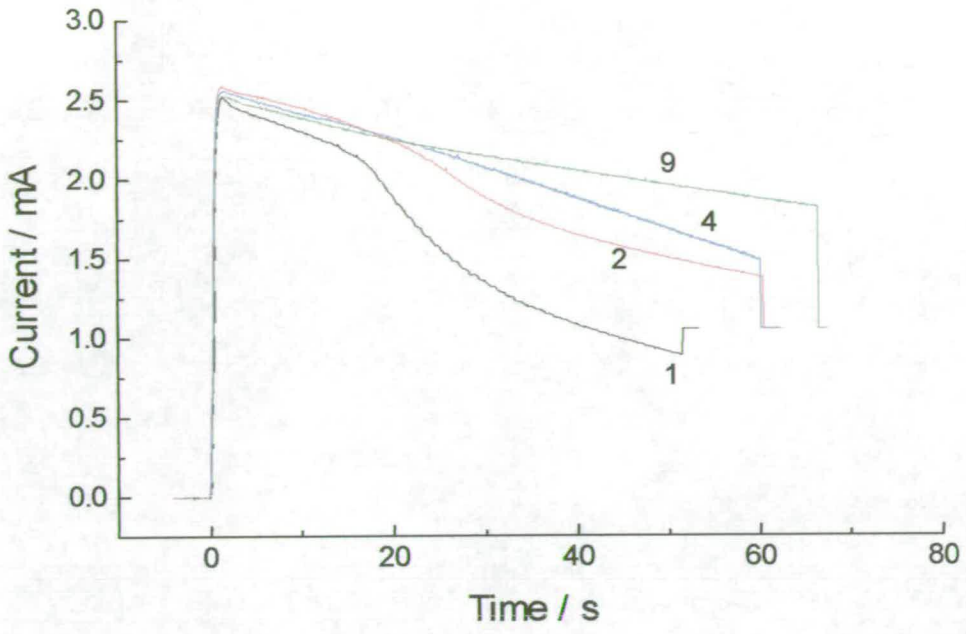

Figure 5.14: Current-time transients for polymerisations of PC from a mM solution of PC in electrolyte at rotation speeds of 1 Hz (black), 2 Hz (red), 4 Hz (blue) and 9 Hz (green).

The data shown in Figure 5.14 suggests that the reason the polymerisation current for PC drops with time may be something other than the formation of an intrinsically non-conducting film. For example, there may be some soluble impurities formed at the electrode. This is a plausible explanation as PC is more reactive than IC and therefore may have undergone some oxidation in air during storage. The absence of a steady-state current with time for the PC polymerisation meant that Koutecky-Levich analysis was not possible.

The PC films were found to be completely soluble in DMSO and partially soluble in DMF. This was also found to be the case for indole polymer films [1, 2].

5.7 Conclusions

The peak oxidation potentials of the IC and PC monomers have been measured experimentally using linear sweep voltammetry. These potentials have enabled the calculation of polarographic half-wave potentials, which have been compared to oxidation potentials calculated using B3PW91/6-311G(2d,2p) for the organic neutral and radical cations and B3PW91/6-31G(d,p) for Fc and Fc^+, as described in chapter four. The polarographic half-wave potential of IC is 1.00 V vs Fc/Fc^+ and of PC is 0.76 V vs Fc/Fc^+. The calculated value for the oxidation potential of IC is 0.21 V lower than the experimental value, which is in line with the systematic error for this type of calculation, as observed in the test calculations described in chapter four. However the calculated value for the oxidation potential of PC is greater than the experimental value. This suggests that there may be something different about the oxidation of PC at the electrode surface compared to the oxidation of the other molecules at the electrode surface. Suitable potentials for the polymerisation of IC and PC with potential step voltammetry are 1.10 V vs Fc/Fc^+ and 0.82 V vs Fc/Fc^+ respectively.

The spin density distributions of $IC^{\bullet+}$ and $PC^{\bullet+}$ have been calculated with B3PW91/6-31G(d,p) in order to predict the possible linkage sites of these molecules to form dimers. From the calculation of the spin density distribution of $IC^{\bullet+}$ four dimers are predicted. These are the 4,7', 7,7', cis-4,10' and trans-4,10' dimers. From the calculation of the spin density distribution of $PC^{\bullet+}$ it is predicted that two $PC^{\bullet+}$ molecules will link *via* their 9 positions only.

The electropolymerisation of IC by potential step voltammetry produces a green-black electroactive film, which is insoluble in acetonitrile, on the electrode surface. This film is completely soluble in DMF and DMSO. A steady-state current was observed in the potential step voltammetry experiments, which shows that the IC film is conducting. The steady-state current observed is the current associated with electrooxidation of IC onto an oxidised polymer film surface. There is evidence to suggest that initial IC film formation occurs in solution, in a manner similar to indole polymerisation. CVs of the IC films in background electrolyte show two overlapping oxidation peaks and two overlapping reduction peaks. Neither of these oxidation peaks stabilise with repeated cycling and the second (higher potential) oxidation appears to cause the IC film to become soluble in acetonitrile. As the film dissolves off the electrode surface with repeated cycling a change in the coat structure is observed. A Koutecky-

Levich analysis was performed on data collected for the IC polymerisation. This showed that the oxidation reaction of IC is first order in monomer and the diffusion coefficient of IC has been measured as 5.9×10^{-5} cm^2 s^{-1} ($\pm 2.0 \times 10^{-5}$). At concentrations of IC in electrolyte above 10 mM the rate of film formation is limited by the area of the electrode surface and is independent of the bulk concentration of IC. This suggests that IC film formation proceeds *via* a surface adsorbed intermediate in a similar mechanism to indole film formation. The limiting current under such circumstances is 5.5 mA (±0.6). The rate of film formation for IC is approximately 0.9 times that of indole-5-carboxylic acid and 0.4 times that of 5-cyanoindole.

FAB mass spectroscopy on a sample of IC film is consistent with an IC dimer, in which the IC monomers have coupled forming one bond with each losing an H, being a product of IC electropolymerisation. The ^{1}H NMR spectrum of a sample of IC film shows that it does not contain significant amounts of large polymer and that there are two different IC dimers present. These are the 7,3' and 7,4' dimers. Therefore the spin density calculation was unsuccessful in predicting the linkage sites of IC, and so the success of such calculations in predicting the linkage sites in indole electropolymerisation cannot necessarily be extrapolated to other aromatic monomers. The linkage of IC at a different site to those predicted may be because such calculations do not take into account a perturbation of the electron density of the radical cation caused by the approach of a second radical cation, which alters the positions at which the spin electron density is high from those predicted by the calculation. Some other effect, such as surface adsorption only in specific orientations, may also limit the products of electropolymerisation to only two dimers.

The electropolymerisation of PC by potential step voltammetry produces a brown-black electroactive film, which is insoluble in acetonitrile, on the electrode surface. This film is completely soluble in DMSO and partially soluble in DMF. A steady-state current was not observed in the potential step voltammetry experiments. Rather the current was observed to decrease with time, with the rate of decrease increasing with decreasing rotation speed. Therefore there may be some soluble impurity being formed at the electrode.

5.8 References

1. J.Gordon Mackintosh and Andrew R.Mount, *J.Chem.Soc. Faraday Trans.*, 1994, **90(8)**, 1121-1125

2. J.Gordon Mackintosh, Craig R.Redpath, Anita C.Jones, Patrick R.R.Langridge-Smith and Andrew R.Mount, *J.Electroanal.Chem.*, 1995, **388(1-2)**, 179-185

3. Peter Jennings, Anita C.Jones, Andrew R.Mount and Alastair D.Thomson, *J.Chem.Soc. Faraday Trans.*, 1997, **93(21)**, 3791-3797

4. Andrew R.Mount and Mark T.Robertson, *Phys.Chem.Chem.Phys.*, 1999, **1**, 5169-5177

5. Lorna J.Kettle, Simon P.Bates and Andrew R.Mount, *Phys.Chem.Chem.Phys.*, 2000, **2**, 195-201

6. Peter Jennings, Anita C.Jones and Andrew R.Mount, *J.Chem.Soc. Faraday Trans.*, 1998, **94**, 3619-3624

7. Jean Clavilier, Vesna Svetlicic and Vera Zutic, *J.Electroanal.Chem.*, 1995, **386**, 157-163

Chapter Six

STEADY-STATE SPECTROSCOPY OF INDOLO{3,2,1-*jk*}CARBAZOLE AND PYRROLO{3,2,1-*jk*}CARBAZOLE AND THEIR POLYMERS

6.1 Introduction

This thesis is concerned with the electropolymerisation of the monomers indolo{3,2,1-*jk*}carbazole (IC) and pyrrolo{3,2,1-*jk*}carbazole (PC) and the characterisation of their polymers, with particular emphasis on their photophysical properties. The electropolymerisation of IC and PC was described in chapter five. In this chapter, the steady-state fluorescence spectroscopy of the monomers and polymers is discussed. In section 6.2, the experimental details for this chapter are given. In section 6.3, the solution phase steady-state fluorescence spectroscopy of the monomers is investigated in both DMF and cyclohexane, in order to provide a background to the investigation of the photophysical properties of the polymers. This work is followed by a comparison of the solution phase, room temperature steady-state fluorescence spectroscopy of IC and PC polymers formed under different conditions. Finally the results of steady-state fluorescence spectroscopy on drop-coated polymer films are given.

6.2 Experimental details

All the solution phase steady-state fluorescence spectroscopy experiments conducted for this thesis used solutions of concentration 10^{-6} M or less to minimise any self-absorption or inner filter effects. Excitation spectra were recorded at a range of emission wavelengths spanning the width of the emission spectra and emission spectra were recorded at a range of excitation wavelengths spanning the width of the excitation spectra. The spectra were not corrected for spectral response.

The IC and PC polymers were electropolymerised from 30 mM solutions of monomer in electrolyte using the technique of potential step voltammetry at a rotating disc electrode (RDE). The working electrode was held at a potential of 1.10 V (IC) and 0.82 V(PC) vs Fc/Fc^+ and the

RDE was rotated at a speeds of 1, 2, 4, 9 or 16 Hz. The films were rinsed in acetonitrile to remove monomer before being dissolved in DMF.

6.3 Solution phase steady-state fluorescence spectroscopy of the IC and PC monomers

6.3.1 Steady-state fluorescence spectroscopy in DMF

The steady-state fluorescence emission and excitation spectra of the IC and PC monomers were measured in the solvent DMF. This solvent was chosen because the polymer films formed from IC were found to be completely soluble in DMF. Therefore analysis of the fluorescence of the IC monomer in DMF would facilitate comparison with the fluorescence of the IC polymers in DMF later. To enable comparison between the IC and PC data the steady-state spectra of both the PC monomer and polymers were also measured in DMF, although the PC polymer is not completely soluble in this solvent.

For both IC and PC it was found that the shape of the emission spectrum is independent of the excitation wavelength, in other words Kasha's rule is obeyed. This means that the emission in each case is always from the same state, the lowest vibrational level of the first singlet excited state S_1. It also means that there are unlikely to be any other emitting species present that are excited and emit in the same region as IC and PC, such as impurities or aggregates.

Examples of emission and excitation spectra for IC and PC in DMF are shown in Figure 6.1. The excitation spectra are shown with the $S_1 \leftarrow S_0$ band normalised to the $S_0 \leftarrow S_1$ emission band.

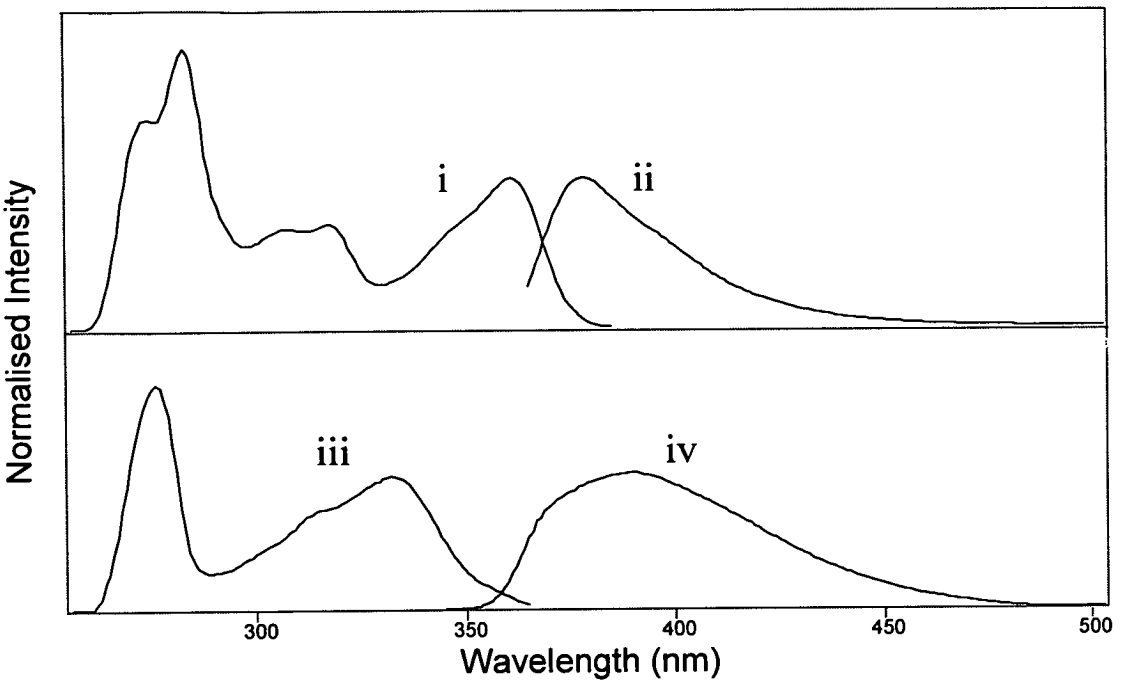

Figure 6.1: Excitation and emission spectra for IC (i and ii) and PC (iii and iv) dissolved in DMF, with emission wavelengths: i 400 nm; iii 380 nm and excitation wavelengths: ii 350 nm; iv 330 nm.

The emission spectrum of IC in DMF is the mirror image of the $S_1 \leftarrow S_0$ band of its excitation spectrum. This shows that for IC there is no large difference between the spacings of the vibrational levels in the ground state, S_0, and the spacings of the vibrational levels in the S_1 state. In other words the adiabatic (equilibrium) geometry of IC in the S_0 state is very similar to that in the S_1 state. However for PC in DMF there is an asymmetry between the emission and excitation spectra. The emission is broad and featureless whereas the $S_0 \leftarrow S_1$ band of the excitation spectrum shows some vibronic structure. This means that there is a significant difference between the absorbing S_0 state and the emitting S_1 state of PC in DMF. This difference could be due to a large difference between the adiabatic geometries of the S_0 and S_1 states of PC. If this geometry difference is intrinsic to the nature of these states the asymmetry between the excitation and emission spectra will be present in a variety of different solvents. Alternatively the broad and featureless nature of the emission of PC in DMF could be due to an interaction between the S_1 state of PC and the polar solvent. However, before investigating these possibilities it was decided to check that the fluorescence excitation and emission spectra

of PC in DMF were not being affected by the presence of impurities, aggregation or excimer formation.

6.3.2 Impurities

In order to investigate the possibility of the presence of impurities the method of synthesis of PC was investigated. The sample of PC used to record the initial fluorescence spectra in DMF was made using the route shown in Figure 6.2(i). After purification by flash chromatography it was found that some of the 5H-dibenzo[*b,f*]azepine starting material remained in the sample [1](Lynns thesis). To exclude the possibility that the presence of this starting material could be contaminating the sample and influencing the shape of the recorded emission spectrum of PC in DMF a sample of PC was synthesised using the alternative route shown in Figure 6.2(ii). This route does not involve any materials with an aromatic system of a similar size to PC and so it is unlikely that any remaining impurities will absorb or emit in the same wavelength region as PC. The emission and excitation spectra of this sample in DMF was measured and it was found that the fluorescence spectra of this second batch of PC was exactly the same as the first batch shown in Figure 6.1. Therefore contamination by the 5H-dibenzo[*b,f*]azepine starting material was excluded. Samples of PC were then re-purified using the technique of flash chromatography, with a 69.6% yield. The flash chromatography purified PC also produced emission and excitation spectra with no change from those shown in Figure 6.1. Therefore the influence of impurities on the fluorescence spectra of PC in DMF was excluded.

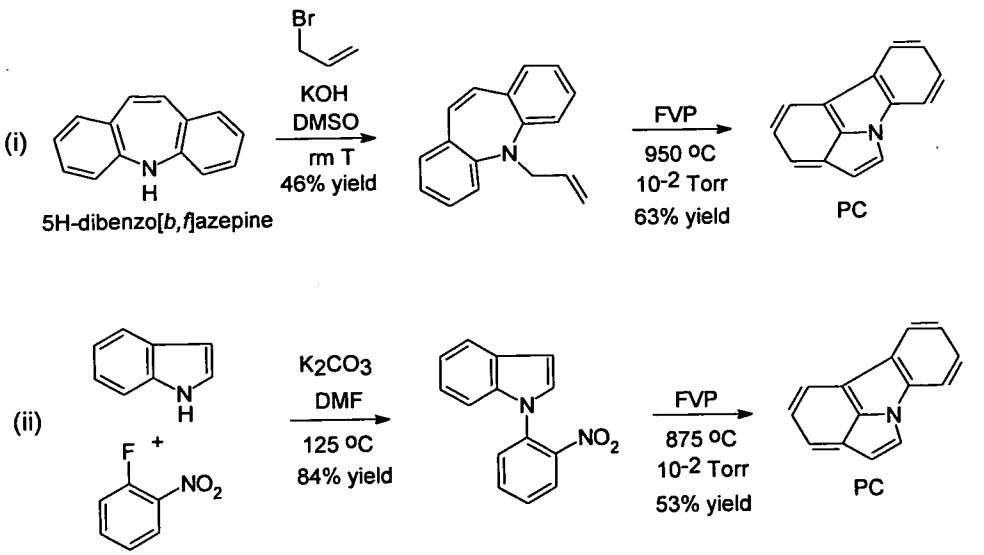

Figure 6.2: Outline of the method of synthesis of PC (i) for the first sample used in fluorescence spectroscopy and (ii) for the second sample used in fluorescence spectroscopy.

6.3.3 Aggregation

The formation of complexes by ground state molecules in solution is called aggregation. These complexes may comprise two, three or more individual molecules bound together by, for example, π-stacking. Such complexes may absorb and emit radiation at higher, lower or the same wavelengths as the individual molecules, depending on the relative energies of the ground and excited states of these species. The presence of aggregates may have a number of effects on the fluorescence spectra of a species. For example the shapes of the emission and excitation spectra may show a dependence on excitation and emission wavelengths respectively, or the shape of the emission spectrum may show a concentration dependence. However such a dependence was not observed in either the IC or PC fluorescence spectra in DMF, suggesting that aggregation is not significant at the concentration of 10^{-6} M used to record these spectra.

Provided that the individual molecules and the aggregate have different individual molar absorption coefficients, aggregation may be detected by recording the UV-visible absorption spectrum as a function of concentration. Where aggregation is present a plot of absorbance against concentration will show deviation from the straight line predicted by the Beer-Lambert law (see chapter 2). Therefore, in order to confirm that aggregation is not affecting the

fluorescence spectra of IC and PC in DMF, UV-visible spectra of both IC and PC were recorded at various concentrations and the Beer-Lambert law plotted as absorbance versus concentration. These plots are shown in Figure 6.3.

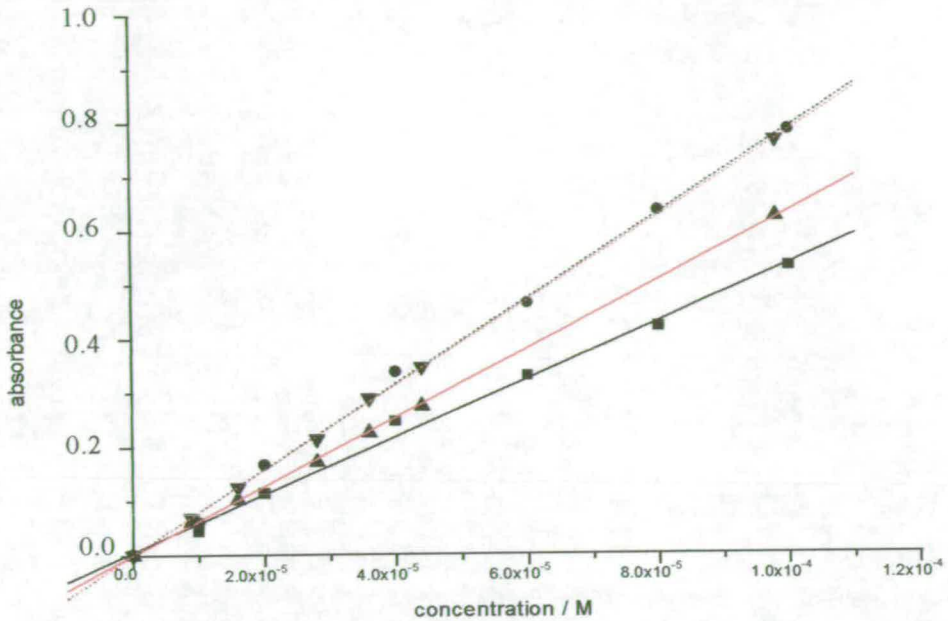

Figure 6.3: Beer-Lambert law plots for IC and PC in DMF. The absorbance has been corrected for the baseline absorbance in each spectrum. The absorbance at two different wavelengths were plotted for each molecule. The black lines are the IC data: ●, 362 nm; ■, 347 nm. The red lines are the PC data: ▲,314 nm; ▼,333 nm.

It can be seen in Figure 6.3 that there is no deviation from the Beer-Lambert law over the concentration range from 10^{-6} M to 10^{-4} M for either IC or PC. This confirms that there is no significant aggregation of either molecule over this range of concentrations and that aggregation is not affecting the shapes of the emission and excitation spectra of IC and PC in DMF, which were recorded at 10^{-6} M.

6.3.4 Excimer formation

An excimer (excited state dimer) is formed when a molecule in its excited state forms a complex with a ground state molecule. Where the other molecule is a different species, such as a solvent molecule, the complex is called an exciplex. An excimer or exciplex may decay to form two ground state molecules by emitting a photon, as illustrated in Figure 6.4. This emission from excimers is characteristically structureless, as the lower state is a continuum.

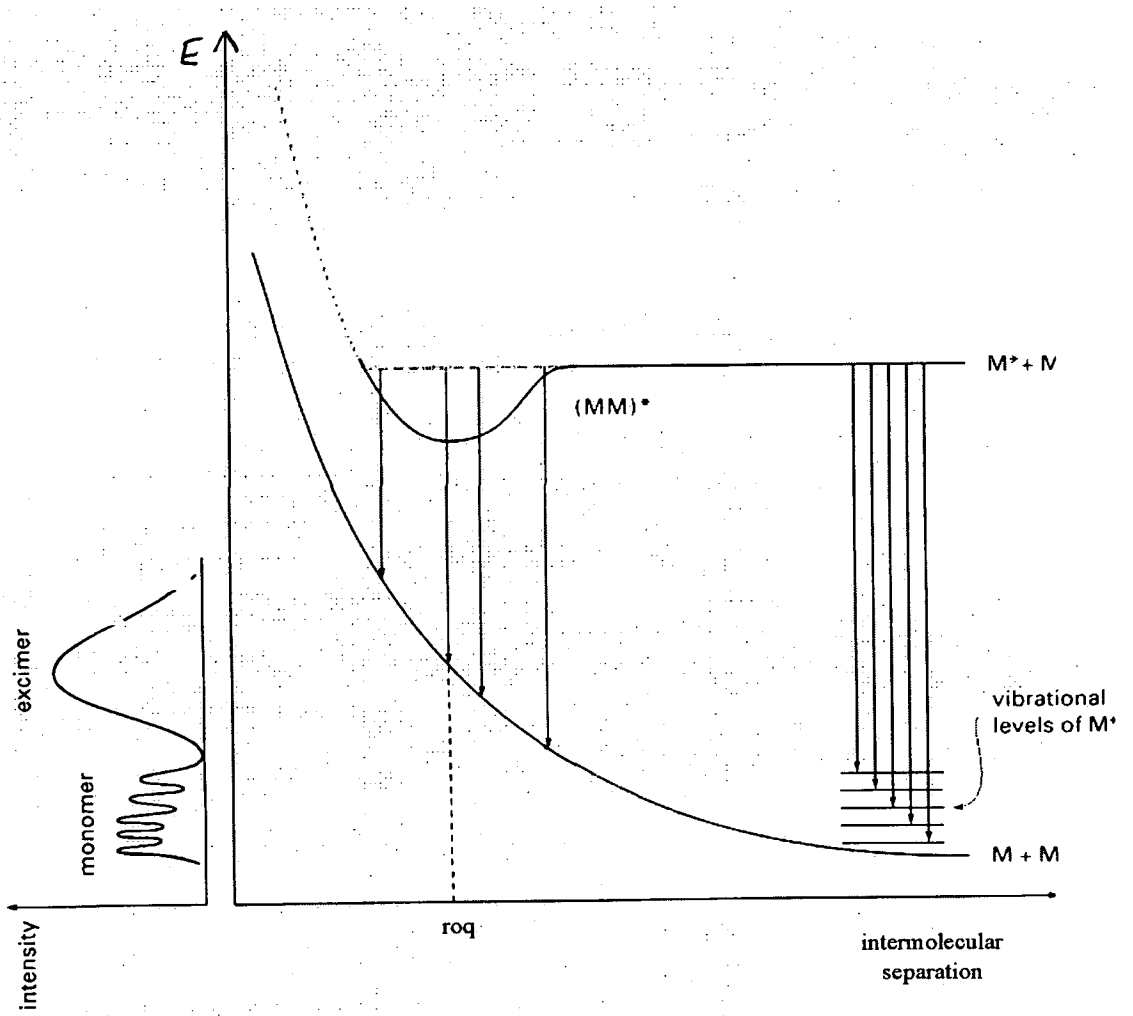

Figure 6.4: Intermolecular potential energy curves for monomer, M, and excimer, (MM)*. Taken from reference 2.

The presence of excimers or exciplexes in solution has no effect on the fluorescence excitation or the UV-visible absorption spectrum of a molecule. Also the shape of the emission spectrum will be independent of the excitation wavelength, as observed for both IC and PC in DMF. However the shape of the emission spectrum will show a concentration dependence. This is because, as in the case of aggregation, the proportion of excimer to uncomplexed excited states in solution is concentration dependent. As exciplex emission always occurs at higher wavelengths than the uncomplexed emission, as the concentration of the solution is decreased the emission intensity at long wavelength will decrease relative to that at shorter wavelength. In

order to investigate the possibility that the PC molecules were forming excimers the fluorescence excitation and emission spectra were examined at different concentrations.

The 10^{-6}M solution of PC in DMF used to record the spectra shown in Figure 6.1 was diluted to 10^{-7}M and the spectra re-measured. The emission recorded at the lower concentration showed no change in shape compared with that at 10^{-6}M, which showed that the broad, featureless emission of PC in DMF is not due to the formation of excimers.

6.3.5 Solvent effects

As shown above, the asymmetry between the excitation and emission spectra of PC in DMF was not due to the presence of impurities, aggregation or excimers. Therefore the effect of the nature of the solvent on the fluorescence spectra of IC and PC was considered. The theory of the effect of the nature of a solvent on fluorescence spectra is given in chapter 2.

The function f(D,n):

$$f(D,n) = 2\left[\frac{D-1}{D+2} - \frac{n^2-1}{n^2+2}\right] \tag{6.1}$$

where D is the static dielectric constant of the solvent and n is the refractive index of the solvent, is commonly used to quantify the dielectric properties of solvents and is useful for studying the effects of such properties on excited state energies [3]. Data for various solvents are shown in Table 6.1 for comparison.

Solvent	Dielectric Constant, D	Refractive Index, n	f(D,n)
Cyclohexane	2.023	1.426	0
Isopentane	1.843	1.356	0.003
DMSO	4.7	1.477	0.539
Ether	4.33	1.352	0.619
THF	7.6	1.405	0.885
DMF	36.7	1.431	1.328
EtOH	24.3	1.361	1.329
MeOH	31.2	1.329	1.412
MeCN	38.8	1.344	1.429
H_2O	81	1.333	1.516

Table 6.1: The dielectric properties of various commonly used solvents.

The steady-state fluorescence spectra of IC and PC were measured in cyclohexane, a nonpolar solvent with f(D,n) = 0, and compared with those measured in DMF, a polar solvent with f(D,n) = 1.328. Typical excitation and emission spectra in cyclohexane and DMF are shown for IC in Figure 6.5 and for PC in Figure 6.6 and data from these spectra are summarised in Table 6.2.

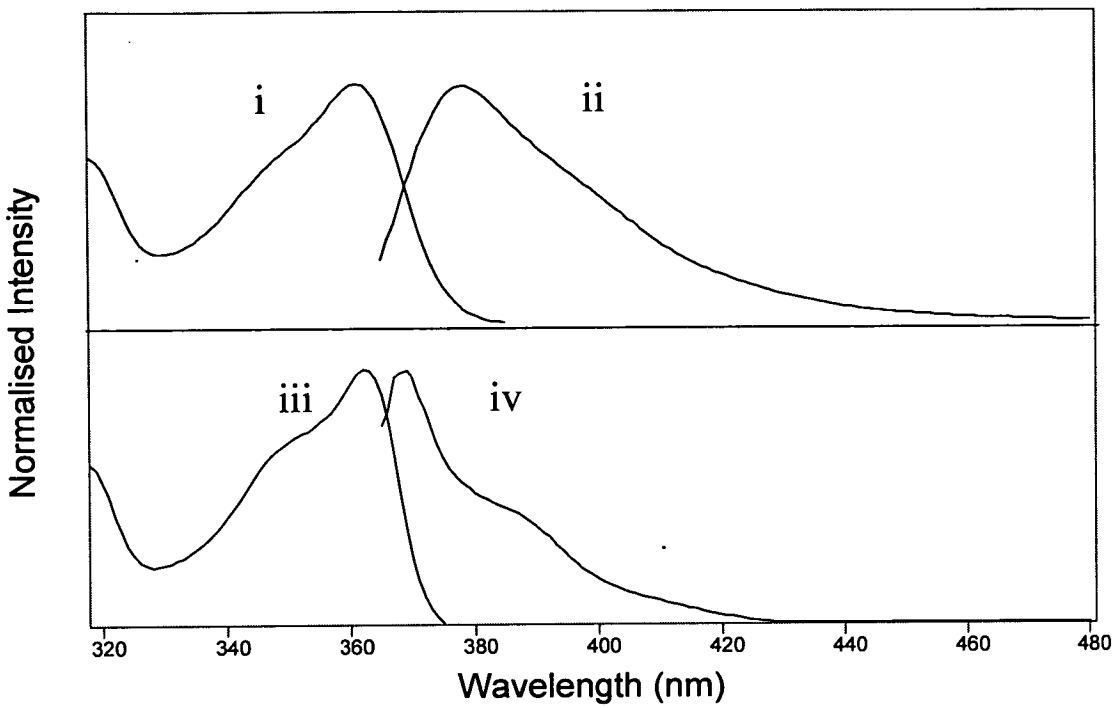

Figure 6.5: Fluorescence excitation and emission spectra of IC in DMF (i and ii) and cyclohexane (iii and iv), with emission wavelengths: i 400 nm; iii 390 nm and excitation wavelength 350 nm for both ii and iv.

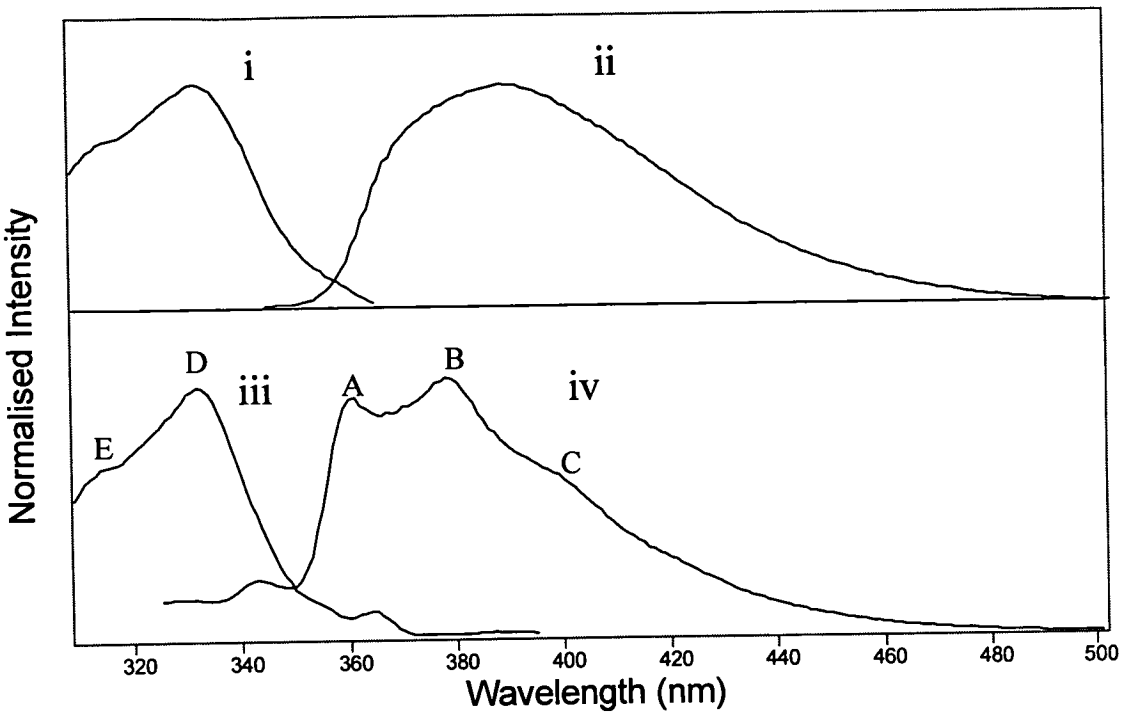

Figure 6.6: Fluorescence excitation and emission spectra of PC in DMF (i and ii) and cyclohexane (iii and iv), with emission wavelengths: i 380 nm; iii 410 nm and excitation wavelengths: ii 330 nm; iv 310 nm.

Solvent	Molecule	Excitation maximum ($\lambda_{max,ex}$) / nm	Emission maximum ($\lambda_{max,em}$) / nm	Stokes Shift / cm^{-1} ($\bar{\nu}_{max,ex} - \bar{\nu}_{max,em}$)	Wavenumber at which excitation and emission spectra cross / cm^{-1}
Cyclohexane	IC	363	369	448	27,322
DMF	IC	361	378	1,246	27,100
Cyclohexane	PC	332	361, 378	2,419	28,571
DMF	PC	332	390	4,479	28,011

Table 6.2: Excitation and emission data for IC and PC in DMF and cyclohexane. The excitation maximum is the wavelength of maximum intensity for the $S_1 \leftarrow S_0$ band.

The emission spectrum of IC in cyclohexane is independent of the excitation wavelength (Kashas rule is obeyed) and is the mirror image of the $S_1 \leftarrow S_0$ band of the excitation spectrum, as found for IC in DMF. The shapes of both the excitation and emission spectra of IC in cyclohexane are similar to those in DMF but are noticeably sharper and less broad. The change in polarity of the solvent from DMF to cyclohexane has virtually no effect on the position of the

excitation spectrum of IC. Therefore the Franck-Condon excited state is not stabilised more by one solvent than the other. However, the emission band is shifted to higher energy, with the Stokes shift for IC reduced by 798 cm^{-1} on moving from DMF to cyclohexane. Therefore the excited state of IC undergoes more solvent relaxation in DMF than in cyclohexane. This is common and originates from the fact that the S_1 states of many molecules are more polarisable and/or have greater permanent dipole moments than their S_0 states.

As for IC, the position of the excitation spectrum of PC undergoes very little change from DMF to cyclohexane. Therefore the Franck-Condon excited state of PC is not stabilised more by one solvent than the other. However the emission spectrum of PC in cyclohexane is very different to that in DMF. In DMF the emission was broad and featureless whereas in cyclohexane vibronic structure is visible. The shape of the emission of PC in cyclohexane is unusual as it is not the mirror image of the excitation spectrum. It has two sharp peaks at 361 nm and 378 nm with a shoulder to the red of the 378 nm peak at ~400 nm. The small feature at 343 nm and the intensity to lower wavelengths of this feature are due to Raman scattering in the solvent. This shape of the emission spectrum of PC in cyclohexane was seen for two different solutions of PC in cyclohexane, one of PC used as received in cyclohexane (Prolabo, Rectapur™, 99%) and the other of PC purified by flash chromatography in cyclohexane (Aldrich, HPLC grade, 99.9+%). Therefore the lack of mirror symmetry is unlikely to be due to an impurity. Also, the overall shape is not due to interference by a Raman band, as it is retained when the excitation wavelength is changed. The possibility of reabsorption affecting the shape of the emission of PC in cyclohexane was excluded by recording the spectra of solutions of 10^{-6}, 5×10^{-7} and 10^{-7}M, for which there was no change in the shape of the emission band. Therefore the lack of mirror symmetry between the excitation and emission spectra of PC in cyclohexane must be due to either a difference in the equilibrium geometries of the S_0 and S_1 states of PC or to a difference in the shape of their potential energy surfaces.

The wavenumbers of the five features labelled A, B, C, D and E in the emission and excitation spectra of PC in cyclohexane shown in Figure 6.6, and the energy separations between them, are given in Table 6.3. The separations between the three features observed in the emission spectrum are approximately the same at ~1,200 cm^{-1}. It is, therefore, likely that they are members of a vibronic progression with a frequency of ~1200 cm^{-1}. The energy separation

between the features in the excitation spectrum is 1,721 cm^{-1}. Therefore these features may be members of a vibrational progression built on a different vibrational mode to those observed in the emission, or they may be members of the same vibrational mode having a different vibrational frequency in the excited state to that in the ground state. This confirms the conclusion that there is a change in geometry or in the shape of the potential energy surface between the S_0 and S_1 states of PC.

Peak	Position / cm^{-1}	Peak separation	Peak separation / cm^{-1}
A	27,725	A to B	1,273
B	26,452	B to C	1,198
C	25,254	D to E	1,721
D	30,108		
E	31,829		

Table 6.3: The peak positions and peak separations for the excitation and emission spectra of PC in cyclohexane.

In Table 6.2 the Stokes shifts for IC and PC in DMF and cyclohexane are shown. The Stokes shift for PC in cyclohexane is 2,419 cm^{-1}, whereas the Stokes shift for IC in cyclohexane is only 448 cm^{-1}. The larger Stokes shift observed for PC than for IC in this solvent is further evidence for a geometry change or change in the potential energy surface of PC which is not present for IC.

The Stokes shift for PC in DMF of 4,479 cm^{-1} is larger than the Stokes shift observed for PC in cyclohexane, which suggests that the excited state of PC undergoes solvent relaxation in DMF. However, since the emission spectrum of PC in DMF is so broad, the maxima in the emission spectrum may not correspond to the maxima of the excitation spectrum in that solvent, and therefore the value for the Stokes shift of PC in DMF may be inaccurate. The point at which the emission and excitation spectra cross in each solvent may be a more accurate measure of the energy separation of the excitation and emission spectra of PC than the Stokes shift. These values are therefore shown in Table 6.2 for both monomers. The point at which the excitation and emission spectra of PC cross shifts by 560 cm^{-1} to the blue when the solvent changes from DMF to cyclohexane. This suggests that there is indeed solvent relaxation occuring for PC in DMF.

The emission of PC appears to be more perturbed by the change in solvent from cyclohexane to DMF than the emission of IC, as some vibronic structure is retained in the emission of IC in DMF but the emission of PC in DMF is broad and featureless. This is supported by the observation that the point at which the excitation and emission spectra of IC cross shifts by only 222 cm^{-1} to the blue when the solvent is changed from DMF to cyclohexane, compared the 560 cm^{-1} blue-shift observed for PC. Therefore there is more solvent relaxation around the excited state PC molecule than around the excited state IC molecule, which means that the change in dipole moment from the ground to the excited state must be larger for PC than for IC.

6.4 Steady-state fluorescence spectroscopy of IC polymers

6.4.1 IC polymer formed at 1 Hz

As described in the previous chapter, IC polymer was formed by the electropolymerisation of IC monomer at a rotating disc electrode (RDE). Use of a RDE allows control of the conditions during polymer formation by controlling the speed of rotation. The effect of increasing the rotation speed is to increase the rate at which monomer is brought to the electrode surface during polymerisation. Electropolymerisation of IC was carried out at rotation speeds of the RDE ranging from 1 to 16 Hz and the effect of rotation speed on the steady-state fluorescence of the IC polymers is discussed in the next section. In this section the steady-state fluorescence of the IC polymer formed at the slowest rotation speed of 1 Hz is described. The IC polymers were found to be completely soluble in DMF and all steady-state spectra for the IC polymers were measured in this solvent.

The steady-state excitation and emission spectra of the IC polymer formed at a 1 Hz rotation speed were measured. Figure 6.7 shows the emission spectra of the IC monomer and this polymer, both excited at 340 nm.

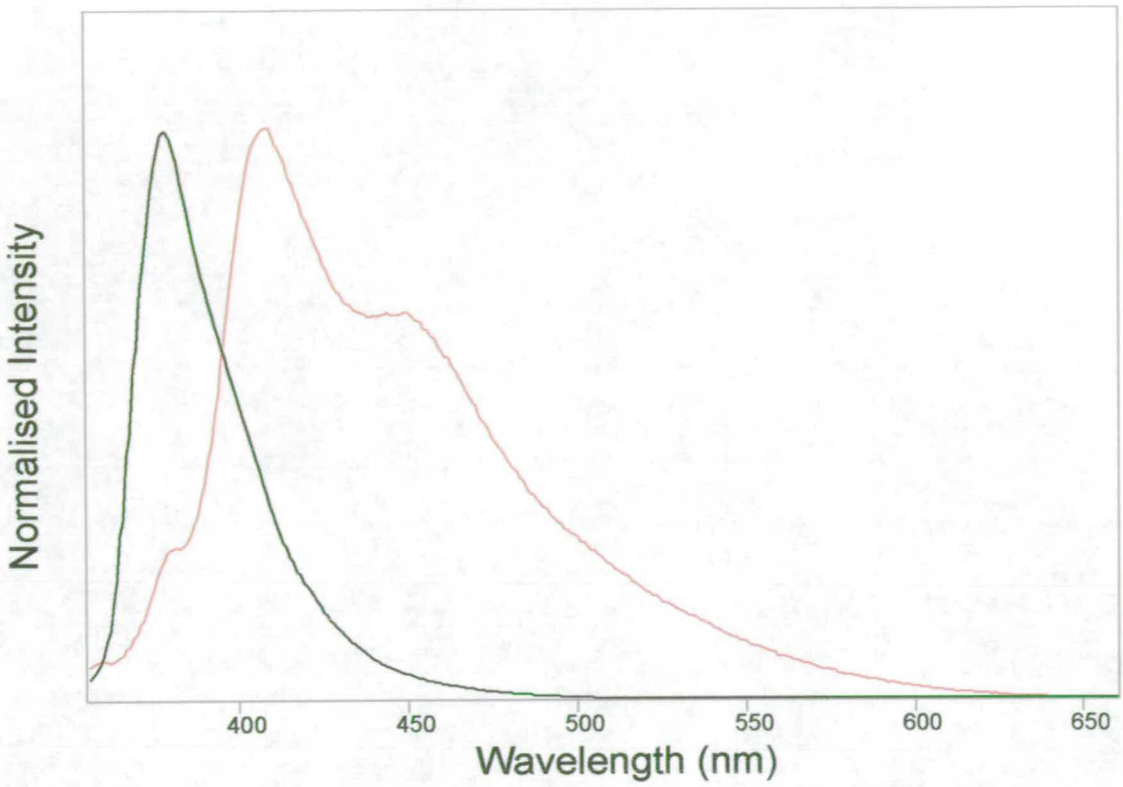

Figure 6.7: Emission spectra of IC monomer (black) and IC polymer (red), both excited at 340 nm.

The emission spectra of the monomer and the polymer shown in Figure 6.7 are quite different in shape. There are peaks at 408 nm and 455 nm in the polymer emission which are absent from the monomer emission, which has only one peak at 378 nm. This shows that the electropolymerisation of IC has formed emitting species which are not monomer. There is a Raman band at 378 nm in the emission spectrum of the pure solvent when exciting at 340 nm. Therefore the small feature at 382 nm in the polymer emission may be due either to some IC monomer which remained in the film after rinsing in acetonitrile or to Raman scattering from the solvent.

The new species formed by the electropolymerisation of IC emit to lower energy than the IC monomer. This shows that the electropolymerisation reaction has formed emitting species which have more extensive π-electron delocalisation than the IC monomer. These species could be dimer, trimer or longer polymers. The wavelength of maximum emission of the IC polymer is at 408 nm, which is 1,945 cm^{-1} to the red of the wavelength of maximum emission of the IC

monomer at 378 nm. A red-shift in the wavenumber of maximum emission of 3,435 cm^{-1} has previously been observed for the emission of the 5-cyanoindole trimer with respect to the 5-cyanoindole monomer in ethanol [4]. The IC polymer has already been shown to contain dimer by mass spectrometry (see chapter five) and the shift of 1,945 cm^{-1} for the IC polymer with respect to the IC monomer is consistent with the presence of IC dimer. Therefore the band peaking at 408 nm can be attributed to dimer emission.

Emission from the 5-cyanoindole trimer in DMF peaks at 424 nm and varying the substituent produces trimers with very similar emission spectra [4]. The IC dimer emission in DMF peaks at 408 nm, which is 925 cm^{-1} to the blue of the 5-cyanoindole trimer emission. This small energy difference is comparable to the effect that changing the indole substituent has on the emission maxima of the indole trimers. For example, the emission maximum of the indole-5-carboxylic acid trimer in ethanol is at 408 nm, whereas for the 5-chloroindole trimer in ethanol it is at 420 nm. Therefore the electropolymerisation of IC produces a dimer which emits in the same region as the indole trimers. This is because, although the IC product is a dimer and the indole product is a trimer, both have conjugation systems of a similar size, as the IC monomer is larger than the indole monomer.

When measuring fluorescence spectra, it is sometimes possible to selectively excite or detect different species by a judicious choice of excitation or emission wavelength, provided that the different species absorb or emit in different regions. The emission bands at 408 and 455 nm shown in Figure 6.7 overlap. However exciting at 320 nm was found to produce an emission spectrum in which the peak at 455 nm is lost and only the emission band due to the IC dimer, which peaks at 408 nm, can be seen. This emission spectrum is shown in Figure 6.8. This dependence of the shape of the IC polymer emission spectrum on the excitation wavelength confirms that there is more than one emitting species present in solution (other than monomer). It also shows that the band at 455 nm is not vibronic structure associated with the 408 nm emission band. Since it emits to longer wavelength than the IC dimer it is likely to be some longer chain polymer. Detecting at 410 nm similarly produces an excitation spectrum mainly due to dimer, also shown in Figure 6.8. The Stokes shift, measured as the difference between the emission and $S_1 \leftarrow S_0$ excitation maxima, for the IC dimer in DMF is 2,517 cm^{-1}. This is more than twice as large as the Stokes shift for the 5-cyanoindole trimer in DMF of 1,200 cm^{-1} [4], suggesting that the IC dimer interacts more with the polar solvent DMF than the 5-cyanoindole

trimer. Therefore the difference between the ground and excited state dipole moments for the IC dimer is larger than that for the 5-cyanoindole trimer.

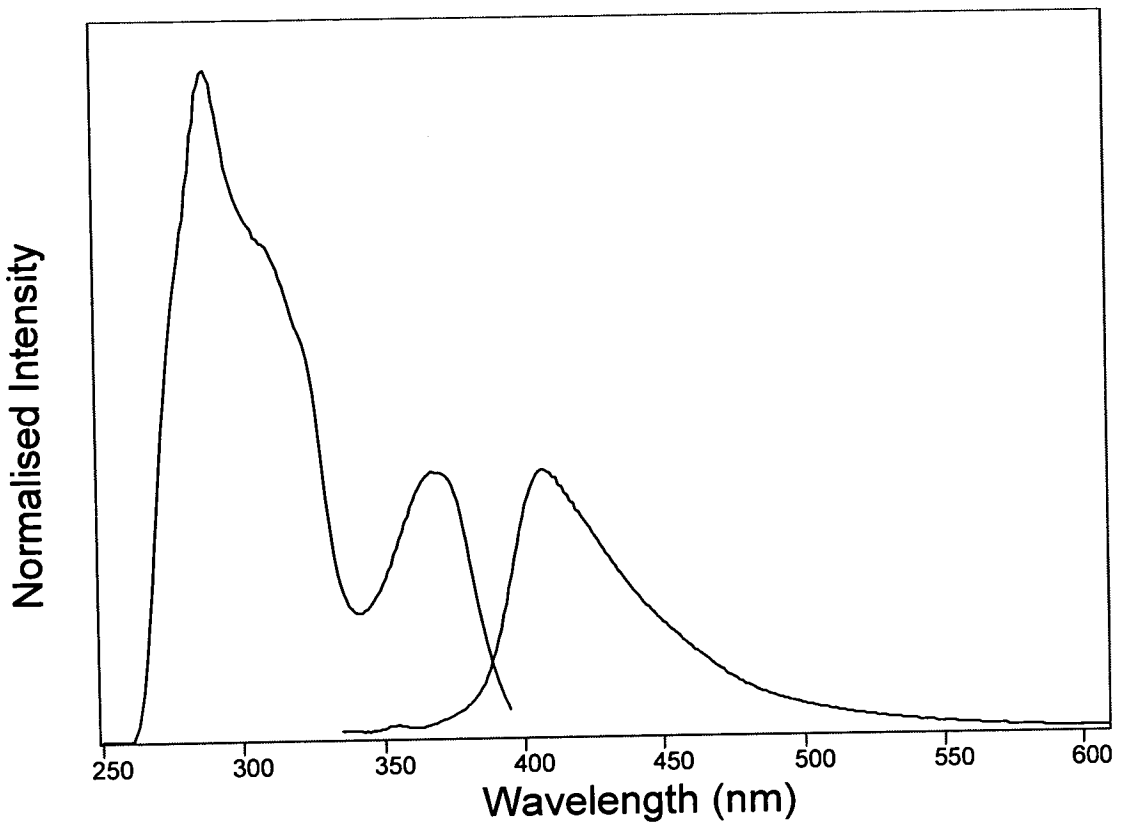

Figure 6.8: Excitation and emission spectra of the IC dimer, with emission wavelength of 410 nm and excitation wavelength of 320 nm respectively.

The excitation spectrum of the IC polymer, recorded at an emission wavelength of 480 nm, is shown in Figure 6.9 (i). At this emission wavelength emission from both the dimer and the species with emission band peaking at 455 nm, should be detected. The excitation spectrum has two relatively weak excitation peaks at ~420 and ~440 nm and a much more intense excitation maximum at ~370 nm due to IC dimer. Exciting at both 420 and 440 nm produces an emission spectrum composed of the 455 nm emission band. Therefore the excitation peak at ~440 nm is the $S_1 \leftarrow S_0$ band of the 455 nm emission and the excitation peak at ~420 nm may be the $S_2 \leftarrow S_0$ band of the 455 nm emission, or could be vibronic structure. Also shown in Figure 6.9 are excitation spectra for the IC polymer recorded at emission wavelengths of 450 and 410 nm. These show that the shape of the excitation spectrum is dependent on the emission wavelength.

As the emission wavelength is decreased the intensity of the excitation spectrum decreases at long wavelengths, as emission from the longer chain length species is no longer being detected.

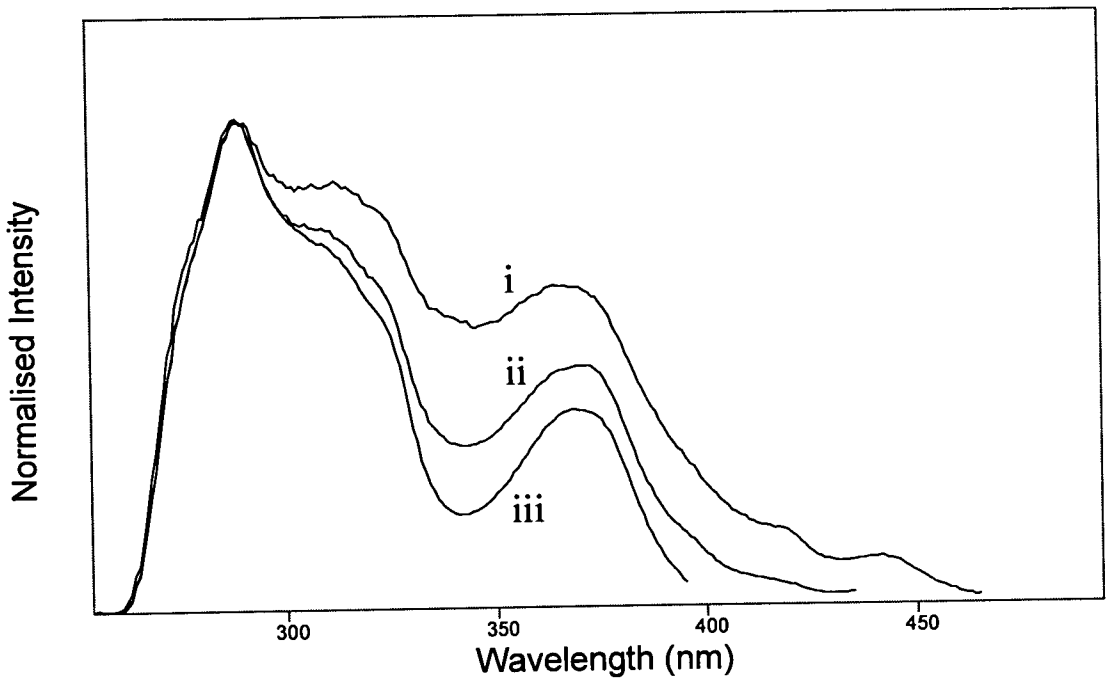

Figure 6.9: IC polymer excitation spectra, at emission wavelengths (i) 480 nm (ii) 450 nm and (iii) 410 nm.

Figure 6.10 shows the relative intensities of the emission of the dimer and the species emitting at 455 nm when excited at 320 and 400 nm respectively. These spectra show that the dimer emission, which peaks at 408 nm, is much more intense than the longer wavelength emission peaking 455 nm, suggesting that there is a great deal more dimer present in solution than longer chain length species. However, it is important to remember that the difference in intensity does not necessarily reflect a difference in the relative amounts of the two emitting species in solution. This is because the different species may have different quantum yields. In fact long chain length polymers usually have lower quantum yields than short chain length polymers, as they have more competing non-radiative de-excitation pathways. Therefore there may be more of the longer wavelength emitting species present in solution relative to dimer than is suggested by Figure 6.10. However the ^{1}H NMR spectrum of the IC polymer (see chapter 5) shows well resolved peaks, which were attributed to the IC dimer and indicate that the sample does not contain significant amounts of long chain polymer. Therefore it is likely that there is indeed much more IC dimer present in solution than the longer chain length emitting species.

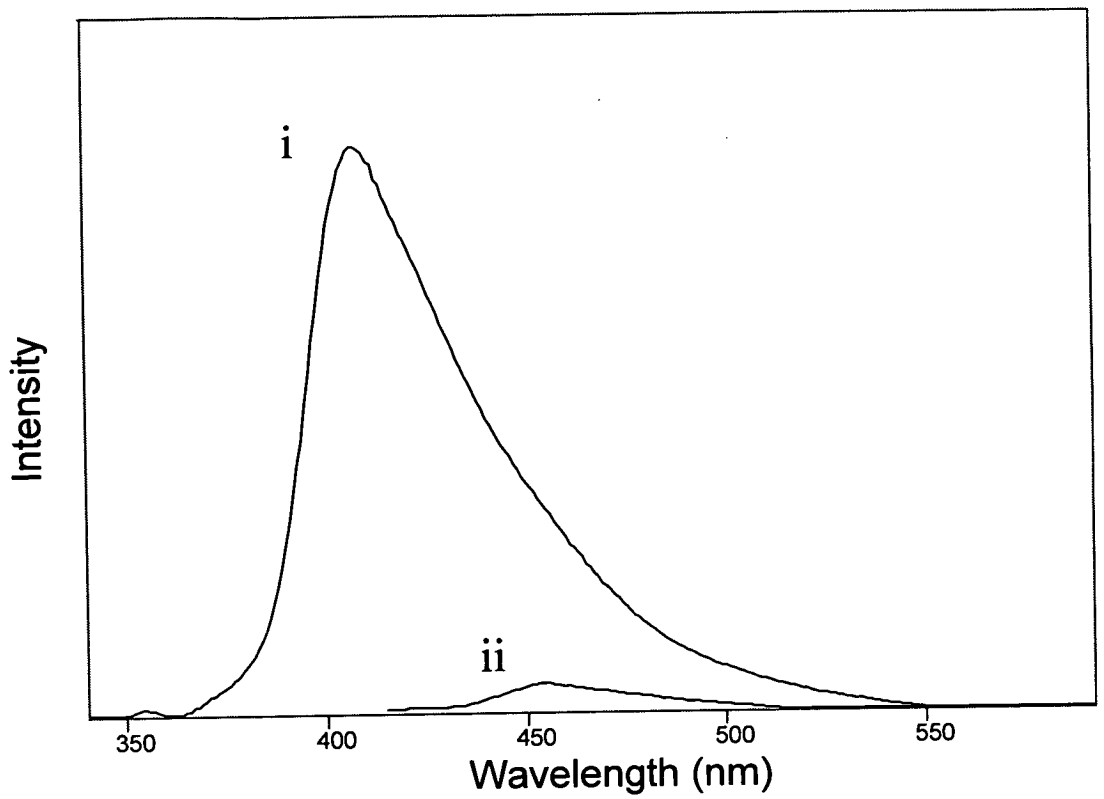

Figure 6.10: Emission spectra of IC polymer at excitation wavelengths of (i) 320 nm and (ii) 400 nm.

As the excitation wavelength is increased the emission of the IC polymer shifts to lower energy and three discrete bands are seen with emission maxima at 408, 455 and 507 nm. These three emission bands are shown in Figure 6.11. Thus, there appears to be at least three different emitting species in the IC polymer solution apart from any IC monomer. The absolute intensity of the band peaking at 507 nm is so low relative to the band peaking at 408 nm that it barely appears above the baseline. However, as discussed above, this may not reflect the actual relative amounts of the two species present in solution.

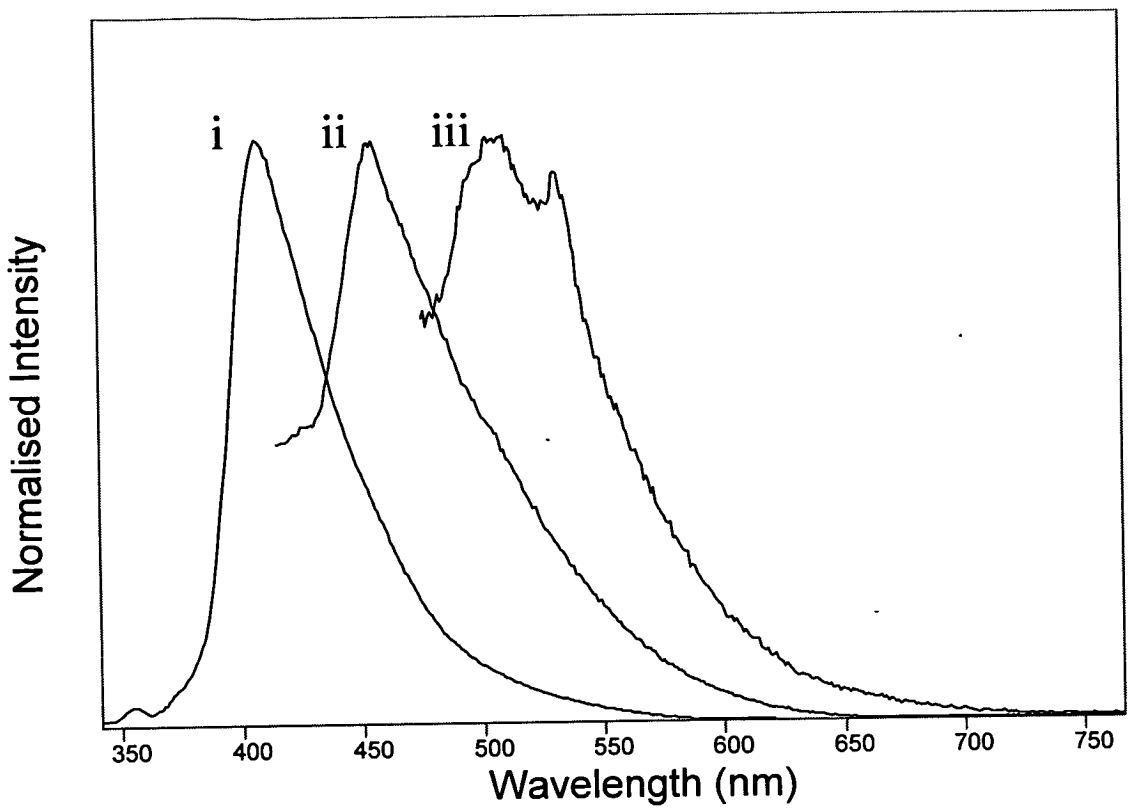

Figure 6.11: The emission of the IC polymer at excitation wavelengths of (i) 320 nm (ii) 400 nm and (iii) 460 nm. The small feature at 530 nm in the emission excited at 460 nm is due to Raman scattering.

A summary of the excitation and emission data for the IC monomer and polymer formed at 1 Hz in DMF is given in Table 6.4.

	Excitation maxima / nm	Emission maxima / nm	Stokes shift / cm^{-1}
IC monomer	361	378	1,246
IC dimer	370	408	2,517
Other polymer	<u>418</u>, 442	455	
Other polymer	-	507	-

Table 6.4 Summary of the excitation and emission data for the IC monomer and the IC polymer formed at 1 Hz, both in DMF at room temperature. The underlined value is the excitation maximum of the $S_2 \leftarrow S_0$ band, all other values refer to the $S_1 \leftarrow S_0$ band.

6.4.2 The effect of varying the conditions of polymer formation

Electropolymerisation at a RDE allows control of the conditions during polymer formation by controlling the speed of rotation. The effect of increasing the rotation speed is to increase the rate at which monomer is brought to the electrode surface during polymerisation. Studies of indole electropolymerisation [5, 6] have shown that, at a given concentration of monomer in electrolyte, use of a fast rotation speed results in formation of a polymer rich in trimer, which emits at shorter wavelengths than the polymer made up of linked trimer units. Use of a slow rotation speed results in formation of a polymer rich in linked trimer. The effect of varying the conditions of polymer formation on the fluorescence spectra of IC polymers was investigated by recording the spectra of polymers formed at rotation speeds of 1, 2, 9 and 16 Hz.

As noted above, the relative intensities of the different bands in an emission spectrum does not necessarily reflect the relative amounts in solution of the different emitting species which contribute to those bands. This is because these different species may have different quantum yields. However, comparing the changes in the relative intensities of the bands in samples formed under different conditions should allow the effect of the different conditions on the amounts of the species present to be determined. The emission spectra with excitation wavelength of 340 nm for polymers formed at different rotation speeds are shown in Figure 6.12. The excitation wavelength 340 nm was chosen because it results in emission across the bands with maxima at 408 and 455 nm.

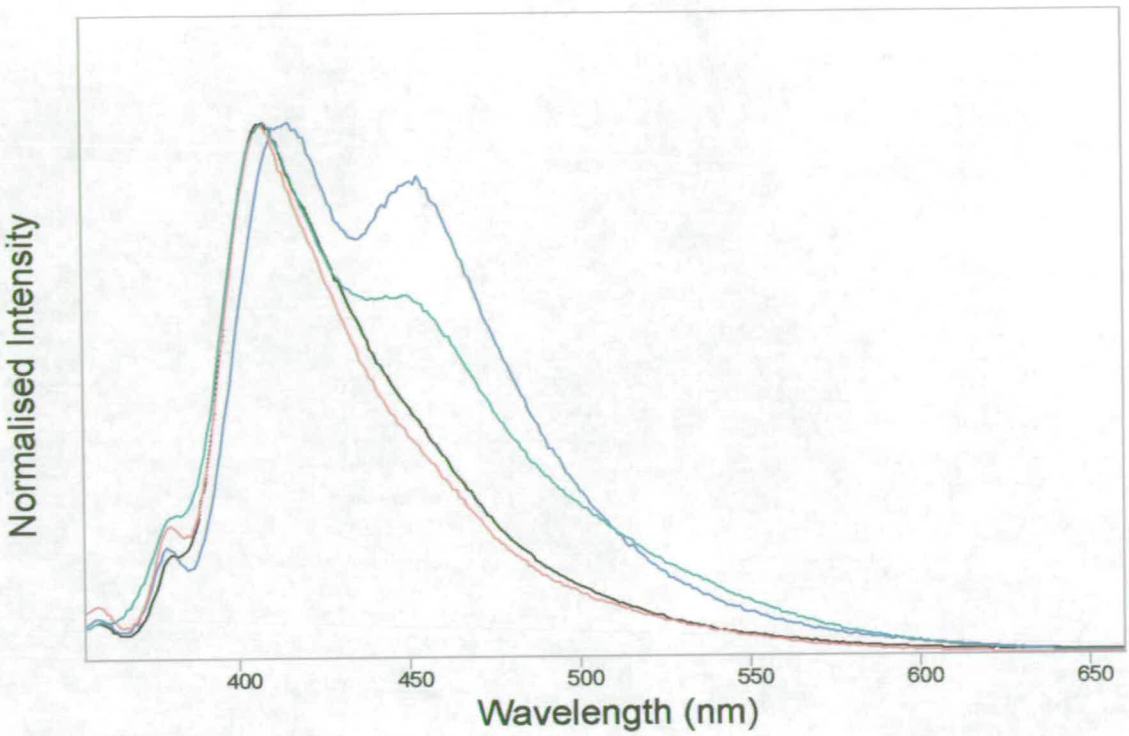

Figure 6.12: Emission spectra, all excited at 340 nm, of IC polymers formed at different rotation speeds; blue is 2 Hz, green is 1 Hz, black is 16 Hz and red is 9 Hz.

In Figure 6.12 it can be seen that the emission of the polymers formed under conditions of fast rotation speed (9 and 16 Hz) is dominated by the dimer emission peak at 408 nm, with very low intensities across the 455 and 507 bands. In contrast, in the emission of the polymers formed at slow rotation speed (1 and 2 Hz) the peak at 455 nm is clearly visible and there is increased intensity across the region where the 507 nm band lies. This is similar to the behaviour of the indole polymers and implies that a similar mechanism is occurring during IC electropolymerisation. The first step in the electropolymerisation is formation of dimer, which emits at 408 nm, and this is followed by linkage of the dimer units to form longer polymer species, which emit at 455 and 507 nm. At fast rotation speeds the first step, dimer formation, dominates. At slow rotation speeds the linkage of the dimer units increases in importance. An apparent anomaly is that the 455 nm emission decreases in intensity relative to the dimer emission on moving from 2 to 1 Hz. However the emission at longer wavelengths, around 510-600 nm, increases in intensity on moving from 2 to 1 Hz. This implies that the species emitting at 507 nm and above is/are formed from the species emitting at 455 nm.

6.5 Steady-state fluorescence spectroscopy of PC polymers

6.5.1 PC polymer formed at 1 Hz

In the previous chapter the electropolymerisation of the PC monomer to form polymer was described. In similar experiments to those described in section 6.4 of this chapter, the steady-state solution phase fluorescence spectra of the PC polymers produced using different rotation speeds of the RDE were measured. The spectra of the PC polymer produced at a 1 Hz rotation speed are discussed in this section and the effect of changing the rotation speed on the spectra of the PC polymers is described in the following section. As for the IC polymers, all the fluorescence spectra were measured for PC polymer dissolved in DMF. However it should be noted that the PC polymers were not completely soluble in this solvent. Therefore the electropolymerisation of PC may produce emitting species which are not observed in this work.

Emission spectra of the PC monomer and the PC polymer formed at a 1 Hz rotation speed, both excited at 330 nm, are shown in Figure 6.13.

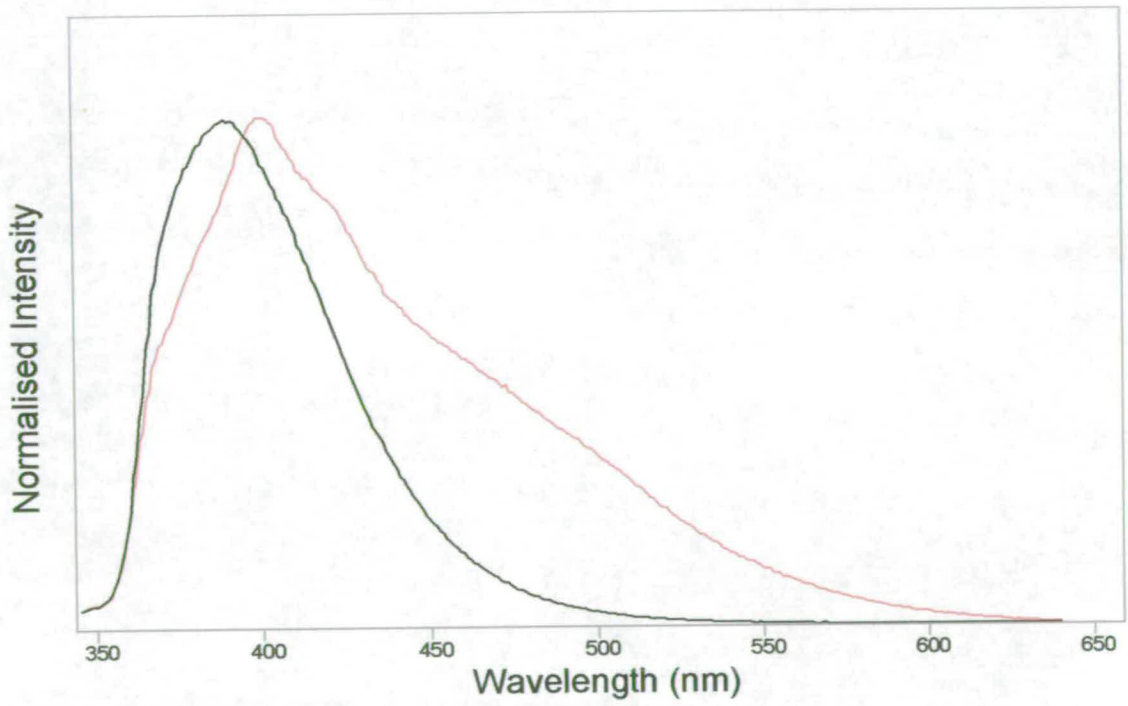

Figure 6.13: Emission spectra of PC monomer (black) and PC polymer (red), both excited at 330 nm. Note there is a Raman band in the solvent at 367 nm.

Overall the emission spectra of the PC monomer and polymer are very different. The emission maximum has shifted from 390 nm for the monomer to 400 nm for the polymer. There is also a large increase in the intensity of the emission to longer wavelengths in moving from the monomer to the polymer, with shoulders on the 400 nm emission band at 420 and 460 nm. This shows that, as was the case for IC, electropolymerisation of PC forms emitting species which are different to the monomer. However the spectra of the monomer and the polymer are very similar at the blue edge. This suggests that there is some PC monomer in the polymer solution, which remained in the film after it was rinsed in acetonitrile.

The increase in the emission to longer wavelengths on going from monomer to polymer indicates that, as with IC, species which have more extensive π-electron delocalisation than the monomer have been formed during the electropolymerisation. In the case of the IC polymer the lowest wavelength peak of the polymer emission was assigned to the IC dimer (see above). However, in the case of the PC polymer, the lowest wavelength emission of the polymer species appears to overlap to a significant degree with the emission of the monomer. This means that the shape of this polymer emission band could be affected by the emission band of the monomer. Therefore the peak at 400 nm in the emission spectrum of the polymer solution may not be the true emission maximum of a polymer species. To check this, emission spectra of the polymer solution were recorded at different excitation wavelengths. Examples are shown in Figure 6.14.

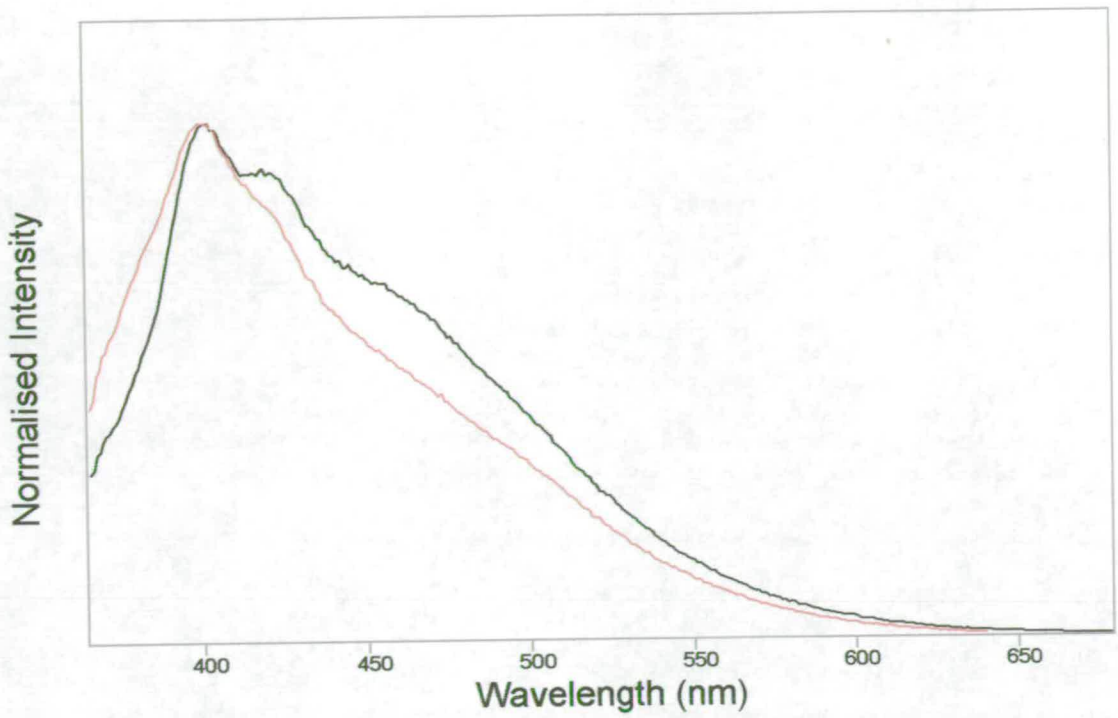

Figure 6.14: Emission spectra of the PC polymer at excitation wavelengths of 330 nm (red) and 350 nm (black).

As shown in Figure 6.14, in moving from a 330 to a 350 nm excitation wavelength the emission spectrum of the PC polymer solution loses intensity at the blue edge, which is where the emission of any monomer in solution will occur. However, the position of the peak at 400 nm in the emission excited at 330 nm remains unchanged in the emission excited at 350 nm. This shows that the position of this maximum is not affected by the proximity of the monomer emission band and that therefore this is the true maximum of the lowest wavelength polymer emission. There is, therefore, a red-shift of 641 cm^{-1} from the monomer emission maximum of 390 nm to the polymer emission maximum. This is a small shift when compared with the shifts in emission maximum from monomer to polymer for 5-cyanoindole of 3,435 [4] and for IC of 1,945 cm^{-1}, and suggests that this emitting species is the PC dimer. However, in the absence of any other evidence from, for example, NMR spectroscopy, this assignment is tentative.

The emission maximum at 400 nm of the, possibly dimeric, PC species is at a slightly shorter wavelength than the emission maxima of similar polymeric species. For example, in DMF the emission maximum of the indole-5-carboxylic acid trimer is at 407 nm [7], the 5-cyanoindole

trimer at 424 nm [4] and the IC dimer at 408 nm. This shows that, in principle, using monomers with different sizes of conjugation system can alter the wavelength of emission of the electropolymerised species in solution. However, the wavelength change is small and all of the species above emit violet light. Also, in order to be of use in an LED, such polymers must emit in the solid state.

In Figure 6.14 it can be seen that the relative intensities of the emission maximum at 400 nm and the shoulders at 420 and 460 nm in the emission of the PC polymer solution are dependent on the excitation wavelength. Therefore different emitting species in solution are responsible for each of these features. To investigate further the different emitting species present in the PC polymer solution, excitation spectra were measured at different emission wavelengths. Examples of these are shown in Figure 6.15 together with the excitation spectrum of the PC monomer for comparison.

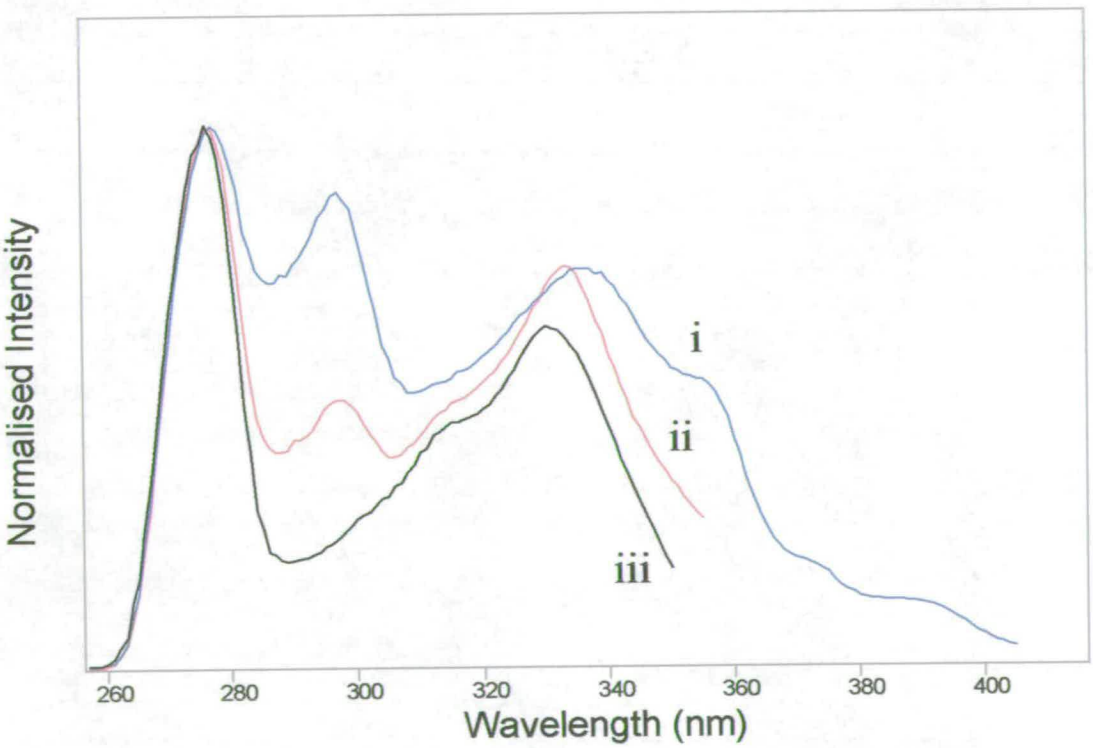

Figure 6.15: Excitation spectra of PC polymer with emission wavelengths of (i) 420 nm and (ii) 370 nm and (iii) PC monomer in DMF with emission wavelength 365 nm.

As was observed for the IC polymer, the emission of the PC polymer is dependent on the excitation wavelength. As the emission wavelength is increased the intensity of the excitation spectrum to longer wavelengths increases. Also a new band appears at 297 nm in the polymer excitation spectra shown in Figure 6.15, which is not present in the monomer spectrum. The excitation spectrum recorded at an emission wavelength of 420 nm shows bands at 390, 375, 355 and 335 nm. Therefore emission spectra excited at approximately these wavelengths were measured and are shown in Figure 6.16.

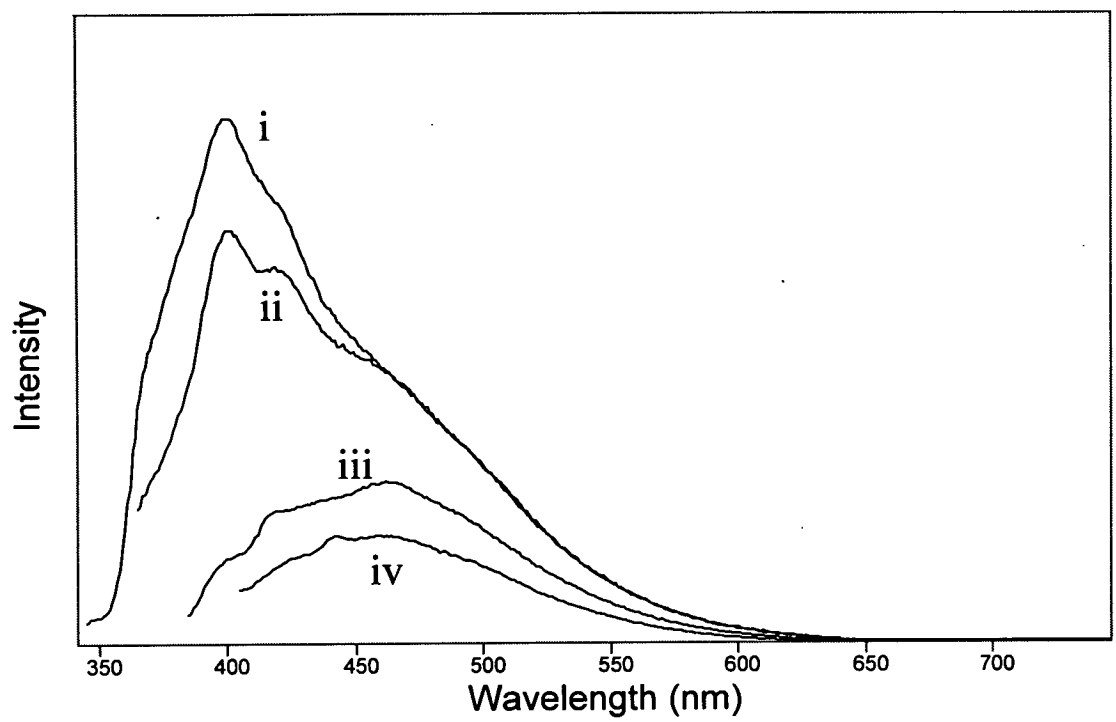

Figure 6.16: Emission spectra of PC polymer at excitation wavelengths of (i) 330 nm (Raman band at 367 nm), (ii) 350 nm (Raman band at 391 nm), (iii) 370 nm (Raman band at 416 nm) and (iv) 390 nm (Raman band at 441 nm).

There are three main emission bands peaking at 400, 420 and 460 nm in the PC polymer emission shown in Figure 6.16. In fact, by exciting at the longer wavelength of 430 nm, it can be seen that the emission of this last band actually peaks at 473 nm. The shift to 460 nm at shorter exciting wavelengths is caused by the overlap with the 420 nm emission band, which is no longer excited at 430 nm. Emission from the 473 nm band has been observed using excitation wavelengths up to 480 nm and the excitation spectrum recorded at an emission wavelength of 500 nm shows additional peaks at ~435 and ~407 nm.

Three emission bands were also observed for the IC polymer solution at 408 (dimer), 455 and 507 nm. The relative intensities of the different emission bands in the spectra of the IC and PC polymers depends on the excitation wavelength used. However, it is clear from Figures 6.9 and 6.16 that, whilst for the IC polymer the intensity of the dimer emission band at 408 nm is far greater than the intensities of the 455 and 507 nm emission bands, the two PC polymer emission bands at 400 and 420 nm have fairly similar intensities. Furthermore, for the PC polymer the emission band at 473 nm is more intense relative to the 400 nm emission band than the 507 nm band is relative to the 408 nm band in the IC polymer emission. This difference in relative intensities may reflect either a difference in relative quantum yields and/or a difference in relative amounts of the different emitting species in solution.

Another difference between the emission spectra of the IC and PC polymers is that for the IC polymer all three emission bands were approximately the same width and were quite sharp, as shown in Figure 6.10. For the PC polymer however, the 473 nm emission band appears to be quite broad compared to the 400 and 420 nm emission bands. Similar broad long wavelength emission was observed for the indole system [4] and was attributed to linked trimer species of varying conjugation lengths. Similarly, the 473 nm emission of the PC polymer could arise from a number of different species of varying conjugation lengths.

A summary of the excitation and emission data for the PC monomer and polymer formed at 1 Hz in DMF is given in Table 6.5.

	Excitation maxima / nm	Emission maxima / nm	Stokes shift / cm^{-1}
PC monomer	332	390	4,479
PC polymer	435, 407, 390, 375, 355, 335	400, 420, 473	-

Table 6.5 Summary of the excitation and emission data for the PC monomer and the PC polymer formed at 1 Hz, both in DMF at room temperature.

6.5.2 The effect of varying the conditions of polymer formation

The effect of varying the conditions of polymer formation on the fluorescence spectra of PC polymers was investigated by recording the emission spectra of polymers formed at rotation speeds of 1, 2, 4, 9 and 16 Hz. Examples of such emission spectra, all excited at 350 nm, are shown in Figure 6.17.

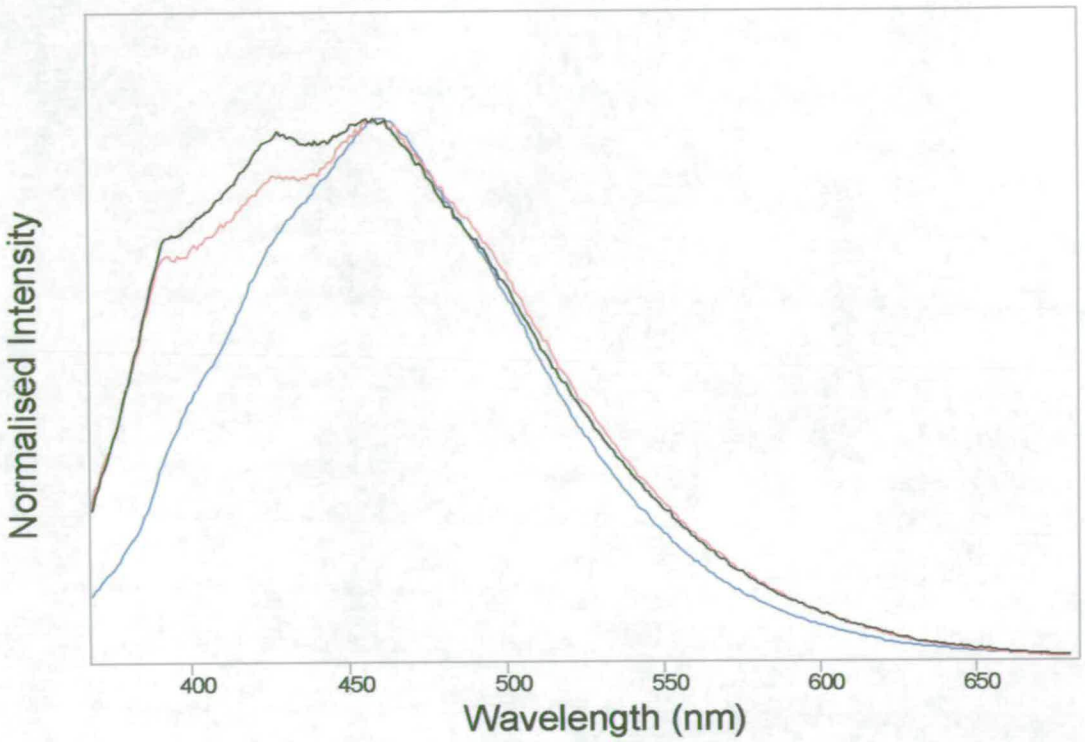

Figure 6.17: Emission spectra, all excited at 350 nm, of PC polymers formed at different rotation speeds; black is 16 Hz, red is 9 Hz and blue is 2 Hz.

As discussed earlier (see section 6.4.2), the effect of increasing the rotation speed is to increase the rate at which monomer is brought to the electrode surface during electropolymerisation. At fast rotation speeds this results in the formation of polymer rich in shorter chain length species such as dimer (IC) and trimer (indoles). Conversely use of a slow rotation speed results in the formation of polymer rich in longer chain length species such as linked dimer or trimer. In Figure 6.17 it can be seen that the intensity of the shorter wavelength PC polymer emission (the 400 and 420 nm bands) decreases relative to the longer wavelength emission (the 473 nm band) as the rotation speed of the RDE is decreased from 16 to 2 Hz. Similar intensity changes have been observed for electropolymerised indoles and also for electropolymerised IC. Therefore it is

likely that a similar mechanism of electropolymerisation is occurring during PC electropolymerisation, ie a two step process with the first step the formation of the short chain length species and the second step the linkage of these species.

In the case of the IC polymer the intensity of the shortest wavelength emission band at 408 nm (dimer) decreases with decreasing rotation speed relative to the second shortest wavelength emission band at 455 nm. However with the PC polymer the intensities of both the two shortest wavelength emission bands, at 400 and 420 nm, decrease relative to the longest wavelength emission band at 473 nm. This suggests that the species that emit at 473 nm are longer chain polymer(s) made up of both the shorter chain polymers which emit at 400 and 420 nm linked together.

However, the trend described above is not followed by the emission from the PC polymer formed at 1 Hz. Rather, as the rotation speed is decreased from 2 to 1 Hz, the intensity of the emission at short wavelengths (400 and 420 nm) increases rather than decreases relative to the emission at long wavelengths (473 nm). This is shown in Figure 6.18. Another anomaly in the 1 Hz PC polymer emission is that the 400 nm band becomes higher in intensity than the 420 nm band. In the emission of the polymers formed at faster rotation speeds the 420 nm band is more intense that the 400 nm band. All this suggests that a different mechanism of electropolymerisation of PC is operating at this slowest rotation speed than that which operates at the faster rotation speeds. This mechanism must favour the formation of short chain length species over long chain length species. It has been shown for the electropolymerisation of indoles that, once the initial layer of polymer is formed on the electrode surface, polymerisation proceeds *via* the linkage of surface adsorbed monomer radical cations [8]. One possibility for the PC polymer formed at 1 Hz is that linkage of monomer radical cations is now occurring in solution rather than on the electrode surface. The probability of monomer radical cations meeting in solution is lower than it is for adsorbed species on the electrode surface. Therefore, with this mechanism, linkage to form long chain length species becomes less likely.

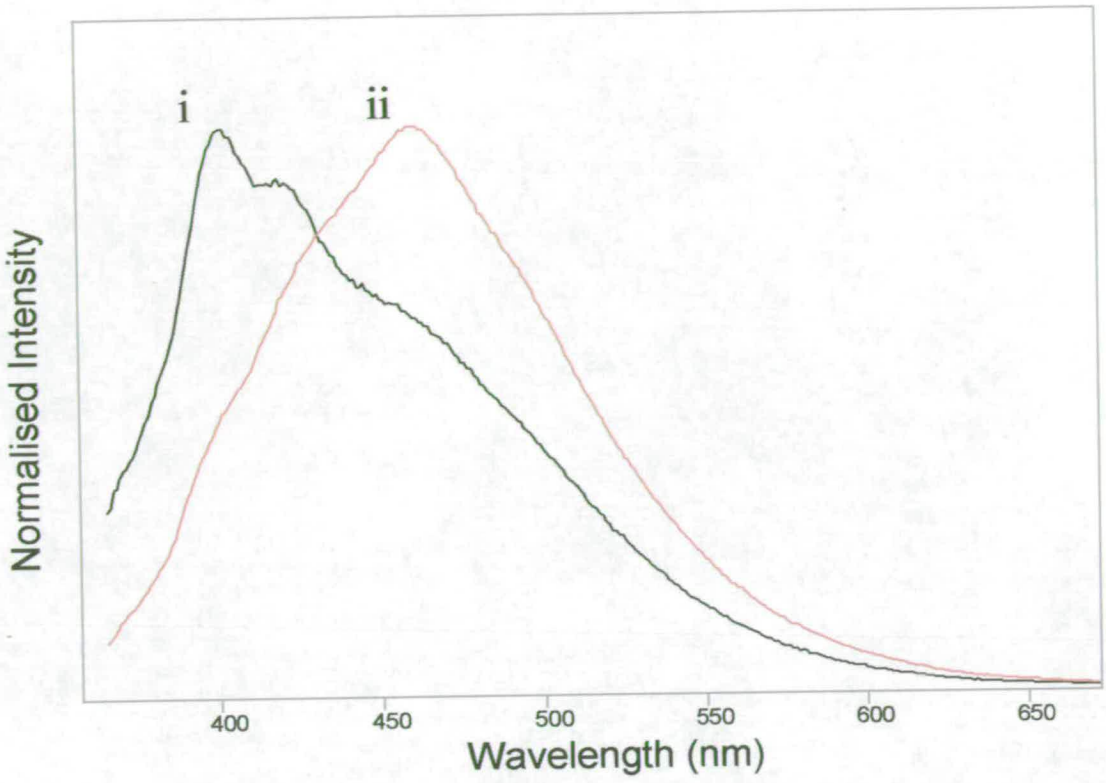

Figure 6.18: Emission spectra, both excited at 350 nm, of PC films formed at rotation speed of (i) 1 Hz (black) and (ii) 2 Hz (red).

6.6 Steady-state fluorescence spectroscopy of a drop coated IC film

If organic conducting polymers are to be of use as the light-emitting layer in a LED they must be fluorescent in the solid state. So far, only the solution-phase steady state fluorescence of IC and PC polymers has been discussed. To determine whether such systems are fluorescent in the solid state, the IC polymer formed at a 1 Hz rotation speed was drop coated onto a glass slide and its steady-state fluorescence spectra measured. Fluorescence has previously been observed in a similar manner for a drop coated 5-cyanoindole film [7].

Figure 6.19 shows a background emission spectrum of the glass slide and the emission spectrum of the drop coated IC film, both excited at 320 nm.

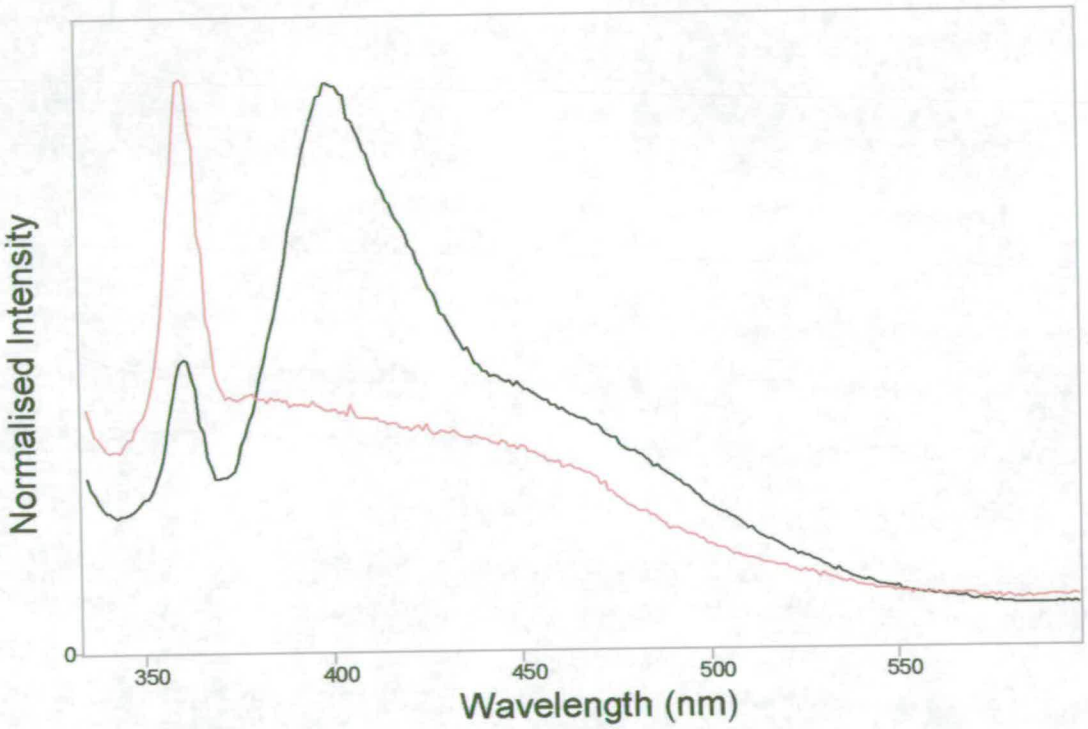

Figure 6.19: Emission spectra of blank microscope slide (red) and drop coated IC film (black), both with excitation wavelength of 320 nm.

The background emission from the glass slide shows scattered light across the region in which IC polymers emit. However there is a peak at 400 nm in the emission of the drop coated IC film which is absent from the background emission of the glass slide. This shows that the IC film is fluorescent in the solid state.

Figure 6.20 shows the emission of the drop coated IC film and of the same IC polymer dissolved in DMF, both excited at 320 nm.

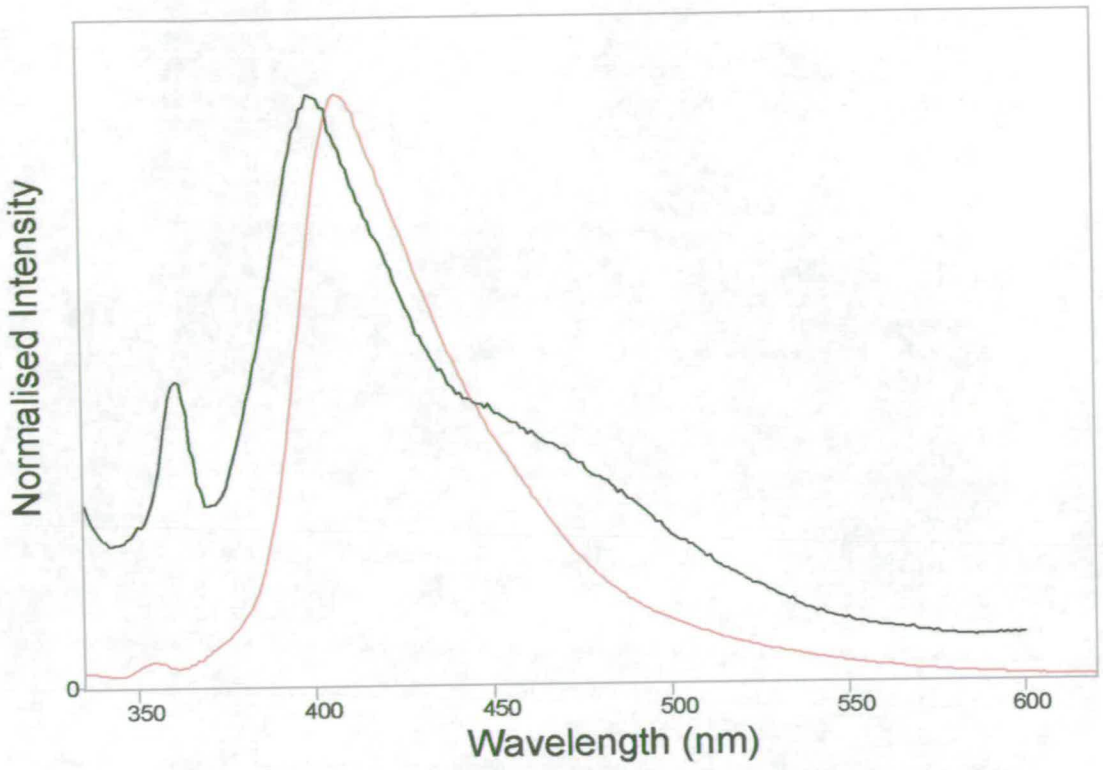

Figure 6.20: Emission spectra of drop-coated IC film (black) and IC polymer dissolved in DMF (red), both with excitation wavelength 320 nm.

The emission maximum of the drop-coated IC film is at 400 nm and is shifted 490 cm^{-1} to shorter wavelength than the emission maximum of the solution-phase IC polymer at 408 nm. Apart from this shift the spectra are similar.

6.7 Conclusions

The room temperature steady-state emission and excitation spectra of IC and PC have been measured in DMF. For both monomers the shape of the emission spectrum is independent of excitation wavelength and so all emission occurs from the same state, the lowest vibrational level of the first singlet excited state S_1. The emission from IC is the mirror image of the excitation spectrum and therefore there is no significant difference between the equilibrium geometries or the potential energy surfaces of the S_0 and S_1 states. In contrast, the emission from PC in DMF is not the mirror image of the IC emission, but is broad and featureless. It has been shown that this asymmetry is not due to the influence of impurities, aggregation or excimer formation.

The room temperature steady-state emission and excitation spectra of IC and PC in cyclohexane have been measured. Again, the emission spectra of both monomers are independent of excitation wavelength and so emission occurs from the same state in each case. The positions of the excitation spectra of IC and PC remain unchanged as the solvent changes from DMF to cyclohexane, which shows that the stability of the Franck-Condon excited state of each monomer is not influenced by the solvent polarity. The emission spectrum of IC is the mirror image of the excitation spectrum in cyclohexane, as it was in DMF. The emission spectrum of PC in cyclohexane, however, is not the mirror image of the excitation spectrum. This asymmetry has been shown not to be due to the influence of impurities, Raman bands or the effects of reabsorption. The three features observed in the emission spectrum of PC in cyclohexane have been shown to be members of a vibronic progression with frequency ~1,200 cm^{-1}. The two features observed in the excitation spectrum have a different energy separation and therefore may be members of a vibrational progression built on a different vibrational mode to those observed in the emission, or they may be members of the same vibrational mode having a different vibrational frequency in the excited state to that in the ground state. Therefore the asymmetry between the excitation and emission spectra of PC in cyclohexane is caused by a difference between the geometries or the shapes of the potential energy surface of the S_0 and S_1 states of PC.

For both IC and PC the Stokes shift decreases when the solvent is changed from DMF to cyclohexane. This shows that there is more solvent relaxation in DMF than in cyclohexane. The change in Stokes shift accompanying the change in solvent is greater for PC than for IC, which

suggests that PC is more perturbed by the increase in solvent polarity than IC. This is likely to be the reason for the broad and featureless nature of the emission of PC in DMF. The Stokes shift observed for PC in cyclohexane is greater than the Stokes shift observed for IC in cyclohexane, which is further evidence of a geometry or potential energy surface difference between the ground and excited states of PC which is not present for IC.

The steady-state fluorescence spectra of an IC polymer formed at a 1 Hz rotation speed and dissolved in DMF were measured. Differences between the emission spectra of the IC monomer and polymer show that electropolymerisation of IC produces an emitting species which is not monomer. Also, the dependence of the IC polymer emission on the excitation wavelength shows that more than one emitting species is present in the sample. The new species formed by the electropolymerisation of IC emit to lower energy than the IC monomer, which shows that the electropolymerisation reaction has formed emitting species which have more extensive π-electron delocalisation than the monomer. These species could be dimer, trimer or longer polymers. The band in the emission of the IC polymer which peaks at 408 nm is due to dimer emission, which emits in the same region as the indole trimers. The Stokes shift for the IC dimer in DMF is more than twice as large as the Stokes shift for the 5-cyanoindole trimer in DMF, and therefore the difference between the ground and excited state dipole moments for the IC dimer is larger than that for the 5-cyanoindole trimer. The dimer emission is much more intense than the longer wavelength emission peaking 455 nm, suggesting that there may be a great deal more dimer present in solution than longer chain length species, depending on the relative quantum yields of the different species. In addition to the dimer emission band, two other emission bands peaking at 455 and 507 nm are observed for the IC polymer.

The steady-state fluorescence spectra of IC polymer samples produced at rotation speeds of 2, 4, 9 and 16 Hz and dissolved in DMF were measured to investigate the effects of the conditions of electropolymerisation on the products formed. The emission of the polymers formed under conditions of fast rotation speed (9 and 16 Hz) is dominated by the dimer emission peak, with very low intensities to longer wavelengths. The intensities to longer wavelengths than the dimer emission increase as the rotation speed decreases. This shows that a similar mechanism to that found for indole electropolymerisation is occurring during IC electropolymerisation. The first step in the electropolymerisation is formation of dimer and this is followed by linkage of the dimer units to form longer polymer species, which emit at to longer wavelengths. At fast

rotation speeds the first step, dimer formation, dominates. At slow rotation speeds the linkage of the dimer units increases in importance. The longest wavelength emitting species are formed from the linked dimer species.

The steady-state emission and excitation spectra of a PC polymer produced at 1 Hz and dissolved in DMF were measured. A comparison of the PC monomer and polymer emission shows that electropolymerisation of PC forms emitting species which are different to the monomer. The increase in the emission to longer wavelengths on going from monomer to polymer indicates that, as with IC, species which have more extensive π-electron delocalisation than the monomer have been formed during the electropolymerisation. The lowest wavelength PC polymer emission at 400 nm has been tentatively assigned as PC dimer. Therefore the PC dimer emits to slightly shorter wavelengths than the IC dimer, which shows that, in principle, using monomers with different sizes of conjugation system can alter the wavelength of emission of the electropolymerised species in solution. The dependence of the emission of the PC polymer on the excitation wavelength shows that there is more than one emitting species present in the sample. In addition to the PC dimer emission there are emission bands for the PC polymer peaking at 420 and 473 nm. For the IC polymer it was found that the intensity of the shortest wavelength emission is far greater than the intensity of the two longer wavelength emission bands. In contrast, the two shortest wavelength emission bands of the PC polymer have similar intensities. Another difference between the emission spectra of the IC and PC polymers is that for the IC polymer all three emission bands were approximately the same width and were quite sharp, whereas for the PC polymer the longest wavelength emission band is quite broad compared two shorter wavelength emission bands. This broad emission could arise from a number of different species of varying conjugation lengths.

The steady-state fluorescence spectra of PC polymers produced at rotation speeds of 2, 4, 9 and 16 Hz and then dissolved in DMF were measured. The intensity of the shorter wavelength PC polymer emission decreases relative to the longer wavelength emission as the rotation speed of the RDE is decreased from 16 to 2 Hz. Similar intensity changes have been observed for electropolymerised indoles and also for electropolymerised IC and it is therefore likely that a similar mechanism operates during electropolymerisation of PC. However, the trend described above is not followed by the emission from the PC polymer formed at 1 Hz. Rather, as the rotation speed is decreased from 2 to 1 Hz, the intensity of the emission at short wavelengths

increases rather than decreases relative to the emission at long wavelengths. This suggests that a different mechanism of electropolymerisation of PC, which favours the formation of short chain length species over long chain length species, is operating at this slowest rotation speed than that which operates at the faster rotation speeds. One possibility is that linkage of monomer radical cations occurs in solution rather than on the electrode surface at the lowest rotation speed. The probability of monomer radical cations meeting in solution is lower than it is for adsorbed species on the electrode surface and therefore linkage to form long chain length species becomes less likely.

The steady-state fluorescence spectra of an IC polymer drop-coated onto a microscope slide has been measured, showing that the IC polymer is fluorescent in the solid state.

6.8 References

1. Lynne A.Crawford, PhD thesis, University of Edinburgh, 2002

2. *Essentials of Molecular Photochemistry* by Andrew Gilbert and Jim Baggott, Blackwell Scientific Publications, 1991

3. H.Lami and N.Glasser, *J.Chem.Phys.*, 1986, **84(2)**, 597-604

4. P.Jennings, A.C.Jones and A.R.Mount, *J.Chem.Soc. Faraday Trans.*, 1998, **94**, 3619-3624

5. J.G.Mackintosh and A.R.Mount, *J.Chem.Soc. Faraday Trans.*, 1994, **90(8)**, 1121-1125

6. J.G.Mackintosh, C.R.Redpath, A.C.Jones, P.R.R.Langridge-Smith and A.R.Mount, *J.Electroanal.Chem.*, 1995, **388(1-2)**, 179-185

7. PhD Thesis, P.Jennings, University of Edinburgh, 1999

8. P.Jennings, A.C.Jones, A.R.Mount and A.D.Thomson, *J.Chem.Soc. Faraday Trans.*, 1997, **93(21)**, 3791-3797

Chapter Seven

TIME-RESOLVED FLUORESCENCE OF INDOLO{3,2,1-*jk*}CARBAZOLE AND PYRROLO{3,2,1-*jk*}CARBAZOLE AND THEIR POLYMERS

7.1 Introduction

In the previous chapter the results of steady-state solution phase fluorescence measurements on the indolo{3,2,1-*jk*}carbazole (IC) and pyrrolo{3,2,1-*jk*}carbazole (PC) monomers and their polymers were presented. These measurements gave an insight into the fluorescence properties of the polymers and the effects of changing the conditions of electropolymerisation on the products of electropolymerisation. It was shown that the electropolymerisation of each monomer results in the formation of polymer containing a number of different emitting components. Such complex multicomponent systems are well suited to investigation by time-resolved fluorescence methods, which can give a more detailed picture of their fluorescence properties than steady-state measurements alone.

In a typical polymer sample there will be a range of polymers with different chain lengths present, and each polymer chain may be divided into segments of different conjugation length. Short conjugation length segments have higher excitation energies than segments with more extended conjugated systems. The fluorescence lifetime of a species is determined largely by the rate of non-radiative decay, since most aromatic fluorophores have radiative lifetimes of similar magnitude. The shorter the lifetime, the more non-radiative decay pathways are available for that species, ie. the more efficiently quenched is the fluorescence. One mechanism by which fluorescence from a chromophore which is part of a polymer may be quenched is by energy transfer to lower excitation energy (longer conjugation) segments of that polymer. The greater the ratio between the length of the polymer chain and the conjugation length of the chromophore, the more available non-radiative, energy transfer pathways will exist. Also, chromophores which emit to lower energies, ie have more extended conjugated systems, tend to have less scope for energy transfer and therefore have longer lifetimes than chromophores which emit to higher energies. It should be noted that, where there are a number of emitting species

present, multiexponential decays are obtained. Though these can be modelled in terms of discrete lifetimes, they may actually represent distributions of emitting species.

In this chapter the results of time-correlated single photon counting (TCSPC) experiments carried out on solutions of the IC and PC monomers and polymers in DMF are given. As the IC polymers were found to be completely soluble in DMF, and to enable comparison between the PC and IC data, the solvent DMF was chosen for all TCSPC measurements. TCSPC allows measurement of the fluorescence decay function at particular excitation and emission wavelengths and this can be analysed to give the individual fluorescence lifetimes and fractional contribution of each component of the total decay. The theoretical basis of the TCSPC experimental technique and the statistical methods used to analyse the data were described in chapter two. Experimental details are given in chapter three and in the following section.

7.2 Experimental details

As discussed in chapter two, decay curves were fitted to a function where the intensity at time t, I(t), is given by:

$$I(t) = A_1 \exp\left(\frac{-t}{\tau_1}\right) + A_2 \exp\left(\frac{-t}{\tau_2}\right) + \ldots\ldots \qquad (7.1)$$

where τ_1 and τ_2 are the lifetimes of components one and two respectively and A_1 and A_2 are the pre-exponential factors (A factors) for each component. It was found for all decays that the length of the shortest lifetime fitted was at least ten times the full width half maximum of the instrument response (IR). Therefore it was unnecessary to deconvolute the decay and the IR in the fitting procedure and all functions were fitted to the tail of the decay. All lifetime data are presented along with the A factors and %-contributions. The %-contribution is the % of the total steady-state fluorescence intensity at that emission wavelength for the given lifetime component.

In recording a fluorescence decay a stop count condition, governing the point at which data collection finishes, must be chosen. The stop count condition in most of the TCSPC experiments performed for this thesis was that 10,000 counts be detected in the peak channel. A higher stop count condition results in data with a higher resolution. In order to ensure that a 10,000 count stop condition gives high enough resolution for these experiments, decays with stop count conditions of both 10,000 and 20,000 counts were recorded for one emission

wavelength in each set of experiments. In all cases these two decays required the same number of lifetimes to be fitted to achieve an acceptable χ^2 value, and the lifetimes, %-contributions and A factors were very similar for each. Therefore use of a 10,000 count stop condition gives acceptable resolution for this set of experiments. All the data given in this chapter were recorded with a 10,000 count stop condition and across 2048 channels unless otherwise stated.

It was found in similar time-resolved fluorescence studies on the indole polymers that there were differences between batches of sample prepared under the same conditions [1]. This was attributed to the difficulty in reproducing identical conditions, since factors such as the quality of monomer and electrode surface, which are hard to quantitatively control, will affect the sample. Therefore, direct comparisons were only made between samples produced from the same monomer solution and on the same day. This approach was also taken in the present work.

7.3 Time-resolved fluorescence of IC and PC monomers

Fluorescence decays for the monomers IC and PC dissolved in DMF were measured by TCSPC. For the measurement of the decay for the IC monomer an excitation wavelength of 370 nm was used and the emission was recorded at 390 nm. For the measurement of the decay of the PC monomer an excitation wavelength of 320 nm was used and the emission was recorded at 400 nm. These wavelengths were chosen by examination of the steady-state fluorescence excitation and emission spectra of IC and PC in DMF, examples of which are shown in Figure 7.1.

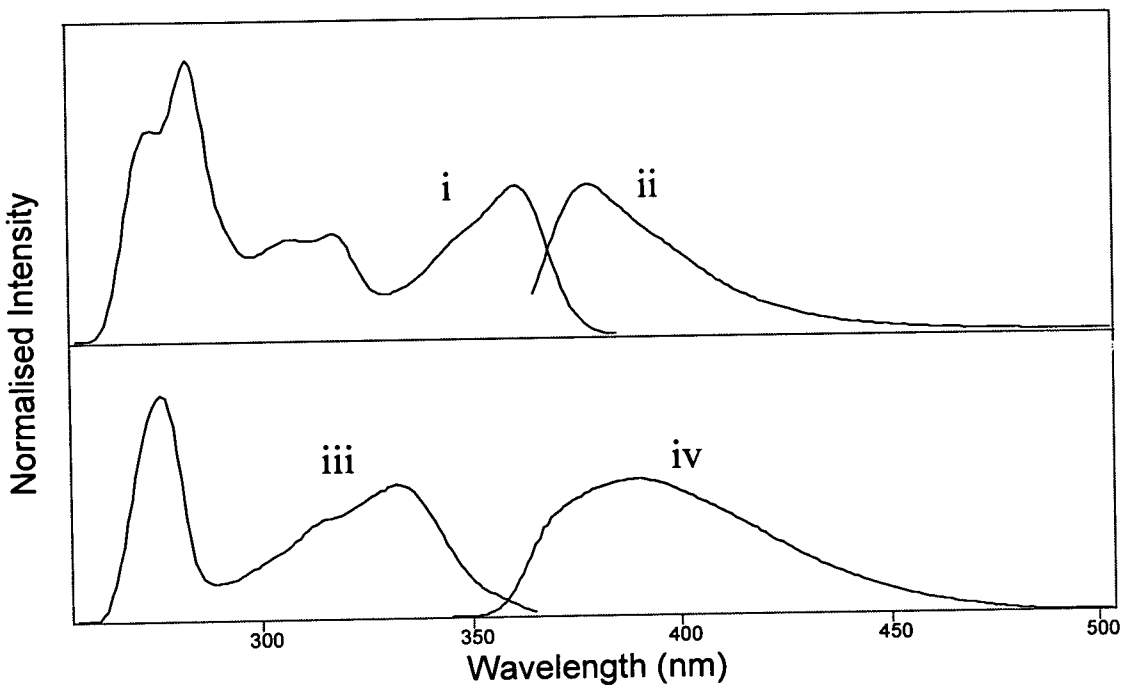

Figure 7.1: Excitation and emission spectra for IC (i and ii) and PC (iii and iv) dissolved in DMF, with emission wavelengths: i 400 nm; iii 380 nm and excitation wavelengths: ii 350 nm; iv 330 nm.

The experimental decay data, fitted single exponential function and residuals for IC are shown in Figure 7.2 and for PC in Figure 7.3. For each monomer the decay was found to be monoexponential. Lifetimes and the χ^2 for each fit are given in Table 7.1. The values of χ^2 shown in Table 7.1 are both ≤ 1.2, which indicates a good fit. Values of 16.1 and 11.5 ns were obtained for the lifetimes of the PC and IC monomers respectively.

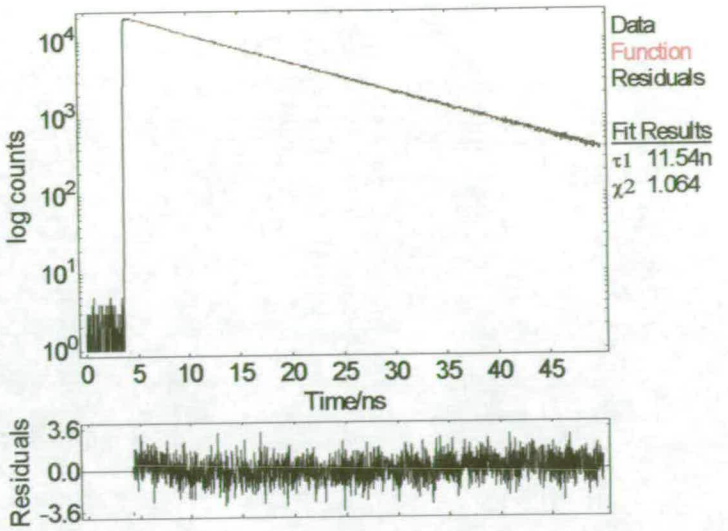

Figure 7.2: The experimental decay data, fitted single exponential function and residuals for IC monomer in DMF.

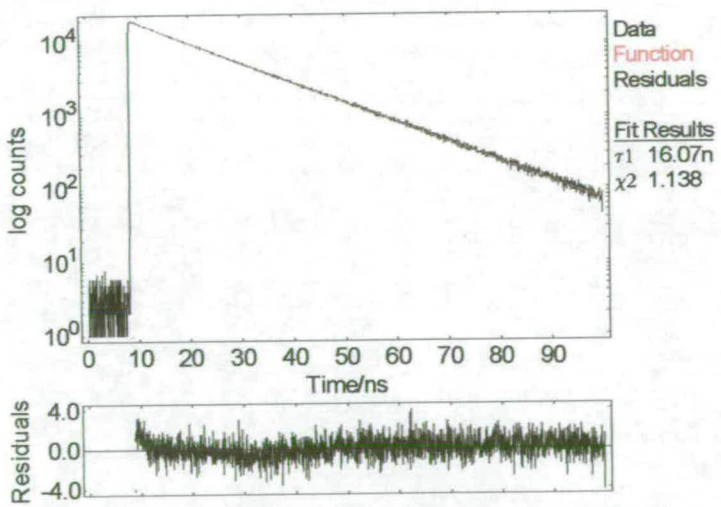

Figure 7.3: The experimental decay data, fitted single exponential function and residuals for PC monomer in DMF.

Monomer	λ_{ex} / nm	λ_{em} / nm	τ / ns	χ^2
IC*	370	390	11.5	1.06
PC*	320	400	16.1	1.14

* both decays collected until 20,000 counts had been recorded in the peak channel

Table 7.1: Excitation and emission wavelengths (λ_{ex} and λ_{em} respectively), fluorescence lifetimes (τ) and χ^2 for the IC and PC monomers.

7.4 Time-resolved fluorescence of IC polymers

7.4.1 Choice of excitation wavelengths

TCSPC measurements were made on samples of IC polymer dissolved in DMF at two different excitation wavelengths. These wavelengths were chosen by examination of the steady-state excitation and emission spectra of the IC polymers, examples of which are shown in Figure 7.4.

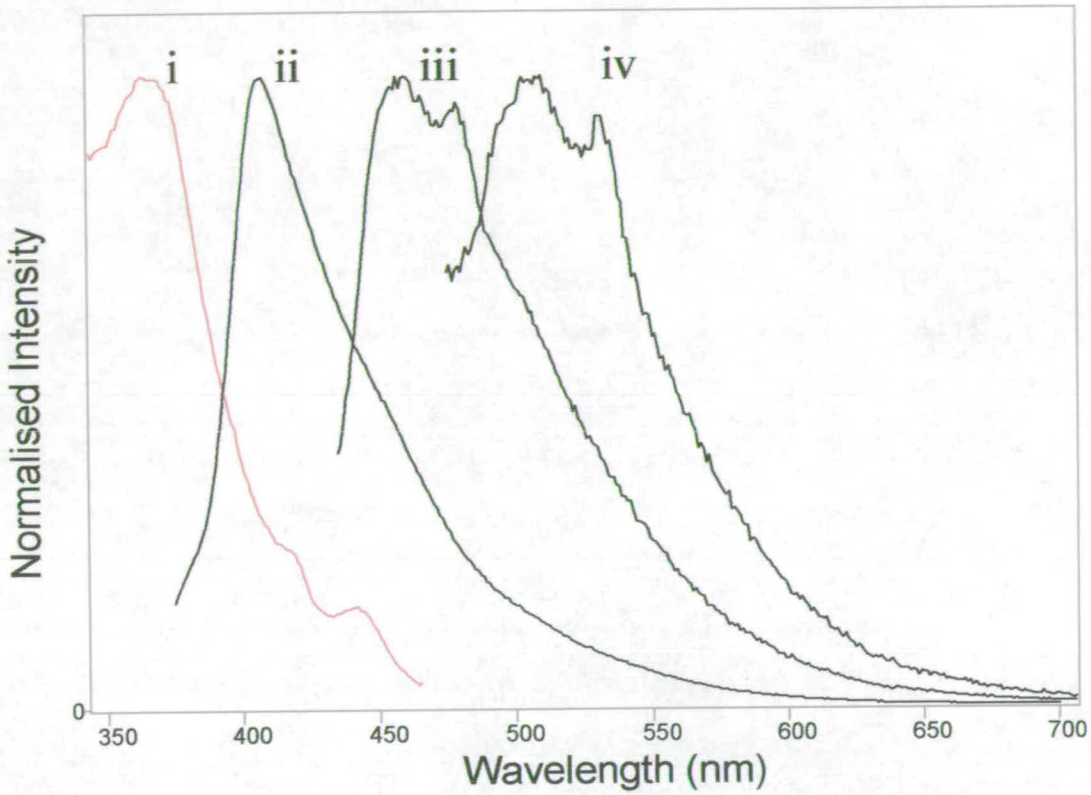

Figure 7.4: Steady-state excitation (red) and emission (black) spectra of IC polymer formed at 1 Hz rotation speed and dissolved in DMF, with (i) emission wavelength 480 nm, (ii) excitation wavelength 360 nm (iii) excitation wavelength 420 nm (Raman scattering at 480 nm) and (iv) excitation wavelength 460 nm (Raman scattering at 533 nm).

As discussed in the previous chapter, there are three emission bands in the IC polymer emission which peak at 408 (Figure 7.4 ii), 455 (Figure 7.4 iii) and 507 nm (Figure 7.4 iv). The band peaking at 408 nm has been attributed to emission from the IC dimer and has a corresponding peak in the excitation spectrum of the IC polymer (Figure 7.4 i) at 370 nm. Therefore the excitation wavelength 370 nm was chosen to investigate the fluorescence lifetime of the dimer species and fluorescence decays were recorded at emission wavelengths from 400 to 540 nm. This excitation wavelength also results in emission from the species forming the 455 nm

emission band and is within the absorption range of IC monomer. Therefore, it has the advantage of allowing the presence of any monomer IC in the sample to be detected, provided that the fluorescence lifetimes of the monomer and polymer species are different.

The second excitation wavelength chosen was 420 nm. This corresponds to an excitation maximum of the species which emit at 455 nm. Exciting at this wavelength produces the emission shown in Figure 7.4 iii. There may be some contribution to this emission from the IC dimer and possibly also from the species giving rise to the 507 nm emission band. Fluorescence decays for this excitation wavelength were recorded at emission wavelengths from 440 to 560 nm.

7.4.2 Sample details

The samples of IC polymer used for the TCSPC experiments were made by electropolymerisation of the IC monomer at a rotating disc electrode (RDE). As discussed in the previous chapter, this allows control of the electropolymerisation conditions by changing the rotation speed of the RDE. The effect of increasing the rotation speed is to increase the rate at which monomer is brought to the electrode surface. TCSPC experiments were performed on IC polymer samples made at rotation speeds of 1 and 9 Hz and at excitation wavelengths of 370 and 420 nm. In section 7.4.3 the results of the experiments on the 1 Hz sample are given and in section 7.4.4 these results are discussed. In section 7.4.5 the effect of changing the rotation speed from 1 to 9 Hz is described.

7.4.3 Results on IC polymer made at 1 Hz

Fluorescence decays were measured for the IC polymer formed at 1 Hz and excited at 370 nm and 420 nm, at various emission wavelengths. The χ^2 values for fitting these decays to a monoexponential function ranged from 2.17 to 10.47, indicating a poor match between the experimental data and the function. However the χ^2 values obtained by fitting each decay to a biexponential function were all ≤ 1.13, indicating a very good match. Also, the residuals for these fits appeared to be randomly distributed around zero. Therefore, all these decays are biexponential. An example of the experimental decay data, fitted biexponential function and residuals obtained for an excitation wavelength of 370 nm and an emission wavelength of 440

nm is shown in Figure 7.5. The lifetimes, A factors and %-contributions for 370 nm excitation are given in Table 7.2.

In Figure 7.6 an example of the experimental decay data, fitted function and residuals obtained for excitation at 420 nm and emission at 500 nm is shown. The lifetimes, A factors and %-contributions for 420 nm excitation are given in Table 7.3.

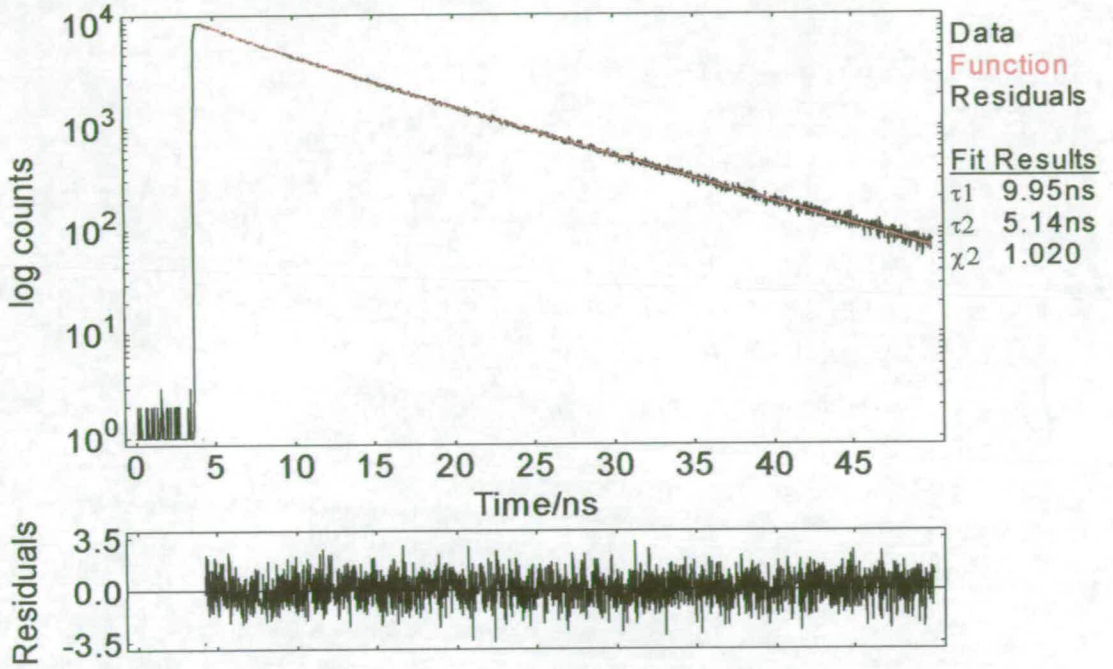

Figure 7.5: The experimental decay data, fitted function and residuals for the IC polymer formed at 1 Hz, with excitation wavelength 370 nm and emission wavelength 440 nm.

λ_{em} / nm	τ_1 / ns	A_1	$\%_1$	τ_2 / ns	A_2	$\%_2$	χ^2
400	10.2	0.72	82	5.8	0.28	18	0.98
410	10.0	0.74	84	5.5	0.26	16	0.99
410*	10.2	0.71	81	5.8	0.29	19	1.02
440	10.0	0.67	80	5.1	0.33	20	1.02
460	9.5	0.58	72	5.0	0.43	28	1.11
500	9.2	0.51	67	4.7	0.49	33	1.02
540	9.2	0.57	72	4.7	0.43	28	1.04

* this decay was collected until 20,000 counts had been recorded in the peak channel

Table 7.2: Fluorescence decay parameters for the decays measured for the IC polymer formed at 1 Hz at various emission wavelengths (λ_{em}), with an excitation wavelength of 370 nm. τ_n is the lifetime of component n, A_n the A factor for component n and $\%_n$ the %-contribution to the steady-state emission intensity of component n.

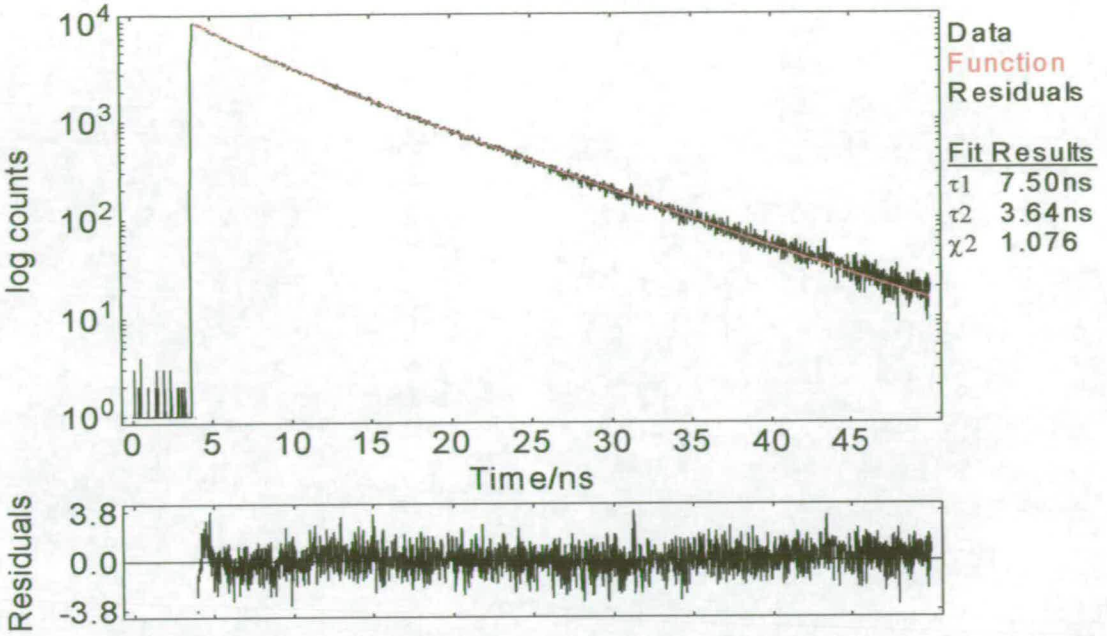

Figure 7.6: The experimental decay data, fitted function and residuals for the IC polymer formed at 1 Hz, with excitation wavelength 420 nm and emission wavelength 500 nm.

λ_{em} / nm	τ_1 / ns	A_1	$\%_1$	τ_2 / ns	A_2	$\%_2$	χ^2
440	7.4	0.58	80	2.6	0.42	20	1.11
460	7.1	0.66	81	3.3	0.34	19	1.06
460*	7.2	0.64	79	3.4	0.36	21	1.13
480	7.3	0.62	77	3.5	0.38	23	1.08
500	7.5	0.60	76	3.6	0.40	24	1.08
540	8.2	0.58	74	4.0	0.42	26	1.12
560	8.4	0.58	74	4.1	0.42	26	1.12

* this decay was collected until 20,000 counts had been recorded in the peak channel

Table 7.3: Fluorescence decay parameters for the decays measured for the IC polymer formed at 1 Hz at various emission wavelengths (λ_{em}), with an excitation wavelength of 420 nm. τ_n is the lifetime of component n, A_n the A factor for component n and $\%_n$ the %-contribution to the steady-state of component n.

The lifetime of any particular emitting species is independent of emission wavelength. Therefore, if the same two species are contributing to two or more different decays, the analysis of each of the decays should yield identical lifetimes. However, since the pre-exponential factor and lifetime for each component (see Equation 7.1) are mathematically correlated in the fitting process, sometimes the lifetimes obtained from such decays are not identical. In such a case a global analysis [2] may be informative. In this type of analysis a number of decays are fitted

simultaneously and the values of certain parameters are held in common between all the decay curves. For example, if it is thought that there are only two species contributing to a number of decays, the values of the two lifetimes may be held in common between all those decays in the global analysis. The generation of acceptable χ^2 values with this process would suggest that there are indeed only two species contributing to all the decays.

In the data shown in Table 7.2, for the decays measured with an excitation wavelength of 370 nm, the lifetimes of components one and two vary by ~1 ns across all the emission wavelengths measured. This small variation in the lifetimes generated by the fitting of each decay individually suggests that the same two species may be contributing to each decay in this data set. To investigate this a global analysis was performed, with the values of τ_1 and τ_2 held in common for all seven decays. The resulting fitted lifetimes, A factors and %-contributions are shown in Table 7.4.

λ_{em} / nm	$\%_1$	A_1	$\%_2$	A_2	Local χ^2
400	85	0.76	15	0.24	0.98
410	85	0.75	15	0.25	0.99
410*	85	0.76	15	0.25	1.03
440	77	0.65	23	0.35	1.03
460	61	0.47	39	0.53	1.14
500	51	0.36	49	0.64	1.10
540	55	0.40	45	0.60	1.13
Global τ and χ^2	τ_1 = 10.0 ns		τ_2 = 5.5 ns		1.06

* this decay was collected until 20,000 counts had been recorded in the peak channel

Table 7.4: Results of global analysis on decays collected for the IC polymer formed at 1 Hz, with excitation wavelength of 370 nm. The values of τ_1 and τ_2 were held in common for all seven decays.

The results of the global analysis of the decays measured with an excitation wavelength of 370 nm, which are shown in Table 7.4, are very good. All the χ^2 values are within acceptable limits and none of the local χ^2 values are significantly greater than those obtained by fitting each decay individually (shown in Table 7.2). Therefore, it is justifiable to conclude that there are only two emitting species, with lifetimes of 10.0 and 5.5 ns, contributing to all seven decays.

In the data shown in Table 7.3, for the decays measured with an excitation wavelength of 420 nm, the lifetimes of components one and two vary by ~1.5 ns across all the emission wavelengths measured. To investigate the possibility of there being only two emitting species contributing to all seven decays a global analysis, where the values of τ_1 and τ_2 were held in common across all the decays, was performed. The resulting fitted lifetimes, A factors and %-contributions and are shown in Table 7.5.

λ_{em} / nm	$\%_1$	A_1	$\%_2$	A_2	Local χ^2
440	60	0.45	40	0.55	2.38
460	58	0.42	42	0.58	1.53
460*	59	0.43	41	0.57	1.72
480	59	0.44	41	0.56	1.33
500	64	0.48	36	0.52	1.13
540	75	0.62	25	0.38	1.41
560	79	0.66	21	0.34	1.67
Global τ and χ^2	τ_1 = 8.0 ns		τ_2 = 4.2 ns		1.60

* this decay was collected until 20,000 counts had been recorded in the peak channel

Table 7.5: Results of global analysis on decays collected for the IC polymer formed at 1 Hz, with excitation wavelength of 420 nm. The values of τ_1 and τ_2 were held in common for all seven decays.

In contrast to the results of the global analysis performed on the decays measured with an excitation wavelength of 370 nm, the results of the global analysis performed on the decays measured with an excitation wavelength of 420 nm are quite poor. The global χ^2 of 1.60 is much higher than the χ^2 values obtained for the individual fits in Table 7.3. Moreover, the local χ^2 values in the global analysis are unacceptably high compared with those given in Table 7.3. Therefore it can be concluded that there are more than two emitting species contributing to the total emission envelope.

It can be seen in the data shown in Table 7.5 that the local χ^2 of 2.38 obtained for the decay measured with an emission wavelength of 440 nm is significantly higher than all the other local χ^2 values. It is also much higher than the χ^2 of 1.11 obtained when fitting this decay individually. Therefore the two species emitting at 440 nm may be different from the species emitting to longer wavelengths. Therefore the global analysis was repeated with the 440 nm decay excluded. The results of this global analysis are shown in Table 7.6.

λ_{em} / nm	$\%_1$	A_1	$\%_2$	A_2	Local χ^2
460	49.6	0.35	50.4	0.65	1.46
460*	50.6	0.36	49.4	0.64	1.68
480	51.0	0.37	49.1	0.63	1.31
500	55.5	0.41	44.6	0.59	1.20
540	68.1	0.54	31.9	0.46	1.37
560	71.6	0.58	28.4	0.42	1.53
Global τ and χ^2	$\tau_1 = 8.2$ ns		$\tau_2 = 4.6$ ns		1.43

* this decay was collected until 20,000 counts had been recorded in the peak channel

Table 7.6: Results of global analysis on decays collected for the IC polymer formed at 1 Hz, with excitation wavelength of 420 nm, with the decay measured with an emission wavelength of 440 nm excluded. The values of τ_1 and τ_2 were held in common for all seven decays.

Excluding the decay measured at an emission wavelength of 440 nm from the global analysis does give a slight improvement in the χ^2 values. Therefore it can be concluded that there are two species with lifetimes of 7.4 and 2.6 ns emitting at 440 nm and that these species are different from those emitting to longer wavelengths. However all the χ^2 values in Table 7.6 are ≥ 1.2 and are still significantly higher than the χ^2 obtained by individual fitting of the decay curves.

A re-examination of the data shown in Table 7.3 for the individual fitting of these decays shows that both the short and long lifetimes vary by only 0.1 ns between the decays measured at the 460 and 480 nm emission wavelengths. Similarly the short and long lifetimes vary by only 0.1 and 0.2 ns respectively between the decays measured at the 540 and 560 nm emission wavelengths. However, the lifetimes obtained for these two subsets of emission wavelengths differ by approximately 1 ns each. Therefore the same two species may be responsible for the emission at 460 and 480 nm and these may be different from the two species responsible for the emission at both 540 and 560 nm. The lifetimes obtained for the 500 nm emission decay lie somewhere between these two sets of lifetimes and so it is uncertain to which set they may belong. To investigate whether this is the case, four sets of global analysis were perfomed, all with the values of the two lifetimes held in common between all the decays involved. In the first global analysis, the results of which are shown in Table 7.7, only the 460 and 480 nm emission decays were included. This global analysis was repeated with the addition of the 500 nm emission decay and the results are shown in Table 7.8. In the third global analysis, the results of which are shown in Table 7.9, only the 500, 540 and 560 nm decays were included. This was

then repeated but with the 500 nm emission decay excluded and these results are shown in Table 7.10.

λ_{em} / nm	$\%_1$	A_1	$\%_2$	A_2	Local χ^2
460	78	0.63	22	0.37	1.07
460*	79	0.64	21	0.36	1.14
480	79	0.64	21	0.36	1.08
Global τ and χ^2	$\tau_1 = 7.2$ ns		$\tau_2 = 3.4$ ns		1.10

* this decay was collected until 20,000 counts had been recorded in the peak channel

Table 7.7: Results of global analysis on the 460 and 480 nm emission decays collected for the IC polymer formed at 1 Hz, with excitation wavelength of 420 nm. The values of τ_1 and τ_2 were held in common for all three decays.

λ_{em} / nm	$\%_1$	A_1	$\%_2$	A_2	Local χ^2
460	75	0.59	25	0.41	1.12
460*	76	0.60	24	0.40	1.15
480	76	0.61	24	0.39	1.08
500	80	0.66	20	0.34	1.24
Global τ and χ^2	$\tau_1 = 7.3$ ns		$\tau_2 = 3.6$ ns		1.15

* this decay was collected until 20,000 counts had been recorded in the peak channel

Table 7.8: Results of global analysis on the 460, 480 and 500 nm decays collected for the IC polymer formed at 1 Hz, with excitation wavelength of 420 nm. The values of τ_1 and τ_2 were held in common for all four decays.

λ_{em} / nm	$\%_1$	A_1	$\%_2$	A_2	Local χ^2
500	55	0.39	45	0.61	1.33
540	67	0.52	33	0.48	1.15
560	70	0.55	30	0.45	1.20
Global τ and χ^2	$\tau_1 = 8.4$ ns		$\tau_2 = 4.4$ ns		1.23

Table 7.9: Results of global analysis on the 500, 540 and 560 nm decays collected for the IC polymer formed at 1 Hz, with excitation wavelength of 420 nm. The values of τ_1 and τ_2 were held in common for all three decays.

λ_{em} / nm	$\%_1$	A_1	$\%_2$	A_2	Local χ^2
540	72	0.56	28	0.44	1.13
560	75	0.59	25	0.41	1.12
Global τ and χ^2	$\tau_1 = 8.3$ ns		$\tau_2 = 4.1$ ns		1.13

Table 7.10: Results of global analysis on the 540 and 560 nm decays collected for the IC polymer formed at 1 Hz, with excitation wavelength of 420 nm. The values of τ_1 and τ_2 were held in common for both decays.

The results of the global analysis shown in Table 7.7 are very good. All the χ^2 values are ≤ 1.14 and the local χ^2 values are close to those obtained by fitting each decay individually (see Table 7.3). This shows that only two species are responsible for the emission at 460 and 480 nm. The results of the global analysis shown in Table 7.10 are also very good, with all the χ^2 values $\leq$ 1.13 and the local χ^2 values close to those obtained by fitting the two decays individually. Therefore only two species are responsible for the emission at 540 and 560 nm. Including the 500 nm emission decay in the global analysis of the 540 and 560 nm decays, the results of which are shown in Table 7.9, significantly worsens the χ^2 values obtained. In particular the local χ^2 for the 500 nm decay in the global analysis is 1.33 compared to the χ^2 of 1.08 obtained by fitting this decay individually. The results obtained by including the 500 nm emission decay in the global analysis of the 460 and 480 nm decays, shown in Table 7.8, are better. Although the χ^2 values are slightly worse than those shown in Table 7.7, they are still acceptable, with all $\chi^2 \leq$ 1.24. The worst χ^2 value in Table 7.8 is for the 500 nm decay. However the lifetimes obtained for fitting this decay individually are close to the global lifetimes in Table 7.8. Therefore, it can be concluded that the species responsible for the emission at 500 nm are the same as those responsible for the emission at 460 and 480 nm and that they have lifetimes of 7.3 and 3.6 ns. The two species responsible for the emission at 540 and 560 nm have lifetimes of 8.3 and 4.1 ns. The accepted values of the lifetimes, A factors and %-contributions for the IC polymer produced at 1 Hz and excited at 420 nm are summarised in Table 7.11.

λ_{em} / nm	τ_1 / ns	A_1	$\%_1$	τ_2 / ns	A_2	$\%_2$
440	7.4	0.58	80	2.6	0.42	20
460	7.3	0.59	75	3.6	0.41	25
460*	7.3	0.60	76	3.6	0.40	24
480	7.3	0.61	76	3.6	0.39	24
500	7.3	0.66	80	3.6	0.34	20
540	8.3	0.56	72	4.1	0.44	28
560	8.3	0.59	75	4.1	0.41	25

* this decay was collected until 20,000 counts had been recorded in the peak channel

Table 7.11: Accepted lifetimes, A factors and %-contributions for the 1 Hz IC polymer sample excited at 420 nm.

7.4.4 Discussion

The steady-state fluorescence spectra of the IC polymer discussed in the previous chapter showed that electropolymerisation of the IC monomer results in the formation of several new emitting species. This is confirmed by the multiexponential nature of the decays measured for the IC polymer samples excited at 370 nm, where only monoexponential decays were recorded for the IC monomer at the same excitation wavelength. The value of 10.0 ns for one of the IC polymer lifetimes is close to the lifetime of the IC monomer, which has been measured as 11.5 ns. This suggests that the component with a lifetime of 10.0 ns in the IC polymer sample may be IC monomer. However, closer examination of the data in Table 7.2 shows that this is not the case. The component with a lifetime of 10.0 ns has the highest %-contribution and therefore contributes the majority of the intensity to the steady-state emission spectrum of the polymer at all the emission wavelengths measured, from 400 to 540 nm. In the steady-state emission spectrum of the IC monomer in DMF (see previous chapter) there is no significant emission intensity at wavelengths longer than 480 nm. Therefore, the species with a lifetime 10.0 ns is not IC monomer and this polymer sample contains no detectable monomer.

In the previous section, it was shown that two emitting species with lifetimes of 10.0 and 5.5 ns contribute to the decays measured with an excitation wavelength of 370 nm. Plots of the %-contributions and A factors against emission wavelength for these two emitting species are shown in Figure 7.7. The A factor for a species is the fraction of the emitting population (at that excitation and emission wavelength) constituted by that species. The %-contribution for a species is the contribution to the steady-state fluorescence intensity of the sample, made by that species at that excitation and emission wavelength. In Figure 7.7 it can be seen that both the A

factors and the %-contribution of the 10.0 ns lifetime species, decrease as the emission wavelength increases from 400 to 540 nm. The plot of A factor against emission wavelength shows that there is more of the 5.5 ns lifetime species emitting above ~460 nm than the 10.0 ns lifetime species, although because of its shorter lifetimes it contributes less to the steady-state spectrum than the 10.0 ns species at these wavelengths. Since species with more extensive π-electron delocalisation generally emit to longer wavelength than species with less delocalisation, this data suggests that the 5.5 ns lifetime component is a species with more conjugation than the 10.0 ns lifetime species.

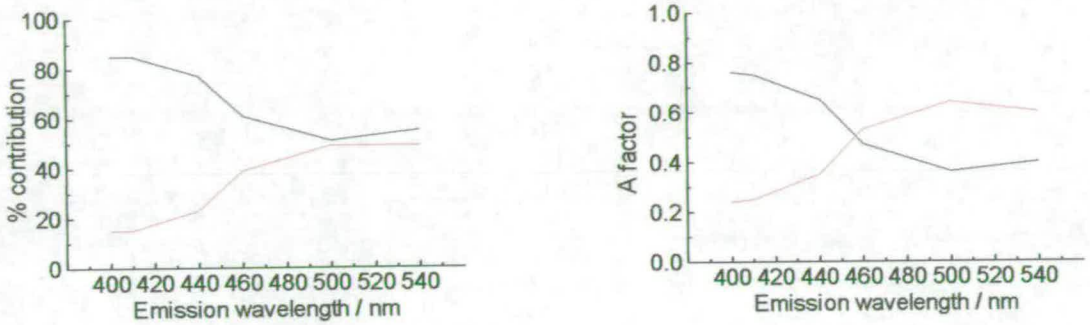

Figure 7.7: Plots of %-contribution and A factor against emission wavelength for the two species with lifetimes 10.0 ns (black) and 5.5 ns (red) for the 1 Hz IC polymer sample. Data taken from results of global analysis shown in Table 7.4.

The values of the %-contribution given in Table 7.4 can be used to separate the overall steady-state emission spectrum of the sample into the individual spectra of each component, as shown in Table 7.12 and Figure 7.8.

λ_{em} / nm	Intensity of steady-state spectrum	$\%_1$	Intensity × $\%_1$	$\%_2$	Intensity × $\%_2$
400	2.3×10^7	85	2.0×10^7	15	3.5×10^6
410	2.7×10^7	85	2.3×10^7	15	4.1×10^6
440	1.6×10^7	77	1.2×10^7	23	3.7×10^6
460	1.1×10^7	61	6.7×10^6	39	4.3×10^6
500	4.6×10^6	51	2.3×10^6	49	2.3×10^6
540	2.1×10^6	55	1.2×10^6	45	9.5×10^5

Table 7.12: Data plotted in Figure 7.8. Intensities at different emission wavelengths taken from the steady-state emission spectrum of the IC polymer with excitation wavelength 360 nm. τ_1 is 10.0 ns and τ_2 is 5.5 ns. %-contributions of each lifetime from global analysis.

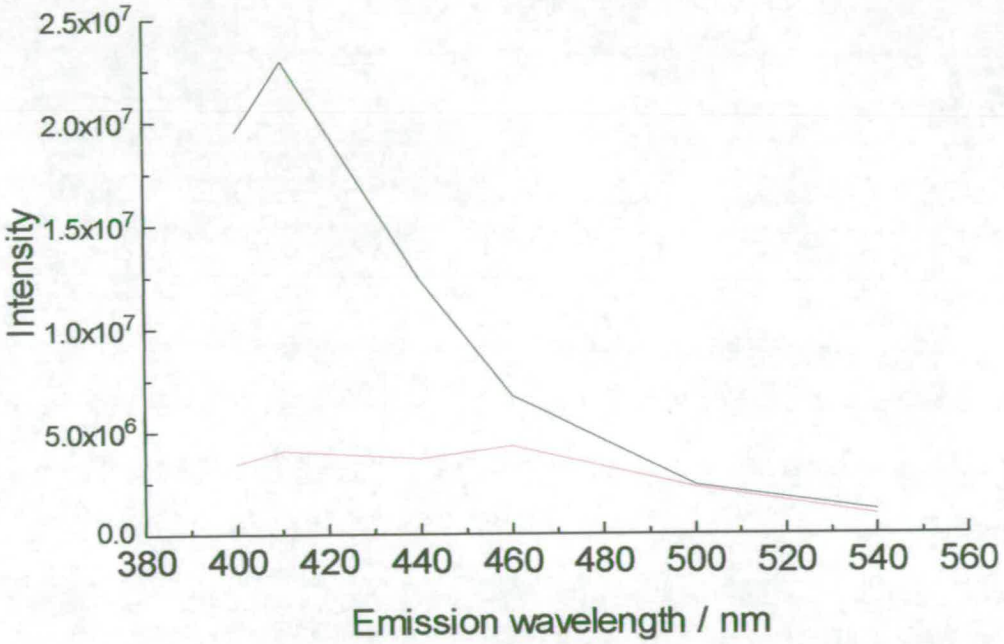

Figure 7.8: Plot of intensity of fluorescence emission for each component where black is 10.0 ns (τ_1) and red is 5.5 ns (τ_2).

As discussed in chapter six, the emission band which peaks at 408 nm, observed in the emission spectrum of the IC polymer excited at 360 nm (see Figure 7.4 ii), is attributed to IC dimer emission. The plot of the emission of the component with lifetime of 10.0 ns shown in Figure 7.8 appears to peak at around 410 nm and so this lifetime can be attributed to the IC dimer. A second emission band peaking at 455 nm was observed in the steady-state spectra of the IC polymer. Although this band is not clearly resolved in the overall steady-state emission excited

at 360 nm, it does contribute some intensity on the red edge of that spectrum. Figure 7.8 suggests that the component with lifetime 5.5 ns may be responsible for this emission band, although there is some contribution from the IC dimer.

In the previous section the analysis of the TCSPC data collected for the IC polymer sample produced at 1 Hz and excited at 420 nm was discussed. It was shown that different species are responsible for the emission at different wavelengths. The emission at 440 nm arises from two species with lifetimes of 7.4 and 2.6 ns, emission in the range 460 to 500 nm arises from two species with lifetimes of 7.3 and 3.6 ns and emission in the range 500 to 560 nm from two species with lifetimes of 8.3 and 4.1 ns. It seems probable that the two species with lifetimes of 7.4 and 7.3 ns are the same and that, therefore, there are five different species emitting when this sample is excited at 420 nm. None of these lifetimes are the same as the two observed when exciting this sample at 370 nm of 10.0 ns (for the IC dimer) and 5.5 ns (for a species with a greater degree of π-electron delocalisation than the dimer). Therefore at least seven different emitting species are present in this sample. It should be noted that some of these lifetimes may be representative of a distribution of similar lifetimes rather than a single species.

Altogether three emission bands peaking at 408, 455 and 507 nm were observed in the steady-state emission spectra of the IC polymer, as discussed in the previous chapter. The band peaking at 408 nm has been attributed to the IC dimer, which has a lifetime of 10.0 ns. In Figure 7.4 ii it can be seen that, when exciting at 360 nm, there is a shoulder in the emission spectrum around 455 nm. The decays measured with an excitation wavelength of 370 nm showed that this emission is from both the IC dimer and a species with lifetime 5.5 ns. The steady-state emission spectrum of the 1 Hz IC polymer sample excited at 420 nm, which is shown in Figure 7.4 iii, appears predominantly to be made up of the emission band which peaks at 455 nm. However, the decays measured with the excitation wavelength of 420 nm show that this emission is not due to the species with lifetimes 10.0 or 5.5 ns, as these lifetimes do not appear in the analysis. Thus, in a complex multicomponent system such as this, fluorescence occuring at the same emission wavelength, but at different excitation wavelengths, is not necessarily due to the same species. For example, in this sample there are several species which emit at ~455 nm.

The species in the IC polymer sample with the shortest lifetime, and therefore the most efficient non-radiative decay, is the 2.6 ns species. This species is observed, when exciting at 420 nm, in

the emission at 440 nm but not in the longer wavelength emission. Therefore this species is a smaller conjugated system than the species whose emission is observed at wavelengths of 460 to 560 nm with the same excitation wavelength. This, together with the short lifetime, is consistent with it being a small chromophore within a larger polymer species. However, 2.6 ns is only four times shorter than 10.0 ns, the lifetime of the IC dimer and the longest lifetime observed. In similar work on indole polymer systems [1, 3] it has been observed that the lifetime of the free indole trimer is 5.5 ns and that this is approximately fifty times the lifetime of the shortest lifetime species, which has been attributed to linked trimer. The very short lifetime observed for the linked indole trimer species compared to the 2.6 ns linked IC species indicates that the linked indole trimer is part of a much longer polymer than the IC species. This is evidence that the size of polymer produced by the electropolymerisation of IC is limited.

At an excitation wavelength of 420 nm, in the emission range 460-500 nm, two decay components with lifetimes 7.4 ns and 3.6 ns were observed. The A factors of these components show little dependence on emission wavelength, indicating that these two species have similar emission spectra and therefore similar conjugation lengths, although they differ significantly in their non-radiative decay rates. This behaviour can be interpreted in terms of differing polymer environments of the two emitting species. Thus, the 7.4 ns lifetime may be due to a free oligomer (or an oligomer with a relatively short polymer chain) and the shorter lifetime to a species of similar conjugation length within a relatively long polymer chain. The latter species would be subject to enhanced non-radiative decay by energy transfer to longer conjugation length (lower excitation energy) segments of the polymer chain, and hence show a shorter fluorescence lifetime. The emission at longer wavelengths (540 and 560 nm), with lifetimes of 8.3 and 4.1 ns, can be attributed to a similar pair of emitting species, but with longer conjugation lengths.

7.4.5 The effects of changing the conditions of polymer formation

As discussed in chapter six, the conditions during electropolymerisation can be controlled by altering the rotation speed of the RDE. The effect of increasing the rotation speed is to increase the rate at which monomer is brought to the electrode surface during polymerisation. It was found that use of a fast rotation speed (9 and 16 Hz) results in spectra dominated by the IC dimer emission, which peaks at 408 nm. Use of a slow rotation speed (1 and 2 Hz) results in an increase in the intensity of the emission band at longer wavelengths, which peaks at 455 nm,

with respect to the 408 nm IC dimer emission band. In order to investigate further the effects of changing the conditions of electropolymerisation on the composition of the polymer, time-resolved fluorescence measurements were made on a sample of IC polymer produced at a rotation speed of 9 Hz. Both the 1 Hz and 9 Hz IC polymer samples were produced on the same day from the same monomer solution and both were the same samples as used in the steady-state spectroscopy reported in chapter six. In this section the results of the TCSPC experiments on the IC polymer samples produced with a 1 and 9 Hz rotation speed are compared.

As for the sample of IC polymer produced at 1 Hz, all the decays measured for the 9 Hz sample of IC polymer, excited at 370 and 420 nm, were found to be biexponential. The results of global analysis of the fluorescence decays excited at 370 nm are given in Table 7.13. It can be seen that, as for the 1 Hz sample, the 9 Hz sample excited at 370 nm contains only two species with lifetimes of 9.8 and 5.0 ns, emitting across this wavelength region.

λ_{em} / nm	$\%_1$	A_1	$\%_2$	A_2	Local χ^2
400	92	0.85	8	0.15	1.06
410	92	0.86	8	0.14	1.03
440	89	0.80	11	0.20	1.00
460	82	0.70	18	0.30	1.01
500	72	0.57	28	0.43	1.03
540	70	0.55	30	0.45	1.03
Global τ and χ^2	$\tau_1 = 9.8$ ns		$\tau_2 = 5.0$ ns		1.03

Table 7.13: Results of global analysis on decays collected for the IC polymer formed at 9 Hz, with excitation wavelength of 370 nm. The values of both τ_1 and τ_2 were held in common for all decays.

Since the lifetimes fitted to the decays measured for the 1 Hz sample of 10.0 ns and 5.5 ns are very similar to those fitted to the decays measured for the 9 Hz sample of 9.8 ns and 5.0 ns, it is reasonable to assume that the same two species are contributing to the decays in each case.

Plots of the %-contribution and A factors for both the 9 Hz and 1 Hz samples, using the data shown in Tables 7.13 and 7.4, are shown in Figure 7.9.

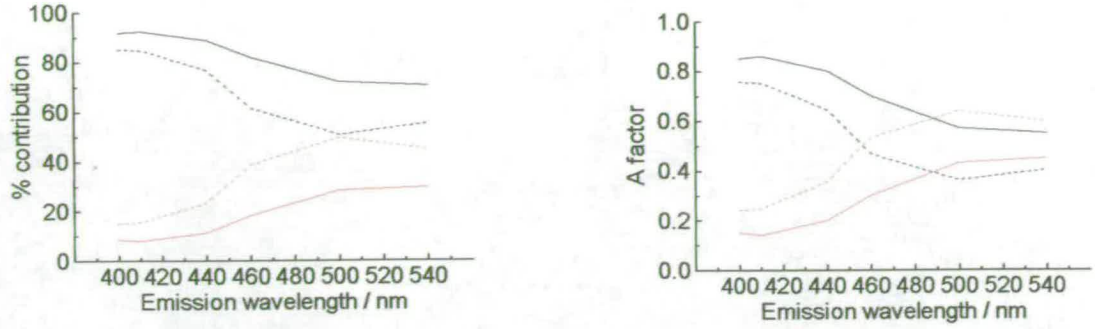

Figure 7.9: Plots of %-contribution and A factor, obtained from the global analyses with both lifetimes held in common for all decays, against emission wavelength for the two component lifetimes of the 9 Hz IC polymer sample (solid lines) and the 1 Hz IC polymer sample (dashed lines), both excited at 370 nm. Black is long lifetime component (~10 ns (τ_1)) and red is short lifetime component (~5 ns (τ_2)).

In the plots shown in Figure 7.9 it can be seen that at all emission wavelengths the A factors and %-contributions for the IC dimer are increased, relative to those for the shorter lifetime species, in the 9 Hz sample compared to the 1 Hz sample. This result supports the conclusion from the steady-state spectra of the IC polymers that IC dimer formation is favoured over the formation of polymer species at fast rotation speeds.

As for the 1 Hz sample, the results of the global analysis with both lifetimes held in common which was carried out on all the decays measured for the 9 Hz sample excited at 420 nm, were poor. Again the 440 nm emission decay gave a particularly high value of χ^2 compared to the other decays and so the global analysis was repeated with the 440 nm decay excluded. The χ^2 values obtained from this global analysis were not sufficiently improved to be acceptable. As before, the individual lifetimes for the remaining decays, with emission wavelengths from 460 to 560 nm, appear to belong to two distinct sets, one for the emission wavelengths from 460 to 480 nm and the other for the emission wavelengths from 540 to 560 nm, with the 500 nm lifetimes somewhere in between. Therefore, as before, four sets of global analysis were performed, the results of which are shown in Tables 7.14, 7.15, 7.16 and 7.17.

λ_{em} / nm	$\%_1$	A_1	$\%_2$	A_2	Local χ^2
460	69	0.52	31	0.48	1.12
460*	69	0.52	31	0.48	1.12
480	73	0.57	27	0.43	1.09
Global τ and χ^2	$\tau_1 = 7.5$ ns		$\tau_2 = 3.7$ ns		1.11

* this decay was collected until 20,000 counts had been recorded in the peak channel

Table 7.14: Results of global analysis on the 460 and 480 nm emission decays collected for the IC polymer formed at 9 Hz, with excitation wavelength of 420 nm. The values of τ_1 and τ_2 were held in common for all three decays.

λ_{em} / nm	$\%_1$	A_1	$\%_2$	A_2	Local χ^2
460	62	0.46	38	0.54	1.21
460*	62	0.46	38	0.54	1.22
480	67	0.50	33	0.50	1.04
500	72	0.57	28	0.43	1.34
Global τ and χ^2	$\tau_1 = 7.7$ ns		$\tau_2 = 3.9$ ns		1.20

* this decay was collected until 20,000 counts had been recorded in the peak channel

Table 7.15: Results of global analysis on the 460, 480 and 500 nm decays collected for the IC polymer formed at 9 Hz, with excitation wavelength of 420 nm. The values of τ_1 and τ_2 were held in common for all four decays.

λ_{em} / nm	$\%_1$	A_1	$\%_2$	A_2	Local χ^2
500	55	0.39	45	0.61	1.17
540	67	0.50	33	0.50	1.06
560	70	0.54	30	0.46	1.12
Global τ and χ^2	$\tau_1 = 8.7$ ns		$\tau_2 = 4.4$ ns		1.12

Table 7.16: Results of global analysis on the 500, 540 and 560 nm decays collected for the IC polymer formed at 9 Hz, with excitation wavelength of 420 nm. The values of τ_1 and τ_2 were held in common for all three decays.

λ_{em} / nm	$\%_1$	A_1	$\%_2$	A_2	Local χ^2
540	69	0.52	31	0.48	1.06
560	73	0.56	27	0.44	1.09
Global τ and χ^2	$\tau_1 = 8.6$ ns		$\tau_2 = 4.2$ ns		1.07

Table 7.17: Results of global analysis on the 540 and 560 nm decays collected for the IC polymer formed at 9 Hz, with excitation wavelength of 420 nm. The values of τ_1 and τ_2 were held in common for both decays.

The results of the global analyses shown in Table 7.14 and 7.17 are very good. All the χ^2 values are ≤ 1.12 and the local χ^2 values are close to those obtained by fitting each decay individually. This shows that only two species are responsible for the emission at 460 and 480 nm and a different two species are responsible for the emission at both 540 and 560 nm. Including the 500 nm emission decay in the global analysis of the 460 and 480 nm decays, the results of which are shown in Table 7.15, significantly worsens the χ^2 values obtained. In particular the local χ^2 for the 500 nm decay in the global analysis is 1.34 compared to the χ^2 of 1.09 obtained by fitting this decay individually. The results obtained by including the 500 nm emission decay in the global analysis of the 540 and 560 nm decays, shown in Table 7.16, are better. Although the χ^2 values are slightly worse than those shown in Table 7.17, they are still acceptable, with all $\chi^2 \leq$ 1.12. Therefore it can be concluded that the species responsible for the emission at 500 nm are the same as those responsible for the emission at 540 and 560 nm and that they have lifetimes of 8.7 and 4.4 ns. The two species responsible for the emission at 460 and 480 nm have lifetimes of 7.5 and 3.7 ns. The results from the individual fit of the 440 nm emission decay were accepted. These were one lifetime of 7.4 ns (74 % and A factor of 0.50) and one lifetimes of 2.6 ns (26 % and A factor of 0.50). It is reasonable to assume that the species with measured lifetimes of 7.4 and 7.5 ns are the same. The accepted results for the 9 Hz IC polymer sample excited at 420 nm are summarised in Table 7.18.

λ_{em} / nm	τ_1 / ns	A_1	$\%_1$	τ_2 / ns	A_2	$\%_2$
440	7.4	0.50	74	2.6	0.50	26
460	7.5	0.52	69	3.7	0.48	31
460*	7.5	0.52	69	3.7	0.48	31
480	7.5	0.57	73	3.7	0.43	27
500	8.7	0.39	55	4.4	0.61	45
540	8.7	0.50	67	4.4	0.50	33
560	8.7	0.54	70	4.4	0.46	30

* this decay was collected until 20,000 counts had been recorded in the peak channel

Table 7.18: Accepted lifetimes, A factors and %-contributions for the 9 Hz IC polymer sample excited at 420 nm.

The lifetimes obtained for the 9 Hz sample are very similar to those obtained for the 1 Hz sample. Therefore it is reasonable to assume that the same emitting species have been produced in the two samples and that changing the rotation speed does not change the products of the

electropolymerisation reaction. However in the 1 Hz sample the same two species were observed at the 460, 480 and 500 nm emission wavelengths whereas in the 9 Hz sample the same two species were observed at the 500, 540 and 560 nm emission wavelengths. A possible explanation for this shift is that at 500 nm all four species are contributing to the emission. Therefore, which set of decays the 500 nm decay appears to belong to depends on the relative amounts of the species contributing to the emission at that wavelength in each sample. However, since such small differences in the relative amounts of species in different samples may be due to the variability of the sample preparation method, the grouping of the 500 nm decay with the 460 and 480 nm decays in one sample and with the 540 and 560 nm decays in the other may not be significant.

The A factors for the five different species observed in the 1 and 9 Hz samples excited at 420 nm are shown in Tables 7.11 and 7.18. These show that the increase in rotation speed from 1 to 9 Hz increases the A factors for the short lifetime species (~2-4 ns) with respect to the A factors for the long lifetime species (~7.5-8.5 ns). However the differences are between 0.04 and 0.08 for all decays except the 500 nm decay, and are therefore small compared to the differences in the A factors observed between the samples when exciting at 370 nm of between 0.09 and 0.21. Therefore, they are probably due only to the variability of the sample preparation method. This suggests that, although a fast rotation speed favours formation of the IC dimer over formation of longer polymers, altering the rotation speed does not significantly change the relative amounts of the different longer polymers which are observed when exciting at 420 nm. This in turn suggests that there is not much variability in the length of polymer species observed at this excitation wavelength.

7.5 Time-resolved fluorescence of PC polymers

7.5.1 Choice of excitation wavelengths

TCSPC measurements were made on samples of PC polymer dissolved in DMF at excitation wavelengths of 355, 420 and 450 nm. These wavelengths were chosen by examination of the steady-state excitation and emission spectra of the PC polymers, examples of which are shown in Figure 7.10.

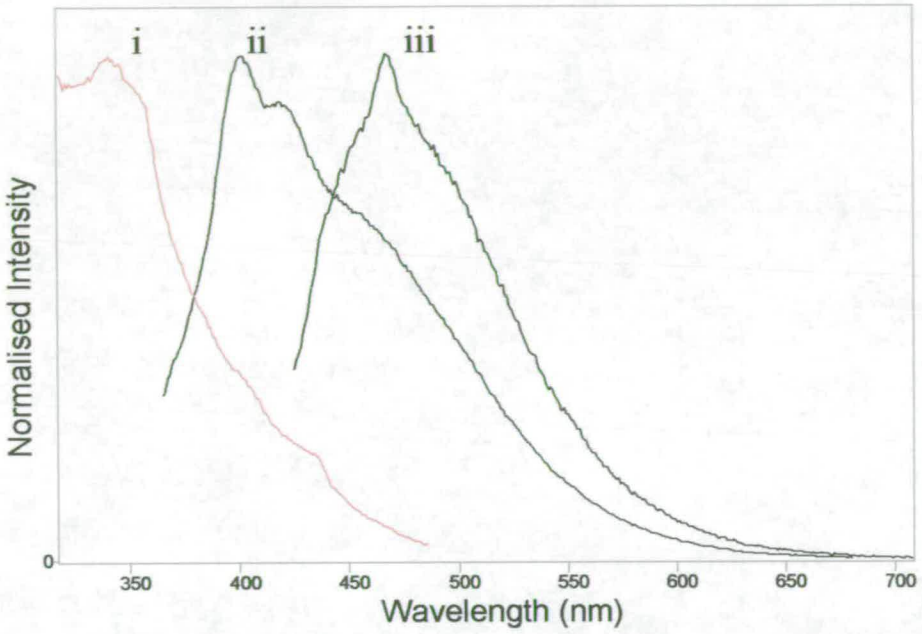

Figure 7.10: Excitation (red) and emission (black) spectra of PC polymer formed at 1 Hz rotation speed in DMF, with (i) emission wavelength 500 nm and excitation wavelengths (ii) 350 nm (Raman band at 391 nm) and (iii) 410 nm (Raman band at 467 nm).

As discussed in chapter six, three overlapping emission bands appear in the steady-state emission of the PC polymers with maxima at 400, 420 and 470 nm. These are visible in the emission spectrum obtained with a 350 nm excitation wavelength, which is shown in Figure 7.10 ii. Therefore, an excitation wavelength of 355 nm and emission wavelengths from 400 to 550 nm were used to investigate the lifetimes of the species which contribute to these three emission bands. This excitation wavelength also has the advantage of being on the long wavelength edge of the PC monomer excitation spectrum and exciting at 355 nm produces a low intensity emission spectrum from the monomer. Therefore, if any PC monomer remains in the sample, it may be detected in the TCSPC experiments at this excitation wavelength. At excitation

wavelengths from 410 nm to 480 nm the emission spectrum appears to be made up of only the broad emission which peaks at 470 nm. The emission obtained by exciting at 410 nm is shown in Figure 7.10 iii. The excitation wavelengths 420 and 450 nm were chosen to investigate the species which contribute to this emission band.

7.5.2 PC polymer made at 1 Hz

Fluorescence decays at various emission wavelengths were measured for the 1 Hz PC polymer sample using excitation wavelengths of 355, 420 and 450 nm. It was necessary to fit three lifetimes, τ_1 (~13 ns), τ_2 (~5 ns) and τ_3 (~2 ns), to each of these decays to achieve acceptable χ^2 values. Examples of the experimental decay data, fitted function and residuals obtained for the experiments carried out at excitation wavelengths of 355 and 450 nm are shown in Figures 7.11 and 7.12 respectively. The lifetimes, A factors and %-contributions for 355, 420 and 450 nm excitation are given in Tables 7.19, 7.20 and 7.21 respectively.

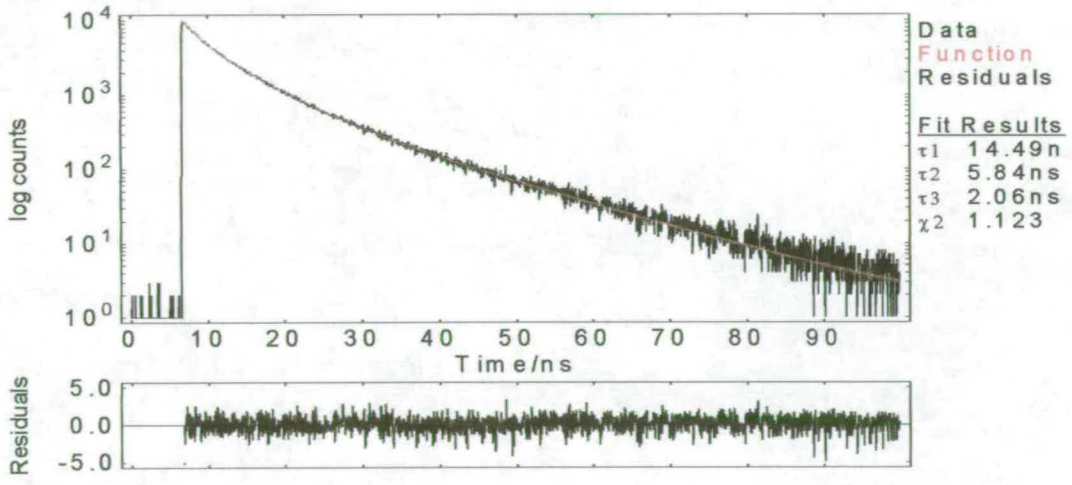

Figure 7.11: The experimental decay data, fitted function and residuals for the PC polymer formed at 1 Hz, with excitation wavelength 355 nm and emission wavelength 430 nm.

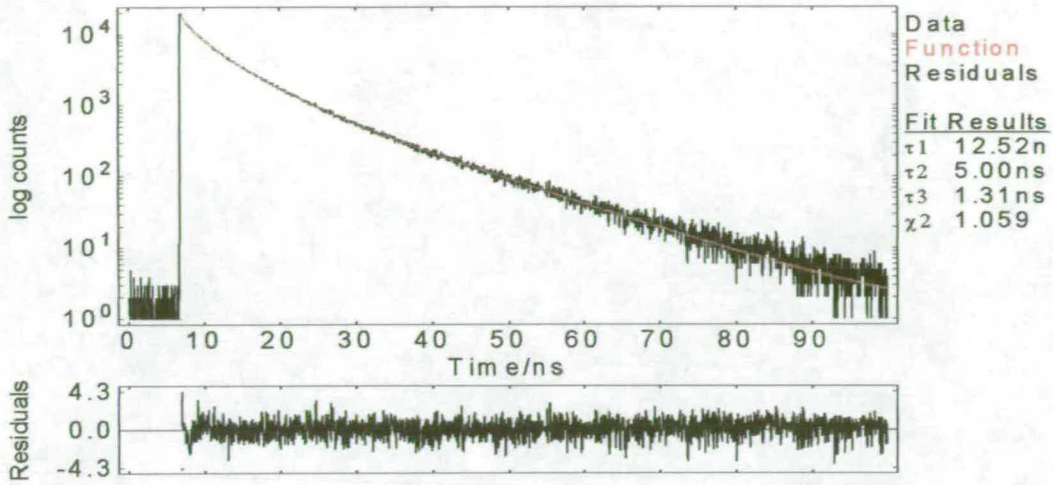

Figure 7.12: The experimental decay data, fitted function and residuals for the PC polymer formed at 1 Hz, with excitation wavelength 450 nm and emission wavelength 550 nm.

λ_{em} / nm	τ_1 / ns	A_1	$\%_1$	τ_2 / ns	A_2	$\%_2$	τ_3 / ns	A_3	$\%_3$	χ^2
400	14.7	0.16	35	6.2	0.61	59	1.9	0.23	7	1.08
430	14.5	0.13	32	5.8	0.54	56	2.1	0.33	12	1.12
470	13.6	0.15	35	5.6	0.56	55	1.9	0.30	10	1.15
490	13.8	0.17	38	5.8	0.54	51	2.1	0.29	10	1.08
550	14.8	0.18	42	6.3	0.52	50	1.7	0.30	8	1.11

Table 7.19: Fluorescence decay parameters for the decays measured for the IC polymer formed at 1 Hz at various emission wavelengths (λ_{em}), with an excitation wavelength of 355 nm. τ_n is the lifetime of component n, A_n the A factor for component n and $\%_n$ the %-contribution to the steady-state emission intensity of component n.

λ_{em} / nm	τ_1 / ns	A_1	$\%_1$	τ_2 / ns	A_2	$\%_2$	τ_3 / ns	A_3	$\%_3$	χ^2
470*	9.9	0.08	20	4.4	0.57	63	2.0	0.35	18	1.05
490*	11.0	0.10	24	4.8	0.54	59	2.0	0.36	17	1.09
550*	12.5	0.14	33	5.4	0.51	54	1.8	0.36	13	1.10

*these decays were collected until 20,000 counts had been recorded in the peak channel, data recorded in 4096 channels

Table 7.20: Fluorescence decay parameters for the decays measured for the IC polymer formed at 1 Hz at various emission wavelengths (λ_{em}), with an excitation wavelength of 420 nm. τ_n is the lifetime of component n, A_n the A factor for component n and $\%_n$ the %-contribution to the steady-state emission intensity of component n.

λ_{em} / nm	τ_1 / ns	A_1	$\%_1$	τ_2 / ns	A_2	$\%_2$	τ_3 / ns	A_3	$\%_3$	χ^2
490*	11.0	0.13	31	4.7	0.57	60	1.2	0.31	8	1.09
550*	12.5	0.15	37	5.0	0.53	54	1.3	0.32	8	1.06

*these decays were collected until 20,000 counts had been recorded in the peak channel

Table 7.21: Fluorescence decay parameters for the decays measured for the PC polymer formed at 1 Hz at various emission wavelengths (λ_{em}), with an excitation wavelength of 450 nm. τ_n is the lifetime of component n, A_n the A factor for component n and $\%_n$ the %-contribution to the steady-state emission intensity of component n.

Global analyses, where all three lifetimes were held in common for all the decays measured, were performed at each excitation wavelength. The results are given in Table 7.22 (excitation wavelength of 355 nm), Table 7.23 (excitation wavelength of 420 nm) and Table 7.24 (excitation wavelength 450 nm). All the χ^2 values obtained from the global analysis of the 355 nm excitation data are ≤ 1.2. Also, the local χ^2 values are similar to those obtained by fitting each decay individually (see Table 7.19). Therefore it can be concluded that the same three species are emitting at each emission wavelength for this data set. The χ^2 values shown in Tables 7.23 and 7.24 are less good. The global χ^2 values are close to 1.2 and two of the local χ^2 values (for the decays measured with excitation at 420 and emission at 550 nm and excitation at 450 and emission at 490 nm) are greater than 1.2. The χ^2 values obtained by fitting these two decays individually (1.10 and 1.09) were not significantly different from the χ^2 values obtained by fitting the other decays in each data set individually, and therefore the poor χ^2 values cannot be attributed to poor data for these decays. Therefore the same three species are not emitting across all emission wavelengths for the 420 and 450 nm excitation wavelengths.

λ_{em} / nm	$\%_1$	A_1	$\%_2$	A_2	$\%_3$	A_3	χ^2
400	38	0.18	56	0.62	6	0.20	1.08
430	32	0.13	55	0.51	13	0.36	1.16
470	30	0.12	58	0.55	12	0.33	1.16
490	36	0.15	54	0.56	10	0.29	1.10
550	46	0.21	45	0.50	9	0.29	1.16
Lifetimes and global χ^2	τ_1 = 14.3 ns		τ_2 = 6.0 ns		τ_3 = 2.0 ns		1.13

Table 7.22: Results of the global analysis on the decays measured for the 1 Hz PC polymer sample excited at 355 nm. $\%_n$ is the %-contribution of τ_n to the steady-state spectrum and A_n is the A factor for τ_n. All three lifetimes were held in common for all decays.

λ_{em} / nm	$\%_1$	A_1	$\%_2$	A_2	$\%_3$	A_3	χ^2
470*	11	0.04	65	0.51	24	0.45	1.16
490*	20	0.08	60	0.51	10	0.41	1.11
550*	40	0.18	45	0.45	15	0.37	1.27
lifetimes and global χ^2	τ_1 = 11.7 ns		τ_2 = 5.1 ns		τ_3 = 2.1 ns		1.18

*these decays were collected until 20,000 counts had been recorded in the peak channel, data recorded in 4096 channels

Table 7.23: Results of the global analysis on the decays collected for the 1 Hz PC polymer sample excited at 420 nm. $\%_n$ is the %-contribution of τ_n to the steady-state spectrum and A_n is the A factor for τ_n. All three lifetimes were held in common for all decays.

λ_{em} / nm	$\%_1$	A_1	$\%_2$	A_2	$\%_3$	A_3	χ^2
490	23	0.09	66	0.58	10	0.33	1.21
550	38	0.15	52	0.50	10	0.35	1.13
lifetimes and global χ^2	τ_1 = 12.3 ns		τ_2 = 5.1 ns		τ_3 = 1.4 ns		1.17

* these decays collected until 20,000 counts had been recorded in the peak channel

Table 7.24: Results of the global analysis on the decays collected for the 1 Hz PC polymer sample excited at 450 nm. $\%_n$ is the %-contribution of τ_n to the steady-state spectrum and A_n is the A factor for τ_n. All three lifetimes were held in common for all decays.

Returning to the results in Tables 7.20 and 7.21, it appears that there is a species with lifetime 12.5 ns which emits at 550 nm in both data sets and also a species with lifetime 11.0 ns which emits at 490 ns in both data sets. The lifetime of 9.9 ns observed in the 470 nm emission is very

close to the 11.0 ns lifetime and these two lifetimes may in fact be due to the same species. Therefore a global analysis between the 470 and 490 nm decays was performed and the results are shown in Table 7.25.

λ_{em} / nm	$\%_1$	A_1	$\%_2$	A_2	$\%_3$	A_3	χ^2
470*	15	0.06	64	0.54	21	0.40	1.07
490*	26	0.11	56	0.52	18	0.37	1.11
lifetimes and global χ^2	$\tau_1 = 10.7$ ns		$\tau_2 = 4.7$ ns		$\tau_3 = 2.1$ ns		1.09

* these decays were collected until 20,000 counts had been recorded in the peak channel, data recorded in 4096 channels

Table 7.25: Results of the global analysis for the decays measured at an excitation wavelength of 420 nm and emission wavelengths of 470 and 490 nm for the 1 Hz PC polymer sample. All three lifetimes held in common for all decays.

All three χ^2 values shown in Table 7.25 are within the acceptable limits and they are very similar to the χ^2 values obtained by analysing these decays individually. Therefore the same three emitting species are responsible for the emission at both 470 and 490 nm when exciting at 420 nm. The lifetime of 10.7 ns obtained from this global analysis is very close to 11.0 ns and therefore it can be concluded that this component is the same as the 11.0 ns component observed when exciting at 450 nm. Comparing the lifetimes shown in Table 7.25 (emission at 470 and 490 nm) and 7.20 (emission at 550 nm) with those in Table 7.22, it appears that a component with lifetime of ~2 ns is common to the emission excited at both 355 and 420 nm. Comparing the lifetimes shown in Table 7.25 with those in Table 7.21 and 7.20, there appears to be a component with lifetime ~5 ns common to the emission excited at 420 and 450 nm. This component may be representative of a distribution of similar lifetimes rather than a single species. Lastly, the 1.2 and 1.3 ns components observed when exciting at 450 nm are likely to be due to the same species.

Thus, overall, the fluorescent species over the range of emission wavelengths from 400 to 550 nm, excited at the three different excitation wavelengths, can be described by seven characteristic lifetimes as follows:

τ / ns	λ_{ex} / nm	λ_{em} / nm
14.3	355	400 to 550
6.0	355	400 to 550
2	355 and 420	400 to 550
5	420 and 450	470 to 550
11	420 and 450	470 to 490
12.5	420 and 450	550
1.3	450	490 to 550

Table 7.26: Accepted lifetimes for the 1 Hz PC polymer sample and the excitation and emission wavelengths at which they are observed.

7.5.3 Discussion

It was concluded from the examination of the steady-state spectra of the PC polymer presented in chapter six that electropolymerisation of the PC monomer results in the formation of a number of emitting species which are not monomer. This is confirmed by the multiexponential nature of the decays measured for the PC polymer samples, where only monoexponential decays were recorded for the PC monomer sample. The value of 14.3 ns for the lifetime of one of the PC polymer species, observed when exciting at 355 nm, is close to the lifetime of the PC monomer, which has been measured as 16.1 ns. This suggests that the species with a lifetime of 14.3 ns in the PC polymer sample may be PC monomer. However a comparison of the %-contributions of this species to the steady-state, $\%_I$ in Table 7.22, and the steady-state emission spectrum of the PC monomer, which is shown in Figure 6.1 in the previous chapter, show that this is not the case. For example, the %-contribution of τ_1 shown in Table 7.22 is 46 % at an emission wavelength of 550 nm, whereas the intensity of the PC monomer steady-state emission spectrum is zero at 550 nm. Therefore the PC polymer sample does not contain any detectable levels of PC monomer.

The global analysis of the decays measured for the 1 Hz PC polymer sample with an excitation wavelength of 355 nm showed the presence of three species with lifetimes of 14.3, 6.0 and 2.0 ns. Plots of the %-contributions and A factors against emission wavelength for each of these three species, taken from the data in Table 7.22, are shown in Figure 7.13. These show that the species which contributes most to the steady-state spectrum at all emission wavelengths has a lifetime of 6.0 ns. This species also has the highest A factors at all emission wavelengths and therefore the highest proportion of excited states present in the sample. The plots in Figure 7.13 also show that the species with a lifetime of 14.3 ns contributes more to the steady-state

spectrum than the species with a lifetime of 2.0 ns at all the emission wavelengths sampled. Interestingly, however, the plot of A factor against emission wavelength shows that the species with a lifetime of 2.0 ns represents a higher fraction of the excited state population than the species with a lifetime of 14.3 ns at all the emission wavelengths sampled. The relative proportions of all three excited states show little dependence on emission wavelength and therefore it is likely that all three species have similar sizes of conjugated system.

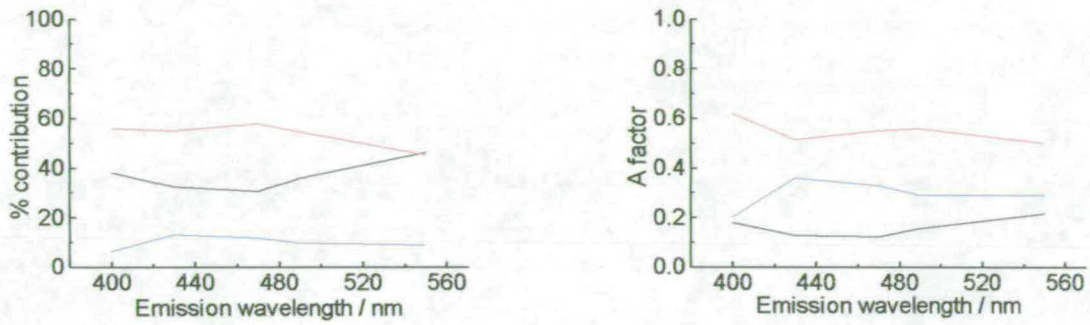

Figure 7.13: Plots of %-contribution and A factor against emission wavelength for the 1 Hz sample of PC polymer excited at 355 nm. Data is taken from the results of the global analysis shown in Table 7.12. Black is the component with lifetime 14.3 (τ_1), red is the component with lifetime 6.0 (τ_2) and blue is the component with lifetime 2.0 ns (τ_3).

The values of the %-contribution given in Table 7.22 were used to separate the overall steady-state emission spectrum of the sample into the individual spectra of each component, as shown in Table 7.27 and Figure 7.14.

λ_{em} / nm	Intensity of steady-state spectrum	$\%_1$	Intensity × $\%_1$	$\%_2$	Intensity × $\%_2$	$\%_3$	Intensity × $\%_3$
400	1.4×10^7	38	5.3×10^6	56	7.8×10^6	6	8.4×10^5
430	1.2×10^7	32	3.8×10^6	55	6.6×10^6	13	1.6×10^6
470	8.7×10^6	30	2.6×10^6	58	5.0×10^6	12	1.0×10^6
490	7.0×10^6	36	2.5×10^6	54	3.8×10^6	10	7.0×10^5
550	2.1×10^6	46	9.7×10^5	45	9.5×10^5	9	1.9×10^5

Table 7.27: Intensities at different emission wavelengths taken from the steady-state emission spectrum of the PC polymer with excitation wavelength 350 nm. %-contributions of each lifetime from Table 7.22. Data plotted in Figure 7.18.

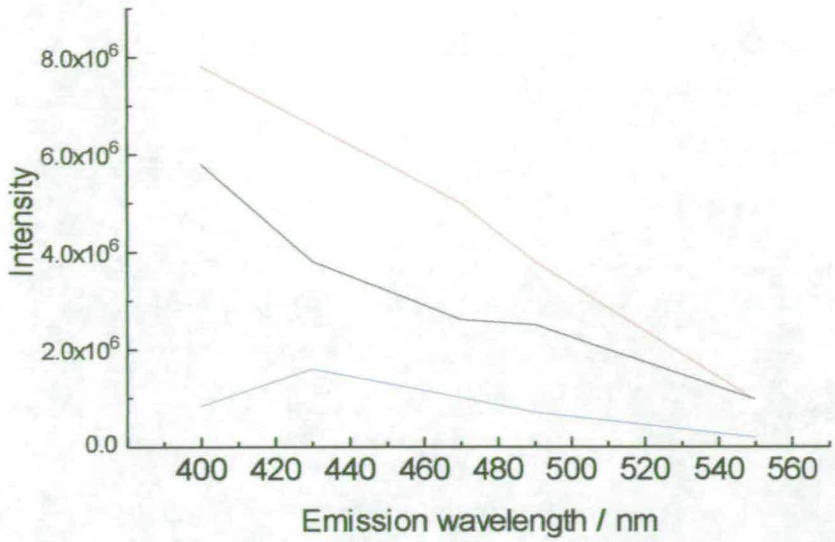

Figure 7.14: Plot of intensity of fluorescence emission for each species observed in the 1 Hz PC polymer sample excited at 355 nm. Black is 14.3 ns (τ_1), red is 6.0 ns (τ_2) and blue is 2.0 ns (τ_3). Data plotted from Table 7.27.

It is clear from Figure 7.10 that the emission spectrum at this excitation wavelength contains a significant contribution from the 14.3 and 6.0 ns components across the entire emission envelope. The 2 ns component makes a much smaller contribution to the steady-state intensity. Comparison of the profiles of the component spectra in Figure 7.14 with the total emission spectrum in Figure 7.10 ii suggests that the 14.3 ns component is largely responsible for the distinct maximum at 400 nm, and probably corresponds to a dimer species similar to that observed for IC (with a lifetime of 10.0 ns). The 6 ns component has a rather broader emission profile and can be identified with the broad shoulder at ~470 nm in the total emission spectrum. The 2 ns component shows a maximum in its emission spectrum at ~430 nm, and is likely to be responsible for the relatively sharp shoulder observed in the total emission spectrum at 420 nm.

The lifetimes of 14.3 and 6.0 ns observed for PC in this emission region are similar in magnitude to those of 10.0 and 5.5 ns observed for IC at an excitation wavelength of 370 nm, and are likely to belong to similar emitting species ie dimer and a higher oligomer (possibly trimer). PC shows a third shorter decay component of lifetime 2 ns which is not observed for IC. This shortest lived species constitutes about a third of the emitting population in this wavelength region, although its contribution to the steady-state emission is only ~10 % because of its relatively low quantum yield. This species is likely to be a short conjugation length segment of a longer

oligomeric (polymeric) chain, which is quenched by energy transfer to longer conjugation length (lower excitation energy) segments of the same chain.

At longer excitation and emission wavelengths, the existence of several emitting species with similar conjugation lengths (excitation energies) but markedly different lifetimes is apparent. As for IC, this can be explained by the existence of species of similar conjugation length in different polymeric environments and hence subject to different rates of non-radiative decay through energy transfer. For PC, four decay components can be identified with lifetimes of 1.3, 5, 11 and 12.5 ns. This is a much greater range of lifetimes than was observed for IC and suggests the existence of a wider range of polymer chain lengths in PC than in IC. In PC, two species of similar conjugation length display lifetimes differing by almost an order of magnitude (12.5 ns and 1.3 ns). The 1.3 ns lifetime can be attributed to an oligomeric segment which constitutes a relatively short conjugation length species in a long polymer chain. The 12.5 ns lifetime can be attributed to a species with similar conjugation length, which is present as a free oligomer or constitutes a relatively long conjugation length segment of a short polymer chain (and hence is free from quenching by energy transfer).

7.6 Conclusions

The technique of time correlated single photon counting (TCSPC) has been used to measure the the fluorescence lifetimes of the IC and PC monomers and also to study the products of the electropolymerisation of IC and PC. The lifetimes of the IC and PC monomers are 11.5 and 16.1 ns respectively.

Fluorescence decays were measured for IC polymer samples produced at a slow rotation speed of 1 Hz and at a fast rotation speed of 9 Hz, at excitation wavelengths of 370 and 420 nm. All the decays recorded for these samples were found to be bi-exponential. It has been confirmed that electropolymerisation of IC monomer produces emitting species which are not monomer and that the sample of IC polymer, produced by electropolymerisation of the IC monomer and rinsed in acetonitrile before dissolution in DMF, is free from monomer.

Seven different emitting species with lifetimes of 2.6, 3.6, 5.5, 4.1, 7.4, 8.3 and 10.0 ns are present in the IC polymer sample produced at 1 Hz. Both the 10.0 and 5.5 ns lifetime species are excited at 370 nm and the 2.6, 3.6, 4.1, 7.4 and 8.3 ns lifetime species are excited at 420 nm. The species with lifetime 10.0 ns has been assigned as IC dimer by a comparison with the steady-state emission spectrum produced by exciting at 360 nm. The species with lifetime 5.5 ns has been shown to have a more extended conjugated system than the IC dimer. It has been shown that in a complex multicomponent system such as this, fluorescence occuring at the same wavelengths, but as a result of excitation at different wavelengths, is not necessarily due to the same species. For example, there are several species in the sample which emit at ~455 nm; the 5.5 ns lifetime species when exciting at 370 nm and the 7.4 and 3.6 ns lifetime species when exciting at 420 nm. The 2.6 ns species has been assigned as a small chromophore within a larger polymer species. The fact that the lifetime of this species is only four times shorter than the longest lifetime observed shows that the size of polymer produced by the electropolymerisation of IC is limited compared to the size of polymer produced by the electropolymerisation of indoles. The 7.4 and 3.6 ns lifetimes are due to two similar conjugation length species in different polymer environments. The 7.4 ns lifetime may be due to a free oligomer (or an oligomer with a relatively short polymer chain) and the 3.6 ns lifetime to a species within a relatively long polymer chain. The 8.3 and 4.1 ns lifetime species are attributed to a similar pair of emitting species, but with longer conjugation lengths.

Increasing the rotation speed of the RDE during the electropolymerisation of IC, from 1 Hz to 9 Hz, does not change the products of the electropolymerisation reaction. However, as the rotation speed is increased the amount of IC dimer in the sample increases with respect to the amount of the 5.5 ns lifetime species. This supports the conclusion from the steady-state spectra, discussed in chapter six, that the mechanism of IC electropolymerisation is similar to the mechanism of indole electropolymerisation. However, altering the rotation speed does not significantly change the relative amounts of the different longer polymers which are observed when exciting at 420 nm. This suggests that the polymers observed with the excitation wavelength of 420 nm are all of similar size.

Fluorescence decays were measured for a sample of PC polymer produced at a 1 Hz rotation speed, at excitation wavelengths of 355, 420 and 450 nm. All the decays recorded for these samples were found to be tri-exponential. It has been confirmed that electropolymerisation of PC monomer produces emitting species which are not monomer and that the sample of PC polymer, produced by electropolymerisation of the PC monomer and rinsed in acetonitrile before dissolution in DMF, is free from monomer.

Seven different emitting species with lifetimes of 14.3, 6.0, ~2, 1.3, 12.5, ~11 and ~5 ns are present in the PC polymer sample produced at 1 Hz. The 14.3, 6.0 and ~2 ns lifetime species are excited at 355 nm and these three species have been shown to have similar sizes of conjugated system. The 14.3 ns species is largely responsible for the distinct maximum at 400 nm in the steady-state emission spectrum of this sample and probably corresponds to a dimer species similar to that observed for IC. The 6.0 ns component has been identified with the broad shoulder at ~470 nm in the total emission spectrum and the ~2 ns component is likely to be responsible for the relatively sharp shoulder observed in the total emission spectrum at 420 nm. This ~2 ns component is likely to be a short conjugation length segment of a longer oligomeric (polymeric) chain, which is quenched by energy transfer to longer conjugation length (lower excitation energy) segments of the same chain. At 420 nm the ~11, 12.5, ~5 and ~2 ns species are excited and at 450 nm the ~11, 12.5, ~5 and 1.3 ns species are excited. This is a much greater range of lifetimes than was observed for IC and suggests the existence of a wider range of polymer chain lengths in PC than in IC.

7.7 References

1. P.Jennings, PhD thesis, University of Edinburgh, 1999

2. Jay R.Knutson, Joseph M.Beechem and Ludwig Brand, *Chem.Phys.Lett.*, 1983, **102(6)**, 501-507

3. Private communications, Alice Williams, University of Edinburgh

Chapter Eight

CONCLUSIONS

In this thesis it has been shown, for the first time, that indolo{3,2,1-*jk*}carbazole (IC) and pyrrolo{3,2,1-*jk*}carbazole (PC) may each be electropolymerised to form electroactive polymers. Electrochemical techniques have been used to probe the mechanism of electropolymerisation of IC. The photophysical behaviour of the IC and PC monomers and their polymers has been investigated using both steady-state and time-resolved spectroscopic methods. The use of quantum chemical calculations has been investigated for the calculation of the oxidation potentials, radical cation spin density distributions and excited states of small organic heterocycles. In this chapter the main conclusions of this work are summarised.

The density functional theory (DFT) functional B3PW91 and the solvation model COSMO, with the 6-311G(2d,2p) basis set for the organic molecules and the 6-31G(d,p) basis set for Fc and Fc^+ has been shown to systematically underestimate the oxidation potentials of a range of small heterocyclic molecules, and reproduces the experimental half wave potentials to within 0.19 V. The calculation method B3PW91/6-31G(d,p) has been shown to successfully reproduce the qualitative radical cation spin density distributions of indoles previously obtained with DMol[3]. The semiempirical method ZINDO has been shown to correctly predict the order of the energies of the two lowest excited states of indole and carbazole and the vertical excitation energies obtained with this method are closer to the experimental energies than those obtained with time-dependent DFT. The *ab initio* excited state method configuration interaction singles (CIS) incorrectly predicts the energetic ordering of the two lowest excited states of both carbazole and indole. However, this method correctly predicts the dipole moment of the ^1L_a state of indole to be larger than the dipole moment of the ^1L_b state.

It has been shown that both IC and PC may be electropolymerised to form electroactive films. IC forms a conducting film, which is completely soluble in DMF. The mechanism of IC film formation has been shown to be similar to that of indole electropolymerisation, with initial IC polymer formation in solution, followed by deposition of the polymer onto the electrode surface. This deposited layer then acts as a site for electrooxidation and adsorption of the monomer

radical cation. The second (higher potential) oxidation peak observed in CVs of the IC films in background electrolyte appears to cause the IC film to become soluble in acetonitrile. As the film dissolves off the electrode surface with repeated cycling a change in the coat structure is observed. The diffusion coefficient of IC has been measured as 5.9×10^{-5} cm^2 s^{-1} ($\pm$ 2.0×10^{-5}). The rate of film formation for IC is approximately 0.9 times that of indole-5-carboxylic acid and 0.4 times that of 5-cyanoindole. NMR and mass spectroscopy have shown that the product of IC electropolymerisation is largely composed of two different IC dimers; 7,3' and 7,4'. The radical cation spin density calculation of $IC^{\bullet+}$ was unsuccessful in predicting the linkage sites of IC, and so the success of such calculations in predicting the linkage sites in indole electropolymerisation cannot necessarily be extrapolated to other aromatic monomers.

Steady-state fluorescence spectroscopy has shown that the PC monomer is more perturbed by an increase in solvent polarity than the IC monomer and that there is a geometry or potential energy surface difference between the ground and excited states of PC, which is not present for IC. The lifetimes of the IC and PC monomers are 11.5 and 16.1 ns respectively. Steady-state and time-resolved spectroscopy of the IC and PC polymers has shown that electropolymerisation of each of these monomers produces a number of emitting species which have more extensive π-electron delocalisation than the monomers. IC dimer has a lifetime of 10.0 ns and has been shown to emit in the same wavelength region as the indole trimers, with a peak in the steady-state spectrum at 408 nm. The shortest PC oligomer (possibly dimer) emits to slightly shorter wavelengths than the IC dimer, which shows that, in principle, using monomers with different sizes of conjugation system can alter the wavelength of emission of the electropolymerised species in solution. It has been shown that a similar mechanism to that found for indole electropolymerisation is occurring during both IC and PC electropolymerisation. The first step in the electropolymerisation is formation of dimer (shortest oligomer) and this is followed by linkage of the dimer units to form longer polymer species, which emit at to longer wavelengths. Seven different emitting species are present in both the IC and PC polymer samples produced at 1 Hz and increasing the rotation speed to 9 Hz does not change the products of the electropolymerisation of IC. The size of polymer produced by the electropolymerisation of IC is limited compared to the size of polymer produced by the electropolymerisation of indoles. However, there appears to be a wider range of polymer chain lengths present in the PC polymer sample than in the IC polymer sample. There are a number of species present in both the IC and

PC polymer samples with similar conjugation lengths, but which are in different polymer environments and therefore have different lifetimes.

The steady-state fluorescence spectrum of an IC polymer drop-coated onto a microscope slide has been measured, showing that the IC polymer is fluorescent in the solid state.

The results presented in this thesis suggest that IC polymer may be a suitable candidate for the emissive layer in light emitting diodes, as it emits in the blue with a high quantum yield and is fluorescent in the solid state.

Appendix

Courses Attended

Unix 1: Introduction to Unix

Introduction to computer programming

Computational methods

Molecular wave mechanics

Managing health and safety in the laboratory

Physical section meetings, Firbush

Colloquia and physical section meetings